

Land-atmosphere interactions and their effect on Australian precipitation

Chiara M. Holgate

November 2020

A thesis submitted for the degree of
Doctor of Philosophy
of the Australian National University



Australian
National
University

© Copyright by Chiara M. Holgate 2020

All rights reserved

Candidate's declaration

The work presented in this thesis is an accurate account of original research performed during the degree of Doctor of Philosophy at the Australian National University. This thesis is presented as a compilation of articles published during the degree. The data processing, analysis, interpretation and preparation of each article were all primarily carried out by C.Holgate, with contributions from co-authors. Author and co-author contributions to each article are specified in a Statement of Contribution provided in this thesis alongside each publication.

Chiara Holgate

November 2020

Acknowledgements

During the course of this PhD, Australia has experienced the most intense drought in the instrumental record, the hottest year on record, diminishing town water supplies, mass fish kills, mega bushfires and floods. Our need to better understand our climate, and prepare for and adapt to its extremes, has never been more apparent.

This research was undertaken to deepen, in some way, our collective understanding of Australia's rainfall, for those who need it most - farmers, rural industries, water resource managers and emergency services. I am thankful for the resilience and perseverance of my family that has enabled them to succeed in farming in Australia, and as a consequence enabled me to receive a university education, and now, a PhD.

I am thankful to my supervisors, Albert, Jason and Andy, for their sustained interest and support in this work. I am especially grateful for the confidence Albert has shown in me from the beginning - hopefully it was well-founded.

Finally, I am most grateful to my husband for his ever-present optimism and support. What a big five years it has been.

Abstract

The aim of the research presented in this thesis is to determine the influence of land-atmosphere interactions on Australian precipitation, both under average conditions and during drought. This aim is addressed using a combination of statistical and numerical atmospheric water accounting techniques.

The first part of the research examines soil moisture, a key variable that underpins the analysis of land-atmosphere interactions. Due to the range of estimation techniques and variety of applications utilising soil moisture information, numerous data sets are available. This thesis evaluates soil moisture from ground, satellite and model estimates across Australia and identifies data sets suitable to the study of land-atmosphere interactions and other applications.

Soil moisture information was then combined with observations of precipitation to identify where land-atmosphere interactions have a detectable influence on Australian precipitation. Analysing the statistical relationship between soil moisture and subsequent precipitation, the results showed detectable relationships in north and southeast Australia and the importance of scale in interpreting physical relationships with a statistical metric.

With regions of land-atmosphere interaction identified, the next stage of the research quantified the interaction with the precipitation recycling ratio — a measure of how much of a region's precipitation is derived from evaporation in that same region. Precipitation recycling was quantified using a “back-trajectory” model that identified the evaporative moisture sources of Australia's precipitation. Strongest land-atmosphere interactions and recycling were found in the north and southeast of the continent in spring and summer, along with long term trends in regional moisture sources.

The importance of land-atmosphere interaction during drought was the subject of the final stage of the research. Focusing on the Murray-Darling Basin in southeast Australia, the research analysed the sources of moisture supplying precipitation and the degree to which the land surface amplified precipitation anomalies during drought onset, persistence and ter-

mination. The results indicate that major droughts were driven by reduced moisture supply from the ocean, as moisture was circulated away from the region, combined with an absence of precipitation-generating mechanisms over land. Droughts terminated when moist easterly flows from the Tasman and Coral Seas strengthened, promoting high precipitation. Terrestrial moisture sources played a secondary role, amplifying precipitation anomalies by less than 6%.

In summary, the research presented in this thesis has determined the influence of land-atmosphere interactions on Australian precipitation, both under average conditions and during drought. The analysis demonstrates that Australian precipitation is predominantly driven by large scale processes transporting marine moisture to the continent for precipitation, with terrestrial moisture sources forming an important contribution to precipitation in the north and southeast of the continent. In the southeast, drought is driven by atmospheric circulation anomalies redirecting ocean moisture away from the region, with land-atmosphere interactions playing a secondary role.

Contents

| | |
|--|------------|
| Candidate's declaration | ii |
| Acknowledgements | iii |
| Abstract | iv |
| 1 Introduction | 1 |
| 1.1 What are land-atmosphere interactions? | 1 |
| 1.2 Why are land-atmosphere interactions important? | 4 |
| 1.3 Land-atmosphere interactions in Australia | 5 |
| 1.4 How land-atmosphere interactions are identified and measured | 7 |
| 1.4.1 Statistical approaches | 8 |
| 1.4.2 Moisture accounting approaches | 10 |
| 1.4.3 Thermodynamic approaches | 11 |
| 1.4.4 Comparison of approaches | 14 |
| 1.5 Thesis motivation and objectives | 16 |
| 1.6 Thesis structure | 17 |
| 2 Soil moisture - the link between the land and the atmosphere | 18 |
| 2.1 Overview | 18 |
| 2.2 Published manuscript 1 | 21 |
| 2.3 Chapter summary | 43 |
| 3 Identifying land-atmosphere interactions with soil moisture-precipitation relationships | 45 |
| 3.1 Overview | 45 |
| 3.2 Published manuscript 2 | 48 |

| | | |
|----------|---|------------|
| 3.2.1 | Supplementary material | 60 |
| 3.3 | Chapter summary | 62 |
| 4 | Quantifying the strength of land-atmosphere interaction over Australia | 63 |
| 4.1 | Overview | 63 |
| 4.2 | Published manuscript 3 | 65 |
| 4.2.1 | Supplementary material | 80 |
| 4.3 | Chapter summary | 91 |
| 5 | The role of land-atmosphere interactions during drought | 92 |
| 5.1 | Overview | 92 |
| 5.2 | Published manuscript 4 | 94 |
| 5.2.1 | Supplementary material | 104 |
| 5.3 | Chapter summary | 109 |
| 6 | Conclusion | 110 |
| 6.1 | Research summary | 111 |
| 6.2 | Future work | 113 |
| | Bibliography | 116 |

List of Tables

| | | |
|------|--|-----|
| 1.1 | Summary of main methods for identifying or quantifying land-atmosphere interaction | 13 |
| 2.1 | Summary of in situ stations | 24 |
| 2.2 | Summary of comparison data sets | 28 |
| 2.3 | Correlation between in situ data and satellite and model products, longer period (2001-2014) | 29 |
| 2.4 | Correlation between 0 and 90 cm in situ measurements and model products . . | 29 |
| 2.5 | Correlation between in situ data and satellite and model products, common period (2012-2013) | 30 |
| 2.6 | Correlation of temporal anomalies, common period (2012-2013) | 32 |
| 3.1 | Proportion of statistically significant grid cells | 53 |
| 4.S1 | Mean correlation between observed and modelled annual and seasonal minimum and maximum temperature and precipitation | 87 |
| 4.S2 | Mean bias of modelled annual and seasonal minimum and maximum temperature and precipitation | 88 |
| 4.S3 | Proportion of cells with bias greater than 10 mm month ⁻¹ | 88 |
| 4.S4 | Proportion of total moisture sourced from outside the model domain by season | 89 |
| 4.S5 | Trends in seasonal evaporation over ocean regions | 90 |
| 5.1 | Drought amplification factors | 101 |
| 5.S1 | Percentile- and SPI-based drought stages, northern Murray-Darling Basin . . . | 107 |
| 5.S2 | Percentile- and SPI-based drought stages, southern Murray-Darling Basin . . . | 108 |

List of Figures

| | | |
|---------|---|----|
| 1.1 | The hydrological cycle | 2 |
| 1.2 | Complex interactions between the land surface and the atmospheric boundary layer | 3 |
| 2.1 | In situ network station locations with climate zones | 23 |
| 2.2 | Minimum, maximum and standard deviation of correlation between in situ and satellite soil moisture estimates | 28 |
| 2.3 | Correlation across climate zones by product | 31 |
| 2.4 | Soil moisture from SMOS_LPRM_A and SMOS_LMEB_A at NSW-03 | 32 |
| 2.5 | Soil moisture from AMSR2_LPRM_D at NT-01 | 33 |
| 2.6 | Soil moisture from ASCAT_TUW_D at NT-02 | 33 |
| 2.7 | Soil moisture from CABLE, WaterDyn and API at NSW-02 | 33 |
| 2.8 | Soil moisture from AWRA-L, KBDI and MSDI at NT-01 | 34 |
| 2.A1-12 | Cluster dendrograms | 43 |
| 3.1 | Station locations and seasonal precipitation climatology | 51 |
| 3.2 | Probability and cumulative density functions for Australian wind speed | 52 |
| 3.3 | Autumn soil moisture-precipitation correlation when the 1D assumption is upheld and when it is not, for spatial scales 0.05° , 0.5° , 1° and 2.5° | 53 |
| 3.4 | Seasonal soil moisture-precipitation correlation when 1D assumption upheld | 54 |
| 3.5 | Difference in correlation between spatial scales, considering initially positive correlation coefficients | 55 |
| 3.S1 | Seasonal soil moisture-precipitation correlation with alternative data inputs | 60 |
| 3.S2 | Seasonal soil moisture-precipitation correlation with alternative temporal filtering | 60 |
| 3.S3 | Difference in correlation between spatial scales, considering initially negative correlation coefficients | 61 |

| | | |
|-------|---|-----|
| 4.1 | Australian hydrological basins and mean annual precipitation, set within back-trajectory model domain | 68 |
| 4.2 | Mean seasonal moisture contribution to Australian precipitation | 70 |
| 4.3 | Mean summer moisture contribution to selected basins | 71 |
| 4.4 | Mean seasonal contributions to precipitation by basin | 71 |
| 4.5 | Interannual variability in marine and terrestrial moisture contribution | 72 |
| 4.6 | Contribution to variance in moisture supplied by ocean region | 73 |
| 4.7 | Mean monthly precipitation recycling by region | 74 |
| 4.8 | Trends in seasonal moisture contribution | 75 |
| 4.S1 | Annual maximum temperature bias of back-trajectory forcing data | 81 |
| 4.S2 | Winter maximum temperature bias of back-trajectory forcing data | 82 |
| 4.S3 | Summer maximum temperature bias of back-trajectory forcing data | 82 |
| 4.S4 | Annual minimum temperature bias of back-trajectory forcing data | 83 |
| 4.S5 | Winter minimum temperature bias of back-trajectory forcing data | 83 |
| 4.S6 | Summer minimum temperature bias of back-trajectory forcing data | 84 |
| 4.S7 | Annual mean precipitation bias of back-trajectory forcing data | 84 |
| 4.S8 | Winter mean precipitation bias of back-trajectory forcing data | 84 |
| 4.S9 | Summer mean precipitation bias of back-trajectory forcing data | 85 |
| 4.S10 | Annual, summer and winter evapotranspiration bias of back-trajectory forcing data | 85 |
| 4.S11 | Mean moisture contribution by basin | 86 |
| 4.S12 | Same as Figure 4.S11 for remaining basins. | 87 |
| 5.1 | Timeseries of droughts in the northern and southern Murray-Darling Basin . . . | 96 |
| 5.2 | Moisture source anomalies during drought, northern Murray-Darling Basin . . . | 98 |
| 5.3 | Moisture source anomalies during drought, southern Murray-Darling Basin . . . | 99 |
| 5.4 | Cumulative variables during drought years | 100 |
| 5.S1 | Seasonal climatology of moisture contribution to precipitation | 104 |
| 5.S2 | SPI-based drought definition, northern Murray-Darling Basin | 105 |
| 5.S3 | SPI-based drought definition, southern Murray-Darling Basin | 106 |
| 5.S4 | Moisture source anomalies during SPI-based drought | 107 |

Chapter 1

Introduction

1.1 What are land-atmosphere interactions?

The overarching aim of this thesis is to determine the influence of land-atmosphere interactions on Australian precipitation. To understand what land-atmosphere interactions are and how they are linked to precipitation, let us first consider the hydrological cycle. The Earth's hydrological cycle transports water between the ocean, atmosphere and reservoirs on land including soils, rivers, lakes and ice (Figure 1.1). Traditionally, each component has been studied in isolation (Evans et al. 2011; Santanello et al. 2018). Yet interactions occur as water, energy, momentum and chemical compounds are exchanged between the land, atmosphere and ocean. The exchange of water and energy between the land surface and overlying atmosphere (the 'boundary layer') creates complex interactions that ultimately impact the occurrence and intensity of precipitation (Figure 1.2). The 'interplay' of these variables are what are referred to as *land-atmosphere interactions* (Betts et al. 2014; Findell and Eltahir 1997).

There are two main pathways by which the land and the atmosphere interact with one another: the 'hydrological' and 'thermal' pathways. The 'hydrological' pathway is the direct influence of landscape water on the state of the boundary layer (Dirmeyer 2011). Water in the landscape can evaporate directly from bare soils, from wet vegetation canopies or from transpiration by vegetation drawing water from near the soil surface, or deeper root zones (Betts et al. 1996). As water moves through the hydrological cycle it links the land and the atmosphere through evaporation and precipitation. Energy utilised in the evaporation of water ('latent heat flux') from the surface of the Earth is sourced from the balance of incoming and outgoing solar shortwave and terrestrial longwave radiation. This net available

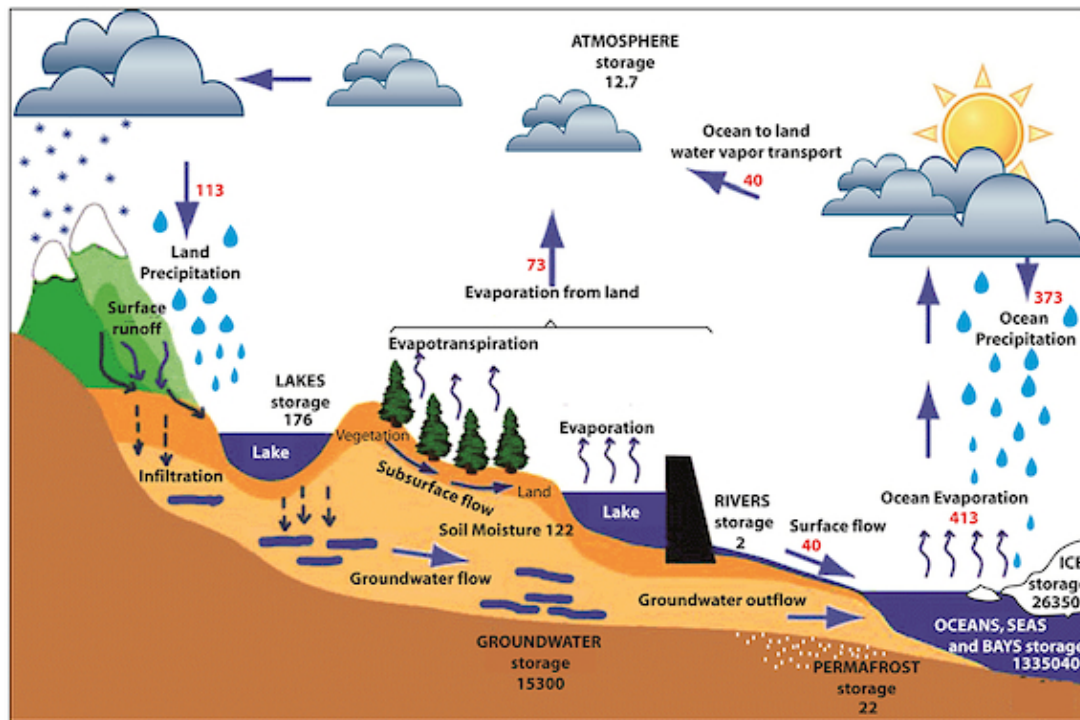


Figure 1.1: The hydrological cycle. Estimates of the observed main water reservoirs (black numbers, in 10^3 km^3) and the flow of moisture through the system (red numbers, in $10^3 \text{ km}^3 \text{ yr}^{-1}$). Adjusted from Trenberth et al. (2007) for the period 2002–2008 as in Trenberth et al. (2011). Source: Gimeno et al. (2012).

energy varies diurnally with the cycle of solar heating and is modified by heat storage, surface reflectivity ('albedo'), cloud cover and the presence of aerosols. The partitioning of available energy toward latent heat fluxes modifies the dynamic and thermodynamic structure of the atmospheric boundary layer (Seneviratne et al. 2010). The partitioning is strongly controlled by atmospheric humidity, temperature, soil and vegetation processes and entrainment of air from above the boundary layer (Betts et al. 1996). The modified structure of the boundary layer in turn affects winds, turbulence, the formation of clouds, convection and ultimately precipitation (Figure 1.2; Santanello et al. 2018).

Net radiative energy not used in the evaporative process is principally used to heat the atmosphere ('sensible heat flux'), and to a lesser degree the soil and vegetation ('soil heat flux'; Figure 1.2). The 'thermal' pathway is driven by these surface heat fluxes. Surface sensible heat fluxes warm the overlying air and cause the atmospheric boundary layer to grow, allowing moisture in the air to reach heights at which it can cool, saturate and condense (i.e. above the 'lifting condensation level' or LCL), forming clouds (Betts 2004; Dirmeyer et al. 2014) that may precipitate (Figure 1.2).

Land-atmosphere interactions occur over a range of temporal and spatial scales. Parti-

1.1. What are land-atmosphere interactions?

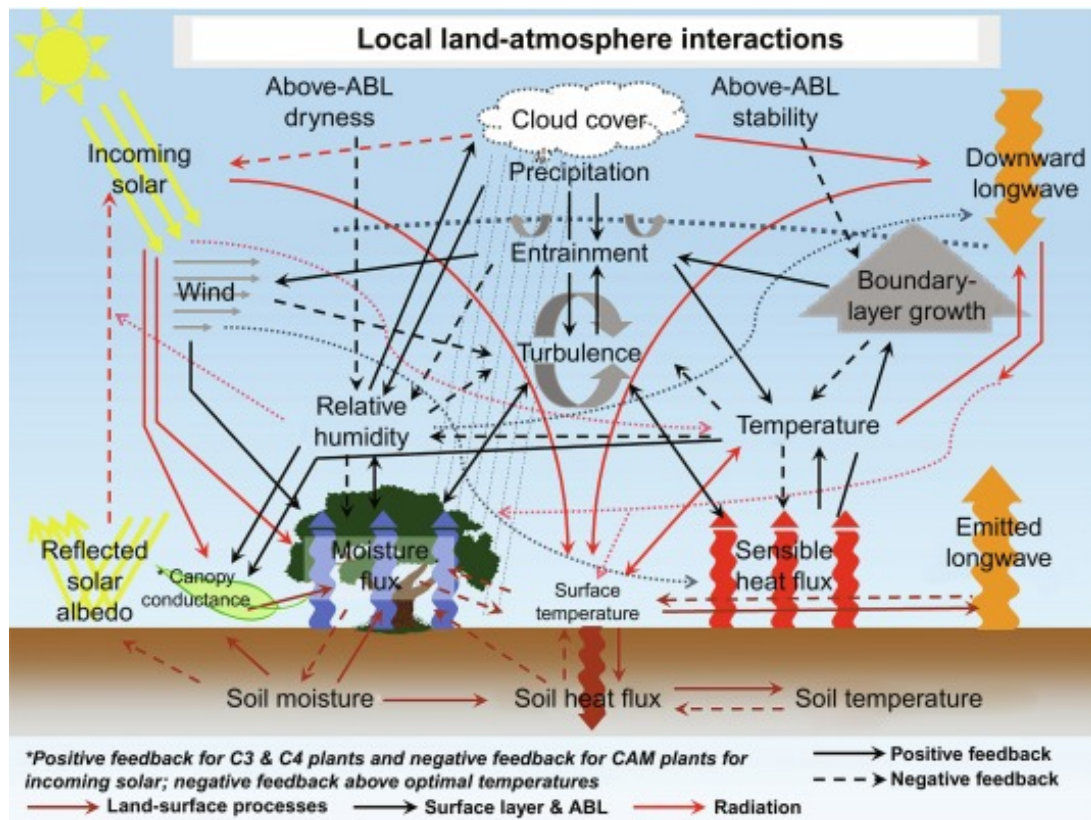


Figure 1.2: Schematic of the complex interactions among the land surface, atmospheric boundary layer, and radiation. These interactions are not all well understood and are often poorly represented in numerical models. Source: Dirmeyer et al. (2019).

tioning of available energy into latent and sensible heat fluxes occurs instantaneously, but integrates over time scales ranging from diurnal (Betts 2004; Findell and Eltahir 2003) to multi-day (Santanello et al. 2007) to seasonal (Meng et al. 2014) to create ‘fast’ and ‘slow’ interactions (Meng et al. 2014). Spatially, land surface properties can influence those of the atmosphere on small, local scales (hundreds of metres to tens of kilometres), especially through convection, as well as regionally (hundreds of kilometres) via mesoscale circulation (e.g. Sharmila and Hendon 2020; Taylor et al. 2012).

Different terms are often used interchangeably to describe the linked processes, such as land-atmosphere ‘interaction’, ‘feedback’ and ‘coupling’ (Lorenz et al. 2015). In this thesis, ‘interactions’ refer to processes in one sphere (e.g. land surface) influencing another sphere (e.g. atmosphere) without specifying a direction of causality (Seneviratne et al. 2010). ‘Interactions’ are thus used as an umbrella term encompassing both ‘coupling’ (a one-way control of one sphere on the other) and ‘feedback’ (a two-way coupling). Two-way feedbacks are distinguished from one-way coupling processes where relevant.

1.2 Why are land-atmosphere interactions important?

The importance of land-atmosphere interactions lies in their impact on our understanding of the climate around us, and hence our ability to interpret past, and predict future, hydroclimatic conditions. Accurate prediction of surface climate is only possible with realistic representation of land-atmosphere interactions (Betts 2004; Santanello et al. 2018). Realistic representation of land-atmosphere interactions is important in hydroclimatic prediction, including prediction of droughts (e.g. Roundy et al. 2013; Zhou et al. 2019), heatwaves (e.g. Hirsch et al. 2019; Miralles et al. 2014), monsoon variability (e.g. Sharmila and Hendon 2020), convection (e.g. Taylor et al. 2012) and cloud formation (e.g. Ek and Holtslag 2004).

Improved prediction of precipitation in Australia is critical given the continent's highly variable precipitation (Nicholls et al. 1997) and vulnerability to climate extremes like droughts (Kiem et al. 2016) and floods (Johnson et al. 2016) that cause significant effects on people, the environment and the economy (Van Dijk et al. 2013). The most recent drought in Australia (2017-2020) led to increased food prices (Australian Bureau of Statistics 2020) and entrenched a longer term shift to warmer and drier conditions in the agriculturally significant parts of Australia, where significant negative impacts to agriculture profitability and productivity have occurred (Hughes et al. 2019, 2017). Perhaps unsurprisingly then, the estimated value of improved seasonal hydroclimatic prediction is substantial, amounting to over \$AUD1 billion per annum for the Australian agricultural sector alone (Centre for International Economics 2014).

Despite their potential to improve hydroclimate prediction, land-atmosphere interactions remain poorly observed and incompletely understood (Ferguson and Wood 2011; Santanello et al. 2018). Previous land-atmosphere research has focused on the northern hemisphere, where it has been shown that land-atmosphere interactions may hold greater importance in transitional climates (Guo et al. 2006; Koster et al. 2004). The transitional nature of much of Australia's climate suggests understanding of these processes is important here. Process knowledge of land-atmosphere interactions is needed to grasp what role they play now, and in a future Australian climate (Evans et al. 2011) where they may become increasingly important (Dirmeyer et al. 2014, 2012), while they are also necessary to improve climate projections, in which they currently represent a key source of uncertainty (Wulfmeyer et al. 2018). This thesis aims to contribute process knowledge of land-atmosphere interactions in Australia's current climate.

1.3 Land-atmosphere interactions in Australia

Important contributions to understanding land-atmosphere interactions in Australia have been made by past studies, but process-level understanding in the Australian region is limited. This limits Australia's weather and hydrological predictive capabilities. This section summarises the state of knowledge in Australia as learned from past studies, pointing out what is known and not known about the impact of land-atmosphere interactions on Australian climate.

Hydrological and thermal feedback pathways

Soil moisture-atmosphere interactions have been shown to exert control on air temperatures in Australia (Hirsch et al. 2014b; Hope and Watterson 2018; Timbal et al. 2002; Zhang 2004). However, the influence of land-atmosphere interactions on precipitation is unclear from past studies. Dirmeyer et al. (2014) combined the hydrological and thermal feedback pathways to demonstrate that soil moisture affects surface fluxes and boundary layer height, suggesting an indirect impact of the land surface state on Australian precipitation. Other studies also suggest soil moisture exerts some control on precipitation (Meng et al. 2014; Notaro 2008; Timbal et al. 2002), but others indicate little to no link between soil moisture and precipitation in Australia (Ferguson and Wood 2011; Hirsch et al. 2014b; Koster et al. 2006). Differences in spatio-temporal scale and methodological approach between studies make it difficult to draw general conclusions. This issue is not limited to Australia, but a global issue that has been noted as an impediment to scientific consensus on land-atmosphere processes (Santanello et al. 2018).

Vegetation-atmosphere interactions may be an important hydrological feedback pathway influencing Australian precipitation. A positive vegetation-precipitation feedback (i.e. more vegetation leads to more evapotranspiration, which increases precipitable water in the boundary layer, enhancing precipitation) has been shown to exert control on north Australian precipitation (Notaro 2018). This result aligns with a strong soil moisture-atmosphere relationship found by others (Decker et al. 2015; Ferguson et al. 2012). Liu et al. (2006) suggested the vegetation-precipitation relationship in north Australia is modest, explaining less than 10% of precipitation variance. More recent studies suggest precipitation in monsoonal northwest Australia is influenced by a combined wind-evaporation-precipitation feedback (Sekizawa et al. 2018; Sharmila and Hendon 2020). Westerly wind anomalies during the monsoon season enhance proximate marine evaporation and the supply of atmospheric moisture to the region.

The additional moisture promotes precipitation, wetter soils, and further precipitation.

Precipitation recycling and moisture sources

Previous estimates indicate precipitation recycling may be an important process for precipitation in Australia's northern and eastern regions, with estimates ranging from 5% at a scale of 10^5 km^2 (Dirmeyer and Brubaker 2007; Van Der Ent and Savenije 2011) to 38% for the whole continent (Dirmeyer et al. 2009b).

Australia's precipitation is mainly sourced from moisture evaporating from proximate ocean regions and terrestrial evapotranspiration in northern and eastern Australia (Dirmeyer et al. 2009b). While this provides a continental scale picture of Australia's moisture sources, it is not known where moisture originates for precipitation in each part of Australia, or how sources vary seasonally, interannually and over the long term. Identifying Australia's moisture sources can help establish the relative importance of local land surface processes versus remote oceanic processes affecting Australian precipitation, both during periods of average precipitation and during extremes such as droughts and floods.

Drought

A significant challenge in understanding the impact of land-atmosphere interactions on Australian precipitation is the untangling of contrasting feedbacks during drought. During the onset to drought, Meng et al. (2014) showed declining soil moisture levels led to a reduction in atmospheric convective potential, and hence precipitation, which further reduced soil moisture levels, resulting in a relatively fast positive feedback mechanism. In contrast, where soil moisture levels remained low for long enough, vegetation cover decreased, evapotranspiration declined and slowed the reduction in soil moisture, leading to a slower negative soil moisture-precipitation feedback that may have dampened the shorter term positive feedback. The operation of contrasting feedbacks at different points in time and space suggests land-atmosphere interactions play a confounding role in the persistence of Australian drought. How land-atmosphere interactions function during drought, and what their relative role is in determining precipitation (compared to larger scale processes) remains uncertain.

Hydrological prediction and future projections

Realistic initialisation of soil moisture improves prediction of Australian temperature on sub-seasonal to seasonal time scales but has only had a modest impact on precipitation forecast skill (Hirsch et al. 2014c; Timbal et al. 2002; Zhao et al. 2019). The precipitation forecast skill of the Australian Bureau of Meteorology seasonal forecast system, ACCESS-S, currently decreases beyond one to two months, depending on region and season (Hudson et al. 2017; King et al. 2020). It is understandable, then, that climate models struggle to simulate extended periods of anomalous precipitation in Australia, such as during drought (Ukkola et al. 2018).

Simulation of land-atmosphere interactions is not just an issue for model development in Australia, but worldwide. Currently, the representation of land-atmosphere interactions in models is unsatisfactory (Wulfmeyer et al. 2018) and remains a weak link in understanding and predicting coupled processes (Santanello et al. 2009). The representation of land-atmosphere interactions during extreme events also remains inadequate (Wulfmeyer et al. 2018). Improved model representation of land-atmosphere interactions remains a challenge for Australia, where land-atmosphere interactions are projected to play an increasingly important role in the future (Dirmeyer et al. 2012).

1.4 How land-atmosphere interactions are identified and measured

To improve understanding of land-atmosphere interactions and improve weather forecast skill, collective international research efforts have developed and applied numerous methods on a range of spatial and temporal scales. The LoCo ("local coupling") research initiative, set up under the auspices of the World Climate Research Program, has collated a comprehensive list of metrics to evaluate land-atmosphere interaction over the last decade, available at http://cola.gmu.edu/dirmeyer/Coupling_metrics.html. The data requirements, computational expense and ability to validate estimates against observations varies widely across methods. A benefit of applying such a diverse range of methods to enhance process understanding is that compensating errors and causality are not as obscured as they may be in single-variable metrics such as bias or root mean square error (Santanello et al. 2018). The di-

versity of methods has been a valuable approach to tackling the challenge of land-atmosphere interaction quantification. Challenges have arisen due to the lack of long-term observations of the relevant processes (Santanello et al. 2018; Seneviratne et al. 2010) and the difficulty of establishing causality in such a complex and highly non-linear, interconnected system (Koster et al. 2003; Salvucci et al. 2002).

Methods fall into three broad categories: statistical approaches, moisture accounting approaches and thermodynamic approaches. A brief overview of the main methods in each category is provided in the following sections and summarised in section 1.4.4.

1.4.1 Statistical approaches

The GLACE index

General circulation models (GCMs) have been used widely to understand and test the sensitivity of the underlying mechanisms of land-atmosphere interactions, since the interactions are complex, observations are lacking and the parameterisation of many of the relevant physical processes may be manipulated and its effects examined (Koster et al. 2002). In model experiments, the land and the atmosphere can be artificially decoupled, and the results compared to the coupled scenario to infer coupling strength (Lorenz et al. 2015).

However, conclusively identifying land-atmosphere interactions in global studies has been limited by the use of single GCMs, where results reflected the particular parameterisation of the model experiment (Koster et al. 2004). To overcome this, multi-model experiment studies have been undertaken (e.g. Dirmeyer 2001; Koster et al. 2002; Notaro 2008), including the Global Land-Atmosphere Coupling Experiment (GLACE; Guo et al. 2006; Koster et al. 2004, 2006; Seneviratne et al. 2006). In these studies the GLACE coherence index (Ω) was employed to estimate the strength of land-atmosphere interactions. Ω is essentially a measure of similarity between time series generated by different model ensembles, where positive values indicate the time series are similar (e.g. dry years will occur at the same time in different models, as will wet years) and a value near zero indicates the time series are very different, or independent, of each other (Koster et al. 2002).

Correlation analysis

Santanello et al. (2011) argued that global scale studies cannot reveal the nature of the underlying mechanisms driving land-atmosphere interactions. Global studies such as those using the GLACE index were limited by a lack of direct observations to test model outputs (Seneviratne et al. 2010). Instead, Santanello et al. (2011) suggested the identification and measurement of land-atmosphere interactions may be improved through local scale analysis at diurnal time scales. Studying the nature of land-atmosphere interactions on this scale was possible due to field measurements available in the US (e.g. LAFE campaign, see Wulfmeyer et al. 2018), including observations of atmospheric structure and thermal properties, surface fluxes and soil moisture. Using field measurements, Findell and Eltahir (1997) sought to understand the degree to which the land surface controls atmospheric conditions by correlating soil moisture with subsequent precipitation. Numerous studies subsequently applied correlation analysis using data from observations, reanalysis and model output (e.g. Duerinck et al. 2016; Liu et al. 2016; Mei and Wang 2011; Wei et al. 2008; Yang et al. 2018).

The difficulty in establishing a causal relationship with correlation analysis has been reflected upon by a number of authors (e.g. Alfieri et al. 2008; Koster et al. 2003; Orlowsky and Seneviratne 2010; Tuttle and Salvucci 2016; Wei et al. 2008). In response, some authors have employed alternative measures of land-atmosphere interaction alongside correlation analysis, allowing interpretation of several lines of evidence (e.g. Duerinck et al. 2016).

Two-legged coupling index

The two-legged coupling index measures the strength of land-atmosphere interactions via the hydrological and thermal pathways; that is, the linkage between soil moisture and boundary layer growth (Dirmeyer et al. 2014). The first part of the index represents the terrestrial 'leg' of the coupling: the degree to which soil moisture controls surface latent heat fluxes (Dirmeyer 2011), taken as the linear regression slope of surface flux on soil moisture. The atmospheric 'leg' measures the slope of surface heat fluxes on the LCL (Dirmeyer et al. 2014). The overall sensitivity of the LCL to soil moisture is then taken as the product of the two slopes. While the relationship was originally formulated to test the coupling strength between soil moisture and the LCL, other atmospheric variables may be used instead. For example, Lorenz et al. (2015) assessed the relationship between soil moisture, sensible heat flux and air temperature.

1.4.2 Moisture accounting approaches

Numerical models of precipitation recycling

The precipitation recycling ratio may be defined as the proportion of precipitation falling in a region that originated as evapotranspiration in that same region (Dirmeyer et al. 2009a). A high precipitation recycling ratio may be indicative of a strong land-atmosphere interactions (Brubaker et al. 1993), where drying soil may lead to a decrease in local evapotranspiration and precipitation (Zhang et al. 2008), potentially contributing to the persistence of droughts (Brubaker et al. 1993).

Precipitation recycling has been assessed using different methods, but all estimate the origin of moisture supplying a region's precipitation. The precipitation recycling ratio can then be calculated as the proportion of moisture originating within the region where the precipitation occurred.

Early assessments of precipitation recycling used 'bulk' estimates (Brubaker et al. 1993; Budyko 1974). Bulk estimates consider a simplified two-dimensional (2D) control volume over a land area. The precipitation recycling ratio is computed by distinguishing precipitation coming from moisture advected from outside the control volume from that originating within the control volume as evapotranspiration. Another approach to estimate precipitation recycling has been the use of passive tracers in climate models to identify precipitation source regions (e.g. Bosilovich 2002; Bosilovich and Chern 2006).

More recent applications of Lagrangian 'back-trajectory' methods use mass conservation to track the path of moisture contributing to precipitation events backward in time to identify its evaporative origin (e.g. Dirmeyer and Brubaker 1999, 2007; Wei et al. 2016). The back-trajectory method tracks air parcels from the location of precipitation events within a numerical model and traces their motion across the model grid to the location of most recent evaporation (Dirmeyer and Brubaker 1999, 2007). The precipitation recycling ratio is then calculated as the proportion of moisture originating in the region of precipitation. The back-trajectory approach has been applied two-dimensionally by vertical averaging atmospheric properties (e.g. Dominguez et al. 2006; Van Der Ent et al. 2010) as well as three-dimensionally (e.g. Dirmeyer and Brubaker 1999; Stohl and James 2004).

Precipitation recycling with isotopic tracers

Isotopic tracers may be used to estimate precipitation recycling and as a tool to validate numerical moisture accounting models. Isotopes of hydrogen (deuterium) and oxygen (^{18}O) can help identify the origin of atmospheric water vapour and precipitation due to the process of isotopic fractionation during phase change. As atmospheric vapour condenses, the heavier isotopes are preferentially precipitated, depleting the vapour of heavier concentrations and enriching surface water stores. On the other hand, surface evaporation preferentially evaporates the lighter isotopes, enriching the remaining liquid. By measuring these relative concentrations, and accounting for geographic and seasonal differences, the source and pathway of water vapour and precipitation may be estimated (Gimeno et al. 2012). By quantitatively understanding water isotopic fractionation through the hydrological cycle in this way, the amount of regional evapotranspiration contributing to precipitation in the same region — that is, the precipitation recycling ratio — may be estimated (e.g. Kurita and Yamada 2008).

1.4.3 Thermodynamic approaches

Mixing diagrams

Mixing diagrams are a way of visualising the balance of surface fluxes (sensible and latent heat fluxes) and upper level entrainment in the boundary layer on a diurnal time scale (Betts 2009). They relate the diurnal evolution of specific humidity and potential temperature, which are integrative of local feedback processes, to the boundary layer energy balance in order to quantify land-atmosphere interaction (Santanello et al. 2009). Mixing diagrams constructed using observations are also useful in evaluating coupled models, particularly in identifying shortcomings in simulation of turbulent fluxes (Santanello et al. 2009).

Relative humidity tendency

The aim of the relative humidity tendency method is to determine the comparative dominance of different and competing interaction pathways, to deduce whether or not clouds will form (Ek and Holtslag 2004). Like the mixing diagram method, this metric relates a number of surface and atmospheric parameters to understand feedback processes, but with a focus on the relative likelihood of cloud development.

Convective triggering potential

The convective triggering potential (CTP) method aims to identify the likelihood for convective precipitation given the interactions between land surface fluxes and atmospheric structure. Like the mixing diagram and relative humidity tendency methods, this method seeks to understand how the land surface and the boundary layer co-evolve to result in different feedback regimes. The CTP is calculated from a thermodynamic diagram of atmospheric temperature profiles. Findell and Eltahir (2003) combine the CTP with an index of humidity in the lower atmosphere to distinguish a boundary layer with stability conditions (a) conducive to convection but too dry, from (b) those with sufficient moisture to trigger convection. The combined index framework may be used to classify conditions into one of four categories: (1) 'atmospherically controlled - wet', if the atmosphere is unstable and humid and precipitation will occur regardless of soil moisture conditions; (2) 'wet soil advantage', if the atmosphere is unstable and high levels of soil moisture can promote precipitation formation; (3) 'dry soil advantage', if dry soils promoting heating of the atmosphere cause air to be lifted above the LCL to promote precipitation, and (4) 'atmospherically controlled - dry', if the atmosphere is stable and precipitation is unlikely to occur regardless of soil moisture state. Roundy et al. (2013) later extended the CTP method to form the Coupling Drought Index (CDI), which accounts for the temporal variation in the land-atmosphere state.

Table 1.1: Summary of main methods for identifying or quantifying land-atmosphere interaction

| Category | Name | Brief description | Examples | Required data |
|--------------------------------|--|---|---|---|
| Statistical approaches | GLACE index | A relative measure of time series similarity of climate model outputs. | Koster et al. 2002, 2006 | Time series of precipitation from coupled and uncoupled climate model ensembles. |
| | Correlation analysis | Correlation between land and atmospheric parameter time series. Can also include regression relationships, often after removing the effects of large-scale climate modes. | Findell and Eltahir 1997; Wei et al. 2008 | Time series of parameters of interest, e.g. soil moisture, precipitation, temperature. |
| | Two-legged coupling index | A relative measure of the degree to which soil moisture changes drive boundary layer growth, using regression relationships weighted by standard deviation. | Dirmeyer 2011; Dirmeyer et al. 2014 | Soil moisture, latent or sensible heat fluxes, lifting condensation level. |
| Moisture accounting approaches | Numerical precipitation recycling models | Tracks origin of precipitation to estimate fraction of precipitation over an area derived from evapotranspiration in that same area. | Dirmeyer and Brubaker 2007; Van Der Ent et al. 2010 | Precipitation, humidity, temperature, wind, pressure, evaporation. |
| | Isotopic models | Estimates moisture origin and pathway by analysing concentrations of hydrogen and oxygen isotopes. | Kurita and Yamada 2008 | Isotopic samples of precipitation and atmospheric moisture, temperature, humidity, precipitation. |
| Thermodynamic approaches | Mixing diagrams | Determines the contribution of surface fluxes and entrainment on boundary layer moisture and heat. | Betts 2009; Santanello et al. 2011, 2009, 2015 | Surface fluxes, mixing ratio, vertical profiles of temperature and pressure. |
| | Relative humidity tendency | Determines likelihood of cloud development through contribution of dry air entrainment, boundary layer properties and surface fluxes to changes in relative humidity and the top of boundary layer using vertical profiles. | Ek and Holtslag 2004; Ek and Mahrt 1994 | Surface fluxes, boundary layer height, vertical profiles of temperature, humidity and pressure. |
| | Convective triggering potential | Estimates whether convection is more likely to be initiated over wet or dry soils based on the stability of the boundary layer. | Ferguson and Wood 2011; Findell and Eltahir 2003 | Soil moisture, precipitation, vertical profiles of temperature and humidity. |

1.4.4 Comparison of approaches

The diversity of coupling metrics, described in the previous sections, are summarised in Table 1.1. The advantages and disadvantages of each approach are briefly explored in this section.

While global models and the GLACE index have been useful in identifying areas of the globe where land-atmosphere interactions are likely to be relatively strong, the low spatial resolution of global approaches strongly limits its ability to deepen understanding on a regional or local scale, which is currently needed in Australia. Utilising a global model with low spatial resolution within Australia would not allow certain topographical features, or land use, vegetation or soil types to be resolved — factors important in understanding the mechanisms underlying any potential interaction. In principle, this limitation may be overcome with the use of higher resolution regional climate models (RCMs). The strongest limitation of this method, however, is that it is largely theoretical, meaning sensitivity experiments set up to calculate the GLACE index cannot be replicated in the field and so cannot be validated (Seneviratne et al. 2010).

Other statistical approaches, such as correlation analysis and the two-legged coupling index, are advantageous in that they are, firstly, simple measures, and secondly, may be directly applied to land and climate observations across a range of spatial and temporal scales. Soil moisture and precipitation data are readily available across Australia and have not yet been applied to study the effect of land-atmosphere interactions on precipitation. Detailed process understanding of the land-atmosphere system on a local level will be limited with correlation, owing to the difficulty of establishing causality (Salvucci et al. 2002). However, correlation analysis presents a useful starting point to identify regions of detectable land-atmosphere interaction across Australia, which can then be investigated with more process-based approaches.

The thermodynamic approaches require a considerable input of observational information, including observations of surface fluxes and vertical atmospheric profiles of temperature, pressure and humidity (Table 1.1). While mixing diagrams and relative humidity tendency methods may be used purely with modelled information beyond the field observation scale, verification is limited to radiosonde stations (or temporary field programs where vertical profiles are measured) — a strong limitation for application within Australia at present. Although the CTP method was originally based on radiosonde profiles (Findell and Eltahir 2003), Ferguson and Wood (2011) demonstrated the use of the method with remotely sensed observations of atmospheric temperature and humidity, as well as precipitation and soil moisture. Use of remote sensing data may be a viable alternative for application of the CTP method in Australia, but

1.4. How land-atmosphere interactions are identified and measured

satellite estimates will still need to be validated with ground-based radiosonde observations, which are currently lacking.

Quantifying land-atmosphere interaction through precipitation recycling presents several advantages. Firstly, by using modelled or reanalysis data, precipitation recycling can be estimated continent-wide, providing information on land-atmosphere interaction across Australia's diverse climate zones, including regions of sparse ground observations. Secondly, the precipitation recycling method effectively deals with geographically remote influences on local land-atmosphere interaction, a challenge in the application of field scale thermodynamic approaches. However, using numerical moisture accounting models to estimate precipitation recycling presents several challenges, including considerable computational expense, and accounting for certain assumptions that may not always be representative, such as a vertically well-mixed atmosphere (Goessling and Reick 2013). The paucity of isotopic observations across Australia not only prevents the use of isotopic models for precipitation recycling estimation at present, but also makes validation of numerical moisture accounting models difficult. Provided these challenges can be managed, numerical moisture accounting models provide an additional benefit; they can provide information on the sources of moisture supplying precipitation at any given time and place. Understanding moisture source regions for precipitation, particularly during extreme events, is considered a 'grand challenge' in atmospheric science (Gimeno 2013).

In a practical sense, the use of any individual method is largely determined by the availability of the observations or model simulations required as input. Many of the thermodynamic approaches require sub-daily observations of vertical atmospheric properties, information which is simply not available across Australia at present. Some of the statistical approaches may be more readily applied with available gridded or gauge-based land and climate observations. For example, estimates of soil moisture and precipitation are readily available continent-wide from multiple data sources. Lastly, moisture accounting models that make use of existing RCM simulations present a viable option for investigating land-atmosphere interactions across Australia.

On balance, the methods able to provide the most information using the data currently available include correlation analysis and precipitation recycling. Therefore, these are the primary methods used in this thesis.

1.5 Thesis motivation and objectives

The overarching aim of this thesis is to answer the question: What role to land-atmosphere interactions play in controlling Australian precipitation, both under average conditions and during drought? The review of process knowledge presented in section 1.3 revealed several key knowledge gaps that need to be addressed to answer this overarching question. This thesis and its research questions are motivated by these knowledge gaps, and are outlined below.

- An array of methods have been used to study land-atmosphere interactions across the world (section 1.4). Most methods require some estimation of soil moisture, typically sourced from models, reanalysis data sets or from remotely sensed products. At the commencement of this research the suitability of different soil moisture data sets for study in the Australian context was unknown. By comparing a suite of modelled and remotely sensed soil moisture estimates to ground observations across Australia, this thesis answers **Research Question 1: How does the performance of different soil moisture data sets vary across Australia?**
- Where in Australia land-atmosphere interactions may have a detectable influence on precipitation is unclear, with inconclusive results evident in the literature (e.g. Hirsch et al. 2014b; Timbal et al. 2002). This thesis leverages available observations of soil moisture and precipitation to address **Research Question 2: Where do land-atmosphere interactions affect precipitation across Australia, and how do the interactions vary in time and with spatial scale?**
- Estimates of the strength of land-atmosphere interactions over Australia are few. To contribute knowledge of the processes controlling Australian precipitation, this thesis presents the first spatiotemporally varying estimates of precipitation recycling to address **Research Question 3: How strongly do land-atmosphere interactions affect precipitation across Australia?**
- Very little is known about how land-atmosphere interactions vary during extreme periods such as drought, and what role they play in drought persistence and termination. This thesis combines estimates of precipitation recycling, moisture sources and atmospheric circulation to present the first answer to **Research Question 4: What role do land-atmosphere interactions play during drought in Australia?**

1.6 Thesis structure

This thesis is primarily comprised of peer-reviewed publications that are presented in the journal format without modification, supported by introductory and summary text. The thesis is structured as follows.

- Chapter 2 evaluates the performance of a suite of soil moisture data sets and presents the publication '*Comparison of remotely sensed and modelled soil moisture data sets across Australia*' (Holgate et al. 2016).
- Chapter 3 identifies where land-atmosphere interactions may have a detectable influence on Australian precipitation, accounting for spatial scale, and presents the publication '*The importance of the one-dimensional assumption in soil moisture-rainfall depth correlation at varying spatial scales*' (Holgate et al. 2019).
- Chapter 4 quantifies the strength of land-atmosphere interactions with the precipitation recycling ratio, identifies the regions supplying moisture to Australian precipitation and presents the publication '*Australian precipitation recycling and evaporative source regions*' (Holgate et al. 2020b).
- Chapter 5 quantifies the relative role of remote processes and land-atmosphere interactions during drought and presents the publication '*Local and remote drivers of southeast Australian drought*' (Holgate et al. 2020a).
- Chapter 6 provides conclusions to the research presented in this thesis, highlights the contribution to the field through addressing identified knowledge gaps, and proposes future research avenues.

Chapter 2

Soil moisture - the link between the land and the atmosphere

2.1 Overview

Soil moisture is a key variable that controls processes and feedbacks within the climate system (Seneviratne et al. 2010) and is the most important land surface variable for seasonal climate prediction (Dirmeyer et al. 2019). Most methods used to identify and quantify land-atmosphere interactions (Table 1.1), including those used in this thesis, require information on soil moisture. Besides land-atmosphere interactions, other important applications of soil moisture include numerical weather forecasting (e.g. Hirsch et al. 2014c), drought monitoring and evaluation (e.g. Pozzi et al. 2013), bushfire danger warning (e.g. Holgate et al. 2017), national water resource accounting (e.g. Frost et al. 2018) and flood prediction (e.g. Wanders et al. 2014).

Different applications source soil moisture information from different data sets. Soil moisture may be directly measured with ground-based in situ sensors, estimated with land surface models or remotely sensed with satellites. Such a variety of applications and estimation techniques has led to the development of numerous soil moisture data sets. Which data sets are most suitable for application across Australia, and appropriate for analysing land-atmosphere interactions, is uncertain.

This chapter resolves this issue by comparing a suite of soil moisture data sets to assess their relative strengths and weaknesses and inform the next stage of research. Six model-based and five satellite-based data sets are compared to ground-based measurements taken from three monitoring networks, covering temperate, tropical and arid parts of Australia.

2.1. Overview

The soil moisture estimates are compared in a common framework by quantifying their level of agreement with ground-based measurements using Pearson correlation. In addition hierarchical clustering analysis is used to identify products that closely associate with each other, to identify which data sets share similar errors and which are complementary. This chapter therefore addresses research question 1: **How does the performance of different soil moisture data sets vary across Australia?**

The research presented in this chapter has been peer-reviewed and published in *Remote Sensing of Environment*, and is provided in its published form. Author contributions are outlined in the Statement of Contribution below.

Statement of Contribution

This thesis is submitted as a Thesis by Compilation in accordance with https://policies.anu.edu.au/ppl/document/ANUP_003405

I declare that the research presented in this Thesis represents original work that I carried out during my candidature at the Australian National University, except for contributions to multi-author papers incorporated in the Thesis where my contributions are specified in this Statement of Contribution.

Title: Comparison of remotely sensed and modelled soil moisture data sets across Australia

Authors: C.M Holgate , R.A.M. De Jeu, A.I.J.M van Dijk, Y.Y Liu, L.J. Renzullo, Vinodkumar, I. Dharssi, R.M. Parinussa, R. Van Der Schalie, A. Gevaert, J. Walker, D. McJannet, J. Cleverly, V. Haverd, C.M. Trudinger and P.R. Briggs


Publication outlet: Remote Sensing of Environment

Current status of paper: Published

Citation: Holgate, C. M., De Jeu, R. A. M., Dijk, A. I. J. M. van, Liu, Y. Y., Renzullo, L. J., Vinodkumar, Dharssi, I., et al. (2016) Comparison of remotely sensed and modelled soil moisture data sets across Australia. Remote Sensing of Environment 186, 479–500. doi:10.1016/j.rse.2016.09.015

Contribution to paper: C.M Holgate collated the model and satellite data, and electronically retrieved ground observations from each co-author. C.M Holgate designed the comparison framework with significant contribution from R.A.M. De Jeu and A.I.J.M van Dijk. C.M Holgate carried out the data processing, analysis, figure preparation and drafting of the manuscript. All co-authors contributed to the refinement of the draft manuscript. C.M Holgate prepared the submission to the journal and led the revisions of the manuscript following peer-review.

Senior author or collaborating authors endorsement: _____

| | | |
|------------------------|---|------------------|
| Chiara Holgate |  | 26 November 2020 |
| Candidate – Print Name | Signature | Date |

Endorsed

| | | |
|----------------------------------|---|-----------|
| Albert Van Dijk |  | 9/11/2020 |
| Primary Supervisor – Print Name | Signature | Date |
| Philip Gibbons |  | 6/11/20 |
| Delegated Authority – Print Name | Signature | Date |



Contents lists available at ScienceDirect

Remote Sensing of Environment

journal homepage: www.elsevier.com/locate/rse

Comparison of remotely sensed and modelled soil moisture data sets across Australia



C.M. Holgate^{a, c, *}, R.A.M. De Jeu^b, A.I.J.M. van Dijk^a, Y.Y. Liu^c, L.J. Renzullo^d, Vinodkumar^{e, f}, I. Dharssi^e, R.M. Parinussa^g, R. Van Der Schalie^{b, h}, A. Gevaert^h, J. Walkerⁱ, D. McJannet^d, J. Cleverly^j, V. Haverd^k, C.M. Trudinger^k, P.R. Briggs^k

^aFenner School of Environment Society, The Australian National University, Canberra, Australia

^bVandersat, Noordwijk, Netherlands

^cARC Centre of Excellence for Climate System Science and Climate Change Research Centre, UNSW Australia, Australia

^dCSIRO Land and Water, Australia

^eBureau of Meteorology, Australia

^fBushfire Natural Hazards Cooperative Research Centre, Australia

^gSchool of Civil and Environmental Engineering, UNSW Australia, Australia

^hFaculty of Earth and Life Sciences, VU University Amsterdam, Netherlands

ⁱDepartment of Civil Engineering, Monash University, Australia

^jSchool of Life Sciences, University of Technology Sydney, Australia

^kCSIRO Oceans and Atmosphere, Australia

ARTICLE INFO

Article history:

Received 21 March 2016

Received in revised form 19 August 2016

Accepted 14 September 2016

Available online 23 September 2016

Keywords:

Soil moisture
SMOS
AMSR2
ASCAT
WaterDyn
CABLE
AWRA-L
KBDI
MSDI
API
Comparison
Cluster analysis
In situ

ABSTRACT

This study compared surface soil moisture from 11 separate remote sensing and modelled products across Australia in a common framework. The comparison was based on a correlation analysis between soil moisture products and *in situ* data collated from three separate ground-based networks: OzFlux, OzNet and CosmOz. The correlation analysis was performed using both original data sets and temporal anomalies, and was supported by examination of the time series plots. The interrelationships between the products were also explored using cluster analyses. The products considered in this study include: Soil Moisture Ocean Salinity (SMOS; both Land Parameter Retrieval Model (LPRM) and L-band Microwave Emission of the Biosphere (LMEB) algorithms), Advanced Microwave Scanning Radiometer 2 (AMSR2; both LPRM and Japan Aerospace Exploration Agency (JAXA) algorithms) and Advanced Scatterometer (ASCAT) satellite-based products, and WaterDyn, Australian Water Resource Assessment Landscape (AWRA-L), Antecedent Precipitation Index (API), Keetch-Byram Drought Index (KBDI), Mount's Soil Dryness Index (MSDI) and CABLE/BIOS2 model-based products. The comparison of the satellite and model data sets showed variation in their ability to reflect *in situ* soil moisture conditions across Australia owing to individual product characteristics. The comparison showed the satellite products yielded similar ranges of correlation coefficients, with the possible exception of AMSR2_JAXA. SMOS (both algorithms) achieved slightly better agreement with *in situ* measurements than the alternative satellite products overall. Among the models, WaterDyn yielded the highest correlation most consistently across the different locations and climate zones considered. All products displayed a weaker performance in estimating soil moisture anomalies than the original data sets (*i.e.* the absolute values), showing all products to be more effective in detecting interannual and seasonal soil moisture dynamics rather than individual events. Using cluster analysis we found satellite products generally grouped together, whereas models were more similar to other models. SMOS (based on LMEB algorithm and ascending overpass) and ASCAT (descending overpass) were found to be very similar to each other in terms of their temporal soil moisture dynamics, whereas AMSR2 (based on LPRM algorithm and descending overpass) and AMSR2 (based on JAXA algorithm and ascending overpass) were dissimilar. Of the model products, WaterDyn and CABLE were similar to each other, as were the API/AWRA-L and KBDI/MSDI pairs. The clustering suggests systematic commonalities in error structure and duplication of information may exist between products. This evaluation has highlighted relative strengths, weaknesses, and complementarities between products, so the drawbacks of each may be minimised through a more informed assessment of fitness for purpose by end users.

© 2016 Elsevier Inc. All rights reserved.

* Corresponding author at: Fenner School of Environment Society, The Australian National University, Building 141, Linnaeus Way, Canberra, ACT 2601, Australia.
E-mail address: chiara.holgate@anu.edu.au (C. Holgate).

1. Introduction

The importance of soil moisture as an environmental variable is evident from its key role in the hydrological cycle. Soil moisture influences rainfall-runoff processes, infiltration, groundwater recharge, and constrains evapotranspiration and photosynthesis. It thus partly governs water and energy exchanges between the land, vegetation and the atmosphere (Albergel et al., 2012; Brocca et al., 2011; Su et al., 2013; Taylor et al., 2012) and influences multi-scale feedbacks (Seneviratne et al., 2010). Understanding how soil moisture varies in time and space is essential for producing environmental forecasts and improving their predictions (Draper, 2011; Owe et al., 2008).

The relevance of soil moisture is also evident in the growing number of applications employing soil moisture data around the world. Some applications include: assimilation into land surface models (e.g. Renzullo et al., 2014) for numerical weather forecasting (e.g. Draper et al., 2009; Dharssi et al., 2011), national water accounting (e.g. Viney et al., 2014) and bushfire danger warning (e.g. Van Dijk et al., 2015; Finkele et al., 2006; Kumar et al., in press), as well as evaluation of regional climate indices and long-term hydrological trends (e.g. Brocca et al., 2014; Liu et al., 2009; Liu et al., 2007), evaluation and improvement of convective processes in climate models (Taylor et al., 2012), drought monitoring and evaluation (e.g. Van Dijk et al., 2013; Pozzi et al., 2013), and flood prediction (e.g. Wanders et al., 2014), among others. Many of these applications have been or are currently being employed in Australia in an effort to better understand and predict the water resources of a country with long-standing climatic variability.

There are several operational or near-operational sources of soil moisture information for Australia. Sources of soil moisture information are generally from one of three broad categories: *in situ* measurements, satellite remotely sensed estimates, and model predictions. Ground-based approaches measure *in situ* soil moisture at a point scale using techniques that utilise the dielectric constant of the soil (e.g. time domain reflectometry (TDR) and soil capacitance measurements) or matric potential of the soil (e.g. tensiometer and resistance unit measurements) typically on a sub-daily time step. Alternatively *in situ* measurements may also be taken over a broader scale (tens of hectares) using cosmic-ray neutron detectors, also on a sub-daily time step. Remotely sensed soil moisture estimates may be obtained on an even larger scale (tens or hundreds of square kilometres) from a growing number of satellite platforms that are able to provide data on a daily basis or every few days. Active or passive satellite instruments operating in the microwave bands are suited to the acquisition of soil moisture due to the large contrast in the dielectric constant between water and soil (Schmugge, 1983). Several radiative transfer models and a change detection algorithm have been developed (e.g. Maeda and Taniguchi, 2013; Owe et al., 2001; Wagner et al., 1999) to retrieve soil moisture from the microwave and radar measurements and are currently in use.

Soil moisture may also be estimated through land surface schemes or hydrological models, with spatial and temporal resolution depending on model structure and purpose. The accuracy of the modelled soil moisture is significantly influenced by the accuracy and spatial coverage of the input precipitation and soil hydraulic property data, in addition to the adequacy of the model structure and assumptions. Soil moisture data sets from remotely sensed and modelled sources are systematically different in the way they estimate soil moisture, and may be better suited to some climatic and environmental conditions than others. The objective of this study is therefore to answer the following research questions:

1. How do currently used remotely sensed and modelled products of surface soil moisture compare across Australia, and what are the driving processes?

2. Which products are most similar to each other and demonstrate similar error structures?

A number of previous studies have compared satellite and/or modelled soil moisture with *in situ* data within Australia (e.g. Brocca et al., 2014; Renzullo et al., 2014; Liu et al., 2009). Although the agreement between the data sets may be well established for the locations of the *in situ* stations, previous efforts have mainly focused on ground data from south-eastern Australia, such as the Murrumbidgee River catchment (e.g. Van der Schalie et al., 2015; Panciera et al., 2014; Dorigo et al., 2015; Su et al., 2013; Yee et al., 2013; Albergel et al., 2012; Mladenova et al., 2011; Draper et al., 2009) where a network of *in situ* stations are located, and often cover relatively short observation periods.

In light of the increasing number of important applications that utilise soil moisture data, the increasing number of approaches for its estimation, and the often limited geographical area, time frame and range of climate zones in previous studies, this study builds upon previous comparisons carried out over Australia in several ways.

Firstly, the coverage of *in situ* locations used as a reference for comparison is enlarged by extending the number of stations to include three separate networks, which include the emergent cosmic-ray technology as well as more traditional TDR and frequency-domain sensors. The networks include OzFlux (e.g. Cleverly, 2011), OzNet (Smith et al., 2012) and CosmOz (Hawdon et al., 2014), which when combined provide *in situ* soil moisture information over a broader range of geographies and climate zones across Australia than any of the networks individually. The entire time period of available data for all networks is considered, beginning with the earliest data (2001) and continuing through 2014.

Secondly, this study collates soil moisture data from multiple relevant sources, which hitherto have not been compared in a single study, across both model and remote sensing platforms. Collation of these different sources of soil moisture data in this comparison has allowed them to be viewed side by side and evaluated in a common framework. Also within individual remote sensing platforms, data sets developed with different radiative transfer algorithms by different research teams are considered.

Thirdly, the interrelationships between the products themselves are explored through cluster analyses. Addressing these research questions will provide a more detailed understanding of the strengths and weaknesses of a number of soil moisture products and further the appreciation of complementarity between sources, allowing the drawbacks of each to be minimised through a more informed assessment of fitness for purpose.

2. Materials

2.1. *In situ* data

The *in situ* data collated for this study forms the reference for comparison with satellite and model derived soil moisture estimates. *In situ* data were obtained and processed from three separate networks: OzFlux, OzNet and CosmOz (Fig. 1). Data from the combined *in situ* network are available for a range of time periods, beginning in 2001.

While *in situ* data has been used as a reference for comparison in this study, the point measurements that largely comprise the data set may or may not be representative of a wider spatial footprint across the landscape as seen by satellite and model products. Which source of soil moisture data may be considered as the 'truth' is debatable. To compare satellite and model products of soil moisture across different regions of Australia, it is practical to utilise a ground-based network as a reference, where a multi-year record of calibrated soil moisture observations is available within most climate regions across Australia.

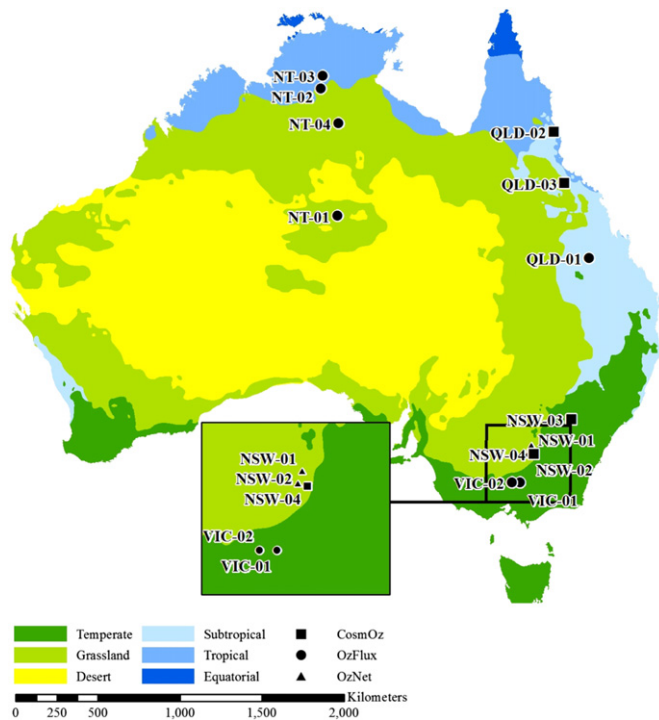


Fig. 1. *In situ* network station locations with major Köppen climate zones (Bureau of Meteorology, 2012).

Soil moisture is measured differently between the networks, and is further described in the following sections. While the systematic differences in measurement approach add complexity to the comparative analysis, the three networks can complement each other when comparing to soil moisture estimated from satellite and model products. For instance the shallower observation depths of the OzNet and OzFlux networks are more comparable to the shallow observation depths of satellites and models; yet the dependence of satellite observation depth with time, mainly depending on soil wetness conditions (e.g. Jackson et al., 2012; see Sections 2.2 and 2.3), is more like the behaviour of the CosmOz sensors. Furthermore the measurement footprint of the CosmOz stations is closer to that of satellite footprints than the point measurements of the OzNet and OzFlux networks. Such systematic differences may be evident from the comparison.

The inclusion of data from an *in situ* station was based on several criteria. Firstly, *in situ* measurements must be available within the study time period (1 January 2001 to 31 December 2014) as well as the shorter period of July 2012 to July 2013, which is common to the satellite and model products. Secondly, station locations were used where the number of coincident daily data points between the *in situ* and time series from all products was greater than or equal to 10 data points per season in both the longer and common periods of comparison. This is to ensure a correlation is made between the *in situ* station and *all* products at a given location, based on data from all seasons. Lastly, the data needed to be publicly available. Table 1 provides an overview of the *in situ* stations meeting these criteria and subsequently focused on in this study. The *in situ* stations considered span a range of environments, situated across wetter and drier areas (annual average rainfall ranged between 175 and 700 mm/year) and multiple climate zones (tropical, sub-tropical, grassland and temperate; Table 1). For this study sites have been named based on the state or territory they reside in, i.e. the Northern Territory (NT), Queensland (QLD), New South Wales (NSW) and Victoria (VIC).

2.1.1. OzFlux

OzFlux is part of a global network of over 500 micrometeorological stations worldwide that provide energy, carbon and water exchange observations with the atmosphere and numerous ecosystem types (www.ozflux.org.au; Baldocchi, 2008). In Australia, OzFlux consists of approximately 37 stations, of which 30 are currently active. Profile soil moisture in the OzFlux network is measured at individual stations using frequency-domain reflectometers (generally Campbell Scientific CS-616 (USA) probes) every 30 min. Data are provided at four levels of processing. Level 3 data has been subject to detailed quality control and has been used in this study. Data sets were downloaded directly from the OzFlux data portal (data.ozflux.org.au/portal) with soil moisture data given in volumetric units. Data from the OzFlux network were publicly available at 22 of the 37 stations across Australia, including 20 active stations and two stations which are no longer operational. Of these 22 stations, seven provided soil moisture data in the topsoil's upper 10 cm and met the criteria for inclusion.

2.1.2. OzNet

OzNet contains 63 monitoring stations within its network spanning the 82,000 km² Murrumbidgee River catchment in south-eastern Australia (Smith et al., 2012; <http://oznet.org.au>). All monitoring stations measure soil moisture, soil temperature and rainfall (Smith et al., 2012), every 20 to 30 min. The first stations were installed in 2001 and focused on root-zone soil moisture measurement (profile to a depth of 90 cm), with later installations measuring the top 0–5 cm (Smith et al., 2012). The older stations use Campbell Scientific (USA) water content reflectometers, and convert to volumetric soil moisture using calibration equations involving soil type and temperature information. The newer stations utilise Stevens Hydraprobe (USA) sensors, inferring volumetric soil moisture from the dielectric constant and conductivity measured (Merlin et al., 2007). Within the OzNet monitoring network two stations satisfied the applied criteria for inclusion.

2.1.3. CosmOz

CosmOz is a network of cosmic-ray sensors currently installed and operating (and calibrated) at nine locations around Australia. Each location houses a CRP-1000b Hydroinnova (USA) cosmic-ray sensor, which counts fast neutrons produced by cosmic rays passing through the earth's atmosphere (Hawdon et al., 2014). The probes are located approximately 2 m above ground and count neutrons in the soil and air above it (Hawdon et al., 2014). The fast neutron count is primarily controlled by the soil water content, where neutrons are moderated by hydrogen atoms within the water molecule. Thus the lower the neutron count, the more scattering that has taken place and the higher the soil moisture, and *vice versa*. Neutron count is corrected for several processes such as the effect of atmospheric pressure, vapour pressure changes and the variation in incoming neutron intensity (Hawdon et al., 2014). Neutron counts can also be affected by water in the vegetation surrounding the probe. In the CosmOz network, the effect of vegetation water on neutron count is effectively eliminated by calibrating each probe to local soil moisture conditions, assuming the hydrogen pool in the vegetation remains stable. This is considered a reasonable assumption for the sites of interest in this study and time period. Once corrections have been made, the neutron count is converted to volumetric soil moisture using a calibration function (Desilets et al., 2010) which is adjusted to known wet and dry soil moisture conditions.

Hourly soil moisture time series data were obtained from Hawdon et al. (2014) (<http://cosmoz.csiro.au>) for this study at four locations (Table 1) consistent with the *in situ* selection criteria.

Table 1
Summary of *in situ* stations.

| | Site name | Network name | Location | Data period | Depth [cm] | Köppen climate zone | Land type | MAR ^a [mm] | MATR ^b [°C] | Reference |
|--------|-----------|---------------------|---------------|-------------|------------|---------------------|----------------------|-----------------------|------------------------|--|
| OzFlux | NT-01 | Alice Springs Mulga | 22.3S, 133.2E | 2010–2013 | 0–10 | Grassland | Semi-arid mulga | 260 | 7–35 | Cleverly (2011) |
| | NT-02 | Dry River | 15.3S, 132.4E | 2008–2013 | 0–5 | Grassland | Open forest savannah | 560 | 14–36 | Beringer (2013) |
| | NT-03 | Red Dirt Melon Farm | 14.6S, 132.5E | 2011–2013 | 0–5 | Tropical | Tropical savannah | 600 | 17–33 | Beringer (2014) |
| | NT-04 | Sturt Plains | 17.2S, 133.4E | 2008–2013 | 0–5 | Grassland | Grassy plain | 670 | 12–36 | Beringer (2013a) |
| | QLD-01 | Arcturus Emerald | 23.9S, 148.5E | 2011–2013 | 0–5 | Subtropical | Pasture | 520 | 9–34 | Schroder (2014) |
| | VIC-01 | Riggs Creek | 36.6S, 145.6E | 2010–2013 | 0–5 | Temperate | Pasture | 310 | 5–34 | Beringer (2014a) |
| | VIC-02 | Whroo | 36.7S, 145.0E | 2011–2013 | 0–10 | Temperate | Box woodland | 575 ^c | 5–32 | Beringer (2013b); Bureau of Meteorology (2016) |
| OzNet | NSW-01 | Y2 | 34.7S, 146.1E | 2003–2014 | 0–5 | Grassland | Dryland cropping | 210 | –1–43 ^c | Smith et al. (2012); Bureau of Meteorology (2016a) |
| | NSW-02 | Y9 | 35.0S, 146.0E | 2003–2014 | 0–5 | Grassland | Dryland cropping | 345 | –1–43 ^c | Smith et al. (2012); Bureau of Meteorology (2016a) |
| CosmOz | NSW-03 | Baldry | 32.9S, 148.5E | 2011–2014 | Variable | Temperate | Pasture | 700 | –1–42 ^c | CSIRO (2015); Bureau of Meteorology (2016b) |
| | NSW-04 | Yanco | 35.0S, 146.3E | 2011–2014 | Variable | Grassland | Grazed | 175 | –1–43 ^c | CSIRO (2015); Bureau of Meteorology (2016a) |
| | QLD-02 | Robson | 17.1S, 145.6E | 2010–2014 | Variable | Subtropical | Tropical rainforest | 510 | 7–37 ^c | CSIRO (2015); Bureau of Meteorology (2016c) |
| | QLD-03 | Weany | 19.9S, 146.5E | 2010–2014 | Variable | Grassland | Grazed open woodland | 650 | 4–41 ^c | CSIRO (2015); Bureau of Meteorology (2016d) |

^a MAR = mean annual rainfall at the site over the stated data period.^b MATR = mean annual temperature range at the site over the stated data period.^c Data from nearest BOM station for the stated data period, with MATR defined as the range between the mean minimum and mean maximum annual values.

2.2. Satellite data

2.2.1. SMOS

The Soil Moisture Ocean Salinity (SMOS) satellite launched in November 2009 carries the Microwave Imaging Radiometer with Aperture Synthesis (MIRAS) radiometer that operates in the L-band, utilising a single channel at 1.4 GHz to estimate volumetric soil moisture to approximately 5 cm depth (Kerr et al., 2010), increasing or decreasing mainly depending on lower or higher soil moisture content. The Y-shaped instrument carries 69 regularly spaced dual-polarisation antennas that achieve an average spatial resolution of approximately 43 km, sampling the earth once every 3 days (Kerr et al., 2010). SMOS has an equatorial crossing time of 0600 h (ascending) and 1800 h (descending) local time.

In this study two SMOS products have been utilised. Firstly, the official product of volumetric soil moisture ‘SMOS_LMEB’ (version RE04) was obtained from the Centre Aval de Traitement des Données SMOS (CATDS), operated for the Centre National d’Etudes Spatiales (CNES, France) by IFREMER (Brest, France) for the period 15 January 2010 to 31 December 2014 (see <http://catds.ifremer.fr/Products>). Secondly, volumetric soil moisture estimates derived by the Land Parameter Retrieval Model (LPRM) algorithm for the period 1 July 2010 to 31 December 2014 were obtained from Van der Schalie et al. (2016), here named ‘SMOS_LPRM’.

The LPRM is a forward radiative transfer model that uses both horizontally and vertically polarised microwave brightness temperatures to partition the detected surface emission into soil and vegetation components using an analytical solution by Meesters et al. (2005). The model is run iteratively, varying the soil moisture term until the simulated brightness temperature converges with the observed. Once the model has converged, a dielectric mixing model (Wang and Schmugge, 1980) and a global database of soil physical properties (Rodell et al., 2004) are applied to determine the absolute soil moisture values (Owe et al., 2001). The official LMEB product similarly uses an iterative forward radiative transfer model. The main

point of difference between the two algorithms is the classification of land cover types within the footprint (estimated from high resolution land use maps) that are used to estimate the contribution of each cover type to the surface microwave emission (Wigneron et al., 2007) in the LMEB approach. Furthermore, the official LMEB algorithm constrains the model based on changes to vegetation optical thickness as measured by overpasses in a given time period (Kerr et al., 2012).

Both the SMOS_LPRM and SMOS_LMEB products were provided as volumetric soil moisture estimates on a global 25 km Equal Area Scalable Earth 2 (EASE2) grid with a cylindrical equal area projection. Each data set was resampled to a daily $0.25^\circ \times 0.25^\circ$ regular grid and quality controlled using flags for open water, snow, frost and coastal areas. The SMOS_LMEB data set was also filtered using the associated SMOS level 3 data quality control index, retaining soil moisture estimates with an uncertainty below $0.06 \text{ m}^3/\text{m}^3$.

2.2.2. AMSR2

The Advanced Microwave Scanning Radiometer 2 (AMSR2) instrument on board the Japan Aerospace Exploration Agency (JAXA) Global Change Observation Mission - Water 1 (GCOM-W1) satellite was launched in May 2012 into the A-Train satellite constellation. The AMSR2 instrument contains seven dual polarised frequency channels centred at 6.9, 7.3, 10.7, 18.7, 23.8, 36.5 and 89.0 GHz (Imaoka et al., 2010). The C-band (6.9 and 7.3 GHz) and X-band frequencies (10.7 GHz) are utilised for volumetric soil moisture estimation at a spatial resolution of approximately 50 km (Imaoka et al., 2010), sensitive to the top 1–2 cm of soil (Escorihuela et al., 2010, Owe et al., 2008). AMSR2 has an equatorial overpass time of 1330 h (ascending) and 0130 h (descending) local time, with near complete earth coverage approximately every two days.

In this study soil moisture data from two different retrieval algorithms were obtained: the official JAXA soil moisture product (here named ‘AMSR2_JAXA’) utilising X-band retrievals, and the soil moisture product derived using the LPRM (here named ‘AMSR2_LPRM’) for both the C-band and X-band retrievals. The JAXA algorithm is

a forward radiative transfer model that simulates brightness temperatures under various combinations of land parameters (such as vegetation signal attenuation and optical depth properties; fraction of pixel covered by vegetation) to develop look-up tables of soil moisture and vegetation water content (Maeda and Taniguchi, 2013; Jackson et al., 2010). The JAXA algorithm has been calibrated to *in situ* data obtained in south-eastern Australia, Mongolia and Thailand (Maeda and Taniguchi, 2013).

The AMSR2_JAXA product was obtained from JAXA GCOM-W1 Data Providing Service (<https://gcom-w1.jaxa.jp/auth.html>) for the period 3 July 2012 to 31 December 2014. Product version 1.1 has been used in this study (the most recent version 2.0 was not available for the whole study period). The AMSR2_LPRM volumetric soil moisture data were obtained from Parinussa et al. (2015) for the period 2 July 2012 to 31 December 2014. Both products were provided as daily volumetric soil moisture estimates on a global $0.25^\circ \times 0.25^\circ$ regular grid, quality controlled for open water, frozen conditions and coastal areas.

2.2.3. ASCAT

The Advanced Scatterometer (ASCAT) instrument on board the Meteorological Operational-A (Metop-A) satellite was launched in October 2006, and is a real aperture radar with six sideways-looking antennae operating in the C-band (5.3 GHz) with a vertical polarisation (Wagner et al., 2013).

ASCAT measurements are available at spatial resolutions of 50 km and 25 km (Wagner et al., 2013), with global coverage achieved approximately every 1.5 days. Measurements are taken over Australia approximately twice a day (Su et al., 2013) with an equatorial crossing time of 2130 h (ascending) and 0930 h (descending) local time (Wagner et al., 2013). ASCAT is a radar instrument that measures the backscatter of transmitted C-band pulses (Wagner et al., 2013). The production and subsequent retrieval of the backscattered signal is what makes ASCAT an 'active' satellite platform, as distinguished from the previous satellites which 'passively' detect radiation upwelling from the earth's surface.

The six antennae (three either side) of Metop-A provide three independent measurements of backscatter coefficients, which allows radar backscatter at different incidence and azimuth angles to be registered (Wagner et al., 1999a). The influence of soil moisture can be observed from the backscatter observations by removing the effect of vegetation through the employment of a time series based change detection algorithm, developed by Wagner et al. (1999). The effect of vegetation is removed by estimating the typical yearly phenological cycles around the world (Brocca et al., 2011). Surface roughness also has a strong influence on backscatter values (Wagner et al., 2013; Verhoest et al., 2008) but is assumed to remain constant in time (Brocca et al., 2011). In this algorithm the backscatter, extrapolated to a reference angle of 40° , is scaled based on the minimum and maximum historical values (Albergel et al., 2012). Assuming land cover remains relatively static over long periods of time changes are attributed to variations in soil moisture, yielding soil moisture in relative terms (Wagner et al., 2013). A time series of relative soil moisture is then obtained between 0% (dry) and 100% (wet) of reference conditions, for a depth of less than 2 cm (Wagner et al., 2013; Schmugge, 1983). The reference 'dry' and 'wet' values are estimated from extremes in backscatter measurements taken between August 1991 and May 2007 (Naeimi et al., 2009).

The 25 km operational resolution soil moisture product (here named 'ASCAT_TUW') on a discrete global grid produced by Vienna Institute of Technology (<http://rs.geo.tuwien.ac.at/products/surface-soil-moisture/ascat/>) was used in this study for the period 1 January 2007 to 31 December 2013. The data were resampled to a daily $0.25^\circ \times 0.25^\circ$ regular grid commensurate with the other satellite data sets, and quality controlled for open water, frozen conditions and coastal areas.

2.3. Model data

The models considered in this study have been developed by a number of research teams and are diverse in approach and purpose. Inevitably different modelling approaches lead to different representations of soil moisture, and with estimations made at different depths and times. This reality is reflected in the range of products considered in this study, all of which are currently utilised in Australia for various purposes. In an effort to limit the impact of model estimates at different times and depths on the assessment, an additional period common to all products is considered, as well as an additional and deeper uniform depth where possible.

Despite differences in model approach, all models considered in this study share common precipitation forcing prepared by Jones et al. (2009) as part of the Australian Water Availability Project (AWAP). The gridded data set contains daily precipitation at 0.05° resolution and is based solely on interpolated station data. The accuracy of the spatial product was assessed through a cross-validation procedure which repeatedly deleted 5% of stations at a time and the error in the analysis of the remaining stations calculated (Jones et al., 2009). For the period 2001–2007 the daily rainfall values have a root mean square error of 3.1 mm and a mean absolute error of 0.9 mm (Jones et al., 2009). In the context of this study common precipitation forcing among model products is seen as an advantage, as precipitation is a key driver of soil moisture variability and therefore differences between products may instead be related to other model-specific factors.

2.3.1. WaterDyn

The AWAP project, developed by the Commonwealth Scientific and Industrial Research Organisation (CSIRO), the Australian Bureau of Meteorology (BOM) and the Australian Bureau of Agricultural and Resource Economics and Sciences, implements a continental-scale water balance over Australia using the WaterDyn model at a resolution of 0.05° (Raupach et al., 2009).

Water balance calculations are carried out for two spatially-varying soil layers: a shallow soil layer with thicknesses ranging from 8 to 70 cm (typically 20 cm at the sites considered in this study), and a lower layer with thicknesses between 50 and 190 cm, depending on soil type (Raupach et al., 2009; Briggs, 2016, pers. comm). In this study estimates from the upper soil layer are considered. The mass balance of water flux across the boundaries of the upper layer is estimated based on a precipitation input, and a combined output from transpiration, soil evaporation, surface runoff and drainage to the deeper layer (Raupach et al., 2009). An estimate of relative water content is then made based on the saturated volumetric water content and depth of the layer.

Time series of daily average relative soil water content (between 0 and 1) for the whole of Australia were obtained for this study for the period 1 January 2001 to 31 December 2013, based on AWAP WaterDyn model version 26M.

2.3.2. CABLE

The CSIRO Atmosphere Biosphere Land Exchange (CABLE) is a land surface scheme that simulates coupled carbon and water cycles and was configured here on a 0.05° grid. For this study volumetric soil moisture estimates were extracted from a modified version of CABLE in the BIOS2 modelling environment (Haverd et al., 2013). In BIOS2, the soil and carbon modules of CABLE v1.4 were replaced by the SLI soil model (Haverd and Cuntz, 2010) and CASA-CNP biogeochemical model (Wang et al., 2007), respectively (Haverd et al., 2013). CABLE/BIOS2 was forced with soil data mapped in the Digital Atlas of Australian Soils (Northcote et al., 1960, 1975); and vegetation cover of each grid cell, which was subdivided into woody and grassy vegetation and assigned a Leaf Area Index (LAI; Haverd et al., 2013).

The model was run at an hourly timestep between 1990 and 2014, with the period 1990–2000 used to initialise soil moisture. The model defines 10 soil layers including 0–2.2 cm, 2.2–8 cm, 8–15 cm, 15–30 cm, 30–60 cm, 60–90 cm, 90–120 cm, 120–240 cm, 240–540 cm and 540–990 cm. To compare with *in situ* measurements, soil moisture estimates from the shallowest two model layers have been aggregated using a weighted arithmetic mean to produce a time series for the 0–8 cm layer.

2.3.3. AWRA-L

The Australian Water Resource Assessment (AWRA) system was developed by BOM and CSIRO as part of an effort to deliver comprehensive water accounting information across the country (Vaze et al., 2013; Stenson et al., 2011). The AWRA landscape model (AWRA-L) is a grid-based distributed biophysical model of the water balance between the atmosphere, soil, groundwater and surface water stores (Viney et al., 2015). AWRA-L estimates a daily running water balance on a $0.05^\circ \times 0.05^\circ$ grid across Australia (Viney et al., 2015) commensurate with meteorological forcing data sourced from AWAP.

The water balance is computed for each grid cell for two hydrological response units: shallow-rooted vegetation and deep-rooted vegetation (Viney et al., 2015). The unsaturated zone is partitioned into three layers, each with a maximum spatially varying water holding capacity: top layer (0–10 cm), shallow root zone layer (10–100 cm) and a deep root zone layer (100–600 cm). Water enters the top soil layer as net precipitation (precipitation minus interception) and may leave as soil evaporation, surface runoff or drainage through to deeper layers (Viney et al., 2015).

In this study the AWRA-L (version 5) water storage values [mm] from the top layer (0–10 cm) have been utilised. In order to evaluate soil moisture estimates alongside the other products, the AWRA-L water storage estimates have been scaled between local minimum and maximum values to produce a time series of relative soil wetness values between 0 and 1 for the period 1 January 2001 to 31 December 2014.

2.3.4. API

The Antecedent Precipitation Index (API) is an empirical relation describing soil wetness conditions that has historically been utilised in rainfall-runoff calculations (Choudhury and Blanchard, 1983; Kohler and Linsley, 1951). API has been used in the past to estimate catchment wetness conditions prior to storm events given the strong influence of soil wetness on runoff generating processes and the difficulty in accurately measuring soil moisture over large areas. The API is commonly of the form shown in Eq. (1).

$$API_t = \gamma API_{t-1} + P_t \text{ [mm]} \quad (1)$$

The index of the preceding day (API_{t-1}) [mm] is multiplied by a recession coefficient (γ) [–], and P_t [mm] is the amount of rainfall recorded on day (t) the index is to be calculated. The recession coefficient is a measure of the decline of the influence of past precipitation (Kohler and Linsley, 1951), i.e. the decline in memory of the soil column. The recession coefficient of the product used in this study was represented by the function:

$$\gamma = 0.85 + \delta(20 - T_{max,t}) \text{ [–]} \quad (2)$$

where $T_{max,t}$ is the maximum daily temperature [$^\circ\text{C}$] and δ is a sensitivity parameter [$^\circ\text{C}^{-1}$] (Crow et al., 2005). The API data set was generated by Kumar et al. (in press) on a daily time step for the whole of Australia on a $0.05^\circ \times 0.05^\circ$ grid for the period 1 January 2012 to 31 December 2014. Since API values are precipitation depths, the time series was scaled to the local minimum and maximum values to produce a data set of relative soil wetness between 0 and 1. API

is simply a proxy representing soil moisture due to a precipitation depth, and does not relate to a specific soil column depth.

2.3.5. KBDI

The Keetch-Byram Drought Index (KBDI; Keetch and Byram, 1968) is an empirical relation describing the cumulative soil moisture deficit of shallow soil layers. KBDI is currently in use in some parts of Australia as part of a suite of tools used to predict and manage bushfire hazard. KBDI is a simplified, running, daily water balance where soil moisture deficit (SMD) is determined by the difference between the daily effective rainfall ($P_{eff,t}$) and daily evapotranspiration (ET_t), as shown by Eq. (3).

$$SMD_t = SMD_{t-1} - P_{eff,t} + ET_t \text{ [mm]} \quad (3)$$

$P_{eff,t}$ [mm] is the portion of rainfall falling on a catchment that infiltrates into the soil, and is lessened by a constant 5 mm of the first part of an event (Finkele et al., 2006). ET_t [mm] is calculated through an empirical equation which is controlled by the previous day's KBDI value (SMD_{t-1}), the previous day's maximum temperature and the mean annual rainfall (Finkele et al., 2006). Conceptually ET is expected to be a function of vegetation density, which is itself considered to be an exponential function of mean annual rainfall (Keetch and Byram, 1968).

The SMD_{t-1} [mm] calculated through the running water balance represents the amount of water required to bring the soil column back to field capacity, and ranges between 0 and 200 mm (Finkele et al., 2006). The value of 200 mm comes from the original depth of water selected by Keetch and Byram (1968) to represent the field capacity of a soil profile depth where drought events are thought to have a clear impact on bushfire hazard. The actual depth of soil this represents thus depends on the soil type, where a greater depth would be represented in a sandy soil for example, compared to a clayey soil with a higher porosity. For this study the converse of the soil moisture deficit has been scaled to its local minimum and maximum values to produce a relative soil moisture time series between 0 and 1 (i.e. 200 mm deficit at wilting point = 100% deficit = 0% soil moisture; 0 mm deficit at field capacity = 0% deficit = 100% soil moisture).

KBDI values have been generated by Kumar et al. (in press) for the period 1 January 2001 to 31 December 2014 using rainfall and temperature data from AWAP on a daily time step for the whole of Australia on a $0.05^\circ \times 0.05^\circ$ grid.

2.3.6. MSDI

Mount's Soil Dryness Index (Mount, 1972) is a similar empirical relation to KBDI in that it is a cumulative soil moisture deficit index, and is also currently used in Australia for bushfire hazard management. MSDI is represented by the same formula as KBDI (see Eq. (3)), but differs in its determination of the P_{eff} and ET terms. To estimate ET the MSDI model assumes a linear relation between mean monthly pan evaporation and mean monthly maximum temperature data measured in Australian capital cities. To calculate $P_{eff,t}$ and partition precipitation into infiltration, runoff or interception, the MSDI model considers the type of vegetation present and assigns each vegetation class their own values of canopy interception, canopy storage, wet evaporation rates and a flash runoff fraction Finkele et al. (2006). For the data set used in this study the vegetation type of each model cell has been estimated through a linear relationship between vegetation class and leaf area index detailed in Finkele et al. (2006). Like the KBDI data set, the converse of the MSDI soil moisture deficit has been scaled to its local minimum and maximum values to produce a relative soil moisture time series. The MSDI time series has been generated by Kumar et al. (in press) for the period 1 January 1974 to 31 December 2014 using rainfall and temperature data from AWAP

on a daily time step for the whole of Australia on a $0.05^\circ \times 0.05^\circ$ grid.

3. Methodology

Direct comparison between the *in situ* data and the satellite and model soil moisture products is challenging due to the systematic differences between each data source. Soil moisture measurements differ in terms of (a) observation depth, (b) temporal change of the observation depth, (c) horizontal support and (d) sampling frequency. For instance the fixed observation depth of the OzNet and OzFlux networks (often taking measurements at several integrated depths, including measurements from the top 0–10 cm or 0–5 cm of soil) contrasts with the variable depth of the CosmOz sensors, which vary in their observation depth depending on soil conditions (Hawdon et al., 2014; Zreda et al., 2008; Franz et al., 2012) and in this study typically vary between 0–7 and 0–50 cm. These contrast with the typical observation depth of the top ≈ 1 –5 cm as seen by satellites, depending on wavelength, soil conditions, moisture content and cover (Kerr et al., 2010; Owe et al., 2008).

Contrasts exist between the point scale measurement of the OzNet and OzFlux networks and the intermediate spatial scale of the CosmOz network. The horizontal support of the cosmic-ray probes is a circle of approximately 600 m diameter around the probe, i.e. approximately 30 ha (Hawdon et al., 2014). Furthermore the model and satellite products represent estimates over tens of square kilometres. Analysis of comparison between products with different spatial support is further complicated by soil moisture variability being controlled by the processes at play at different scales (Vinnikov et al., 1999), and at different levels of wetness (Brocca et al., 2014).

Lastly, soil moisture measurements differ in their sampling frequency, and in the networks considered in this study range from 20 min in the OzNet network, to 30 min in the OzFlux network, to hourly in the CosmOz network.

Compounding these issues of scale are the different sources of uncertainty and error associated with each data source. These systematic differences prevent absolute agreement between the different products (Brocca et al., 2011; Draper et al., 2009).

For these reasons the comparisons of satellite and model products are based on their relative temporal agreement with the *in situ* data, using the Pearson correlation coefficient as the primary statistical metric. From this, four methods were implemented to compare the satellite and model products to the *in situ* measurements to assess their relative performance across Australia, and potential interrelationships, and are outlined in the sections following.

3.1. Pearson correlation coefficient

The degree of association between the *in situ* reference data and product data sets was calculated using the Pearson correlation coefficient (R) according to Eq. (4).

$$R = \frac{\frac{1}{n} \sum_{t=1}^n (\theta_{t,p} - \bar{\theta}_p)(\theta_{t,i} - \bar{\theta}_i)}{\sqrt{\frac{1}{n} \sum_{t=1}^n (\theta_{t,p} - \bar{\theta}_p)^2 \frac{1}{n} \sum_{t=1}^n (\theta_{t,i} - \bar{\theta}_i)^2}} \quad (4)$$

$\theta_{t,p}$ and $\theta_{t,i}$ refer to the daily average soil moisture of a product (p ; either satellite or model) and *in situ* (i) respectively, and $\bar{\theta}_p$ or $\bar{\theta}_i$ its average over the time series from $t = 1$ to n days. Correlations were only performed when at least 10 coincident data points each season were present between the reference *in situ* data set and the comparison product, to ensure a sufficient sample size in determining if the

calculated correlation is likely to be different from zero. At stations where this threshold was met or exceeded, correlation analysis was performed using the maximum number of coincident observations in the study time period (1 January 2001 to 31 December 2014), as well as in a shorter period (July 2012 to July 2013). The longer period allowed interannual cycles to be studied with multi-year climatology. The shorter time period was chosen to constrain the correlation to a period common to all products. By studying both the longer and common periods, the correlation analysis avoids being strongly influenced by data gaps and the inclusion or exclusion of extreme events (Loew, 2014). In both cases the correlation statistic was only analysed at sites where the entire seasonal cycle was observed. The significance of each correlation was also calculated using a p -value of 0.01.

The data from each *in situ* station were transformed into a time series of daily averages, bringing the range of measurement frequencies into a common format. This time series of daily *in situ* soil moisture for the study time frame forms the reference for comparison with other products.

Each satellite soil moisture product was resampled to a common $0.25^\circ \times 0.25^\circ$ regular grid. The satellite pixel whose centroid is co-located with each *in situ* station coordinate on the grid was chosen and the corresponding daily soil moisture time series extracted. Where several satellite pixels fall within the reprojected grid cell the arithmetic average was taken. Soil moisture data from each of the models were provided as daily time series at the location coordinates of the *in situ* stations. In this way time series of daily soil moisture values were compiled at each station for each of the *in situ*, satellite and model estimates.

Product soil moisture estimates have not been weighted to specific depth fractions of overlap with the *in situ* measurements, since most products provide soil moisture estimates at depths varying with soil conditions (i.e. all but the WaterDyn, CABLE and AWRA-L products). To compare the different products the correlation has been calculated between *in situ* measurements (for measurement depths listed in Table 1) and product soil moisture estimates (for the indicative depths listed in Table 2).

Consistent with the shallow nature of satellite observing depths, soil moisture estimates have been taken from the top layer of each model. Where models provide estimates at deeper defined intervals (i.e. WaterDyn, AWRA-L and CABLE), additional *in situ* soil moisture observations were considered to provide some assessment of how the evaluation differs when a uniform corresponding depth interval is used. Deeper *in situ* observations were available at OzNet sites NSW-01 and NSW-02 for the intervals 0–30 cm, 30–60 cm and 60–90 cm. Using a weighted arithmetic mean, a single *in situ* soil moisture time series for the depth interval 0–90 cm was calculated for both NSW-01 and NSW-02. The *in situ* measurements were then correlated with each of the WaterDyn, CABLE and AWRA-L time series based on their respective overlapping layer fractions.

3.2. Temporal anomaly

Correlation was also determined for the temporal anomalies of each data set. The performance of each product was evaluated using both the original and anomaly time series to respectively highlight agreement in soil moisture seasonality (Dorigo et al., 2015; Brocca et al., 2011; Reichle et al., 2004), as distinct from the skill of a product in detecting single events (Brocca et al., 2011).

Typically, the temporal anomaly time series is calculated using the difference between the soil moisture measurement and its long-term mean; however as the time periods covered by the different products evaluated in this study vary significantly, the soil moisture anomalies (θ_{anom}) were calculated using a 29-day moving average in the common time period (based on Albergel et al., 2009;

Table 2
Summary of comparison data sets.

| | Product | Algorithm | Version | Overpass | Frequency [GHz] | Data period | Spatial resolution [km] | Depth [cm] |
|------------|----------|-----------|---------|----------|-----------------|-------------|-------------------------|--------------------------|
| Satellites | SMOS | LPRM | 2016 | A | 1.4 | 2010–2014 | ≈43 | ≈0–5 |
| | SMOS | LMEB | RE04 | A | 1.4 | 2010–2014 | ≈43 | ≈0–5 |
| | AMSR2 | LPRM | 1.1 | D | 6.9 | 2012–2014 | ≈50 | ≈0–2 |
| | AMSR2 | JAXA | 1.1 | A | 10.7 | 2012–2014 | ≈50 | ≈0–2 |
| | ASCAT | TUW | WARP5.5 | D | 5.3 | 2007–2013 | ≈25 | ≈0–2 |
| Models | WaterDyn | – | 26M | – | – | 2001–2013 | ≈5 | 0–8 to 0–70 ^b |
| | CABLE | – | BIOS2 | – | – | 2001–2014 | ≈5 | 0–8 ^a |
| | AWRA-L | – | 5.0 | – | – | 2001–2014 | ≈5 | 0–10 |
| | API | – | – | – | – | 2012–2014 | ≈5 | Variable |
| | KBDI | – | – | – | – | 2001–2014 | ≈5 | Variable |
| | MSDI | – | – | – | – | 2001–2014 | ≈5 | Variable |
| | – | – | – | – | – | – | – | – |

^a Weighted mean of 0–2.2 cm & 2.2–8 cm intervals.^b Typically 0–20 cm at sites considered in this study.

Kim et al., 2015). For each soil moisture measurement (either *in situ* or product) at time t (θ_t), a period of 14 days prior and 14 days after was defined. Provided at least seven measurements were available in this period, the average soil moisture ($\bar{\theta}_{anom}$) and standard deviation (σ) were calculated in order to calculate the anomaly as per Eq. (5).

$$\theta_{anom} = \frac{\theta_t - \bar{\theta}_{(t-14:t+14)}}{\sigma_{(t-14:t+14)}} \quad (5)$$

3.3. Time series visualisation

The comparison of products based on the correlation was supported by visual analysis of the soil moisture time series plots. The aim of studying the time series plots was to identify and highlight features of product temporal behaviour not apparent in the correlation analysis, lending insight to the processes driving temporal behaviour of each product across Australia.

3.4. Cluster analysis

A cluster analysis was conducted to explore the interrelationships between the products themselves. While the ability of a product to successfully reproduce *in situ* temporal behaviour was measured using R , the purpose of the cluster analysis was to show those products that closely associate with each other. Close association between products indicates similarity. Identifying similarity or lack thereof helps determine which data sets have duplicate content and may share commonalities in error structure, and which are complementary, potentially providing useful information given that multiple products are currently employed in single applications (e.g. data assimilation).

Hierarchical cluster analyses were performed at each station location to construct dendrograms where products are grouped when their degree of association is maximal. Each dendrogram is developed by ranking all possible pairs of products based on their degree of association. A hierarchy tree (dendrogram) is then created based on the ranking, beginning with the two products with the closest degree of association, all the way to the products with the least association, with the height of each link in the tree reflecting the relative degree of association between the products. The analysis was based on the Euclidean distance between product pairs of $1-R^2$ values.

3.5. Satellite overpass and frequency band selection

Prior to the product comparison, a preliminary analysis was undertaken to determine which satellite overpass (ascending or descending part of the orbit) and frequency band data sets should be used in the comparison. Fig. 2 shows the range of correlation coefficients R and standard deviation for ascending and descending passes for each of the satellite soil moisture products: SMOS_LPRM L-band, SMOS_LMEB L-band, AMSR2_LPRM C-band, AMSR2_LPRM X-band, AMSR2_JAXA X-band, and ASCAT_TUW C-band. The correlation was calculated between *in situ* and the satellite product over the longer time period of comparison and at all sites (Table 1).

Particularly interesting from Fig. 2 are the lower minimum correlations of AMSR2_LPRM C-band in the daytime overpass (ascending) compared to its night-time overpass. Data from night-time satellite overpasses are often considered more suitable for comparison with *in situ* soil moisture as night-time conditions are considered to provide better soil moisture estimates due to the increased thermal equilibrium conditions of the surface soil, canopy and near-surface air (Owe et al., 2008). The wider range of correlation for the

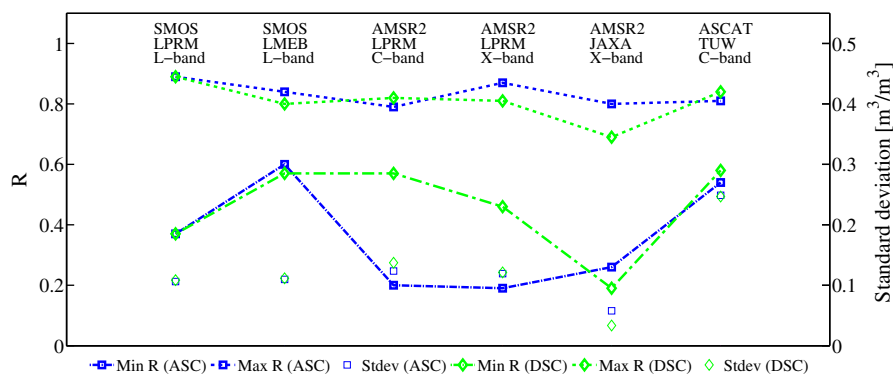


Fig. 2. Minimum and maximum coefficients of correlation between *in situ* and satellite soil moisture estimates across all stations (left axis) and standard deviation (right axis), for different satellite overpasses and frequency bands. Note the units of standard deviation for ASCAT are percentage relative wetness. ASC = ascending overpass, DSC = descending overpass.

AMSR2_LPRM C-band daytime ascending overpass is a result of a lower correlation result at the northern Australian station location NT-04 ($R = 0.20$).

Considering the night-time descending overpass, AMSR2_LPRM C-band yields a more favourable range of correlation than AMSR2_LPRM X-band. This is consistent with the expectation that X-band retrievals are more susceptible to scattering and absorption due to vegetation influences due to its shorter wavelength (De Jeu et al., 2008) and represent a shallower soil depth compared to C-band retrievals, and therefore yield poorer correlation results. Considering these factors and the difference in the range of correlation between ascending and descending for SMOS and ASCAT was less than 0.01 (Fig. 2), the night-time or early morning data sets have been selected for further analysis in this study. For the AMSR2_JAXA product, correlations were generally better under day-time ascending passes, leading to a higher correlation coefficients compared to the night-time descending data set in Fig. 2.

In summary, from this analysis the following products have been used for subsequent analysis: SMOS_LPRM_A, SMOS_LMEB_A, ASCAT_TUW_D, AMSR2_LPRM_D (C-band) and AMSR2_JAXA_A (where products are named as *satellite_algorithm_overpass*).

4. Results

4.1. Comparison of products

The comparisons in terms of the correlation coefficient (R) between *in situ* soil moisture measurements and satellite or model products are presented in Tables 3 and 5. All correlations are between the *in situ* soil moisture depth intervals listed in Table 1, and the product depth intervals listed in Table 2. Correlation coefficients are shown for both the longer period of coincident data within the study timeframe of 2001–2014 (Table 3) and common period of July 2012–July 2013 (Table 5). Values in bold indicate the highest correlation among either satellite or model products. A relative comparison of R (longer period) for each product across Australia is illustrated in Fig. 3, shown with major Köppen climate classification zones.

The results of the additional comparison between *in situ* soil moisture and modelled estimates at deeper depths are provided in Table 4 for the longer period of comparison.

Overall the satellite products yielded roughly similar ranges of correlation coefficients, with the possible exception of AMSR2_JAXA_A. The SMOS products performed slightly better than the alternative

Table 4

Summary of correlation between 0 and 90 cm *in situ* measurements and model products, longer period (2001–2014).

| Station | Models | | |
|---------|----------|-------|--------|
| | WaterDyn | CABLE | AWRA-L |
| NSW-01 | 0.68 | 0.76 | 0.80 |
| NSW-02 | 0.66 | 0.72 | 0.66 |

satellite-based data sets, yielding higher correlation coefficients than the other satellite products at 11 out of 13 sites. In the longer period of comparison, SMOS_LMEB_A achieved correlation coefficients in the range 0.64–0.83 and 0.48–0.88 in the common period. SMOS_LPRM_A yielded a range between 0.37 and 0.89 in the longer period, or 0.67 and 0.89 when omitting QLD-02, where SMOS_LMEB_A returned a non-significant correlation. SMOS_LPRM_A achieved a better correlation with *in situ* measurements than SMOS_LMEB_A at over half of the locations in the longer period of comparison, and showed the highest skill among all satellite products on eight occasions compared to three occasions for SMOS_LMEB_A. However SMOS_LMEB_A returned fewer non-significant correlations than SMOS_LPRM_A in the common period owing to a comparatively larger number of data points available at each site (e.g. NT-01, QLD-01, VIC-01 and NSW-03). With the exception of QLD-02, Fig. 3 highlights that the strong, long-term agreement of the SMOS products is consistent across climate zones.

ASCAT_TUW_D and AMSR2_LPRM_D performed similarly well, with correlation coefficients in the range of 0.57–0.82 and 0.58–0.84, respectively, in the longer time period of comparison. ASCAT_TUW_D and AMSR2_LPRM_D were slightly less similar to each other in the common period of comparison, yielding a range of 0.54–0.87 and 0.39–0.89 respectively, similar to SMOS_LMEB for a comparable number of data points.

The AMSR2_JAXA_A product performed most poorly among the satellite data sets, achieving a larger range of 0.26–0.80 in the longer period, and 0.38–0.86 in the common period. Approximately half the sites yielded $R < 0.6$ in both periods of comparison. The wider range of correlation coefficients from AMSR2_JAXA_A reflects a more variable agreement across climate zones than the other satellites (Fig. 3). The higher correlation coefficients found at stations NSW-01 and NSW-02 suggest a potential calibration effect in this area, as data from this area have been used in the AMSR2_JAXA algorithm calibration process (Maeda and Taniguchi, 2013).

Table 3

Summary of correlation between *in situ* data and satellite and model products, longer period (2001–2014). Values in bold indicate the highest correlation among either satellite or model products.

| Station | | Satellites | | | | | Models | | | | | |
|---------|-----------|-------------|-------------|--------------|--------------|-------------|-------------|-------------|-------------|-------------|-----------|-------------|
| | | SMOS LPRM A | SMOS LMEB A | AMSR2 LPRM D | AMSR2 JAXA A | ASCAT TUW D | WaterDyn | CABLE | AWRA-L | API | KBDI | MSDI |
| OzFlux | NT-01 | 0.74 | 0.68 | 0.65 | 0.52 | 0.63 | 0.79 | 0.81 | 0.77 | 0.79 | 0.45 | 0.58 |
| | NT-02 | 0.87 | 0.73 | 0.68 | 0.71 | 0.84 | 0.88 | 0.89 | 0.89 | 0.84 | 0.75 | 0.75 |
| | NT-03 | 0.77 | 0.65 | 0.78 | 0.77 | 0.81 | 0.83 | 0.82 | 0.79 | 0.84 | 0.72 | 0.71 |
| | NT-04 | 0.74 | 0.72 | 0.57 | 0.55 | 0.73 | 0.84 | 0.85 | 0.73 | 0.64 | 0.86 | 0.87 |
| | QLD-01 | 0.67 | 0.64 | 0.64 | 0.51 | 0.58 | 0.78 | 0.80 | 0.72 | 0.72 | 0.64 | 0.55 |
| | VIC-01 | NS | 0.79 | 0.66 | 0.38 | 0.70 | 0.83 | 0.70 | 0.58 | 0.76 | 0.59 | 0.72 |
| | VIC-02 | 0.75 | 0.71 | 0.63 | 0.26 | 0.59 | 0.78 | 0.67 | 0.69 | 0.82 | 0.50 | 0.71 |
| OzNet | NSW-01 | 0.74 | 0.78 | 0.77 | 0.78 | 0.68 | 0.84 | 0.80 | 0.80 | 0.72 | 0.45 | 0.66 |
| | NSW-02 | 0.78 | 0.81 | 0.80 | 0.80 | 0.69 | 0.83 | 0.80 | 0.80 | 0.77 | 0.42 | 0.68 |
| CosmOz | NSW-03 | 0.85 | 0.81 | 0.82 | 0.67 | 0.83 | 0.87 | 0.77 | 0.61 | 0.71 | 0.63 | 0.84 |
| | NSW-04 | 0.80 | 0.75 | 0.73 | 0.57 | 0.72 | 0.76 | 0.68 | 0.63 | 0.68 | 0.25 | 0.44 |
| | QLD-02 | 0.37 | NS | 0.62 | 0.43 | 0.75 | 0.82 | 0.87 | 0.70 | 0.63 | 0.84 | 0.73 |
| | QLD-03 | 0.89 | 0.83 | 0.75 | 0.63 | 0.84 | 0.88 | 0.89 | 0.77 | 0.82 | 0.73 | 0.77 |
| | Range | 0.37–0.89 | 0.64–0.83 | 0.57–0.82 | 0.26–0.80 | 0.58–0.84 | 0.76–0.88 | 0.67–0.89 | 0.58–0.89 | 0.63–0.84 | 0.25–0.86 | 0.44–0.87 |
| | N (sum) | 5104 | 6650 | 4861 | 5363 | 6740 | 16,171 | 17,456 | 17,456 | 10,103 | 17,456 | 17,456 |
| | N (range) | 212–590 | 265–716 | 225–612 | 236–681 | 251–896 | 619–2250 | 619–2309 | 619–2309 | 531–1096 | 619–2309 | 619–2309 |

NS: not significant.

Table 5
Summary of correlation between *in situ* data and satellite and model products, common period (2012–2013). Values in bold indicate the highest correlation among either satellite or model products.

| | Station | Satellites | | | | | Models | | | | | |
|--------|-----------|----------------|----------------|-----------------|-----------------|----------------|-------------|-------------|-----------|-------------|-------------|-------------|
| | | SMOS LPRM A | SMOS LMEB A | AMSR2 LPRM D | AMSR2 JAXA A | ASCAT TUW D | WaterDyn | CABLE | AWRA-L | API | KBDI | MSDI |
| OzFlux | NT-01 | NS | 0.62 | 0.66 | 0.45 | 0.45 | 0.57 | 0.69 | 0.67 | 0.72 | −0.15 | 0.31 |
| | NT-02 | 0.72 | 0.70 | 0.70 | 0.78 | 0.83 | 0.89 | 0.90 | 0.88 | 0.89 | 0.72 | 0.70 |
| | NT-03 | 0.81 | 0.69 | 0.78 | 0.77 | 0.89 | 0.90 | 0.90 | 0.81 | 0.88 | 0.86 | 0.82 |
| | NT-04 | 0.57 | 0.53 | 0.54 | 0.55 | 0.39 | 0.80 | 0.71 | 0.66 | 0.61 | 0.74 | 0.84 |
| | QLD-01 | NS | 0.48 | 0.63 | 0.45 | 0.41 | 0.63 | 0.64 | 0.58 | 0.58 | 0.70 | 0.52 |
| | VIC-01 | NS | 0.84 | 0.66 | 0.39 | 0.75 | 0.90 | 0.78 | 0.66 | 0.81 | 0.67 | 0.76 |
| | VIC-02 | 0.79 | 0.78 | 0.71 | 0.38 | 0.74 | 0.79 | 0.72 | 0.56 | 0.70 | 0.70 | 0.85 |
| OzNet | NSW-01 | 0.69 | 0.79 | 0.82 | 0.79 | 0.73 | 0.79 | 0.80 | 0.74 | 0.69 | 0.56 | 0.75 |
| | NSW-02 | 0.81 | 0.83 | 0.87 | 0.82 | 0.80 | 0.86 | 0.86 | 0.84 | 0.80 | 0.54 | 0.78 |
| CosmOz | NSW-03 | NS | 0.85 | 0.85 | 0.72 | 0.86 | 0.90 | 0.77 | 0.58 | 0.76 | 0.64 | 0.92 |
| | NSW-04 | 0.87 | 0.88 | 0.78 | 0.86 | 0.85 | 0.90 | 0.79 | 0.79 | 0.84 | 0.36 | 0.80 |
| | QLD-02 | 0.35 | NS | 0.57 | 0.40 | 0.78 | 0.85 | 0.85 | 0.64 | 0.69 | 0.83 | 0.73 |
| | QLD-03 | NS | 0.80 | 0.85 | 0.55 | 0.73 | 0.78 | 0.90 | 0.70 | 0.80 | 0.70 | 0.78 |
| | Range | 0.35–0.87 | 0.48–0.88 | 0.54–0.87 | 0.38–0.86 | 0.39–0.89 | 0.57–0.90 | 0.64–0.90 | 0.56–0.88 | 0.58–0.89 | −0.15–0.86 | 0.31–0.92 |
| | N (sum) | 1455 | 2147 | 2684 | 3226 | 2002 | 4696 | 4696 | 4696 | 4696 | 4696 | 4696 |
| | N (range) | 75–151 | 68–194 | 173–253 | 211–273 | 130–176 | 330–366 | 330–366 | 330–366 | 330–366 | 330–366 | 330–366 |

NS: not significant.

One difficulty in comparing time series from different satellite platforms, or different retrieval algorithms for a single platform, is the discrepancy in sampling times. The correlation results presented thus far have been based on all days within the study period where both in *in situ* time series and the product to be correlated with had finite values. Inevitably this leads to a different number of sampling points to compare (see N in Table 3 for example), as well as a difference in the timing of those points between products. Preliminary tests were carried out to provide some indication of how the correlation varies when sampling points are colocated in time between the satellite products. The agreement between a satellite product and *in situ* estimates was re-assessed using data points colocated in time between satellite product pairs.

For instance when the two SMOS products were colocated in time, the range of *R* varied little to previous estimates shown in Table 3. The correlation between SMOS_LPRM_A and *in situ* measurements ranged between 0.40 and 0.89, and SMOS_L3_A between 0.61 and 0.81. Changes at individual sites were within approximately $\pm 5\%$ of values listed in Table 3 for *N* = 6650. Similarly little change in the range of *R* was observed when the two AMSR2 products were colocated in time. AMSR2_LPRM_D ranged between 0.52 and 0.82, and AMSR2_JAXA_A between 0.26 and 0.79, for *N* = 4903.

The comparison was extended to compare *R*-values when temporally colocating products from different satellite platforms. When SMOS_L3_A and ASCAT_TUW_D were colocated in time, the correlation coefficients between SMOS_L3_A and *in situ* measurements ranged between 0.63 and 0.85. This is similar to the range previously estimated (Table 3), for a reduced number of points (*N* = 3551). ASCAT_TUW_D ranged between 0.58 and 0.84, the same range as previous (Table 3) where almost twice the number of data points were considered.

When AMSR2_LPRM_D and ASCAT_TUW_D were colocated in time, AMSR2_LPRM_D *R*-values ranged between 0.49 and 0.85. Correlation coefficients at individual sites varied approximately $\pm 10\%$, with the exception of QLD-02 (reducing from 0.62 previously to 0.50); however this was based on considerably fewer data points (*N* = 1891 compared to 4861 previously, Table 3). The range in ASCAT_TUW_D *R*-values changed little (0.45–0.89) but NT-04 saw a considerable reduction in *R*, from 0.73 (Table 3) to 0.45, again based on fewer data points.

Lastly, when SMOS_L3_A and AMSR2_LPRM_D were colocated in time, AMSR2_LPRM_D varied little from previous estimates, ranging between 0.55 and 0.82 (*N* = 3436). The correlation between SMOS_L3_A and *in situ* measurements did vary considerably at

NT-04, reducing to 0.53. Otherwise, correlation coefficients remained within approximately $\pm 10\%$ of previous estimates shown in (Table 3).

Correlation between the *in situ* measurements and modelled predictions varied between products. The WaterDyn product was the clear front runner, followed closely by CABLE. WaterDyn achieved the strongest agreement with *in situ* measurements among all the models in both the longer and common periods, and indeed was stronger than all satellite products. The higher correlation coefficients of WaterDyn compared to all satellite products was based on notably more data points (Tables 3 and 5). The correlation between WaterDyn and *in situ* measurements ranged between 0.76 and 0.88 in the longer period of comparison, and 0.57 and 0.90 in the common period. The highly consistent strength of WaterDyn across climate zones is reflected in Fig. 3. CABLE and API also performed well and were generally strong across climate zones (Fig. 3), with CABLE yielding somewhat higher correlation coefficients with *in situ* measurements than API. Despite the simplicity of API, agreement with *in situ* data was strong, ranging between 0.63 and 0.84 in the longer period and 0.58 and 0.89 in the common period. AWRA-L yielded similar ranges in both the longer and common periods of comparison (0.58–0.89 and 0.56–0.88 respectively). MSDI yielded a smaller range in correlation than KBDI in the longer period of comparison (0.44–0.87 and 0.25–0.86 respectively). In the common period the range in KBDI was wider still (−0.15–0.86), with the negative correlation value at NT-01 a result of several smaller wetting events being missed in the model output. KBDI was most variable across climate zones, displaying particular variability among the grassland stations (Fig. 3).

It is noted that the deeper and variable observation depth of the CosmOz stations was not detrimental to the correlation compared to the stations with fixed, shallower TDR and frequency-domain sensors. Significant, positive correlation coefficients were found at all CosmOz stations for all products, in both the longer and common period of comparison (with the exception of SMOS at two sites where the number of satellite data points was relatively low). This suggests that the temporal evolution of soil moisture in the deeper soil zone of CosmOz readings is similar to the shallower soil zone as estimated by the satellite and some model products, indicating hydraulic coupling of the layers.

Similarly, the strong correlation between the WaterDyn and *in situ* data sets indicates the greater depth interval of the upper WaterDyn model layer effectively simulates the temporal dynamics of the shallower surface layer measured by the *in situ* stations.

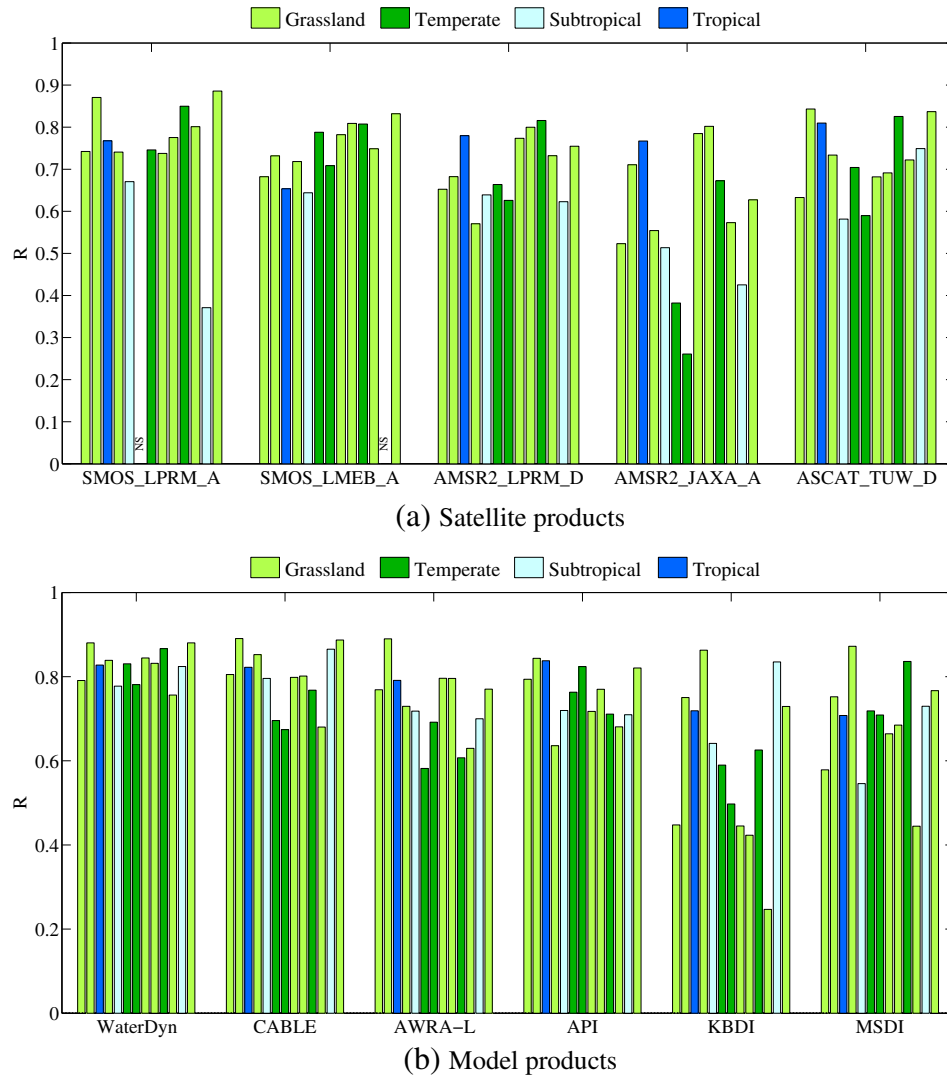


Fig. 3. Correlation across climate zones by product, longer period (2001–2014). Sites are in the same order (from top to bottom) as Table 3.

However, when looking at the results of the correlation (longer period) between OzNet measurements and each of the WaterDyn, CABLE and AWRA-L models constrained to the same depth (0–90 cm) in Table 4, correlation coefficients either remained the same or decreased. WaterDyn decreased by 0.16 and 0.17 at NSW-01 and NSW-02 respectively. AWRA-L remained the same at NSW-01 and decreased by 0.14 at NSW-02. CABLE decreased to a lesser extent, by 0.04 and 0.08 at NSW-01 and NSW-02 respectively.

4.2. Comparison of temporal anomalies

The results of the correlation between *in situ* data and satellite and model anomalies are presented in Table 6. The range of correlation coefficients between the products was similar. SMOS_LPRM_A ranged between 0.27 and 0.54, similar to SMOS_LMEB_A (0.20–0.55). A significant correlation between *in situ* measurements and SMOS estimates was not found at a number of sites, particularly SMOS_LPRM_A, due to a comparatively low number of data points; however a significant correlation was possible in many instances at a significance level of $p = 0.05$ (not shown). At sites where both products yielded a significant correlation, values were similar between products (Table 6). AMSR2_LPRM_D and AMSR2_JAXA_A yielded a

similar range of correlation coefficients, ranging between 0.20 and 0.55 and 0.24 and 0.56, respectively. ASCAT_TUW_D achieved a similar range (0.22–0.49) for relatively fewer data points.

The models showed greater skill in simulating *in situ* temporal anomalies than the satellite products. WaterDyn and CABLE continued to perform strongly relative to the other products, ranging between 0.38 and 0.77 and 0.33 and 0.78, respectively, with AWRA-L following closely with 0.34–0.76. As in the relative product comparison, the agreement of KBDI was somewhat weaker than MSDI, ranging between 0.25 and 0.70 compared to 0.29 and 0.78.

The temporal anomaly of all products showed a weaker correlation with *in situ* data than the original time series, indicating all products are more effective at detecting interannual and seasonal patterns than single events. This is likely a result of the disparity between product and *in situ* spatial support. Single events measured by *in situ* sensors represent a small point in space and thus the influence of local conditions. Even the spatial support of the CosmOz *in situ* estimates, covering approximately 30 ha surrounding the instrument, represent at best only 1.2% of the grid cell of the highest resolution products (WaterDyn, CABLE, AWRA-L, API, KBDI, MSDI) and at worst 0.05% of the lower resolution satellite products (SMOS_LPRM_A, SMOS_LMEB_A, AMSR2_LPRM_D, AMSR2_JAXA_A).

Table 6

Summary of correlation of temporal anomalies, common period. Values in bold indicate the highest correlation among either satellite or model products.

| | Station | Satellites | | | | | Models | | | | | |
|--------|-----------|----------------|----------------|-----------------|-----------------|----------------|-------------|-------------|-------------|-------------|-------------|-------------|
| | | SMOS LPRM A | SMOS LMEB A | AMSR2 LPRM D | AMSR2 JAXA A | ASCAT TUW D | WaterDyn | CABLE | AWRA-L | API | KBDI | MSDI |
| OzFlux | NT-01 | NS | 0.40 | 0.39 | NS | NS | 0.55 | 0.71 | 0.76 | 0.72 | 0.47 | 0.55 |
| | NT-02 | NS | 0.20 | 0.30 | 0.36 | 0.43 | 0.50 | 0.46 | 0.39 | 0.43 | 0.53 | 0.41 |
| | NT-03 | 0.37 | 0.23 | 0.35 | 0.54 | 0.53 | 0.76 | 0.78 | 0.66 | 0.65 | 0.70 | 0.67 |
| | NT-04 | NS | NS | 0.24 | NS | 0.22 | 0.57 | 0.38 | 0.45 | 0.38 | 0.57 | 0.53 |
| | QLD-01 | NS | 0.30 | 0.20 | 0.44 | NS | 0.68 | 0.63 | 0.61 | 0.61 | 0.48 | 0.60 |
| | VIC-01 | NS | 0.34 | 0.32 | 0.36 | NS | 0.77 | 0.67 | 0.59 | 0.65 | 0.70 | 0.78 |
| OzNet | VIC-02 | NS | NS | 0.22 | 0.24 | NS | 0.47 | 0.33 | 0.34 | 0.40 | 0.40 | 0.40 |
| | NSW-01 | 0.38 | 0.34 | 0.46 | 0.38 | 0.30 | 0.52 | 0.51 | 0.52 | 0.51 | 0.38 | 0.41 |
| CosmOz | NSW-02 | 0.54 | 0.55 | 0.52 | 0.56 | 0.26 | 0.67 | 0.69 | 0.68 | 0.65 | 0.48 | 0.57 |
| | NSW-03 | NS | 0.33 | 0.48 | 0.27 | 0.33 | 0.58 | 0.59 | 0.55 | 0.62 | 0.32 | 0.51 |
| CosmOz | NSW-04 | 0.27 | 0.22 | 0.39 | 0.30 | 0.30 | 0.38 | 0.37 | 0.37 | 0.37 | 0.25 | 0.29 |
| | QLD-02 | NS | NS | NS | NS | 0.44 | 0.47 | 0.49 | 0.47 | 0.48 | 0.43 | 0.35 |
| CosmOz | QLD-03 | NS | 0.39 | 0.55 | 0.39 | 0.49 | 0.50 | 0.56 | 0.46 | 0.51 | 0.44 | 0.50 |
| | Range | 0.27–0.54 | 0.20–0.55 | 0.20–0.55 | 0.24–0.56 | 0.22–0.49 | 0.38–0.77 | 0.33–0.78 | 0.34–0.76 | 0.37–0.72 | 0.25–0.70 | 0.29–0.78 |
| CosmOz | N (sum) | 1455 | 1999 | 2721 | 3003 | 1859 | 4354 | 4354 | 4354 | 4354 | 4354 | 4354 |
| | N (range) | 75–151 | 64–178 | 158–235 | 202–254 | 125–164 | 317–337 | 317–337 | 317–337 | 317–337 | 317–337 | 317–337 |

NS: Not significant.

At the larger product scales soil moisture dynamics are more likely to be influenced by broad atmospheric controls (Brocca et al., 2014).

4.3. Time series visualisation

Visual inspection of the time series at each station location provided further insight into the differences in agreement of satellite and model soil moisture products with *in situ* measurements. The purpose of this section is to summarise the main features of interest within the time series to complement the findings of the correlation analysis.

The SMOS_LPRM_A and SMOS_LMEB_A products were shown to yield slightly higher correlation coefficients than other satellite products in the correlation analysis overall. This was reflected in the time series plots, where both products had a good visual fit to the *in situ* data. An example plot is shown in Fig. 4 at station NSW-03. Seasonal and annual cycles had a better visual fit to the *in situ* data than shorter term dynamics, particularly at the drier northern locations. Both SMOS products displayed a reduced sensitivity to soil moisture change during dry periods (e.g. soil moisture < 0.1 m³/m³), especially at the drier sites of the Northern Territory. It is noted that SMOS_LMEB_A often showed contrary short-term temporal behaviour to SMOS_LPRM_A during the periods of reduced sensitivity. The two AMSR2 soil moisture products were not as similar

as the two SMOS products. AMSR2_LPRM_D showed a tendency to dry down more slowly than *in situ*, displaying a more concave drying process. This behaviour was evident at all stations to some extent, but was most apparent at the end of the wet season at the drier Northern Territory locations, reflected in their lower correlation values there. An example of this effect is shown for NT-01 in Fig. 5. This effect was not observed in the AMSR2_JAXA_A time series. At some south-eastern Australian stations the winter wet period was on one occasion lagged by several months in the AMSR2_JAXA_A time series (NSW-04) or missed entirely (VIC-01 and VIC-02), resulting in a poorer correlation at these locations compared to the other satellite products (Table 3).

Similar to the other satellite products, the ASCAT_TUW_D product had a good visual fit to the *in situ* data, more so at annual and seasonal scales than for short-term dynamics. The time series of the ASCAT_TUW_D product was smoother than *in situ* at the drier, northern Australia stations, particularly those characterised by open wooded vegetation (e.g. NT-02, illustrated in Fig. 6).

Analysis of the WaterDyn, CABLE and API time series consistently showed a good visual temporal fit to *in situ* data across station locations (e.g. Fig. 7).

Analysis of the KBDI product time series showed a tendency to dry too slowly after wet periods and individual rainfall events (e.g. Fig. 8). The visual fit of the time series to *in situ* was generally better at the northern and eastern Australian locations. Long-term soil moisture

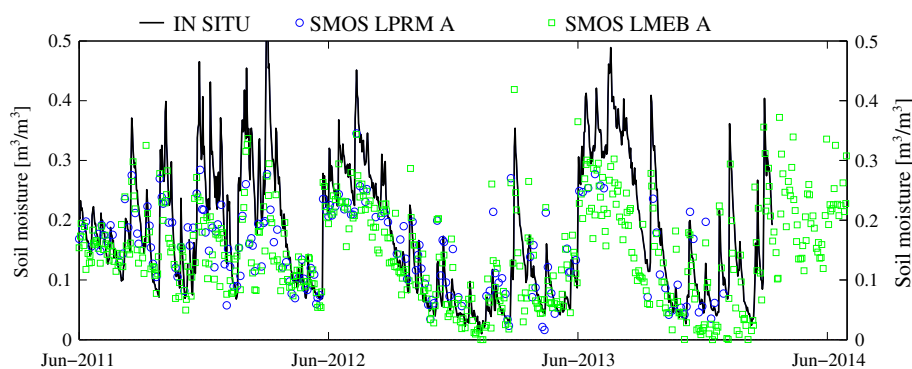


Fig. 4. SMOS_LPRM_A and SMOS_LMEB_A at NSW-03 (CosmOz network). *In situ* time series on left axes; product time series on right axes.

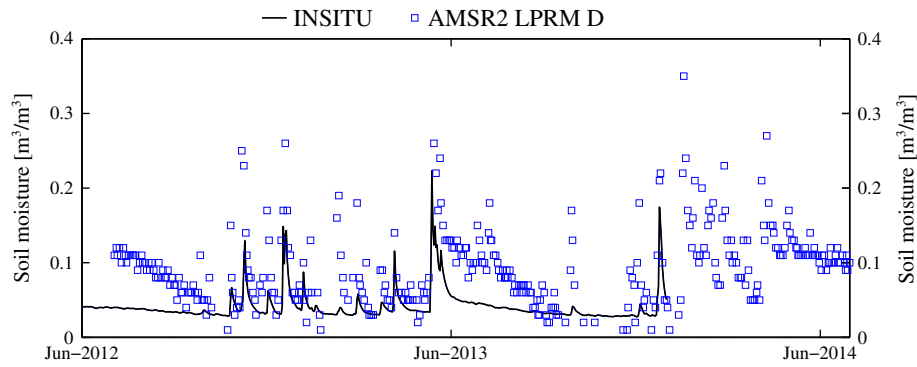


Fig. 5. AMSR2_LPRM_D at NT-01 (OzFlux network). *In situ* time series on left axes; product time series on right axes.

dynamics were not represented well at most stations in the south-east, as reflected in Fig. 3.

MSDI showed similar characteristics to KBDI in the time series plots. Dry down dynamics were also slow compared to the *in situ*, but to a lesser extent than KBDI at all sites and therefore MSDI achieved more favourable correlation values in both the longer and common periods of comparison.

Unlike the KBDI product, the AWRA-L time series occasionally showed a tendency to dry down too quickly compared to *in situ* measurements (Fig. 8). While this observation was evident at all stations, it was most prominent at the northern Australian locations where *in situ* measurements showed a prolonged period of decreasing soil moisture following the wet season. Nonetheless the overall wet/dry seasonal patterns were reflected well in the AWRA-L time series.

The short-term variability in *in situ* anomalies was noticeably larger at locations where cosmic-ray instruments were used. Soil moisture measurements from cosmic-ray sensors are subject to correction procedures, the largest of which relates to changes in atmospheric pressure (Hawdon et al., 2014), and may account for the increased short-term variability. This pattern of higher short-term variability at cosmic-ray sites compared to TDR and frequency-domain sensor sites in a similar location was also visible in the time series of absolute soil moisture values, but with more pronounced differences in correlation between products in the anomaly time series.

4.4. Cluster analysis

The cluster analysis was based on a matrix of $1-R^2$ values, with the aim of highlighting products that closely associate with each other.

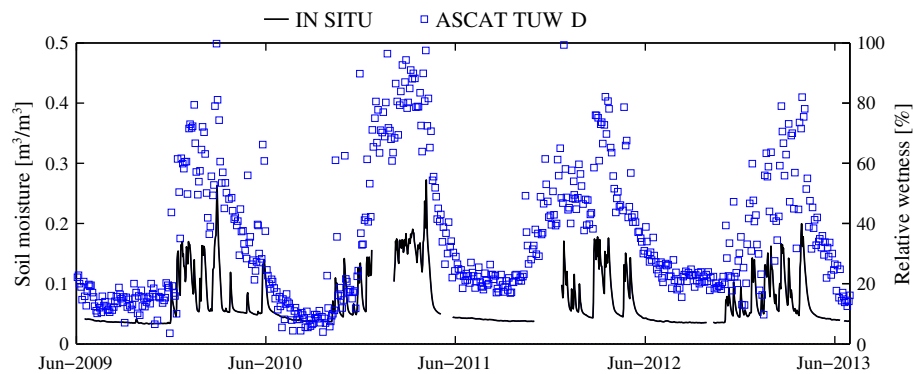


Fig. 6. ASCAT_TUW_D at NT-02 (OzFlux network). *In situ* time series on left axes; product time series on right axes.

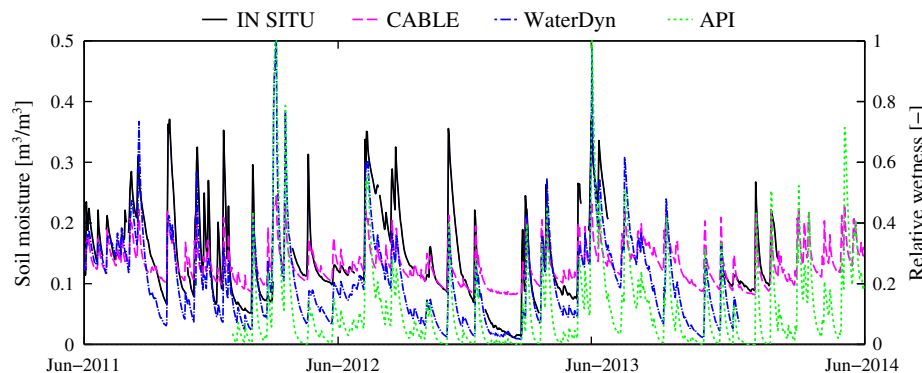


Fig. 7. CABLE, WaterDyn and API at NSW-02 (OzNet network). *In situ* and CABLE time series on left axes; WaterDyn and API time series on right axes.

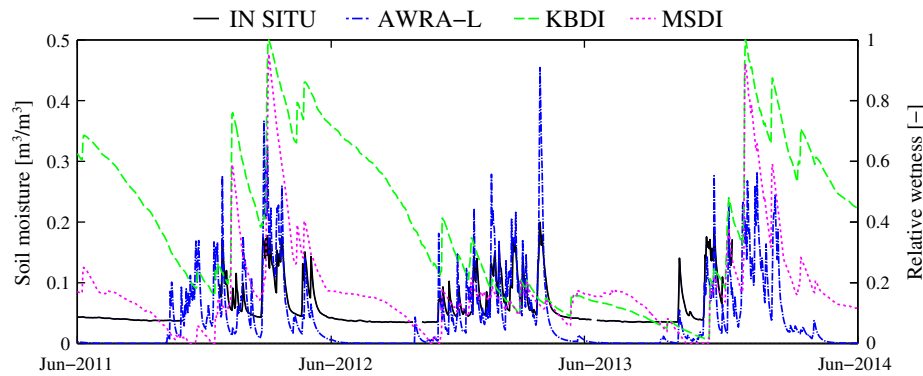


Fig. 8. AWRA-L (0–10 cm), KBDI and MSDI at NT-01 (OzFlux network). *In situ* time series on left axes; product time series on right axes.

Products that group together may indicate similarities in their error structure. Grouping is expected given that dependence exists among some products (e.g. model products use the same AWAP forcing data and both SMOS products use the same input brightness temperature data, as do the AMSR2 products).

A cluster analysis was carried out for each station location. The 1- R^2 matrices included all products (and *in situ* estimates) with the exception of SMOS_LPRM_A, which could not be correlated with some products due to a lack of coincident data, and so could not be included in the clustering matrices. Furthermore a cluster analysis could not be performed at QLD-02 due to a lack of significant correlation between SMOS_LMEB_A and other products at the $p = 0.01$ level. The hierarchical cluster dendrograms are provided in the Appendix for the longer period of comparison.

In general, satellite products clustered with other satellite products, and model products with model products, this being clearest at grassland climate zone locations NT-01, NT-04, NSW-01, NSW-02 and NSW-04, and temperate zone location VIC-02. At the remaining sites, the satellite/satellite and model/model groupings were less evident, often due to ASCAT_TUW_D, AMSR2_LPRM_D or AMSR2_JAXA_A grouping with one or more of the model products. Interestingly, SMOS_LMEB_A and ASCAT_TUW_D grouped at eight out of the 12 locations; however, no clear patterns between climate zones or vegetation types/density were apparent. As expected, KBDI and MSDI showed a close association and paired at all but one site. The WaterDyn, CABLE, AWRA-L and API products grouped together at most locations, with AWRA-L grouping with API at nine locations. WaterDyn and CABLE paired closely, particularly at the NT grassland zone stations. AMSR2_LPRM_D and AMSR2_JAXA_A did not group (*i.e.* were different to each other) at 10 out of 12 sites. *In situ* measurements grouped closely with models at nine out of 12 sites, but did not show a preference for a particular model product.

It is noted that filtering of the product time series, or analysis of the time series on a longer time scale (e.g. monthly), may potentially bring out similarities not observed here. Strong variability in the soil moisture record is present at daily time scales. On a daily time scale, there is a mismatch of sampling times between satellites and *in situ* measurements, and often models are forced with inexact timing of precipitation events (Reichle et al., 2004).

5. Discussion

5.1. Comparison with previous studies

The results of the correlation analysis are comparable to other studies, which mainly focus on the OzNet *in situ* network in

south-eastern Australia. For example Van der Schalie et al. (2015) compared SMOS_LPRM (ascending) to OzNet sites NSW-01 and NSW-02 for the period 2010–2011. The LPRM was run for the SMOS data set using two alternative sources of effective soil temperature input data and several incidence angles. Their study estimated correlation coefficients at sites NSW-01 and NSW-02 (on average for all incidence angles and input sources) of 0.75 and 0.88, respectively. This compared well to the findings in this study ($R = 0.74$ and $R = 0.69$ in the longer and common periods at NSW-01, and $R = 0.78$ and 0.81 at NSW-02; Tables 3 and 5). Van der Schalie et al. (2015) also compared *in situ* data to the SMOS_LMEB product, and estimated very similar correlation coefficients to SMOS_LPRM.

Su et al. (2013) also compared OzNet *in situ* data to satellite products, including ASCAT_TUW and SMOS_LMEB, for the period 2001–2012. Average correlation between all sites and ASCAT_TUW was estimated to be 0.67 (descending overpass), similar to that found in this study for the period 2001–2014 (range of 0.68–0.72 of stations NSW-01, NSW-02 and NSW-04; Table 3). The association between SMOS_LMEB and *in situ* was weaker in the previous study ($R = 0.71$ compared to 0.78–0.81 here, ascending overpass) noting that the 2013 study used an earlier version of the SMOS_LMEB product.

Frost et al. (2015) compared monthly 0–5 cm *in situ* surface soil moisture measurements from 38 sites in the OzNet network (December 2001–May 2012) to estimates derived from CABLE, WaterDyn and AWRA-L models, as well as ASCAT_TUW. CABLE and WaterDyn were found to perform more strongly than AWRA-L and ASCAT_TUW_D at OzNet sites, consistent with the findings in this study. Furthermore, Frost et al. (2015) found that CABLE and AWRA-L were better than WaterDyn when compared to deeper profile (0–90 cm) *in situ* measurements, a result reflected in this study.

Lastly, Kumar et al. (in press) compared KBDI and MSDI estimates with OzNet data for the period September 2009 to May 2011. Kumar et al. (in press) reported the average correlation between the 0–30 cm *in situ* measurements and KBDI as 0.60, and 0.71 for MSDI. These values are higher than those found in this study between the 0–10 cm *in situ* measurements and KBDI (0.45 and 0.42 at NSW-01 and NSW-02 respectively) and MSDI (0.66 and 0.68 at NSW-01 and NSW-02 respectively).

5.2. Satellite performance

The range of agreement with *in situ* estimates was similar among the satellite products, with the exception of AMSR2_JAXA_A. SMOS_LPRM_A and SMOS_LMEB_A showed a closer association to *in situ* estimates at most sites compared to other satellite products. Both SMOS products better reflected annual and seasonal variation

than short-term events. The process driving the strength of the SMOS L-band instrument is the estimation of soil moisture at a greater observation depth than the other satellites, which utilise the shorter wavelengths of the C- and X-bands. The longer wavelength of the L-band instrument is also beneficial in that it is less influenced by cloud and vegetation cover (De Jeu et al., 2008). These benefits are consistent with the findings of this study, where close association with *in situ* data was found consistently across station locations with different soil and vegetation characteristics and climate zones with the exception of QLD-02, a site located within dense tropical vegetation. At this site both SMOS products showed limited agreement with *in situ* measurements, corresponding to the known limitation of the LPRM over densely forested areas (Van der Schalie et al., 2016). At this particular site, ASCAT_TUW_D was better able to reflect *in situ* temporal dynamics than SMOS. Furthermore, both SMOS products displayed a reduced sensitivity to soil moisture change during dry periods, especially at the drier sites of the Northern Territory. This is in line with De Jeu et al. (2008), where it was shown that the dielectric constant has a reduced sensitivity to changes in soil moisture under dry conditions.

AMSR2_LPRM (C-band) exhibited clear differences in correspondence with *in situ* measurements during the daytime (ascending) and night-time (descending) parts of the orbit (Fig. 2). The process driving this finding is likely in part the differing of canopy and surface soil temperatures from the assumption of equality in the LPRM method. More intense heating of the ground surface in the daytime is noted by Owe et al. (2008) as being a significant problem for arid, semi-arid and possibly temperate regions as well, especially in areas with a high proportion of bare soil, a common feature across much of Australia. The estimation of effective temperature is an area of ongoing improvement in the LPRM development. Furthermore, vegetation density may also be affecting the difference in daytime ascending and night-time descending overpass retrievals, especially at the tropical rainforest site QLD-02. Lei et al. (2015) show that in the United States the relative advantage of night-time retrievals (of AMSR-E, predecessor of AMSR2) degraded over more heavily vegetated areas, and may help explain this result.

The AMSR2_LPRM_D product showed a moderately close association with *in situ* data overall, yet displayed slower dry down behaviour particularly within the grassland and tropical locations of the Northern Territory. The process driving this observation may be the greater influence of vegetation on the brightness temperatures in the C-band, causing the area of the satellite footprint to appear wetter for longer at the end of wet periods than in the deeper penetrating L-band. For example where *in situ* sensors are located in an area of bare soil or grass within a woodland or savannah, the soil moisture as recorded by the sensor would *a priori* be expected to rise and fall more rapidly compared to a smoother signal from the taller, more established vegetation within the satellite footprint. The smoother soil moisture signal of the satellite product is matched by the vegetation optical depth signal, sourced in parallel with AMSR2 C-band soil moisture retrievals.

While the dry down processes observed in the ASCAT_TUW_D time series better matched *in situ* data than AMSR2_LPRM_D, it showed a similarly smooth signal at some locations. However, a strength of ASCAT_TUW is the ability to separate backscatter due to soil moisture and vegetation. The soil moisture data set may be improved in future through the inclusion of dynamic vegetation correction (Vreugdenhil et al., 2016).

Moreover, the success of ASCAT_TUW_D in reflecting *in situ* temporal dynamics at a site of dense tropical vegetation (QLD-02) compared to the SMOS and AMSR2 products may be indicative of a potential relative product strength. This is in line with previous studies that compared soil moisture estimates retrieved from ASCAT with those retrieved from passive microwave sensors (e.g. Al-Yaari et al., 2014).

AMSR2_JAXA_A performed most poorly among the satellite products in terms of correlation of relative soil moisture values. The assumption in the JAXA algorithm of a constant surface and canopy temperature of 295 K ($\approx 22^\circ\text{C}$) at all locations and times is not reflective of the range of Australian conditions (e.g. see mean annual temperature ranges of sites in Table 1), and may represent an important weakness of this product over Australia.

Tests carried out to assess how the correlation varied when different satellite product pairs were colocated in time showed differences of approximately 5–10% compared to the correlation based on all coincident satellite and *in situ* finite values. Considerable differences were observed at site NT-04 (in the SMOS_L3_A data set when colocated with AMSR2_LPRM_D), suggesting the agreement between *in situ* and remotely sensed soil moisture may be more sensitive at this site than at others considered. This is reasonable given that NT-04 is located within a grassy plain in northern Australia where soil moisture is typically quite variable. However, it should be kept in mind that the change in correlation at these two sites when satellite pairs were colocated in time was based on fewer data points than when all coincident satellite and *in situ* points were considered.

5.3. Model performance

In the correlation analysis the WaterDyn product had the strongest agreement with *in situ* measurements across all products considered in this study, and most consistently across locations in different climate zones and with different soil and vegetation characteristics. The calculation of the upper soil layer water mass balance and subsequent conversion to relative soil moisture proved to effectively simulate soil moisture temporal dynamics as measured by the *in situ* sensors. CABLE was similarly able to reproduce *in situ* temporal dynamics, but was less consistent across climate zones (particularly at the temperate locations) compared to WaterDyn.

The API data set was found to be quite successful in simulating annual and seasonal dynamics of soil moisture across all station locations and climate zones considered in this study. The variation in performance across locations may be indicative of variation in the rainfall input data quality, and would need to be further tested, including an inspection of gauge inputs to the gridded data. The success is particularly compelling given the simplified nature of the index, based only on rainfall and temperature data inputs. The simplicity of the API index is considered a strength of this product. However API does not consider ecohydrological processes and energy fluxes. Instead, these are strengths of the AWRA-L model, which is process-based and includes sub-routines for water and energy fluxes, allowing vegetation to adjust accordingly.

Although the AWRA-L product correlated well with shallow *in situ* measurements at most locations, AWRA-L showed poorer agreement than API at seven locations (longer period). While no clear geographical or climatic pattern was discernible in the AWRA-L correlation results, it is possible that the association was affected by the calibration of the model to streamflow observations. When comparing deeper (0–90 cm) soil moisture measurements and AWRA-L, the correlation remained the same at one site (NSW-01) and reduced at another (NSW-02). Frost et al. (2015) undertook a more comprehensive assessment of deeper (0–90 cm) soil moisture measurements with AWRA-L in south-east Australia (at over 30 sites) and found correlation coefficients in the order $0.7 < R < 0.8$, indicating AWRA-L may be able to effectively simulate both surface and root-zone soil moisture in this area. Frost et al. (2015) found CABLE to perform similarly to AWRA-L in the deeper profile in this area, and WaterDyn slightly worse.

The weaker agreement of KBDI reflected the poor simulation of drying processes observed in the *in situ* measurements. In terms of mimicking *in situ* soil moisture temporal behaviour, the processes

driving the weakness of KBDI were two-fold. Firstly, ET is a function of vegetation cover in the KBDI model, which is itself a function of mean annual rainfall. It does not consider other factors affecting the likelihood of the vegetation being present such as soil type or latitude (Keetch and Byram, 1968). Moreover, modelled ET was only controlled by rainfall and temperature (and the previous day's soil moisture condition), without consideration of other meteorological factors such as net radiation, wind speed, or relative humidity. Secondly, the KBDI model is simplified and does not consider additional processes such as deep drainage or spatiotemporal changes to infiltration. Overall, KBDI displayed the greatest variability in performance across the sites, showing particular variability among the locations in the grassland climate zone.

While the MSDI model is similar to KBDI, its relative strength lies in the different simulation of rainfall-runoff and ET. In KBDI rainfall infiltrating the soil is lessened by a constant 5 mm of the first part of the event, regardless of vegetation cover or how the loss is partitioned between canopy interception and runoff (Finkele et al., 2006). MSDI treats them separately, and varies them depending on vegetation cover. Each grid cell is assigned one of seven vegetation classes, each with their own values of canopy interception, canopy storage and wet evaporation rates (Finkele et al., 2006). While the estimation of ET in the MSDI model is slightly more comprehensive than in KBDI, a weakness of MSDI is that it uses linear relationships between monthly pan evaporation and monthly maximum temperatures from capital cities in the south-east of Australia only, and yet is applied nation-wide across all climate zones (Kumar et al. in press; Finkele et al., 2006). Lastly, evaporation is again only a function of rainfall and temperature, and vegetation cannot adjust based on water or energy availability as it can in AWRA-L.

Although the model products achieved stronger coefficients of correlation than the satellite products in many instances, it should be noted that the strength of the model products may be in part due to their higher resolution (Table 2). Despite the model products showing stronger agreement with *in situ* measurements than the satellite products in many instances, this was not always the case, and may be partially attributed to the greater number of data points used in the correlation between model and *in situ* estimates (Tables 3 and 5), as well as to the differences in methodological approach.

5.4. Interrelationships between products

The results of the cluster analysis showed some grouping of products. Generally satellite products grouped with other satellite products, and model products with other model products, indicating potential duplication of information and potential similarities in error structures between satellite-satellite and model-model groups. However the general distinction between satellite and model products from each other indicates complementarity may exist between the data sets. Both have implications for applications utilising multiple products such as land surface model data assimilation.

It may be expected that products sharing commonalities in their approach (e.g. models share AWAP forcing data; some satellites share the same microwave sensing frequency) would cluster closely together. However, despite general grouping of satellite products with other satellites and models with models, this was not always the case. For instance, the lack of grouping between the AMSR2 products at most sites highlights the dissimilar nature of these soil moisture estimates, despite their common brightness temperatures, indicating a potential lack of commonality in their error structures and potential complementarity.

On the other hand, despite their very different approaches, the strong intercorrelation ($R > 0.85$) and close grouping of API and AWRA-L in the cluster analyses indicates that the net effect of precipitation infiltration, soil evaporation and drainage of the top soil layer

in the AWRA-L model produces very similar temporal behaviour to the API model, driven only by precipitation and temperature.

WaterDyn and CABLE intercorrelated strongly in the cluster analyses ($R > 0.75$) and particularly at the Northern Territory sites ($R > 0.94$). The two models also yielded similarly strong correlation coefficients with *in situ* at the Northern Territory sites, particularly in the longer period (both $R > 0.79$). This indicates that the models are most similar in their ability to successfully reproduce *in situ* temporal dynamics, and suggests that their model approaches are most similar to each other, at these sites.

Moreover, KBDI and MSDI paired closely, intercorrelating very strongly (range: 0.73–0.99) across the sites. This result confirms the similarity in the index model approaches, and indicates potential similarity in error structure.

Lastly, the tendency of SMOS_LMEB_A and ASCAT_TUW_D to cluster together at most locations reflects their strong temporal intercorrelation (range: 0.64–0.87) despite their differing sensors, algorithms and observation depths. That there was no clear pattern between climate zones and vegetation type/density from the clustering suggests other factors may be influencing the strong similarity in temporal soil moisture dynamics between SMOS_LMEB_A and ASCAT_TUW_D. Future clustering with SMOS_LPRM_A may help distinguish whether the similarity is algorithm-based, or more attributable to instrument features such as spatial resolution, microwave frequency and observation depth, or other factors.

6. Conclusions

This study sought to compare a wide range of sources of surface soil moisture information in a common framework, to understand how their relative performance varies across Australia and how products interrelate. To this end, 11 sources of soil moisture data were evaluated; five satellite and six model products, plus *in situ* data from three separate networks across the country. The Pearson correlation coefficient was used as the primary statistical metric to evaluate the relative temporal fit between satellite and model data sets with *in situ* measurements, which served as a reference.

The comparison of the products, as measured by their correlation with *in situ* estimates, varied between products and locations around Australia. The satellite products displayed an overall similar level of temporal association with *in situ* measurements, with the possible exception of AMSR2_JAXA_A. The two SMOS products showed the closest association with *in situ* estimates at most sites across the climate zones, owing to the deeper observation depth of the L-band sensor, with the exception of one site located in an area of dense tropical vegetation.

The AMSR2_LPRM_D and ASCAT_TUW_D products showed slower dry down behaviour than *in situ* measurements, likely a result of the greater influence of vegetation on the brightness temperatures in the C-band. The poorer temporal association of AMSR2_JAXA_A with *in situ* compared to the other satellite products may be due to the assumption in the retrieval algorithm of a constant surface and canopy temperature at all locations and times, and assumption not reflective of the range of Australian conditions.

The WaterDyn model, followed closely by CABLE, showed the closest association with *in situ* estimates out of the model products. API and AWRA-L also yielded strong agreement with *in situ* estimates.

API highlights how a simplified measure can in this case prove to be almost as successful as comprehensive process-based models in simulating temporal surface soil moisture dynamics on a daily basis. API is an index used as a proxy for soil moisture, and is a function of rainfall and temperature only. The variation in performance across sites may be indicative of variation in quality of the input data, particularly rainfall, and requires further examination. The utility

of satellite-based rainfall may also be considered, and may prove particularly useful in gauge-sparse areas.

KBDI displayed slower dry down behaviour compared to *in situ* measurements and had the highest variability across sites and climate zones of all products. The related index, MSDI, was slightly more successful at reproducing *in situ* temporal dynamics but showed poorer consistency than the strongest performing models.

The comparison of products may differ when considering different temporal and spatial scales, and it is recommended that future work consider this where commensurate with product application. All products were better able to reflect the interannual and seasonal temporal behaviour of the *in situ* reference than short-term dynamics, as reflected in the poorer temporal anomaly correlation results.

In situ soil moisture data sourced from cosmic-ray sensors were evaluated alongside soil moisture data collected from more traditional TDR and frequency-domain sensors. Cosmic-ray sensors vary in effective depth dependent on soil moisture, as satellite observations do. Future research may consider investigating the difference in correlation between satellite remotely sensed estimates and cosmic-ray sensors and their TDR counterparts, where both sets of *in situ* data are available at the same station location.

Clustering analysis revealed a general grouping of satellite products with other satellite products, and model products with model products. The general distinction between model and satellite products indicated potential complementarity between the data sources, whereas clustering of product pairs within the model and satellite

categories suggested potential similarities in error structure and duplicate information may exist between products.

Acknowledgements

This research was undertaken as part of the Australian Energy and Water Exchange research initiative (OzEWEX) Soil Water Estimation and Evaluation Project (SWEEX) whose aim is to evaluate soil moisture products against *in situ* observations across a variety of landscapes in order to identify when and where certain products are better than others. The soil moisture data sets used in this study can be accessed at www.ozewex.org/project_data.

The authors thank all those involved in the provision of soil moisture data, including: the CSIRO funded CosmOz network (cosmoz.csiro.au) and Aaron Hawdon for provision of data; the University of Melbourne and Monash University for provision of data and Xiaoling Wu, Alessandra Monerris-Belda, Frank Winston and Rodger Yound for data processing and network maintenance of the OzNet network; TU Wien for the production of the ASCAT data set; the Japan Aerospace Exploration Agency for the provision of the AMSR2_JAXA data set; the Centre Aval de Traitement des Données in France for the provision of the SMOS_LMEB data set. Vanessa Haverd, Cathy Trudinger and Peter Briggs thank the support of the Australian Climate Change Science Program. The contribution of Richard De Jeu and Robin Van Der Schalie was funded by the European Space Agency through the Climate Change Initiative for Soil Moisture (Contract 4000104814/11/I-NB). Finally, the authors wish to thank the three anonymous reviewers whose comments and suggestions helped improve the paper.

Appendix: cluster dendrograms by station

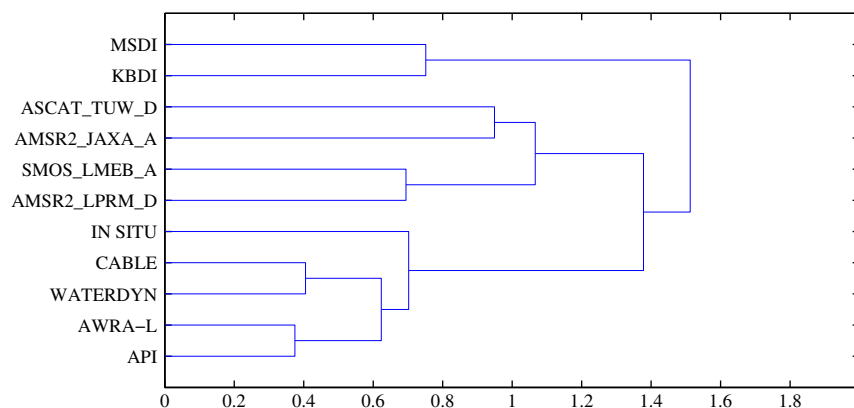


Fig. A1. NT-01.

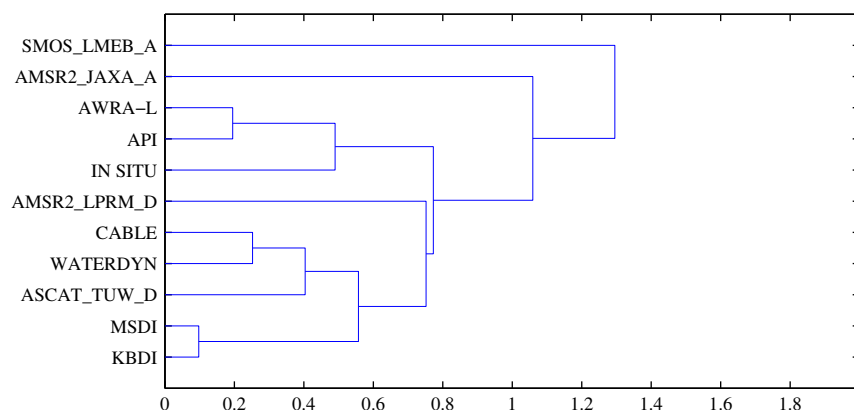


Fig. A2. NT-02.

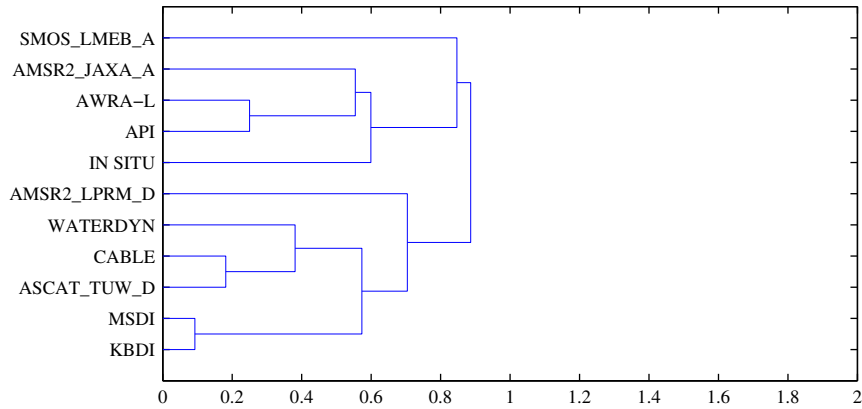


Fig. A3. NT-03.

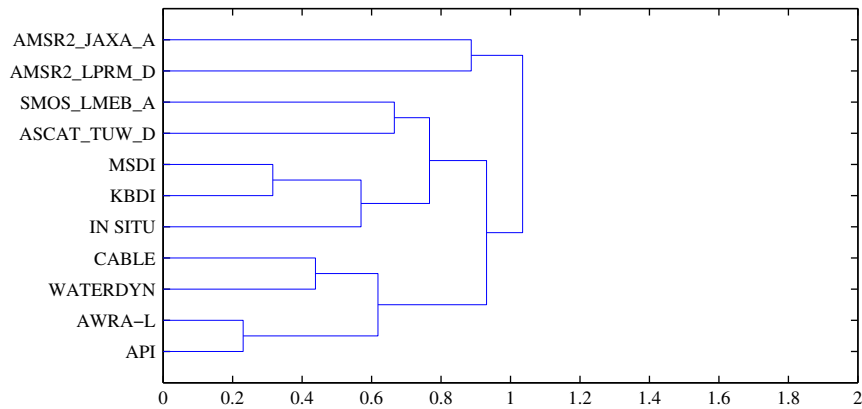


Fig. A4. NT-04.

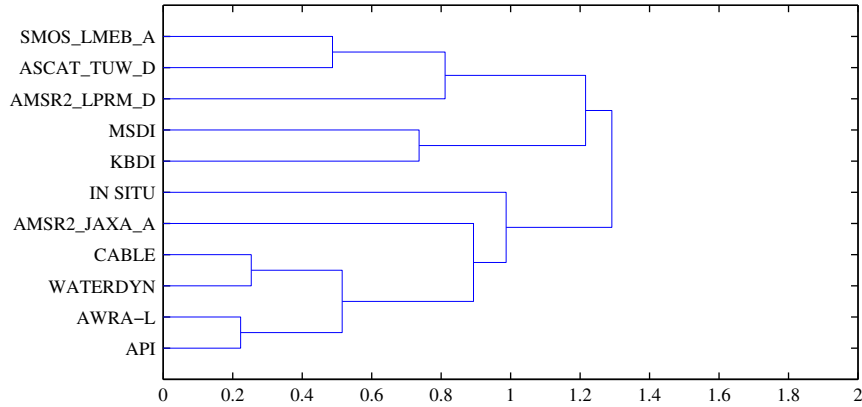


Fig. A5. QLD-01.

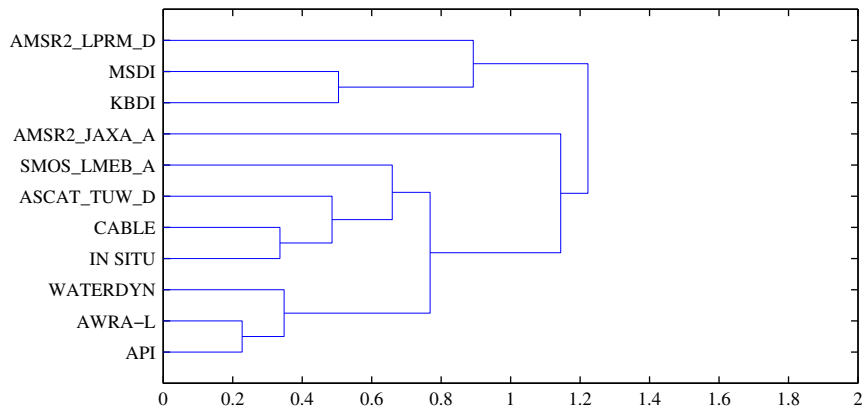


Fig. A6. QLD-03.

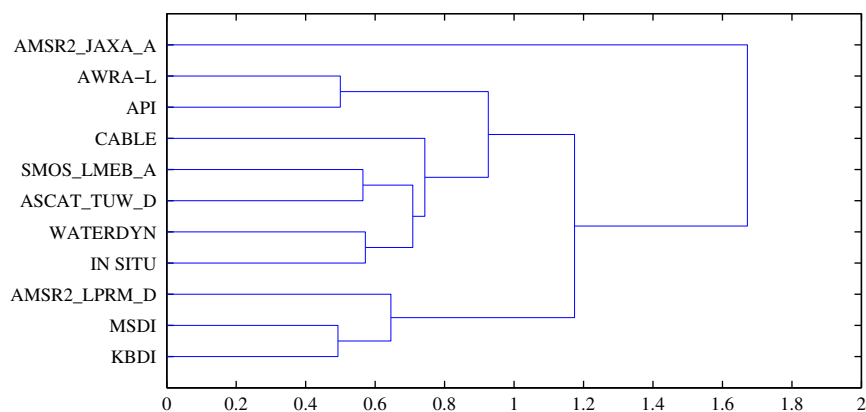


Fig. A7. VIC-01.

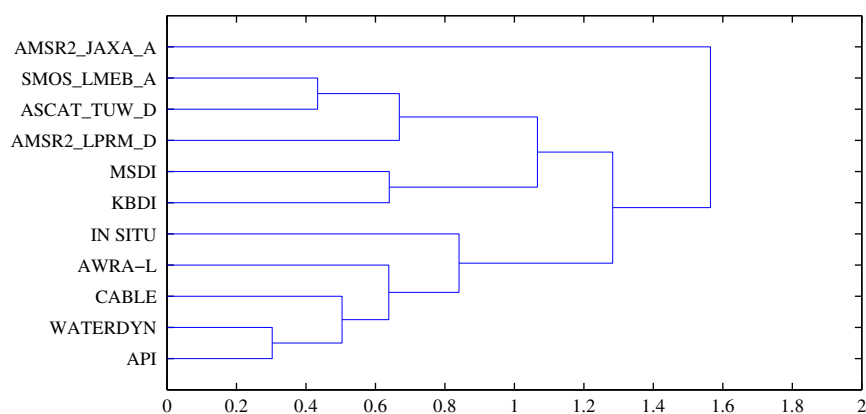


Fig. A8. VIC-02.

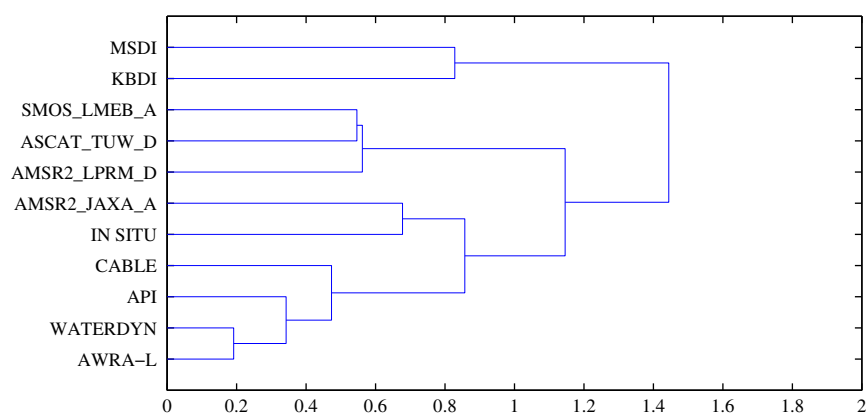


Fig. A9. NSW-01.

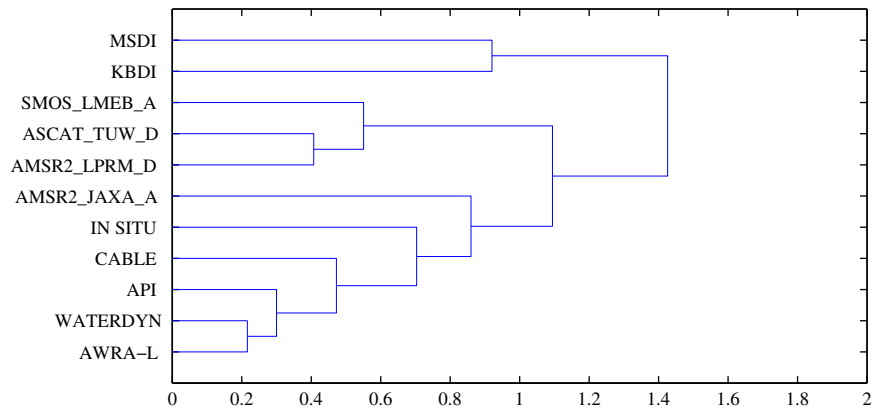


Fig. A10. NSW-02.

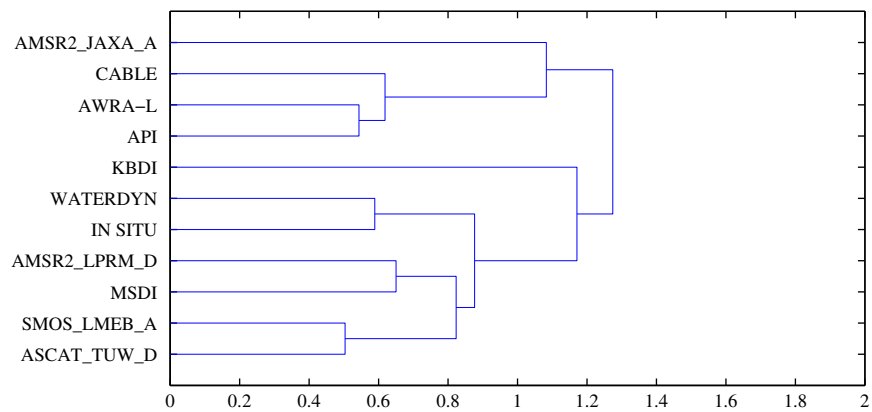


Fig. A11. NSW-03.

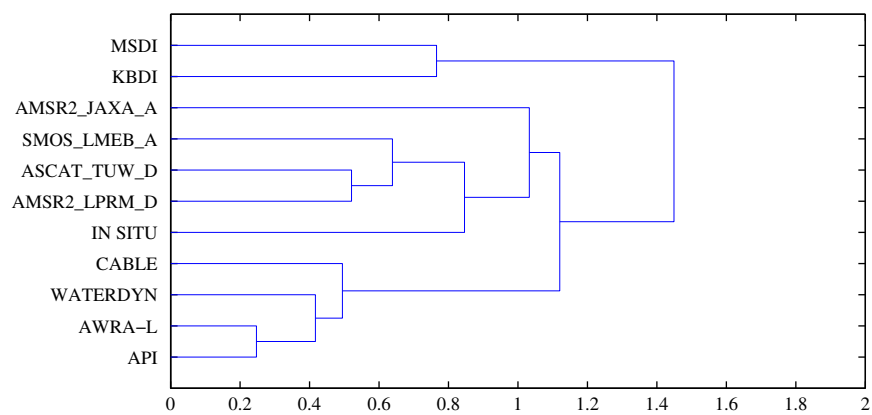


Fig. A12. NSW-04.

References

- Albergel, C., de Rosnay, P., Gruhier, C., Munoz-Sabater, J., Hasenauer, S., Isaksen, I., Kerr, Y., Wagner, W., 2012. Evaluation of remotely sensed and modelled soil moisture products using global ground-based in situ observations. *Remote Sens. Environ.* 118, 215–226.
- Albergel, C., Rüdiger, C., Carrer, D., Calvet, J.C., Fritz, N., Naeimi, V., Bartalis, Z., Hasenauer, S., 2009. An evaluation of ASCAT surface soil moisture products with in-situ observations in southwestern France. *Hydrol. Earth Syst. Sci.* 13, 115–124.
- Al-Yaari, A., Wigneron, J.P., Ducharme, A., Kerr, Y.H., Wagner, W., De Lannoy, G., Reichle, R., Al Bitar, A., Dorigo, W., Richaume, P., Mialon, A., 2014. Global-scale comparison of passive (SMOS) and active (ASCAT) satellite based microwave soil moisture retrievals with soil moisture simulations (MERRA-land). *Remote Sens. Environ.* 152, 614–626.
- Baldocchi, D., 2008. Breathing of the terrestrial biosphere: lessons learned from a global network of carbon dioxide flux measurement systems. *Australian J. Botany* 56, 1–26.
- Beringer, J., 2013. Dry River Ozflux Tower Site Ozflux: Australian and New Zealand Flux Research and Monitoring Hdl: 102.100.100/ 14229.
- Beringer, J., 2013a. Sturt Plains Ozflux Tower Site Ozflux: Australian and New Zealand Flux Research and Monitoring Hdl: 102.100.100/ 14230.
- Beringer, J., 2013b. Whroo Ozflux Tower Site Ozflux: Australian and New Zealand Flux Research and Monitoring Hdl: 102.100.100/ 14232.
- Beringer, J., 2014. Red Dirt Melon Farm Ozflux Tower Site Ozflux: Australian and New Zealand Flux Research and Monitoring Hdl: 102.100.100/ 14245.
- Beringer, J., 2014a. Riggs Creek Ozflux Tower Site Ozflux: Australian and New Zealand Flux Research and Monitoring Hdl: 102.100.100/ 14246.
- Briggs, P.R., 2016. Personal Communications.
- Brocca, L., Zucco, G., Mittelbach, H., Moramarco, T., Seneviratne, S.I., 2014. Absolute versus temporal anomaly and percent of saturation soil moisture spatial variability for six networks worldwide. *Water Resour. Res.* 50, 5560–5576.
- Brocca, L., Hasenauer, S., Lacava, T., Melone, F., Moramarco, T., Wagner, W., Dorigo, W., Matgen, P., Martinez Fernández, J., Llorens, P., Latron, J., Martin, C., Bittelli, M., 2011. Soil moisture estimation through ASCAT and AMSR-e sensors: an inter-comparison and validation study across Europe. *Remote Sens. Environ.* 116, 3390–3408.
- Bureau of Meteorology, 2016. Mangalore Airport monthly rainfall.
- Bureau of Meteorology, 2016a. Yanco Agricultural Institute monthly lowest temperature and monthly highest temperature.
- Bureau of Meteorology, 2016b. Peak Hill Post Office monthly lowest temperature and monthly highest temperature.
- Bureau of Meteorology, 2016c. Walkamin Research Station monthly lowest temperature and monthly highest temperature.
- Bureau of Meteorology, 2016d. Charters Towers Airport monthly lowest temperature and monthly highest temperature.
- Bureau of Meteorology, 2012. Climate classification maps: Köppen major classes.
- Choudhury, B.J., Blanchard, B.J., 1983. Simulating soil water recession coefficients for agricultural watersheds. *Am. Wat. Resour.* 19 (2), 241–247.
- Cleverly, J., 2011. Alice Springs Mulga Ozflux Site Ozflux: Australian and New Zealand flux research and monitoring network.
- Crow, W.T., Bindlish, R., Jackson, T.J., 2005. The added value of spaceborne passive microwave soil moisture retrievals for forecasting rainfall-runoff partitioning. *Geophys. Res. Lett.* 32, L18401.
- CSIRO, 2015. Australian cosmic-ray neutron soil moisture monitoring network. accessed 17/03/2015.
- De Jeu, R.A.M., Wagner, W., Holmes, T.R.H., Dolman, A.J., Van de Giesen, N.C., Friesen, J., 2008. Global soil moisture patterns observed by space borne microwave radiometers and scatterometers. *Surv. Geophys.* 29, 399–420.
- Desilets, D., Zreda, M., Ferre, T.P.A., 2010. Nature's neutron probe: land surface hydrology at an elusive scale with cosmic rays. *Water Resour. Res.* 46. <http://dx.doi.org/10.1029/2009wr008726>.
- Dharssi, I., Bovis, K.J., Macpherson, B., Jones, C.P., 2011. Operational assimilation of ASCAT surface soil wetness at the Met office. *Hydrol. Earth Syst. Sci.* 15, 2729–2746.
- Dorigo, W.A., Gruber, A., De Jeu, R.A.M., Wagner, W., Stacke, T., Loew, A., Albergel, C., Brocca, L., Chung, D., Parinussa, R.M., Kidd, R., 2015. Evaluation of the ESA CCI soil moisture product using ground-based observations. *Remote Sens. Environ.* 162, 380–395.
- Draper, C.S., Walker, J.P., Steinle, P.J., De Jeu, R.A.M., Holmes, T.R.H., 2009. An evaluation of AMSR-e derived soil moisture over Australia. *Remote Sens. Environ.* 113, 703–710.
- Draper, C.S., 2011. Near-surface Soil Moisture Assimilation in NWP. University of Melbourne Australia. Doctor of Philosophy Thesis.
- Escorihuela, M.J., Chanzy, A., Wigneron, J.P., Kerr, Y.H., 2010. Effective soil moisture sampling depth of L-band radiometry: a case study. *Remote Sens. Environ.* 114, 995–1001.
- Finkele, K., Mills, G.A., Beard, G., Jones, D.A., 2006. National daily gridded soil moisture deficit and drought factors for use in prediction of forest fire danger index in Australia. BMRC Research Report no. 119.
- Franz, T.E., Zreda, M., Ferre, T.P.A., Rosolem, R., Zweck, C., Stillman, S., Zeng, X., Shuttleworth, W.J., 2012. Measurement depth of the cosmic ray soil moisture probe affected by hydrogen from various sources. *Water Resour. Res.* 48, W08515.
- Frost, A.J., Ramchurn, A., Hafeez, M., Zhao, F., Haverd, V., Beringer, J., Briggs, P., 2015. Evaluation of AWRA-I: the Australian water resource assessment model. 21st International Congress on Modelling and Simulation 29 November to 4 December 2015.
- Haverd, V., Raupach, M.R., Briggs, P.R., Canadell, J.G., Isaac, P., Pickett-Heaps, C., Roxburgh, S.H., Van Gorsel, E., Viscarra Rossel, R.A., Wang, Z., 2013. Multiple observation types reduce uncertainty in Australia's terrestrial carbon and water cycles. *Biogeosciences* 10, 2011–2040.
- Haverd, V., Cuntz, M., 2010. Soil-litter-iso: a one-dimensional model for coupled transport of heat, water and stable isotopes in soil with a litter layer and root extraction. *J. Hyd.* 388, 438–455.
- Hawdon, A., McJannet, D., Wallace, J., 2014. Calibration and correction procedures for cosmic-ray neutron soil moisture probes located across Australia. *Water Resour. Res.* 50, 5029–5043.
- Imaoka, K., Kachi, M., Fujii, H., Murakami, H., Hori, M., Ono, A., Igarashi, T., Nakagawa, K., Oki, T., Honda, Y., Shimoda, H., 2010. Global Change Observation Mission (GCOM) for monitoring carbon, water cycles and climate change. *Proc. IEEE* 98 (5), 717–734.
- Jackson, T.J., Bindlish, R., Cosh, M.H., Zhao, T., Starks, P.J., Bosch, D.D., Seyfried, M., Moran, M.S., Goodrich, D.C., Kerr, Y.H., Leroux, D., 2012. Validation of soil moisture and ocean salinity (SMOS) soil moisture over watershed networks in the U.S. *IEEE Trans. Geos. Rem. Sens.* 50 (5), 1530–1543.
- Jackson, T.J., Cosh, M.H., Bindlish, R., Starks, P.J., Bosch, D.D., Seyfried, M., Goodrich, D.C., Moran, M.S., Du, J., 2010. Validation of advanced microwave scanning radiometer soil moisture products. *IEEE Trans. Geos. Rem. Sens.* 48 (12), 4256–4272.
- Jones, D.A., Wang, W., Fawcett, R., 2009. High quality spatial climate data sets for Australia. *Aust. Meteor., Ocean., J.* 58, 233–248.
- Keetch, J.J., Byram, G.M., 1968. A drought index for forest fire control. Research Paper SE-380 U.S.D.A Department of Agriculture Forest Service.
- Kerr, Y.H., Waldteufel, P., Richaume, P., Wigneron, J.P., Ferrazzoli, P., Mahmoodi, A., Al Bitar, A., Cabot, F., Gruhier, C., Enache Juglea, S., Leroux, D., Mialon, A., Delwart, S., 2012. The SMOS soil moisture retrieval algorithm. *IEEE Trans. Geos. Rem. Sens.* 50 (5), 1384–1403.
- Kerr, Y.H., Wigneron, J.P., Boutin, J., Escorihuela, M.J., Font, J., Reul, N., Gruhier, C., Enache Juglea, S., Drinkwater, M.R., Hahne, A., Martín-Neira, M., Mecklenburg, S., 2010. The SMOS mission: new tool for monitoring key elements of the global water cycle. *Proc. IEEE* 98 (5), 666–687.
- Kim, S., Liu, Y.Y., Johnson, F.M., Parinussa, R.M., Sharma, A., 2015. A global comparison of alternate AMSR2 soil moisture products: why do they differ? *Remote Sens. Environ.* 161, 43–62.
- Kohler, M.A., Linsley, R.K., 1951. Predicting the Runoff From Storm Rainfall. U.S. Weather Bureau, Washington D.C.
- Kumar, V., Dharssi, I., Bally, J., Steinle, P., McJannet, D., Walker, J., 2016. Verification of soil moisture from multiple models over Australia for fire danger rating application. *Water Resour. Res.* (in press).
- Lei, F., Crow, W.T., Shen, H., Parinussa, R.M., Holmes, T.R., 2015. The impact of local acquisition time on the accuracy of microwave surface soil moisture retrievals over the contiguous United States. *Remote Sens.* 7, 13448–13465.
- Liu, Y., Van Dijk, A.I.J.M., De Jeu, R.A.M., Holmes, T., 2009. An analysis of spatiotemporal variations of soil and vegetation moisture from a 29-year satellite-derived data set over mainland Australia. *Water Resour. Res.* 45, W07405.
- Liu, Y., De Jeu, R.A.M., Van Dijk, A.I.J.M., Owe, M., 2007. TRMM-TMI satellite observed soil moisture and vegetation density (1998–2005) show strong connection with El Niño in eastern Australia. *Geophys. Res. Lett.* 34, L15401. <http://dx.doi.org/10.1029/2007GL030311>.
- Loew, A., 2014. Terrestrial satellite records for climate studies: how long is long enough? A test case for the Sahel. *Theor. Appl. Climatol.* 115, 427–440.
- Maeda, T., Taniguchi, Y., 2013. Descriptions of GCOM-W1 AMSR2 Level 1R and Level 2 Algorithms. Japan Aerospace Exploration Agency Earth Observation Research Centre.
- Meesters, G.C., De Jeu, R.A.M., Owe, M., 2005. Analytical derivation of the vegetation optical depth from the microwave polarisation difference index. *IEEE Geos. Rem. Sens. Lett.* 2 (2), 121–123.
- Merlin, O., Walker, J.P., Panciera, R., Young, R., Kalma, J., Kim, E., 2007. Soil moisture measurement in heterogeneous terrain. In: Oxley, L., Kulasiri, D. (Eds.), MOD-SIM 2007 International Congress on Modelling and Simulation, Modelling and Simulation Society of Australia and New Zealand. pp. 2604–2610.
- Mladenova, I., Lakshmi, V., Jackson, T.J., Walker, J.P., Merlin, O., De Jeu, R.A.M., 2011. Validation of AMSR-e soil moisture using I-band airborne radiometer data from National Airborne Field Experiment 2006. *Remote Sens. Environ.* 115, 2096–2103.
- Mount, A.B., 1972. The derivation and testing of a soil dryness index using runoff data. *Tasmanian Forestry Commission Bulletin No.*, pp. 4.
- Naeimi, V., Scipal, K., Bartalis, S.H., Wagner, W., 2009. An improved soil moisture retrieval algorithm for ERS and METOP scatterometer observations. 47 (7), 1999–2013.
- Northcote, K.H., Beckmann, G.G., Bettenay, E., Churchward, H.M., Van Dijk, D.C., Dimmock, G.M., Hubble, G.D., Isbell, R.F., McArthur, W.M., Murtha, G.G., Nicolls, K.D., Paton, T.R., Thompson, C.H., Webb, A.A., Wright, M.J., 1960. Atlas of Australian Soils, Sheets 1 to 10 With Explanatory Data. CSIRO Australia and Melbourne University Press, Melbourne.
- Northcote, K.H., Hubble, G.D., Isbell, R.F., Thompson, C.H., Bettenay, E., 1975. A Description of Australian Soils. CSIRO Australia.
- Owe, M., De Jeu, R., Holmes, T., 2008. Multisensor historical climatology of satellite-derived global land surface moisture. *J. Geophys. Res.* 113, F01002.
- Owe, M., De Jeu, R.A.M., Walker, J., 2001. A methodology for surface soil moisture and vegetation optical depth retrieval using the microwave polarization difference index. *IEEE Trans. Geos. Rem. Sens.* 39 (8), 1643–1654.

- Panciera, R., Walker, J.P., Jackson, T.J., Gray, D.A., Tanase, M.A., Ryu, D., Monerris, A., Yardley, H., Rudiger, C., Wu, X., Gao, Y., Hacker, J.M., 2014. The Soil Moisture Active Passive Experiments (SMAPEX): toward soil moisture retrieval from the SMAP mission. *IEEE Trans. Geos. Rem. Sens.* 52, 490–507.
- Parinussa, R.M., Holmes, T.R.H., Wanders, N., Dorigo, W., De Jeu, R.A.M., 2015. A preliminary study toward consistent soil moisture from AMSR2. *J. Hydrometeor.* 16, 932–947.
- Pozzi, W., Sheffield, J., Stefanski, R., Cripe, D., Pulwarty, R., Vogt, J.V., Heim, R.R., Jr., Brewer, M.J., Svoboda, M., Westerhoff, R., Van Dijk, A.I.J.M., Lloyd-Hughes, B., Pappenberger, F., Werner, M., Dutra, E., Wetterhall, F., Wagner, W., Schubert, S., Mo, K., Nicholson, M., Bettio, L., Nunez, L., Van Beek, R., Bierkens, M., Goncalves de Goncalves, L.G., Zell de Mattos, J.G., Lawford, R., 2013. Toward global drought early warning capability: expanding international cooperation for the development of a framework for monitoring and forecasting. *Am. Meteorol. Soc.* 94 (6), 776–785.
- Raupach, M.R., Briggs, P.R., Haverd, V., King, E.A., Paget, M., Trudinger, C.M., 2009. Australian Water Availability Project (AWAP): CSIRO Marine and Atmospheric Research Component: final report for phase 3. CAWCR Technical Report No. 013.
- Reichle, R.H., Koster, R.D., Dong, J., Berg, A.A., 2004. Global soil moisture from satellite observations, land surface models, and ground data: implications for data assimilation. *J. Hydrometeor.* 5, 430–442.
- Renzullo, L., Van Dijk, A.I.J.M., Perraud, J.M., Collins, D., Henderson, B., Jin, H., Smith, A.B., McJannet, D.L., 2014. Continental satellite soil moisture data assimilation improves root-zone moisture analysis for water resources assessment. *J. Hydrol.* 519, 2747–2762.
- Rodell, M., Houser, P.R., Jambor, U., Gottschalk, J., Mitchell, K., Meng, C.J., Arsenault, K., Cosgrove, B., Radakovitch, J., Bosilovich, M., Entin, J.K., Walker, J.P., Lohmann, D., Toll, D., 2004. The global land data assimilation system. *Bull. Am. Meteorol. Soc.* 85, 381–394.
- Schmugge, T.J., 1983. Remote sensing of soil moisture: recent advances. *IEEE Trans. Geosci. Rem. Sens.* GE-21 (3), 336–344.
- Schroder, I., 2014. Arcturus Emerald Ozflux Tower Site Ozflux: Australian and New Zealand flux research and monitoring Hdl: 102.100.100/ 14249.
- Seneviratne, S.I., Corti, T., Davin, E.L., Hirschi, M., Jaeger, E.B., Lehner, I., Orlowsky, B., Teuling, A.J., 2010. Investigating soil moisture-climate interactions in a changing climate: a review. *Earth Sci. Reviews* 99, 125–161.
- Smith, A.B., Walker, J.P., Western, A.W., Young, R.L., Ellett, K.M., Pipunic, R.C., Grayson, R.B., Siriwidena, L., Chiew, F.H.S., Richter, H., 2012. The Murrumbidgee soil moisture monitoring network data set. *Water Resour. Res.* 48, W07701.
- Stenson, M.P., Fitch, P., Vleeshouwer, J., Frost, A.J., Bai, Q., Lerat, J., Leighton, B., Knapp, S., Warren, G., Van Dijk, A.I.J.M., Bacon, D., Pena Arancibia, J.L., Manser, P., Shoesmith, J., 2011. Operationalising the Australian Water Resources Assessment system. . Water Information Research and Development Alliance Science Symposium Proceedings
- Su, C.H., Ryu, D., Young, R.L., Western, A.W., Wagner, W., 2013. Inter-comparison of microwave satellite soil moisture retrievals over the Murrumbidgee basin southeast Australia. *Remote Sens. Environ.* 134, 1–11.
- Taylor, C.M., De Jeu, R.A.M., Guichard, F., Harries, P.P., Dorigo, W.A., 2012. Afternoon rain more likely over drier soils. *Nature* 489, 423–426.
- Van der Schalie, R., Kerr, Y.H., Wigneron, J.P., Rodríguez-Fernández, N.J., Al-Yaari, A., De Jeu, R.A.M., 2016. Global SMOS soil moisture retrievals from the land parameter retrieval model. *Int. J. Appl. Earth Obs. Geoinf.* 45, 125–134. Part B.
- Van der Schalie, R., Parinussa, R.M., Renzullo, L., Van Dijk, A.I.J.M., Su, C.H., De Jeu, R.A.M., 2015. SMOS soil moisture retrievals using the land parameter retrieval model: evaluation over the Murrumbidgee Catchment, southeast Australia. *Remote Sens. Environ.* 163, 70–79.
- Van Dijk, A.I.J., Yebra, M., Cary, G., 2015. A Model-data Fusion Framework for Estimating Fuel Properties, Vegetation Growth Carbon Storage and the Water Balance at Hillslope Scale: Feasibility Study in Namadgi National Park ACT. Bushfire and Natural Hazards CRC, Australia.
- Van Dijk, A.I.J.M., Beck, H.E., Crosbie, R.S., De Jeu, R.A.M., Liu, Y.Y., Podger, G.M., Timbal, B., Viney, N.R., 2013. The Millennium Drought in southeast Australia (2001–2009): natural and human causes and implications for water resources, ecosystems, economy and society. *Water Resour. Res.* 49, 1040–1057.
- Vaze, J., Viney, N., Stenson, M., Renzullo, L., Van Dijk, A., Dutta, D., Crosbie, R., Lerat, J., Penton, D., Vleeshouwer, J., Peeters, L., Teng, J., Kim, S., Hughes, J., Dawes, W., Zhang, Y., Leighton, B., Perraud, J.M., Joehnk, K., Yang, A., Wang, B., Frost, A., Elmahdi, A., Smith, A., Daamen, C., 2013. The Australian Water Resources Assessment Modelling System (AWRA). 20Th International Congress on Modelling and Simulation, Adelaide, Australia 1–6 December 2013. pp. 3015–3021.
- Verhoest, N.E.C., Lievens, H., Wagner, W., Alvarez-Mozos, J., Moran, M.S., Mattia, F., 2008. On the soil roughness parameterization problem in soil moisture retrieval of bare surfaces from synthetic aperture radar. *Sensors* 8, 4213–4248.
- Viney, N., Vaze, J., Crosbie, R., Wang, B., Dawes, W., Frost, A., 2015. AWRA-L V5.0: Technical Description of Model Algorithms and Inputs. CSIRO, Australia.
- Viney, N.R., Vaze, J., Vleeshouwer, J., Yang, A., Van Dijk, A., Frost, A., 2014. The AWRA modelling system. *Hydrol. Water Resour. Symp.* 1018–1025.
- Vinnikov, K.Y., Robock, A., Qiu, S., Entin, J.K., 1999. Optimal design of surface networks for observation of soil moisture. *J. Geophys. Res.* 104 (D16), 19743–19749.
- Vreugdenhil, M., Dorigo, W.A., Wagner, W., De Jeu, R.A.M., Hahn, S., Van Marle, M.J.E., 2016. Analyzing the vegetation parameterization in the TU-wien ASCAT soil moisture retrieval. *IEEE Trans. Geosci. Rem. Sens.* 54 (6), 3513–3531.
- Wagner, W., Hahn, S., Kidd, R., Melzer, T., Bartalis, Z., Hasenauer, S., Figa-Salda na, J., de Rosnay, P., Jann, A., Schneider, S., Komma, J., Kubu, G., Brugger, K., Aubrecht, C., Züger, J., Gangkofner, U., Kienberger, S., Brocca, L., Wang, Y., Blöschl, G., Eitzinger, J., Steinnocher, K., Zeil, P., Rubel, F., 2013. The ASCAT soil moisture product: a review of its specifications, validation results and emerging applications. *meteo z.* 22 (1), 5–33.
- Wagner, W., Lemoine, G., Rott, H., 1999. A method for estimating soil moisture from ERS scatterometer and soil data. *Remote Sens. Environ.* 70, 191–207.
- Wagner, W., Lemoine, G., Borgeaud, M., Rott, H., 1999a. A study of vegetation cover effects on ERS scatterometer data. *IEEE Trans. Geosci. Rem. Sens.* 37 (2), 938–948.
- Wanders, N., Karssenber, D., de Roo, A., de Jong, S.M., Bierkens, M.F.P., 2014. The suitability of remotely sensed soil moisture for improving operational flood forecasting. *Hydrol. Earth Syst. Sci.* 18, 2343–2357.
- Wang, Y.P., Houlton, B.Z., Field, C.B., 2007. A model of biogeochemical cycles of carbon, nitrogen, and phosphorus including symbiotic nitrogen fixation and phosphatase production. *Global Biogeochem. Cycles* 21, <http://dx.doi.org/10.1029/2006GB002797>.
- Wang, J.R., Schmugge, T.J., 1980. An empirical model for the complex dielectric permittivity of soil as a function of water content. *IEEE Trans. Geosci. Remote Sens.* 18, 288–295.
- Wigneron, J.P., Kerr, Y., Waldteufel, P., Saleh, K., Escorihuela, M.J., Richaume, P., Ferrazzoli, P., de Rosnay, P., Gurney, R., Calvet, J.C., Grant, J.P., Guglielmetti, M., Hornbuckle, B., Mätzler, C., Pellarin, T., Schwank, M., 2007. L-band microwave emission of the biosphere (I-MEB) model: description and calibration against experimental data sets over crop fields. *Rem. Sens. Environ.* 107, 639–655.
- Yee, M., Walker, J.P., Dumedah, G., Monerris, A., Rudiger, C., 2013. Towards land surface model validation from using satellite retrieved soil moisture. 20Th International Conference on Modelling and Simulation, Adelaide, Australia.
- Zreda, M., Desilets, D., Ferré, T.P.A., Scott, R.L., 2008. Measuring soil moisture content non-invasively at intermediate spatial scale using cosmic-ray neutrons. *Geophys. Res. Lett.* 35, L21402.

2.3 Chapter summary

In this chapter 11 sources of soil moisture data — from observations, models and remote sensing platforms — were statistically compared with Pearson correlation. The results show that remotely sensed estimates provide spatial continuity of data unavailable to other observed data sets, which is particularly useful in data-sparse areas of Australia. However, the relatively low temporal (approximately every few days) and spatial (~ 25 km) resolution of remotely sensed soil moisture will make it difficult to analyse land-atmosphere interactions, where more local and diurnal scales are needed to resolve complex feedback processes (Santanello et al. 2011). The comparison identified that the relatively stronger performance of some remotely sensed products over others was largely a function of instrument type, with performance varying over different landscape types. Overall the SMOS remotely sensed data set was able to best reflect the temporal behaviour of in situ observations at the ground stations considered.

The similarities identified between satellite products indicate potential commonalities in their error structure. Some satellite data sets may be complementary to each other and have the potential to be used together to minimise individual weaknesses. For example, SMOS was found to perform poorly over densely vegetated areas, whereas ASCAT was able to perform better in these areas owing to its different methodological approach. The European Space Agency Climate Change Initiative developed a hybrid global soil moisture product that combines both passive (including SMOS) and active (including ASCAT) microwave retrievals, with promising results over Australia (Liu et al. 2012).

Most models simulated ground-based soil moisture temporal behaviour quite well, and in some cases also simulated the observed magnitude. The WaterDyn model (Raupach et al. 2009) simulated observed temporal dynamics most accurately, and more successfully than other simpler models which simulate comparatively fewer physical processes. WaterDyn also showed stronger agreement with in situ observations than all of the remotely sensed data sets considered. The WaterDyn model provides spatially contiguous data at high spatial and temporal resolution, necessary for assessing local feedback processes. This chapter therefore demonstrates that the WaterDyn model can accurately simulate high resolution soil moisture dynamics observed across a range of landscape and climate types, and is therefore suitable for evaluating land-atmosphere interactions across Australia.

As well as answering the first research question of this thesis, the research presented in this chapter contributes to the broader understanding of soil moisture variability across Australia.

By retrieving soil moisture data from three separate monitoring networks, this research was able to build upon past studies and extend the analysis of soil moisture variability across a broader range of geographies and climate zones. The resulting understanding of complementarity and difference between satellite and model data sources allows for a more informed assessment of suitability across applications and beyond the study of land-atmosphere interactions.

Chapter 3

Identifying land-atmosphere interactions with soil moisture-precipitation relationships

3.1 Overview

The impact of land surface states on the evolution of the boundary layer, and thus precipitation, can be estimated by analysing the relationship between soil moisture and subsequent precipitation. This relationship represents coupling (i.e. one-way feedback) between the two ends of the 'hydrological' pathway described in Chapter 1. Regions of positive coupling show an enhancement of precipitation when soils are wet, or suppression of precipitation when soils are dry. Regions of positive coupling may therefore be identified when higher soil moisture levels are positively correlated with higher precipitation totals. On the other hand, regions of negative coupling may be identified when higher soil moisture levels are negatively correlated with higher precipitation totals. Using up to date observations of precipitation across Australia, and soil moisture data evaluated in Chapter 2, this chapter uses lag correlation to analyse the relationship between soil moisture and next-day rainfall to address research question 2: **Where do land-atmosphere interactions affect precipitation across Australia, and how do the interactions vary in time and with spatial scale?**

Similar correlation techniques have been widely applied to study soil moisture-precipitation relationships in other parts of the world (e.g. Duerinck et al. 2016; Liu et al. 2016; Mei and Wang 2011; Wei et al. 2008; Yang et al. 2018). However, previous studies did not

explicitly uphold the one-dimensional (1D) assumption inherent in the correlation, creating uncertainty in previous interpretations of the statistical measure. When inferring a relationship between colocated soil moisture and precipitation, it is assumed that land surface conditions influence the state of the air mass directly overlying that same surface. Air masses transported over neighbouring grid cells will likely be influenced by neighbouring land surface properties and will not be representative of the local coupling. This highlights the important role that horizontal transport of moisture and energy play in land-atmosphere interaction (Dirmeyer 2006; Froidevaux et al. 2013; Taylor 2015). Therefore the 1D assumption requires spatial and temporal scales to be linked to ensure the 1D coupling is accurately represented. The assumption is explored in this chapter by evaluating soil moisture-rainfall correlation with explicit treatment of spatial and temporal scales.

The research presented in this chapter has been peer-reviewed and published in *Journal of Geophysical Reviews - Atmospheres*, and is provided in its published form. Author contributions are outlined in the Statement of Contribution below.

Statement of Contribution

This thesis is submitted as a Thesis by Compilation in accordance with https://policies.anu.edu.au/ppl/document/ANUP_003405

I declare that the research presented in this Thesis represents original work that I carried out during my candidature at the Australian National University, except for contributions to multi-author papers incorporated in the Thesis where my contributions are specified in this Statement of Contribution.

Title: The Importance of the One-Dimensional Assumption in Soil Moisture - Rainfall Depth Correlation at Varying Spatial Scales

Authors: Holgate, C. M., A. I. J. M. Van Dijk, J. P. Evans, and A. J. Pitman


Publication outlet: Journal of Geophysical Research: Atmospheres

Current status of paper: Published

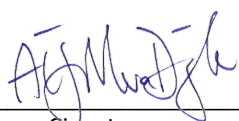
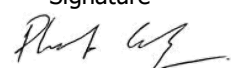
Citation: Holgate, C. M., Dijk, A. I. J. M. V., Evans, J. P., & Pitman, A. J. (2019). The Importance of the One-Dimensional Assumption in Soil Moisture - Rainfall Depth Correlation at Varying Spatial Scales. Journal of Geophysical Research: Atmospheres, 124(6), 2964–2975. <https://doi.org/10.1029/2018JD029762>

Contribution to paper: C. Holgate led the study. C. Holgate designed the study with significant input from A. Van Dijk and J. Evans. C.M Holgate carried out the data processing, analysis, figure preparation and drafting of the manuscript. All co-authors contributed to the refinement of the draft manuscript. C.M Holgate prepared the submission to the journal and led the revisions of the manuscript following peer-review.

Senior author or collaborating authors endorsement: _____

| | | |
|------------------------|---|------------------|
| Chiara Holgate |  | 26 November 2020 |
| Candidate – Print Name | Signature | Date |

Endorsed

| | | |
|----------------------------------|---|-----------|
| Albert Van Dijk |  | 9/11/2020 |
| Primary Supervisor – Print Name | Signature | Date |
| Philip Gibbons |  | 6/11/20 |
| Delegated Authority – Print Name | Signature | Date |

JGR Atmospheres

RESEARCH ARTICLE

10.1029/2018JD029762

Key Points:

- Soil moisture-rainfall depth seasonal relationships over Australia are analyzed in a 1-D framework for the first time
- One-dimensional assumption is not viable at small spatial scales, making method unsuited to detect local land-atmosphere coupling at high resolution
- Correlation magnitude is scale-dependent; therefore spatial scale effects need to be considered as climate model resolutions improve

Supporting Information:

- Supporting Information S1

Correspondence to:

C. M. Holgate,
chiara.holgate@anu.edu.au

Citation:

Holgate, C. M., Van Dijk, A. I. J. M., Evans, J. P., & Pitman, A. J. (2019). The importance of the one-dimensional assumption in soil moisture - Rainfall depth correlation at varying spatial scales. *Journal of Geophysical Research: Atmospheres*, 124, 2964–2975. <https://doi.org/10.1029/2018JD029762>

Received 5 OCT 2018

Accepted 14 FEB 2019

Accepted article online 25 FEB 2019

Published online 18 MAR 2019

The Importance of the One-Dimensional Assumption in Soil Moisture - Rainfall Depth Correlation at Varying Spatial Scales

C. M. Holgate^{1,2} , A. I. J. M. Van Dijk¹ , J. P. Evans^{3,4} , and A. J. Pitman^{3,4} 

¹Fenner School of Environment and Society, Australian National University, Canberra, ACT, Australia, ²ARC Centre of Excellence for Climate System Science, University of New South Wales, Sydney, New South Wales, Australia, ³ARC Centre of Excellence for Climate Extremes, University of New South Wales, Sydney, New South Wales, Australia, ⁴Climate Change Research Centre, School of Biological, Earth and Environmental Sciences, University of New South Wales, Sydney, New South Wales, Australia

Abstract Inferring local land-atmosphere coupling through correlation of colocated soil moisture and future rainfall inherently assumes a one-dimensional (1-D) framing of the coupling mechanism. For the first time we demonstrate the importance of upholding this assumption by examining the statistical relationship between daily soil moisture and rainfall depths over Australia, specifying spatial scales (0.05°, 0.5°, 1°, and 2.5°) to constrain the relationship to local-only physical processes. At small scales, without consideration of the 1-D assumption, strong land-atmosphere coupling is suggested across much of the country. However, when adhering to a 1-D framework, small sample sizes make correlation unsuitable for assessing local coupling at these small scales. When adhering to a 1-D framework, at scales of 0.5° and above, we find positive correlations in northern Australia in the wet and transition seasons and negative correlations in southern Australia in austral winter. The correlation is scale dependent, suggesting that as spatial resolutions increase in the future and land-atmosphere coupling heterogeneity is resolved, spatial distributions of local coupling may differ from larger-scale estimates characteristic of current coarse resolution climate models.

1. Introduction

Land surface fluxes of moisture and heat affect the thermodynamic and hydrodynamic properties of the planetary boundary layer (PBL). Changes to albedo and the partitioning of available energy between sensible and latent heat fluxes (Betts et al., 1996; Pielke, 2001) affect the PBL, upper level entrainment, and cloud formation. These changes can then feedback to the land surface state (Santanello et al., 2018).

Previous studies have assessed land-atmosphere coupling and associated feedbacks by examining the link between soil moisture and subsequent rainfall, for example, by applying covariance-based methods to global climate models, other model output, or observations. Examples include correlation analysis (Findell & Eltahir, 1997; Liu et al., 2016; Zhang et al., 2008), the coherence index (Koster et al., 2006; Yang et al., 2018), the feedback parameter (Notaro, 2008), and the two-legged coupling index (Dirmeyer, 2011).

Inferring the presence of local land-atmosphere coupling through covariance of colocated soil moisture and rainfall at a grid cell or point fundamentally assumes a one-dimensional (1-D) framing of the coupling mechanism. That is, the assumption when correlating gridded soil moisture and rainfall is that the local land surface state influences the overlying air mass within the same grid cell, within the diurnal or daily time scale of PBL evolution (Betts, 2004; Santanello et al., 2018) to produce rainfall. This assumption clearly requires that air masses do not travel through or beyond the grid cell within the daily time frame. If an air mass is horizontally advected (i.e., transported) across the bounds of the grid cell within a day, the air mass has been affected by the land surface state of neighboring grid cells, and the 1-D assumption inherent in the local correlation is broken.

The validity of the 1-D assumption is questionable given the important role advection can play in local land-atmosphere coupling (e.g., Dixon et al., 2013; Doran et al., 1995; Findell & Eltahir, 2003; Froidevaux et al., 2013; Taylor, 2015). The assumption has not been explicitly tested in previous studies analyzing the temporal correlation between soil moisture and subsequent rainfall. For example, Findell and Eltahir

(1997) correlated two weekly soil moisture (interpolated to a daily time scale and spatially averaged over the state of Illinois, USA) on 1 day with daily rainfall accumulated over the subsequent 21 days. Similarly, Duerinck et al. (2016) and Liu et al. (2016) temporally correlated regional soil moisture and future 21-day rainfall totals over Illinois and Asia, respectively. The time the overlying air masses remained over the land surface of given spatial scale was not explicitly connected to the impact of local versus remote processes on the computed relationship. On the other hand, while not directly discussing the 1-D assumption, Alfieri et al. (2008) sought to distinguish the impact of local versus remote processes on point-scale daily soil moisture-rainfall relationships by separating the correlation into days with convective versus stratiform rainfall, respectively. Our study differs from these previous efforts as we intentionally uphold the 1-D correlation assumption.

Modeling studies have found different magnitudes and even different signs in temporal soil moisture-rainfall feedback (i.e., two-way coupling) at varying spatial scales. For example, Hohenegger et al. (2009) found a negative feedback with a 2.2-km grid size model but a positive feedback with a 25-km model. This change is strongly influenced by the convective parameterization present in the 25-km model (and absent in the 2.2-km model). Taylor et al. (2013) also investigated the soil moisture-rainfall feedback using a model run at 4- and 12-km resolution, and they showed that the feedback was highly dependent on the convective parameterization. When convection was explicitly resolved, the probability of rainfall was dependent on spatial scale, but the overall sign of the feedback was consistent across the spatial scales tested (Taylor et al., 2013). In another modeling study using 2-km resolution Froidevaux et al. (2013) showed that the soil moisture-rainfall feedback can be negative under conditions with no background wind and positive when a background wind is present. While the wind speed in this study was not explicitly linked to the grid size, the mechanism invoked—convection initiates preferentially over drier grid cells and then propagates downwind to rain over wet grid cells—naturally provides a link between the grid size and the time it takes for a precipitating system to pass from a dry grid cell to a wet grid cell. Coupling strength has also been shown to be affected by background wind by Cioni and Hohenegger (2017), where simulations initialized with observed wind speed profiles led to a weaker control of the land surface on rainfall compared to simulations where wind velocities were initially set to zero and by Findell and Eltahir (2003) who showed that strong wind shear can suppress convection. Furthermore, in a remote sensing-based study using a base resolution of 0.25°, Guillod et al. (2015) showed that a negative spatial feedback (rains where conditions are drier) coincided with positive temporal soil moisture-rainfall feedback in some geographic regions. Following the methodology of Guillod et al. (2015) and Taylor et al. (2012), Petrova et al. (2018) showed that a negative spatial feedback in North Africa was robust across varying spatial scales (1°, 2.5°, and 5°). Overall, these studies highlight the importance of spatial scale and surrounding land surface conditions, as well as wind speeds and temporal scales, in determining the coupling sign and strength.

To confront the challenges of the 1-D assumption and spatial scale in applying correlation as a coupling metric, we examine the correlation between daily soil moisture and colocated next-day rainfall depth. For the statistical relationship to be indicative of local coupling between the land and the atmosphere (where “local” is defined as the area contained within a single grid cell), we uphold the 1-D assumption by restricting the correlation to a temporal scale short enough for soil moisture to alter overlying PBL properties before the affected air mass passes through and out of the grid cell. The near-surface wind speed is used to represent transport of the air mass, noting that it is likely an underestimate of wind speeds higher in the PBL. Wind speed defines the time it takes for an air mass to cross a grid cell; hence, a maximum wind speed can be defined so that air masses cannot entirely cross a grid cell within a given time frame. Our analysis therefore differs from previous soil moisture-rainfall correlation studies in that we explicitly integrate the spatial and temporal scales and relate the statistical relationship to local-only (1-D) physical coupling processes at spatial scales of 0.05°, 0.5°, 1°, and 2.5°.

Our analysis also differs in the treatment of persistent exogenous weather conditions. Some studies have attempted to deal with the effect of rainfall autocorrelation on the computed soil moisture-rainfall relationship by considering the difference between the correlation of subsequent 21-day rainfall totals and the correlation of soil moisture with subsequent 21-day rainfall totals (e.g., Findell & Eltahir, 1997; Liu et al., 2016; Mei & Wang, 2011). A window length of 21 days was reasoned to be representative of a short climatic period rather than a single weather event (Findell & Eltahir, 1997). Working at such a time scale makes it difficult for the effect of local soil moisture conditions and related overlying PBL properties to be

separated from the effect of larger-scale processes (e.g., remotely generated synoptic systems) on colocated rainfall. Here instead, we filter the time series at each cell to retain only those days without prior rainfall to account for the effect of multiday storm events on the soil moisture-rainfall relationship.

While the methodology used in this study can be applied to any geographic region, we focus on Australia since the soil moisture-rainfall relationship is currently poorly defined in this region and has not yet been statistically assessed using available multiyear observational data. Soil moisture-rainfall correlation over Australia has been considered in a modeled environment by Wei et al. (2008); other studies examined the potential coupling between the land and the atmosphere in the region through different covariance-based methods but with a focus on temperature (Hirsch, Pitman, & Kala, 2014; Hirsch, Pitman, Seneviratne, et al., 2014; Holmes et al., 2017; H. Zhang, 2004).

Identifying a significant statistical relationship between soil moisture and next-day rainfall across Australia does not necessarily imply a direct coupling, but it is a valuable first step toward understanding the physical mechanisms driving land-atmosphere coupling over the continent. Understanding of the local coupling mechanism, and its spatial scale dependence, is needed to grasp what role it may play in near-term hydroclimatic prediction (including prediction of extremes such as droughts and heatwaves) and longer-term climate projections.

The primary objective of this paper is therefore to examine the importance of upholding the 1-D assumption in the application of soil moisture-rainfall correlation as a coupling metric at varying spatial scales. Adhering to a 1-D framework, this paper will also determine, for the first time, whether a significant correlation exists between soil moisture and colocated next-day rainfall over Australia. We pursue these objectives using interpolated ground observations, model outputs, remote sensing retrievals, and reanalysis data.

2. Methods

2.1. Data

To test the correlation between soil moisture and next-day rainfall in a 1-D framework, we used a gridded data set. Gridded rainfall estimates from the Australian Gridded Climate Data data set (D. Jones et al., 2009) are based on interpolation of station observations to a 0.05° resolution grid, are available from 1901 to 2016, and represent daily rainfall totals (mm) in the 24 hr to 0900 local time. Accuracy of the rainfall estimates was assessed by Jones et al. (2009) for the period 2001–2007 using a cross-validation procedure whereby 5% of stations were deleted at a time and the error in the remaining stations calculated. Daily rainfall values in the data set have a root-mean-square error of 3.1 mm and a mean absolute error of 0.9 mm. Figure 1a shows the location of station gauges used in the interpolated product. Gauge density varies across the country, with a greater number of stations located in the more populous coastal regions. Fewer gauges are present in the arid interior where rainfall is low (<50 mm) for at least half the year (Figures 1d and 1e). Areas without rainfall data were removed from our analyses; only grid cells with at least 15 days of rainfall (>1 mm) in each season were utilized. Rainfall estimates from the Multi-Source Weighted Ensemble Precipitation (MSWEP, version 2.2) were also utilized for comparison. MSWEP merges data from station, satellite, and reanalysis products into a global, 3-hourly data set at 0.1° for 1979–2016 (Beck et al., 2017).

Daily average soil moisture is available at 0.05° resolution for 1911–2016 from the WaterDyn continental-scale water balance model. WaterDyn estimates soil moisture for two spatially varying soil layers depending on soil type (Raupach et al., 2009). Gridded estimates of daily average relative soil moisture content (%) from the uppermost layer were utilized, corresponding to a topsoil thickness of ~ 8 –70 cm (typically 20 cm; Raupach et al., 2009) depending on soil type. Based on evaluation against shallow in situ measurements from 13 sites in different climatic regions of Australia, the temporal dynamics of WaterDyn soil moisture estimates appeared more accurate than several alternative model and remote sensing estimates, with correlation coefficients for daily patterns ranging from 0.76 to 0.88 (Holgate et al., 2016). Remotely sensed soil moisture estimates produced by the European Space Agency's Climate Change Initiative (CCI) program (version 3.2) (Y. Y. Liu et al., 2011, 2012; Wagner et al., 2012) were also used for comparison. The daily average CCI surface soil moisture estimates (in volumetric units, m^3/m^3) combine active and passive satellite retrievals over 1979–2015 and are available at 0.25° .

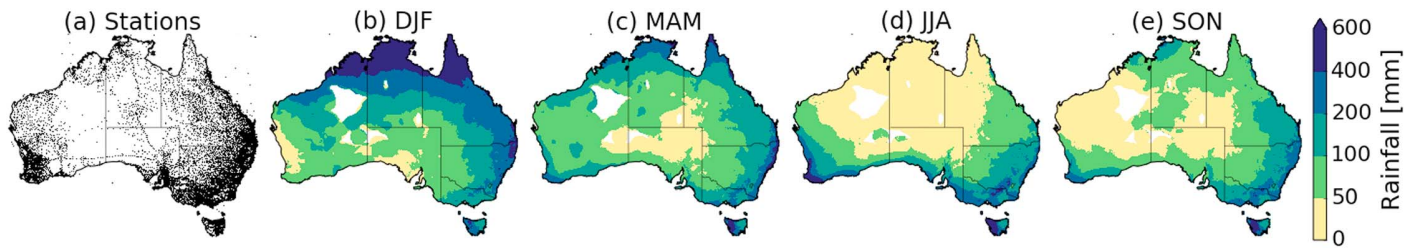


Figure 1. (a) Station locations used in the Australian Gridded Climate Data rainfall data set (sample from 1900–2008 shown) and (b–e) seasonal rainfall climatology (1979–2015). White areas in panels (b) to (e) indicate regions of no data. DJF = December, January, February; JJA = June, July, August; MAM = March, April, May; SON = September, October, November.

Wind speed data from 6-hourly ERA-Interim reanalysis at 0.75° resolution were used. Surface wind speed (m/s) estimates were taken at 0000 UTC (0800–1000 local time across Australia) to approximately coincide with the start of the rainfall measurement period. Wind speed data from McVicar et al. (2008) were also used for comparison. The data set spatially interpolates 24-hr wind run observations from surface anemometers from 1975 to 2017 and is available at 0.1° .

2.2. Correlation

We assessed the degree of association between daily average soil moisture and next-day rainfall totals across Australia using the nonparametric Spearman rank correlation coefficient. Since rainfall is measured as a daily total commencing at 0900 local time, the previous day's average soil moisture value was used as an estimate of early morning soil moisture for correlation with rainfall accumulated in the subsequent 24 hr from 0900. Since we performed the correlation on a 1-day temporal scale utilizing daily gridded soil moisture and rainfall data, to uphold the 1-D assumption inherent in the correlation the spatial grid scale was constrained to the distance an air parcel may be transported across the landscape within a single day. For an air mass to remain within a grid cell of given size from the start of the rainfall measurement period at 0900 local time until the afternoon (say 7 hr), a maximum wind speed must be defined. For example, for an air mass to remain within a 1° grid cell (~ 100 km) between morning and afternoon, the wind speed must be ~ 4 m/s or less. Surface wind speeds of ~ 4 m/s are most common across Australia according to the distribution constructed from ERA-Interim reanalysis (Figure 2).

Soil moisture and rainfall data were remapped from their native grids to the target grid using conservative first-order remapping, which maintains energy and water mass balance between the original and target grids (P. W. Jones, 1999). Wind speed data were remapped to the target grid using bilinear interpolation. The soil moisture and rainfall time series were filtered to retain days when the wind speed was below the threshold to match the 1-D correlation framework assumption.

We controlled for the persistence of exogenous weather conditions and the potentially resulting spurious correlations. This can occur both at the seasonal scale and the scale of days, where the persistence of rainfall seasonality or transient synoptic systems, respectively, can lead to correlation between soil moisture and future rainfall without any suggestion of causation. At a seasonal scale, we avoided this by analyzing individual seasons separately. Within those seasons, we controlled for persistence by only considering the first day of rain if consecutive rainfall days were recorded. That is, the time series were filtered to retain only those days without rainfall (>1 mm) on the previous day. In this way, the effect of single-system rainfall events persisting over consecutive days was accounted for.

The analyses were carried out for all seasons over the period 1979–2015, corresponding to the longest overlapping period of soil moisture, rainfall, and wind speed data available.

2.3. Varying the Spatial Scale

To test the robustness of the analysis results to different spatial scales, we calculated the correlation at different spatial resolutions. The analysis was initially carried out at 1° , corresponding to the most common wind speed across Australia (Figure 2). The analysis was repeated at 0.05° (native resolution of the primary

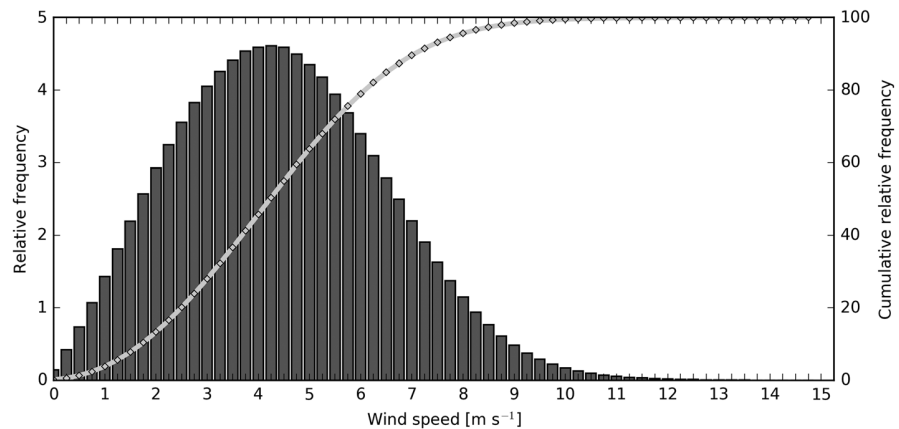


Figure 2. Probability density function (bars, left axis) and cumulative density function (line, right axis) for 0000 UTC wind speeds across Australia, 1979–2015.

soil moisture and rainfall data sets) and 0.5° to test the analysis results at smaller spatial scales. The data were also coarsened to 2.5° to test robustness at a lower resolution. To maintain the correlation analysis 1-D assumption, wind speed thresholds corresponding to each spatial resolution were applied separately; 0.25, 2, 4, and 10 m/s were applied to the 0.05° , 0.5° , 1° , and 2.5° resolution analyses, respectively.

3. Results

3.1. Testing the Correlation Assumption

Figure 3 and Table 1 demonstrate the importance of upholding the 1-D assumption when correlating soil moisture and next-day rainfall. When advection and the 1-D assumption were ignored and the correlation performed without stratification of the time series by wind speed (Figures 3a–3d), the relationship between soil moisture and next-day rainfall appeared significant across Australia at all scales of analysis (18–30% of land grid cells significant across scales in March, April, May; see Table 1). However, when the physical transport of air masses was accounted for and the 1-D assumption upheld using only days below the wind speed threshold, the spatial pattern of correlation (Figures 3e–3h) and the proportion of cells that are statistically significant (Table 1) changed. At the smallest scale tested, 0.05° , low sample sizes were evident everywhere, highlighting the reduction in sample sizes when the time series are partitioned based on the low wind speed threshold of 0.25 m/s (refer to Figure 2). When the assumption was ignored, 18% of land grid cells were statistically significant (Table 1); when the assumption was upheld, 0% of cells were significant (with $N > 15$). At 0.5° much of the inland regions showed a statistically insignificant relationship between soil moisture and next-day rainfall (Figure 3f; 7% of cells overall were significant, compared to 20% when the assumption was ignored; Table 1). A more modest change in the proportion of significant grid cells occurred at 1° (23% reduced to 15% when assumption upheld; Table 1). At the largest scale tested, 2.5° , only minor differences in the spatial pattern occurred between the nonstratified case (Figure 3d) and the stratified case (i.e., after the 1-D assumption was upheld; Figure 3h). This is because most days in the time series were below the relatively high wind speed threshold of 10 m/s (see Figure 2). Clearly, the importance of upholding the 1-D assumption becomes increasingly apparent as the scale gets smaller. If soil moisture-rainfall correlation were to be used as a direct indicator of land-atmosphere coupling without upholding the 1-D assumption, the metric would indicate a strong, widespread coupling present over Australia at the scale of 0.05° , when in fact no such coupling is indicated.

3.2. Spatial Scale Dependence

To test the robustness of the statistical relationships at different spatial scales, we computed the correlation at varying spatial scales, including 0.05° (Figures 4a–4d), 0.5° (Figures 4e–4h), 1° (Figures 4i–4l), and 2.5° (Figures 4m–4p). In all seasons low sample sizes ($N < 15$) are evident everywhere at 0.05° . At 0.5° (Figures 4e–4h) low sample sizes affect substantial areas; outside these areas, the spatial pattern resembles

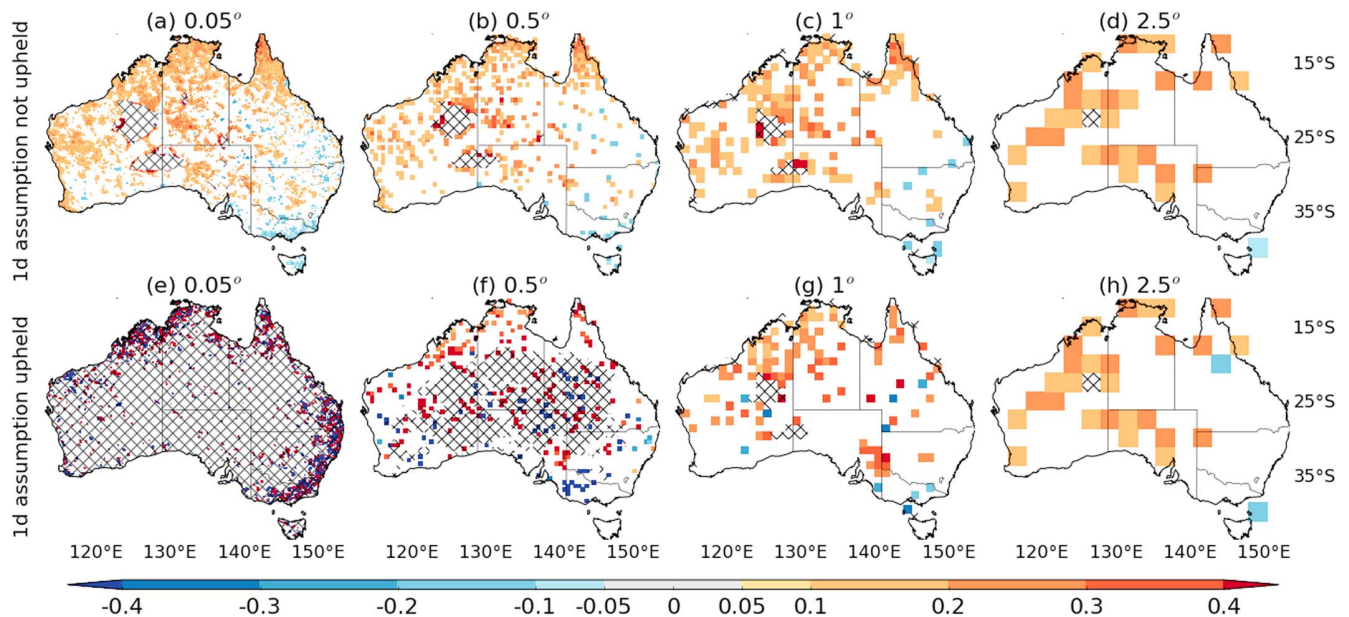


Figure 3. Comparing correlation between soil moisture and next-day rainfall when the 1-D assumption was upheld and when it was not, at varying spatial scales (1979–2015; March, April, May shown). Only grid cells with $p < 0.05$ (two tailed) are colored. Maximum sample size N is 607; $N < 15$ are hatched. Only the first day of consecutive rainfall days was considered. Correlations shown for (a–d) all wind speeds and (e–h) local conditions, that is, 1-D assumption upheld.

that found at 1° (Figures 4i–4l). At 1° , a clear spatial structure of correlation is evident, with positive coefficients (~ 0.1 to 0.4) found across the northern tropical and central arid regions in the northern Australia wet (December, January, February; Figure 4i) and transition seasons (March, April, May and September, October, November; Figures 4j and 4l). The relationship becomes insignificant in northern Australia in the dry season (June, July, August; Figure 4k). Some areas of negative correlation are evident in the semiarid and temperate eastern and southeastern parts of the country in austral winter (~ -0.1 to -0.4 ; Figure 4k). At 2.5° , soil moisture-rainfall correlation broadly resembles the spatial pattern at 1° , although the negative statistical relationship in eastern and southwestern Australia becomes more spatially coherent at 2.5° (Figure 4k).

Table 1
Proportion of Grid Cells Statistically Significant ($p < 0.05$) in Soil Moisture-Next-Day Rainfall Correlation

| Correlation spatial scale | One-dimensional assumption not upheld (%) | One-dimensional assumption upheld (%) |
|------------------------------|---|---------------------------------------|
| March, April, May | | |
| 0.05° | 18 | 0 |
| 0.5° | 20 | 7 |
| 1° | 23 | 15 |
| 2.5° | 30 | 30 |
| June, July, August | | |
| 0.05° | 10 | 0 |
| 0.5° | 11 | 2 |
| 1° | 13 | 7 |
| 2.5° | 16 | 16 |
| September, October, November | | |
| 0.05° | 29 | 0 |
| 0.5° | 21 | 4 |
| 1° | 23 | 13 |
| 2.5° | 28 | 27 |
| December, January, February | | |
| 0.05° | 25 | 0 |
| 0.5° | 25 | 6 |
| 1° | 26 | 16 |
| 2.5° | 20 | 20 |

The overall spatial pattern—a positive correlation in northern Australia during the wet and transition seasons and slight negative correlation in southeastern Australia during austral winter—remains when replacing the WaterDyn soil moisture values with remotely sensed CCI estimates (Figures S1a–S1d in the supporting information), when replacing the rainfall values with MSWEP estimates (Figures S1e–S1h), and when replacing the wind speed data with estimates from McVicar et al. (2008; Figures S1i–S1l). When filtering the rainfall and soil moisture time series to retain only those days without rainfall (< 1 mm) on the previous 2 days or previous 5 days (Figure S2), the overall seasonal spatial pattern remained but with fewer cells showing a statistically significant relationship, as expected due to the reduced sample sizes.

The scale dependence of the soil moisture-rainfall correlation was further assessed by computing the difference in magnitude of correlation coefficients when moving between spatial resolutions. The larger-scale correlation results were first remapped to the smaller scale using nearest neighbor interpolation and the difference taken at each cell. The statistical significance of correlation differences was assessed using Zou's confidence interval test (Zou, 2007). This method constructs approximate confidence

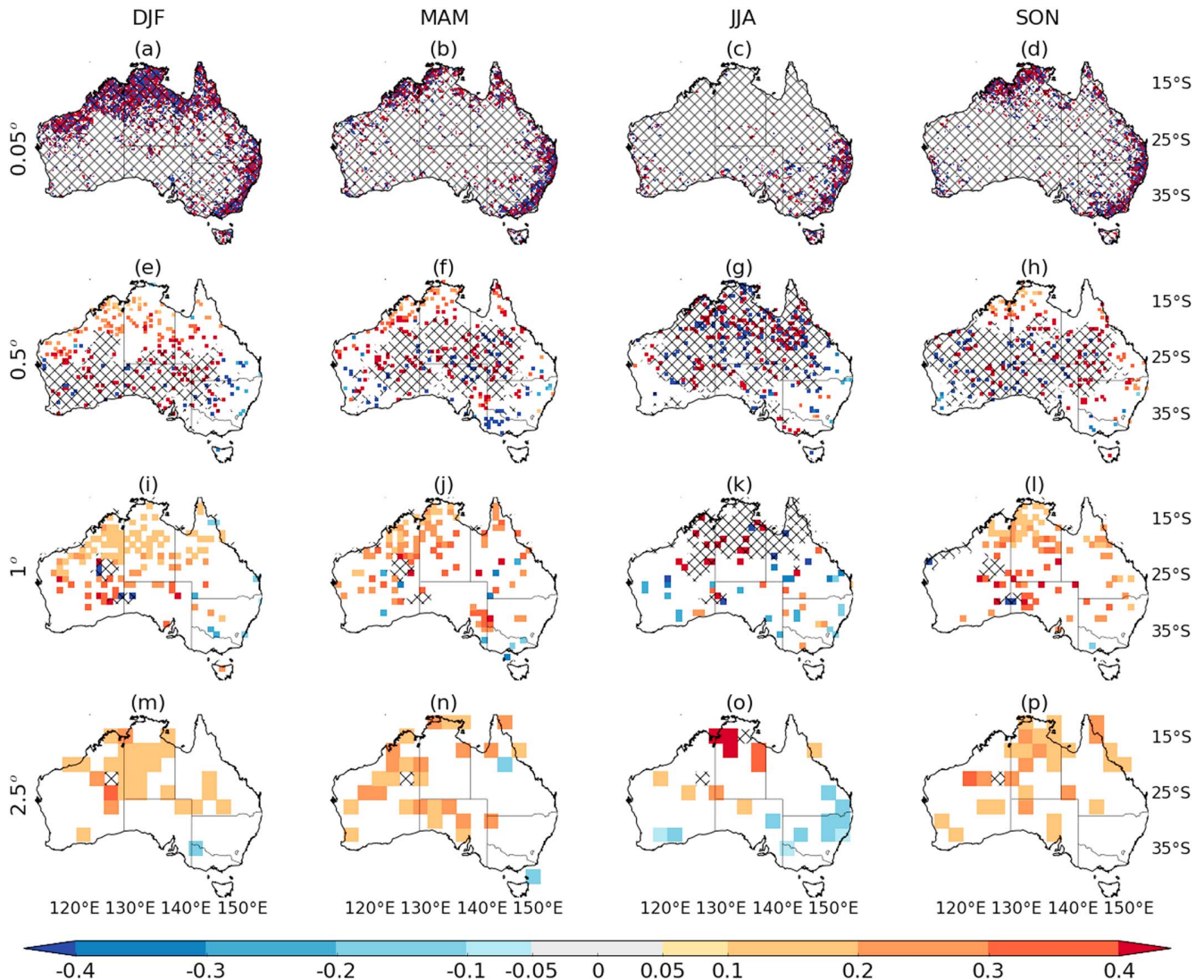


Figure 4. Correlation between soil moisture and next-day rainfall, 1979–2015. Only grid cells with $p < 0.05$ (two tailed) are colored. Maximum sample size N is 590; $N < 15$ are hatched. Only the first day of consecutive rainfall days was considered. Correlations are shown for local conditions (1-D assumption upheld) at (a–d) 0.05° (wind speeds ≤ 0.25 m/s), (e–h) 0.5° (wind speeds ≤ 2 m/s), (i–l) 1° (wind speeds ≤ 4 m/s), and (m–p) 2.5° (wind speeds ≤ 10 m/s). DJF = December, January, February; JJA = June, July, August; MAM = March, April, May; SON = September, October, November.

intervals for the differences between correlations at each spatial scale, by taking into account the dependency between correlations.

When first considering cells with a positive soil moisture-rainfall correlation in both the larger and smaller scales of analysis, decreasing the scale of the correlation from 1° to 0.5° (Figures 5a–5d), and from 2.5° to 0.5° (Figures 5e–5h), yielded a coherent pattern of higher correlation (~ 0 to $+0.4$; 95% confidence) across northern Australia. When decreasing the scale from 1° to 0.5° , 65–73% of the significant correlation differences increased in magnitude across seasons; when decreasing the scale from 2.5° to 0.5° , 71–92% increased. When moving from 2.5° to 1° (Figures 5i–5l), essentially no statistically significant difference in the correlation was evident across seasons. When considering cells with a negative soil moisture-rainfall correlation in both the larger and smaller scales of analysis, fewer cells showed a significant difference in the magnitude of correlation coefficients across Australia (Figure S3), but where a change was present, particularly in the southeast of the country, the correlation became more strongly negative.

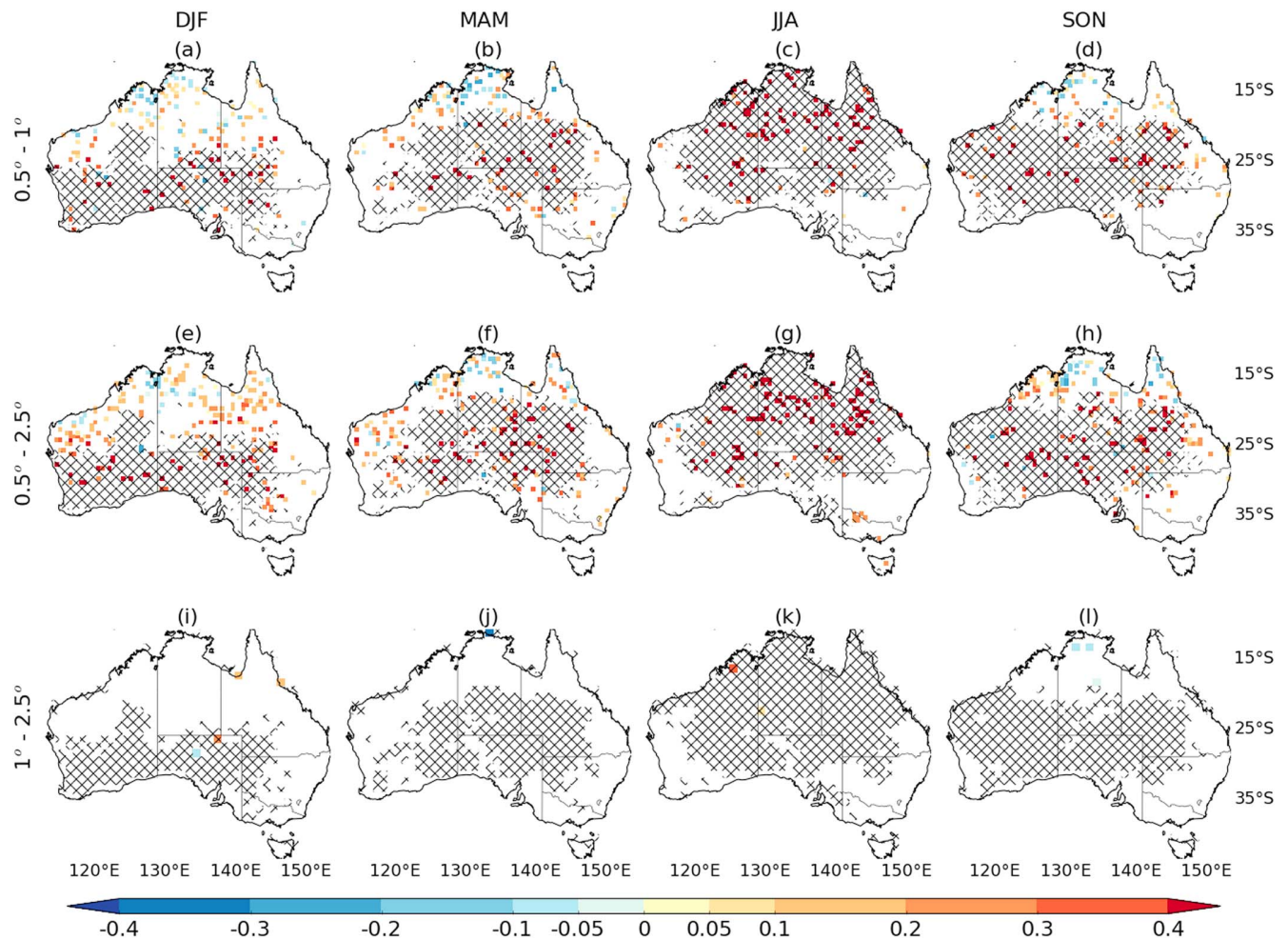


Figure 5. Difference in correlation between spatial scales, 1979–2015, considering grid cell correlation coefficients that were initially positive in both scales of analysis. Only grid cells with statistically significant (95% confidence) correlation differences are colored. $N < 15$ (of smaller scale) are hatched. Only the first day of consecutive rainfall days was considered. (a–d) 0.5–1°, (e–h) 0.5–2.5°, and (i–l) 1–2.5°. DJF = December, January, February; JJA = June, July, August; MAM = March, April, May; SON = September, October, November.

3.3. Statistical Sample Sizes

In this study, we screened the data using wind speed thresholds to isolate days where local surface conditions are the primary influence on the overlying atmosphere and focus on the soil moisture coupling to rainfall by only using the first rain days of storm systems. Despite using 37 years of data, this subselection resulted in data sets containing ~590 or fewer data points.

Findell et al. (2015) suggest that to determine land-atmosphere coupling, strength sample sizes of at least 6–12 summers (at least 552 days) are required to converge on sample means found using 25 summers of data (2,300 days). This would imply that most of our grids points are not adequately sampled. However Findell et al. (2015) assume stationarity in the underlying statistical properties—in our case, the correlation between grid cell soil moisture and rainfall. Findell et al. (2015) do this on a grid cell basis using data from the North American Regional Reanalysis, which has grid cell sizes of ~30 km × 30 km. That is, they are using an implicit 1-D framing of the coupling mechanism. In many locations ~90% of days will have wind speeds high enough that the surface conditions of neighboring grid cells will impact, or even dominate, the relationship between the surface and the atmosphere. That is, on low wind speed days the local surface conditions and atmospheric conditions can be related physically and will present one set of statistical properties. On moderate or high wind speed days the local surface conditions will have little or no influence on the

atmosphere. The implied statistical properties may seem random as they depend on the unknown surface properties of surrounding grid cells. Hence, the statistical properties assessed by Findell et al. (2015) are dependent on wind speed and are not stationary.

While the sample sizes suggested by Findell et al. (2015) are not directly applicable to our study, we caution that some of the results presented in this study may be affected by small sample sizes. We attempt to overcome this by only considering those correlations that are significant with 95% confidence, and we explicitly indicate areas where sample sizes are very small even if the correlation is significant.

4. Discussion

This study applied a 1-D framework to the correlation between soil moisture and next-day rainfall depths. In doing this we have examined the importance of upholding the 1-D assumption when using correlation as a coupling metric at varying spatial scales. By applying the correlation in a 1-D framework, we have shown that a significant correlation between colocated soil moisture and next-day rainfall exists over Australia in all seasons.

The impact of applying correlation with and without upholding the 1-D assumption increased as the spatial scale decreased. The proportion of grid cells showing a statistically significant relationship between soil moisture and rainfall changed considerably when the assumption was upheld. At 0.05° , if correlation was applied without consideration of the 1-D assumption and relative spatial and temporal scales, the metric would lead to the interpretation that the land and atmosphere are significantly coupled across Australia at small scales. In contrast, when the physical transport of air masses was accounted for and the 1-D assumption upheld, the correlation metric did not suggest any meaningful coupling at this scale.

Few rain days in the 1979–2015 time series had estimated wind speeds below the threshold required at 0.05° , resulting in small sample sizes for our high-resolution correlation analysis. While a longer time series may help circumvent this problem, our 37-year time series is already considerably longer than previous correlation studies (e.g., 11, 14, and 20 years in Duerinck et al., 2016; Findell & Eltahir, 1997; D. Liu et al., 2016, respectively). The small sample size highlights the limitation of the local correlation method when applied to small scales. Even if a local relationship exists between soil moisture and rainfall at small scales, the correlation method was not able to identify it, making this statistical method unsuited to the study of local land-atmosphere coupling in this case. This result serves as a caution to the application of the correlation method to the assessment of local land-atmosphere coupling at small spatial scales. Furthermore, it should be noted that application of 1-D soil moisture-rainfall correlation cannot necessarily distinguish the influence of soil moisture on rainfall occurrence from rainfall amount. For instance, Findell et al. (2011) found the land surface, represented by the evaporative fraction, to have a significant influence on rainfall occurrence but not rainfall amount. When using a 1-D correlation approach as in the current study, the time series of soil moisture and rainfall are subselected to uphold the 1-D assumption. This means that days when rainfall did not occur will be filtered out, preventing the method from determining the soil moisture-rainfall relationship on days with rainfall compared to days without rainfall. Rather, the correlation reflects how rainfall amount varies with changes in soil moisture.

This study has shown that when appropriately applying the correlation metric in a 1-D framework, a clear relationship between soil moisture and next-day rainfall is present across Australia in all seasons at scales at and above 0.5° . Significant positive soil moisture-rainfall correlations were found in tropical northern and arid central Australia during the wet and transition seasons. At 1° , a sparse but negative correlation was found in the semiarid and temperate eastern and southeastern regions in austral winter. This negative winter relationship in the eastern and southeastern regions became more spatially coherent as the scale was coarsened to 2.5° .

The negative soil moisture-rainfall relationship contrasts with the results of previous studies at comparable scales showing generally positive or no temporal soil moisture-rainfall coupling over Australia (e.g., Hirsch, Pitman, Seneviratne, et al., 2014; Koster et al., 2004; Notaro, 2008; Wei et al., 2008). While a negative spatial coupling (rains preferentially over areas drier than surrounding) was shown for parts of Australia by Taylor et al. (2012), positive temporal coupling was shown in a complementary study

by Guillod et al. (2015). The opposite sign of the temporal soil moisture-rainfall relationship found in our study compared to previous work suggests that there is uncertainty in the coupling between the land and the atmosphere over eastern and southeastern Australia in particular and warrants detailed examination of the coupling mechanisms over this region to reconcile the contrasting results between studies with differing methodologies.

Comparing soil moisture-rainfall correlation across different spatial scales showed that the statistical relationship is scale dependent, particularly in northern and eastern Australia. A tendency toward a greater correlation magnitude was found in the finer-scale (0.5°) analysis, compared to the coarser scales (either the 1° or 2.5° analyses). In as much as the observationally constrained statistical relationship reflects real-world coupling, this result indicates that coupling appears stronger as the scale is decreased from 2.5° to 0.5° .

The scale dependence suggests that an increase in coupling strength may be expected in a climate model as model resolution increases toward 0.5° . As climate models increase in resolution and move from a variety of tiled approaches to explicit representation of land surface heterogeneity, the related heterogeneity in the coupling between soil moisture and rainfall at smaller scales should become apparent. This might be expected to result in different feedback patterns in comparison to more homogeneous signals simulated with current coarser resolution climate models. Further increases toward extremely high resolutions will limit the usefulness of grid cell correlation-based coupling measures as the implicit 1-D assumption will be routinely broken. If gridded correlation metrics are to be applied to study local land-atmosphere coupling, spatial and temporal scales must be integrated to uphold the 1-D assumption and ensure that local-only physical processes are considered. If such coupling estimates are then to be used for comparison with climate models, comparable spatial scales should be maintained.

5. Conclusion

We sought to determine the correlation between colocated soil moisture and next-day rainfall depth across Australia, where the 1-D assumption inherent in the correlation method was upheld, at different spatial scales.

We have shown that when the 1-D assumption was upheld, the proportion of land area where the soil moisture-rainfall relationship was statistically significant depended on the spatial scale, whereas no such dependence was found when the spatial and temporal scales were not integrated. Consequently, the interpretation of the soil moisture-rainfall statistical relationship as an indicator of land-atmosphere coupling is significantly affected, particularly as scales get smaller.

Analyzing the soil moisture-rainfall relationship in a 1-D framework, we found positive correlation in northern Australia during the wet and transition seasons and limited negative correlation in southeastern Australia during austral winter. The statistical relationship was scale dependent, with stronger correlations in northern and eastern Australia in the 0.5° analysis compared to the 2.5° or 1° analyses.

Remembering that observational analyses such as those used in the present study are inherently limited by the spatiotemporal coverage and quality of the measurements and that statistical methods cannot establish a causative link (Salvucci et al., 2002), the correlation result provides a qualitative indication of the presence of a coupling in this region. This offers the opportunity to next undertake a comprehensive examination of the physical mechanisms driving this relationship.

In summary, we have demonstrated for the first time the importance of upholding the 1-D assumption in the correlation between soil moisture and rainfall, as a metric for land-atmosphere coupling, at varying spatial scales. At small scales correlation is not a viable method for assessing local coupling as adhering to a 1-D framework results in very small sample sizes. At scales of 0.5° and above we have shown that, when the assumption was appropriately handled, a significant correlation between soil moisture and next-day rainfall exists over Australia across all seasons. The dependence of the correlation on spatial scale suggests that as future climate models increase in spatial resolution and heterogeneity in the coupling is resolved, coupling behavior may deviate from current large-scale estimates. The mechanisms driving coupling in different regions and at different spatial scales will therefore need to be reevaluated in order to understand their role in near-term hydroclimatic prediction and longer-term climate projections.

Acknowledgments

This work was made possible thanks to an Australian Government Research Training Scholarship for author C. M. H. and support from the ARC Centre of Excellence for Climate System Science. C. M. H. and A. I. J. M. v. D. were supported through the ARC Discovery Projects funding scheme (project DP40103679). J. P. E. and A. J. P. were supported via the ARC Centre of Excellence for Climate System Science (CE170100023). The authors would like to acknowledge Dr. E. Slavich of the Mark Wainwright Analytical Centre at the University of New South Wales for the statistical support. Rainfall data from the AGCD data set are available from the Bureau of Meteorology (<https://www.bom.gov.au/climate/austmaps/metadata-daily-rainfall.shtml>); MSWEP rainfall data can be obtained upon request via the website (<https://www.gloh2o.org/>). Soil moisture data from WaterDyn can be obtained upon request from P. Briggs at CSIRO (<https://www.csiro.au/awap/>) and CCI soil moisture from ESA (<https://www.esa-soilmoisture-cci.org/node/145>). Wind data from ERA-Interim may be obtained from ECMWF (<https://apps.ecmwf.int/datasets/>) and from McVicar et al. (2008) via the CSIRO data access portal (<https://doi.org/10.4225/08/5a6ffda5bb332>).

References

- Alfieri, L., Claps, P., D'Odorico, P., Laio, F., & Over, T. M. (2008). An analysis of the soil moisture feedback on convective and stratiform precipitation. *Journal of Hydrometeorology*, 9(2), 280–291. <https://doi.org/10.1175/2007JHM863.1>
- Beck, H. E., van Dijk, A. I. J. M., Levizzani, V., Schellekens, J., Miralles, D. G., Martens, B., & de Roo, A. (2017). MSWEP: 3-hourly 0.25° global gridded precipitation (1979–2015) by merging gauge, satellite, and reanalysis data. *Hydrology and Earth System Sciences*, 21(1), 589–615. <https://doi.org/10.5194/hess-21-589-2017>
- Betts, A. K. (2004). Understanding hydrometeorology using global models. *Bulletin of the American Meteorological Society*, 85(11), 1673–1688. <https://doi.org/10.1175/BAMS-85-11-1673>
- Betts, A. K., Ball, J. H., Beljaars, A. C. M., Miller, M. J., & Viterbo, P. A. (1996). The land surface-atmosphere interaction: A review based on observational and global modeling perspectives. *Journal of Geophysical Research*, 101(D3), 7209–7225. <https://doi.org/10.1029/95JD02135>
- Cioni, G., & Hohenegger, C. (2017). Effect of soil moisture on diurnal convection and precipitation in large-Eddy simulations. *Journal of Hydrometeorology*, 18(7), 1885–1903. <https://doi.org/10.1175/JHM-D-16-0241.1>
- Dirmeyer, P. A. (2011). The terrestrial segment of soil moisture–climate coupling. *Geophysical Research Letters*, 38, L16702. <https://doi.org/10.1029/2011GL048268>
- Dixon, N. S., Parker, D. J., Taylor, C. M., Garcia-Carreras, L., Harris, P. P., Marsham, J. H., et al. (2013). The effect of background wind on mesoscale circulations above variable soil moisture in the Sahel. *Quarterly Journal of the Royal Meteorological Society*, 139(673), 1009–1024. <https://doi.org/10.1002/qj.2012>
- Doran, J. C., Shaw, W. J., & Hubbe, J. M. (1995). Boundary layer characteristics over areas of inhomogeneous surface fluxes. *Journal of Applied Meteorology*, 34(2), 559–571. <https://doi.org/10.1175/1520-0450-34.2.559>
- Duerinck, H. M., van der Ent, R. J., van de Giesen, N. C., Schoups, G., Babovic, V., & Yeh, P. J.-F. (2016). Observed soil moisture–precipitation feedback in Illinois: A systematic analysis over different scales. *Journal of Hydrometeorology*, 17(6), 1645–1660. <https://doi.org/10.1175/JHM-D-15-0032.1>
- Findell, K. L., & Eltahir, E. A. B. (1997). An analysis of the soil moisture-rainfall feedback, based on direct observations from Illinois. *Water Resources Research*, 33(4), 725–735. <https://doi.org/10.1029/96WR03756>
- Findell, K. L., & Eltahir, E. A. B. (2003). Atmospheric controls on soil moisture-boundary layer interactions: Three-dimensional wind effects. *Journal of Geophysical Research*, 108(D8), 8385. <https://doi.org/10.1029/2001JD001515>
- Findell, K. L., Gentile, P., Lintner, B. R., & Guillod, B. P. (2015). Data length requirements for observational estimates of land–atmosphere coupling strength. *Journal of Hydrometeorology*, 16(4), 1615–1635. <https://doi.org/10.1175/JHM-D-14-0131.1>
- Findell, K. L., Gentile, P., Lintner, B. R., & Kerr, C. (2011). Probability of afternoon precipitation in eastern United States and Mexico enhanced by high evaporation. *Nature Geoscience*, 4(7), 434–439. <https://doi.org/10.1038/ngeo1174>
- Froidevaux, P., Schlemmer, L., Schmidli, J., Langhans, W., & Schär, C. (2013). Influence of the background wind on the local soil moisture–precipitation feedback. *Journal of the Atmospheric Sciences*, 71(2), 782–799. <https://doi.org/10.1175/JAS-D-13-0180.1>
- Guillod, B. P., Orlowsky, B., Miralles, D. G., Teuling, A. J., & Seneviratne, S. I. (2015). Reconciling spatial and temporal soil moisture effects on afternoon rainfall. *Nature Communications*, 6(1), 6443. <https://doi.org/10.1038/ncomms7443>
- Hirsch, A. L., Pitman, A. J., & Kala, J. (2014). The role of land cover change in modulating the soil moisture-temperature land-atmosphere coupling strength over Australia. *Geophysical Research Letters*, 41, 5883–5890. <https://doi.org/10.1002/2014GL061179>
- Hirsch, A. L., Pitman, A. J., Seneviratne, S. I., Evans, J. P., & Haverd, V. (2014). Summertime maximum and minimum temperature coupling asymmetry over Australia determined using WRF. *Geophysical Research Letters*, 41, 1546–1552. <https://doi.org/10.1002/2013GL059055>
- Hohenegger, C., Brockhaus, P., Bretherton, C. S., & Schär, C. (2009). The soil moisture–precipitation feedback in simulations with explicit and parameterized convection. *Journal of Climate*, 22(19), 5003–5020. <https://doi.org/10.1175/2009JCLI2604.1>
- Holgate, C. M., De Jeu, R. A. M., van Dijk, A. I. J. M., Liu, Y. Y., Renszullo, L. J., Vinodkumar, et al. (2016). Comparison of remotely sensed and modelled soil moisture data sets across Australia. *Remote Sensing of Environment*, 186, 479–500. <https://doi.org/10.1016/j.rse.2016.09.015>
- Holmes, A., Rüdiger, C., Mueller, B., Hirschi, M., & Tapper, N. (2017). Variability of soil moisture proxies and hot days across the climate regimes of Australia. *Geophysical Research Letters*, 44, 7265–7275. <https://doi.org/10.1002/2017GL073793>
- Jones, D., Wang, W., & Fawcett, R. (2009). High-quality spatial climate data-sets for Australia. *Australian Meteorological and Oceanographic Journal*, 58(4), 233–248. <https://doi.org/10.22499/2.5804.003>
- Jones, P. W. (1999). First- and second-order conservative remapping schemes for grids in spherical coordinates. *Monthly Weather Review*, 127(9), 2204–2210. [https://doi.org/10.1175/1520-0493\(1999\)127<2204:FASOCR>2.0.CO;2](https://doi.org/10.1175/1520-0493(1999)127<2204:FASOCR>2.0.CO;2)
- Koster, R. D., Dirmeyer, P. A., Guo, Z., Bonan, G., Chan, E., Cox, P., et al., & GLACE Team (2004). Regions of strong coupling between soil moisture and precipitation. *Science*, 305(5687), 1138–1140. <https://doi.org/10.1126/science.1100217>
- Koster, R. D., Sud, Y. C., Guo, Z., Dirmeyer, P. A., Bonan, G., Oleson, K. W., et al. (2006). GLACE: The global land-atmosphere coupling experiment. Part I: Overview. *Journal of Hydrometeorology*, 7(4), 590–610. <https://doi.org/10.1175/JHM510.1>
- Liu, D., Yu, Z., & Mishra, A. K. (2016). Evaluation of soil moisture-precipitation feedback at different time scales over Asia. *International Journal of Climatology*, 37(9), 3619–3629. <https://doi.org/10.1002/joc.4943>
- Liu, Y. Y., Dorigo, W. A., Parinussa, R. M., de Jeu, R. A. M., McCabe, M. F., et al. (2012). Trend-preserving blending of passive and active microwave soil moisture retrievals. *Remote Sensing of Environment*, 123, 280–297. <https://doi.org/10.1016/j.rse.2012.03.014>
- Liu, Y. Y., Parinussa, R. M., Dorigo, W. A., de Jeu, R. A. M., Wagner, W., van Dijk, A. I. J. M., et al. (2011). Developing an improved soil moisture dataset by blending passive and active microwave satellite-based retrievals. *Hydrology and Earth System Sciences*, 15(2), 425–436. <https://doi.org/10.5194/hess-15-425-2011>
- McVicar, T. R., van Niel, T. G., Li, L. T., Roderick, M. L., Rayner, D. P., Ricciardulli, L., & Donohue, R. J. (2008). Wind speed climatology and trends for Australia, 1975–2006: Capturing the stilling phenomenon and comparison with near-surface reanalysis output. *Geophysical Research Letters*, 35, L20403. <https://doi.org/10.1029/2008GL035627>
- Mei, R., & Wang, G. (2011). Impact of sea surface temperature and soil moisture on summer precipitation in the United States based on observational data. *Journal of Hydrometeorology*, 12(5), 1086–1099. <https://doi.org/10.1175/2011JHM1312.1>
- Notaro, M. (2008). Statistical identification of global hot spots in soil moisture feedbacks among IPCC AR4 models. *Journal of Geophysical Research*, 113, D09101. <https://doi.org/10.1029/2007JD009199>

- Petrova, I. Y., van Heerwaarden, C. C., Hohenegger, C., & Guichard, F. (2018). Regional co-variability of spatial and temporal soil moisture–precipitation coupling in North Africa: An observational perspective. *Hydrology and Earth System Sciences*, 22(6), 3275–3294. <https://doi.org/10.5194/hess-22-3275-2018>
- Pielke, R. A. (2001). Influence of the spatial distribution of vegetation and soils on the prediction of cumulus convective rainfall. *Reviews of Geophysics*, 39(2), 151–177. <https://doi.org/10.1029/1999RG000072>
- Raupach, M. R., Briggs, P. R., Haverd, V., King, E., Paget, M., & Trudinger, C. M. (2009). Australian Water Availability Project (AWAP): CSIRO marine and atmospheric research component: Final report for phase 3. Aspendale: CSIRO Marine and Atmospheric Research. Retrieved from http://www.csiro.au/awap/doc/CTR_013_online_FINAL.pdf
- Salvucci, G. D., Saleem, J. A., & Kaufmann, R. (2002). Investigating Soil Moisture Feedbacks on Precipitation with Tests of Granger Causality. *Advances in Water Resources*, 25(8–12), 1305–1312. [https://doi.org/10.1016/S0309-1708\(02\)00057-X](https://doi.org/10.1016/S0309-1708(02)00057-X)
- Santanello, J. A., Dirmeyer, P. A., Ferguson, C. R., Findell, K. L., Tawfik, A. B., Berg, A., et al. (2018). Land–atmosphere interactions: The LoCo perspective. *Bulletin of the American Meteorological Society*, 99(6), 1253–1272. <https://doi.org/10.1175/BAMS-D-17-0001.1>
- Taylor, C. M. (2015). Detecting soil moisture impacts on convective initiation in Europe. *Geophysical Research Letters*, 42, 4631–4638. <https://doi.org/10.1002/2015GL064030>
- Taylor, C. M., Birch, C. E., Parker, D. J., Dixon, N., Guichard, F., Nikulin, G., & Lister, G. M. S. (2013). Modeling soil moisture–precipitation feedback in the Sahel: Importance of spatial scale versus convective parameterization. *Geophysical Research Letters*, 40, 6213–6218. <https://doi.org/10.1002/2013GL058511>
- Taylor, C. M., de Jeu, R. A. M., Guichard, F., Harris, P. P., & Dorigo, W. A. (2012). Afternoon rain more likely over drier soil. *Nature*, 489(7416), 423–426. <https://doi.org/10.1038/nature11377>
- Wagner, W., Dorigo, W., de Jeu, R., Fernandez, D., Benveniste, J., Haas, E., & Ertl, M. (2012). Fusion of active and passive microwave observations to create an essential climate variable data record on soil moisture. *ISPRS Annals of the Photogrammetry, Remote Sensing and Spatial Information Sciences (ISPRS Annals)*, 7, 315–321.
- Wei, J., Dickinson, R. E., & Chen, H. (2008). A negative soil moisture precipitation relationship and its causes. *Journal of Hydrometeorology*, 9(6), 1364–1376. <https://doi.org/10.1175/2008JHM955.1>
- Yang, L., Sun, G., Zhi, L., & Zhao, J. (2018). Negative soil moisture–precipitation feedback in dry and wet regions. *Scientific Reports*, 8(1), 4026. <https://doi.org/10.1038/s41598-018-22394-7>
- Zhang, H. (2004). Analyzing the potential impacts of soil moisture on the observed and model-simulated Australian surface temperature variations. *Journal of Climate*, 17(21), 4190–4212. <https://doi.org/10.1175/JCLI3141.1>
- Zhang, J., Wang, W.-C., & Wei, J. (2008). Assessing land–atmosphere coupling using soil moisture from the global land data assimilation system and observational precipitation. *Journal of Geophysical Research*, 113, D17119. <https://doi.org/10.1029/2008JD009807>
- Zou, G. Y. (2007). Toward using confidence intervals to compare correlations. *Psychological Methods*, 12(4), 399–413. <https://doi.org/10.1037/1082-989X.12.4.399>

3.2.1 Supplementary material

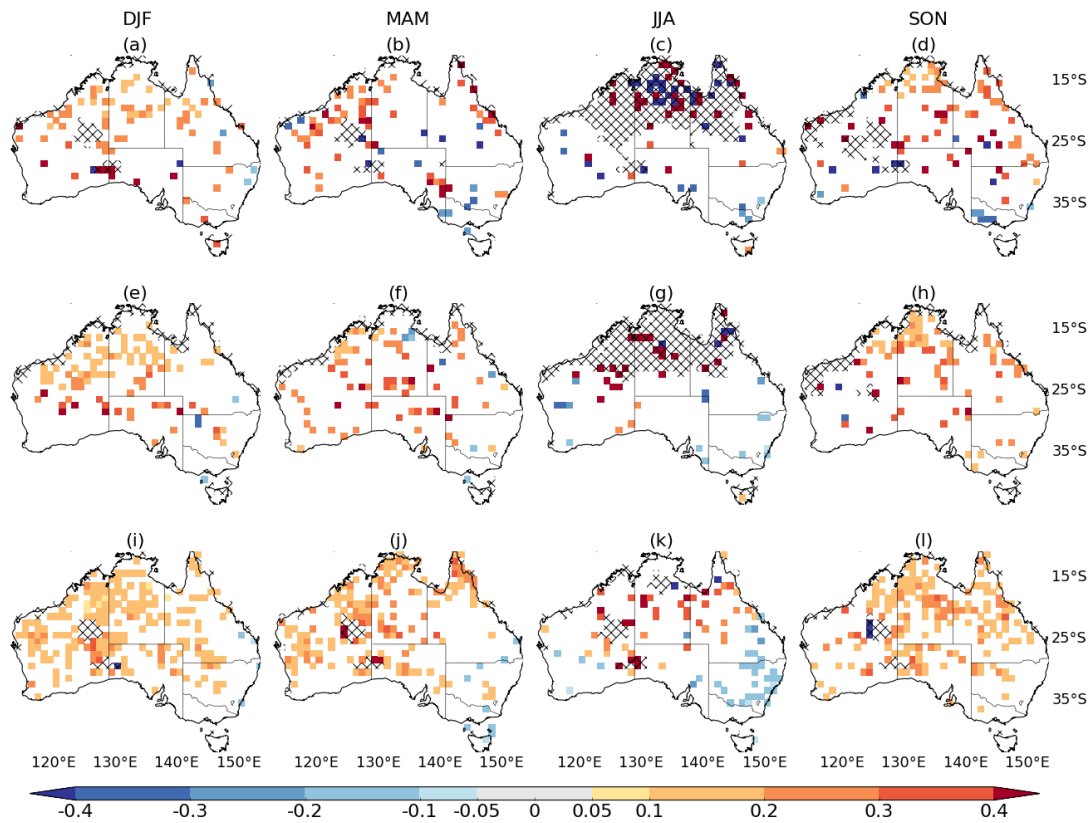


Figure 3.S1: Same as Figure 3.4, but with (a)-(d) WaterDyn soil moisture replaced by CCI estimates; (e)-(h) AGCD rainfall replaced by MSWEP estimates, and (i)-(l) ERA-I wind speed replaced by McVicar et al. (2008) estimates.

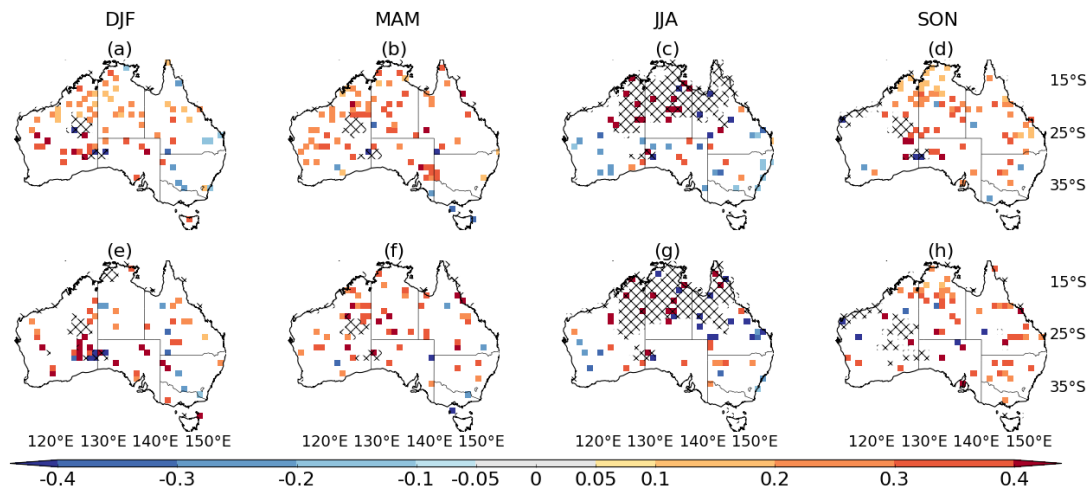


Figure 3.S2: Same as Figure 3.4, but retaining only those days in the time series without rainfall (<1 mm) on either of the previous (a)-(d) 2 days or (e)-(h) 5 days.

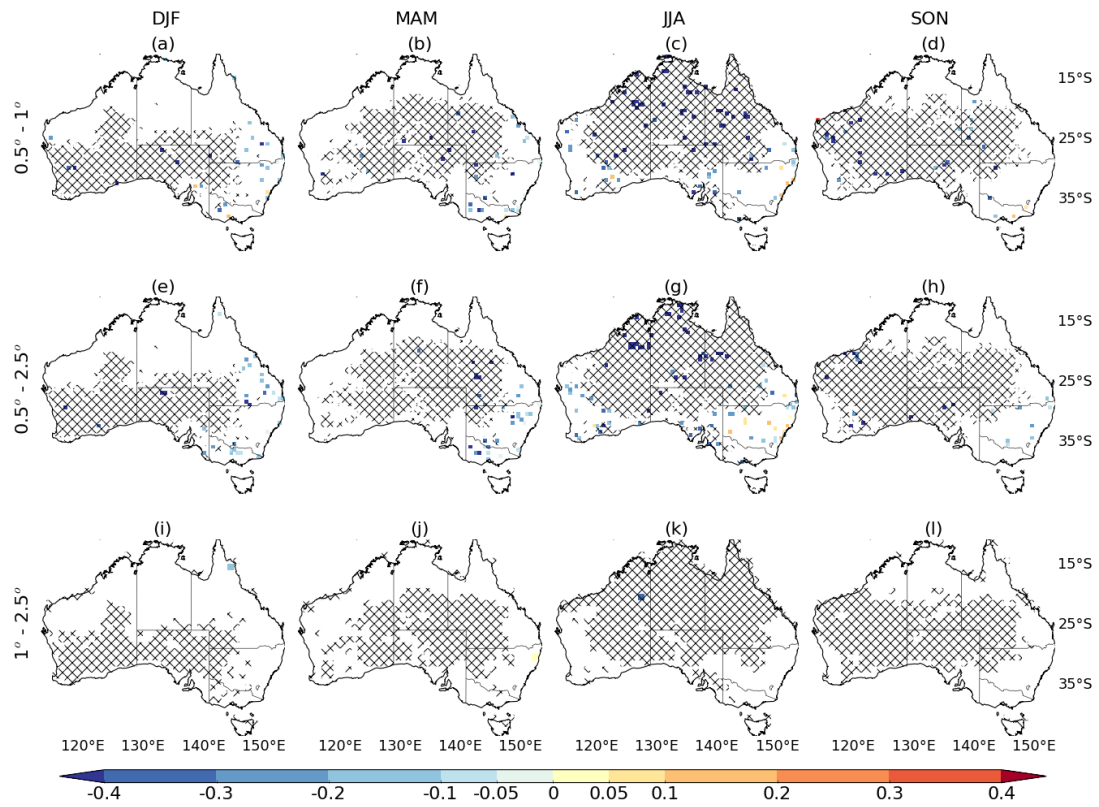


Figure 3.S3: Same as Figure 3.5, but considering correlation coefficients that were initially negative in both scales of analysis.

3.3 Chapter summary

This chapter sought to address research question 2 and identify regions of Australia where land-atmosphere interactions likely influence precipitation. Using multiple observational, modelled and remotely sensed data sets, regions of relatively strong land-atmosphere interaction were identified with lag correlation of soil moisture and next-day precipitation. The results show a positive soil moisture-precipitation relationship in northern Australia during the wet and transition seasons, and a negative relationship in parts of southern Australia during winter.

The analysis demonstrated the importance of upholding the 1D assumption when using correlation to infer land-atmosphere relationships. When the assumption was ignored, statistically significant correlation was shown over large areas, leading to the interpretation that soil moisture and precipitation are significantly coupled over most of the continent. When the assumption was upheld, the correlation only indicated a significant relationship over certain areas, and only at larger spatial scales ($> 0.5^\circ$). At smaller spatial scales the sample sizes became too small to detect a meaningful statistical relationship. This means that correlation — as a metric to infer land-atmosphere relationships — is better suited for use at larger spatial scales. Therefore, in addition to identifying regions where land-atmosphere interactions influence Australian precipitation, this chapter contributes to the land-atmosphere field by providing the first demonstration of the importance of applying the statistical technique in a manner consistent with the physical mechanisms it represents.

The soil moisture-precipitation relationship was also shown to be scale-dependent, with stronger correlation coefficients found at smaller spatial scales. This result suggests that land-atmosphere relationships previously found using large scale climate models may need to be revisited as climate models increase in spatial resolution.

Correlation as a statistical technique cannot itself fully characterise the complex physical mechanisms involved in land-atmosphere interactions. Rather, this analysis empirically identifies those parts of Australia where the land surface state has the clearest influence on precipitation, the seasonal variation of the interaction, and its dependence on spatial scale. With regional land-atmosphere interactions now identified, the next chapter aims to examine and quantify the physical relationships driving this interaction.

Chapter 4

Quantifying the strength of land-atmosphere interaction over Australia

4.1 Overview

The previous chapter identified regions of Australia where land-atmosphere interactions have relatively greater influence on precipitation each season. This chapter quantifies the interaction to address research question 3: **How strongly do land-atmosphere interactions affect precipitation across Australia?** The strength of land-atmosphere interactions is quantified with the precipitation recycling ratio. As described in Chapter 1, precipitation recycling is computed by first identifying the origin of moisture for a region's precipitation, and then calculating the proportion of moisture originating from the same region as the precipitation. The regions supplying moisture for all precipitation events across Australia between 1979 and 2013 are identified with a three-dimensional (3D) Lagrangian back-trajectory model. The results of the back-trajectory analysis presented in this chapter include: the climatological evaporative source regions supplying moisture for seasonal precipitation in each part of Australia; the level of precipitation recycling, and interannual variability and long term trends of moisture supply and recycling.

The research presented in this chapter has been peer-reviewed and published in *Journal of Climate*, and is provided in its published form. Author contributions are outlined in the Statement of Contribution below.

Statement of Contribution

This thesis is submitted as a Thesis by Compilation in accordance with https://policies.anu.edu.au/ppl/document/ANUP_003405

I declare that the research presented in this Thesis represents original work that I carried out during my candidature at the Australian National University, except for contributions to multi-author papers incorporated in the Thesis where my contributions are specified in this Statement of Contribution.

Title: Australian Precipitation Recycling and Evaporative Source Regions

Authors: Holgate, C. M., A. I. J. M. Van Dijk, J. P. Evans, A. J. Pitman and G. Di Virgilio


Publication outlet: Journal of Climate

Current status of paper: Published

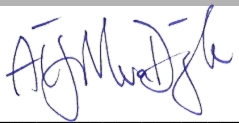

Citation: Holgate, C. M., Evans, J. P., van Dijk, A. I. J. M., Pitman, A. J., & Di Virgilio, G. (2020). Australian Precipitation Recycling and Evaporative Source Regions. Journal of Climate, 33(20), 8721–8735. <https://doi.org/10.1175/JCLI-D-19-0926.1>

Contribution to paper: C. Holgate led the study. C. Holgate designed the study with significant input from A. Van Dijk and J. Evans. C. Holgate made significant changes to the back-trajectory Fortran model originally written by J. Evans. C. Holgate ran the model simulations, conducted the analysis, prepared the figures and drafted the manuscript. All co-authors contributed to the refinement of the draft manuscript. C. Holgate prepared the submission to the journal and led the revisions of the manuscript following peer-review.

Senior author or collaborating authors endorsement: _____

| | | |
|------------------------|---|------------------|
| Chiara Holgate |  | 26 November 2020 |
| Candidate – Print Name | Signature | Date |

Endorsed

| | | |
|----------------------------------|---|-----------|
| Albert Van Dijk |  | 9/11/2020 |
| Primary Supervisor – Print Name | Signature | Date |
| Philip Gibbons |  | 6/11/20 |
| Delegated Authority – Print Name | Signature | Date |

Australian Precipitation Recycling and Evaporative Source Regions^①

C. M. HOLGATE

*Fenner School of Environment and Society, Australian National University, Canberra, Australian Capital Territory, and
ARC Centre of Excellence for Climate System Science, University of New South Wales, Sydney, New South Wales, Australia*

J. P. EVANS

*ARC Centre of Excellence for Climate Extremes, and Climate Change Research Centre, School of Biological, Earth and
Environmental Sciences, University of New South Wales, Sydney, New South Wales, Australia*

A. I. J. M. VAN DIJK

Fenner School of Environment and Society, Australian National University, Canberra, Australian Capital Territory, Australia

A. J. PITMAN

*ARC Centre of Excellence for Climate Extremes, and Climate Change Research Centre, School of Biological, Earth and
Environmental Sciences, University of New South Wales, Sydney, New South Wales, Australia*

G. DI VIRGILIO

*Climate Change Research Centre, School of Biological, Earth and Environmental Sciences, University of New South Wales,
Sydney, New South Wales, Australia*

(Manuscript received 15 December 2019, in final form 12 July 2020)

ABSTRACT

The relative importance of atmospheric advection and local land–atmosphere coupling to Australian precipitation is uncertain. Identifying the evaporative source regions and level of precipitation recycling can help quantify the importance of local and remote marine and terrestrial moisture to precipitation within the different hydroclimates across Australia. Using a three-dimensional Lagrangian back-trajectory approach, moisture from precipitation events across Australia during 1979–2013 was tracked to determine the source of moisture (the evaporative origin) and level of precipitation recycling. We show that source regions vary markedly for precipitation falling in different regions. Advected marine moisture was relatively more important than terrestrial contributions for precipitation in all regions and seasons. For Australia as a whole, contributions from precipitation recycling varied from ~11% in winter up to ~21% in summer. The strongest land–atmosphere coupling was in the northwest and southeast where recycled local land evapotranspiration accounted for an average of 9% of warm-season precipitation. Marine contributions to precipitation in the northwest of Australia increased in spring and, coupled with positive evaporation trends in the key source regions, suggest that the observed precipitation increase is the result of intensified evaporation in the Maritime Continent and Indian and Pacific Oceans. Less clear were the processes behind an observed shift in moisture contribution from winter to summer in southeastern Australia. Establishing the climatological source regions and the magnitude of moisture recycling enables future investigation of anomalous precipitation during extreme periods and provides further insight into the processes driving Australia's variable precipitation.

KEYWORDS: Atmosphere–land interaction; Climatology; Feedback; Water vapor; Semi-Lagrangian models

^① Supplemental information related to this paper is available at the Journals Online website: <https://doi.org/10.1175/JCLI-D-19-0926.s1>.

Corresponding author: Chiara Holgate, chiara.holgate@anu.edu.au

DOI: 10.1175/JCLI-D-19-0926.1

© 2020 American Meteorological Society. For information regarding reuse of this content and general copyright information, consult the [AMS Copyright Policy](https://www.ametsoc.org/PUBSReuseLicenses) (www.ametsoc.org/PUBSReuseLicenses).

1. Introduction

The origin of moisture for regional precipitation indicates the relative importance of local versus remote processes. Regions that receive a large portion of their moisture from local terrestrial sources are likely to experience stronger land–atmosphere coupling relative to regions where precipitation is typically derived from advected marine moisture (Eltahir and Bras 1996). In Australia, the relative importance of local terrestrial versus remote oceanic processes affecting precipitation is currently uncertain (Evans et al. 2011): Where does the moisture come from, and how strongly do land–atmosphere coupling processes attenuate or amplify atmospheric moisture to impact local precipitation depth and timing?

Identifying the evaporative source regions that supply moisture for precipitation can reveal important aspects of a region's hydroclimatology. Knowing the long-term average source regions provides insight into the drivers of precipitation during anomalously dry or wet periods (Dirmeyer et al. 2014). In the case of drought, for example, identifying the long-term average source regions can help reveal whether the low precipitation was due to a reduction in source evaporation, anomalous atmospheric circulation (i.e., the moisture was generated but transported elsewhere), a lack of local precipitation-generating mechanisms, land–atmosphere coupling, or a combination of factors. Second, if a region's precipitation is dependent on precipitation recycling over land, then the land surface state and how it is coupled to the atmosphere becomes important to any explanation of precipitation anomalies. Establishment of the terrestrial sources also allows the identification of areas where distant land-use change may affect local precipitation (van der Ent et al. 2010). Similarly, identifying the marine sources allows investigation of how future changes in sea surface temperatures (SSTs) and atmospheric circulation influence local precipitation changes.

Dirmeyer et al. (2009) estimated the annual average source regions supplying moisture for precipitation to most countries, including Australia, between 1979 and 2003. They found Australian precipitation mainly to originate as moisture from marine evaporation, particularly along the coastlines in all but the southeast corner of Australia, and to originate via terrestrial moisture in northern and eastern Australia. Other studies have explored the source regions for precipitation over individual regions (Stohl and James 2005; Sharmila and Hendon 2020) and in selected wet and dry years (Miralles et al. 2016). Other studies have shed light on where moisture evaporated over predefined ocean

regions falls as precipitation over Australia (van der Ent and Savenije 2013; Gimeno et al. 2012). How source regions vary for precipitation falling in each part of the continent, and how sources vary between seasons and years, has not been previously examined. A more detailed analysis of source regions for each part of the continent, and how these regions vary temporally, is required to examine the interplay between large-scale processes and local coupling mechanisms that attenuate or amplify precipitation within the different hydroclimatic regimes across Australia. Regions need to be studied individually if important coupling mechanisms operating during average versus anomalous periods are to be revealed.

Precipitation recycling is one measure of land–atmosphere coupling strength. The precipitation recycling ratio is the proportion of a region's precipitation that is derived from evapotranspiration in that same region. High recycling levels may be indicative of strong, positive land–atmosphere coupling (Brubaker et al. 1993), whereby a decrease in soil moisture may lead to a decrease in local evapotranspiration and precipitation (Zhang et al. 2008), potentially contributing to the persistence of droughts (Brubaker et al. 1993). Previous estimates indicate that precipitation recycling in Australia may vary from as much as 38% for the whole continent (Dirmeyer et al. 2009) to 5% at a scale of 10^5 km^2 (Dirmeyer and Brubaker 2007; van der Ent and Savenije 2011). Given these uncertainties, a long-term dataset of evaporative source regions and precipitation recycling for each part of Australia could help establish the relative importance of local versus remote processes and the strength of coupling processes across periods of average and anomalous precipitation.

We aim to develop such a long-term dataset. Our objectives are 1) to establish a multidecadal time series of daily evaporative source regions and precipitation recycling across the Australian continent and for its 13 major hydrological basins using the Lagrangian back-trajectory method based on Dirmeyer and Brubaker (1999, 2007); 2) to define interannual and intraseasonal variability of evaporative source regions and precipitation recycling for each part of Australia; and 3) to determine where recycling plays a significant role in the generation of regional precipitation, and when and where large-scale processes dominate precipitation generation through moisture advection. To achieve these objectives, we investigated the period 1979–2013, covering periods of average precipitation and severe drought and flood, and extend the analysis of Dirmeyer et al. (2009) to include the Millennium Drought (2001–09) and a subsequent wet period (2010–11).

2. Data and methods

a. Back-trajectory model

We tracked atmospheric water (vapor, liquid, and solid) from all precipitation events exceeding 2 mm day^{-1} backward in time and space to identify their moisture origin using a Lagrangian back-trajectory model with explicit moisture accounting based on [Dirmeyer and Brubaker \(1999\)](#). Precipitation falling anywhere on the Australian continent between 1979 and 2013 was tracked.

For each day that precipitation occurred at grid cell i , air parcels were launched at a rate proportional to the rate of precipitation. Parcels were released from a random, total-precipitable-water-weighted height in the atmosphere, assuming the vertical distribution of precipitable water indicates where the precipitation forms. Each parcel k , treated as a passive water vapor tracer, was advected through the atmosphere using three-dimensional (3D) wind fields and the fully implicit technique of [Merrill et al. \(1986\)](#):

$$\begin{aligned} x^{n-1} &= x^n + \frac{\Delta t u^n + \Delta t u^{n-1}}{2} \quad \text{and} \\ y^{n-1} &= y^n + \frac{\Delta t v^n + \Delta t v^{n-1}}{2}, \end{aligned} \quad (1)$$

where x and y (both in meters) are the grid coordinates along the trajectory; u and v (both in meters per second) are the zonal and meridional wind components, respectively; Δt (s) is the time interval; and n (s) is the time step. Height displacement of the parcel was determined with the vertical wind component.

At each 10-min time interval of the back trajectory, part of the parcel's water vapor was assumed to have come from evaporation of the grid cell x, y underlying the parcel at that point in its trajectory, assuming the evaporation mixes well throughout the entire atmospheric column during the time step, and that evaporation was the only source of moisture for the parcels. Moisture was added to parcel k according to

$$C_{i,k}(x, y, t) = \frac{E(x, y, t)}{\text{TPW}_i}, \quad (2)$$

where $C_{i,k}$ (fraction) is the contribution of moisture at grid cell x, y at time t to parcel k , E (m) is the estimated evaporation at grid cell x, y at time t , and TPW_i (m) is the total precipitable water above original grid cell i at the time of the precipitation event ([Dirmeyer and Brubaker 1999](#)).

For each 0.5° grid cell across Australia, up to 100 parcels were released every day, dependent on the proportion of time it rained during the day; at least one

parcel per 10-min simulation time step was released for cells where it rained. Parcels were released from the location of each precipitation event and tracked backward until all of the precipitable water for that event had been accounted for, or until the maximum back-trajectory time (set at 30 days) had been reached, or until the parcel reached the boundary of the model domain. The total evaporative contribution $E_A(x, y)$ of parcels $k-m$ over time t to t_{\max} across all grid cells $i-n$ within area A where it rained is therefore

$$E_A(x, y) = \sum_{i=1}^n \sum_{k=1}^m \sum_{t=0}^{t_{\max}} C_{i,k}(x, y, t). \quad (3)$$

When summed over all grid points in the domain, the $E_A(x, y)$ equals P_A , the total precipitation in area A ([Dirmeyer and Brubaker 1999](#)). This process was repeated until all precipitable water from all precipitation events across Australia during 1979–2013 had been accounted for. This yielded the source regions for Australian precipitation; that is, a daily map of evaporated water vapor that contributed to precipitation over the Australian continent each day during the 35-yr time frame. The 3D distribution of $E_A(x, y)$ was then partitioned to obtain the evaporative source regions for precipitation falling in each of Australia's major hydrological basins. Basin boundaries ([Fig. 1](#)) were the major topographic drainage divisions derived from the Australian Hydrological Geospatial Fabric ([Bureau of Meteorology 2012](#)).

This method makes some assumptions that may impact the accuracy of the identified moisture source regions, including that evaporative water is well mixed vertically at the time scale of the back-trajectory model and that the vertical distribution of precipitable water indicates where rain formation occurs vertically. Although testing of these assumptions is beyond the scope of the current study, past studies that addressed these uncertainties indicate that they are likely to have only small influences in our case ([Goessling and Reick 2013](#); see the Text S1 section in the online supplemental material).

b. Precipitation recycling

The 3D time series of evaporative origin was used to determine the precipitation recycling ratio for each hydrological basin, where the recycling ratio ρ is defined as the proportion of basin A precipitation that originated as evaporation from that same basin:

$$\rho = \sum E_A(x, y) / P_A. \quad (4)$$

Recycling ratios are dependent on spatial scale, since recycling necessarily increases from zero at a point, to 100% for the whole globe. Given this scale dependency,

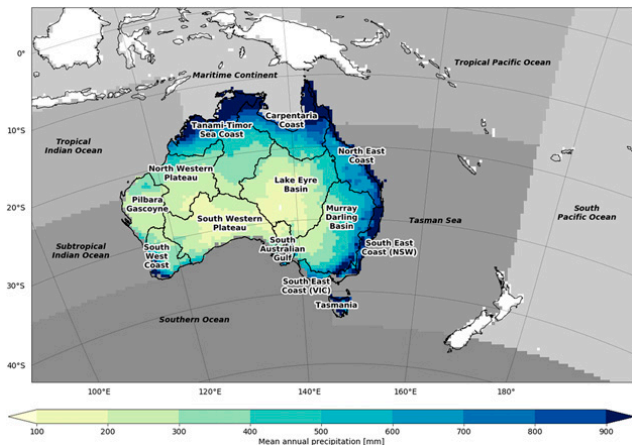


FIG. 1. Australian major hydrological basins and mean annual precipitation (Bureau of Meteorology 2010) set within the model domain. Ocean regions are delineated in grayscale (shades are arbitrary).

we also present scaled recycling ratios ρ_s to allow a comparison between basins of different size and allow comparison with previous studies. Dirmeyer and Brubaker (2007) examined the relationship between recycling ratio and geographic area for different regions globally and empirically found a power law describing the data according to

$$\rho_s = aA^b, \quad (5)$$

where ρ_s is the scaled recycling ratio (%), A is the area (km^2), and a and b are fitting parameters. Dirmeyer and Brubaker (2007) found b to vary little from an average 0.462 across the globe, suggesting that such a universal value of b could be applied. Hence once the recycling ratio ρ for a region of size A has been calculated, the value of a can be calculated by rearranging Eq. (5). A recycling ratio scaled to a new area can then be computed for the region (ρ_s). In this study we find values for a for each hydrological basin and then use $b = 0.462$ and $A = 10^5 \text{ km}^2$ to compute scaled recycling ratios ρ_s for each basin.

c. Back-trajectory forcing data

The back-trajectory analysis was driven by time-varying 3D atmospheric fields of wind, temperature, precipitable water and pressure, and two-dimensional (2D) fields of precipitation and latent heat flux, produced by the ERA-Interim-driven WRFv3.6.1 simulation. The simulation was performed over the Coordinated Regional Climate Downscaling Experiments (CORDEX)-Australasia domain at $\sim 50 \text{ km}$ horizontal resolution and 30 vertical levels spaced closer together in the boundary layer. The model physics parameterizations included the Mellor–Yamada–Janjić planetary boundary layer, Betts–Miller–Janjić cumulus, WRF double-moment 5-class cloud microphysics,

Rapid Radiative Transfer Model longwave radiation, Dudhia shortwave radiation, and the Noah land surface model. This simulation uses spectral nudging of winds and geopotential height above approximately 500 hPa using ERA-Interim (Evans et al. 2013). This ensures that the synoptic-scale weather systems within the WRF simulation remain close to those in the reanalysis but has the advantage of conserving water, which the reanalysis does not do due to its assimilation of observations.

An ensemble of ERA-Interim driven simulations within the CORDEX-Australasia modeling framework was recently evaluated by Di Virgilio et al. (2019) for the period 1981–2010 and included the WRF configuration called UNSW-WRF360K. The simulation used in the present study is UNSW-WRF360K, but with additional spectral nudging of winds and geopotential. The spectrally nudged simulation (WRF360K-Nudged) was not included in Di Virgilio et al. (2019) but is evaluated here following the same evaluation method and is presented in the online supplemental material in comparison with other CORDEX-Australasia models defined in Di Virgilio et al. (2019). The ensemble of regional models was evaluated against observations contained within the Australian Gridded Climate Dataset (AGCD; Jones et al. 2009) on an annual and seasonal basis. WRF-simulated precipitation variability and trends have also been extensively evaluated (Cortés-Hernández et al. 2016; Fita et al. 2017; Olson et al. 2016; Evans et al. 2017) and performed well overall.

In terms of minimum and maximum temperature, the mean bias for UNSW-WRF360K-Nudged was smaller than the ensemble mean for all seasons of the year, with correlation coefficients r ranging between 0.92 and 0.98 (Table S1 in the online supplemental material). Maximum temperature (annual mean bias -0.64 K ; Table S2 in the online supplemental material) tended to be underestimated in eastern Australia (Fig. S1 in the online supplemental material), especially in winter ($\sim -3 \text{ K}$; Fig. S2 in the online supplemental material) and was overestimated in parts of western and northern Australia in summer ($\sim 2 \text{ K}$; Fig. S3 in the online supplemental material). Annual mean bias in minimum temperature was small (0.24 K ; Table S2 and Fig. S4 in the online supplemental material), with winter minimum temperatures underestimated ($\sim -2 \text{ K}$) in the west and parts of the east, with some overestimation occurring in eastern and northern Australia ($\sim 2 \text{ K}$; Fig. S5 in the online supplemental material). In summer, minimum temperatures were overestimated in central and southeastern Australia ($\sim 2 \text{ K}$) and underestimated in the southwest and northeast ($\sim -1.5 \text{ K}$; Fig. S6 in the online supplemental material).

UNSW-WRF360K-Nudged estimated precipitation well overall (annual $r = 0.88$; Table S1) and better than the equivalent nonnudged simulation (UNSW-WRF360K) in all seasons. UNSW-WRF360K-Nudged underestimated annual precipitation in coastal regions (mean bias $-7.6 \text{ mm month}^{-1}$; Table S2 and Fig. S7 in the online supplemental material), but had the lowest proportion of land with annual mean bias exceeding 10 mm month^{-1} (1% as compared with 24% ensemble mean; Table S3 in the online supplemental material). In winter UNSW-WRF360K-Nudged estimated precipitation well [$r = 0.90$ (Table S1) and mean bias over Australia of $-4.9 \text{ mm month}^{-1}$ (Table S2)] but was positively biased along the southern coastline (up to $\sim 40 \text{ mm month}^{-1}$; Fig. S8 in the online supplemental material). Summer precipitation was also well simulated [$r = 0.93$ (Table S1) and mean bias over Australia of $-16.6 \text{ mm month}^{-1}$ (Table S2)] but overestimated precipitation in the monsoonal north (up to $\sim 40 \text{ mm month}^{-1}$; Fig. S9 in the online supplemental material). In both seasons UNSW-WRF360K-Nudged still achieved a much smaller proportion of land with mean bias exceeding 10 mm month^{-1} (2% and 0.8% in summer and winter, respectively; Table S3) relative to the ensemble mean (24% and 19% in summer and winter, respectively; Table S3).

UNSW-WRF360K-Nudged evapotranspiration estimates were compared to the Derived Optimal Linear Combination Evapotranspiration (DOLCE), version 2 (Hobeichi et al. 2018, 2020), a hybrid of 11 global evapotranspiration datasets. Hobeichi et al. (2018) showed the hybrid dataset outperformed its constituent products when compared to global flux tower measurements. UNSW-WRF360K-Nudged estimated evapotranspiration well overall (annual $r = 0.72$), but relative to DOLCE tended to underestimate ($\sim -0.5 \text{ mm day}^{-1}$) values in the interior north and east of Australia in both summer and winter, with bias reaching $\sim -1.3 \text{ mm day}^{-1}$ along the mountainous region of southeast Australia in summer (Fig. S10 in the online supplemental material). Evapotranspiration was overestimated along the coastlines ($>0.5 \text{ mm day}^{-1}$; Fig. S10) in summer, likely a reflection of large ocean–land evaporation differences and differences in dataset land–water masks at the coastlines. The interannual variability was very similar to that of DOLCE for the study period, with both datasets displaying an 11% coefficient of variation. Neither dataset showed statistically significant ($p < 0.05$) trends in annual continentwide estimates during the study period.

Overall, the strong performance of the WRF simulation compared to observed temperature, precipitation and evapotranspiration, and ability of the model to conserve water (unlike reanalysis products) makes the

simulation ideal for driving the back-trajectory analysis over Australia.

3. Results

a. Evaporative source regions

Moisture source regions showed strong seasonal shifts in evaporative contribution (E_A) and spatial domain. In summer (Fig. 2a), moisture for Australia's precipitation was principally sourced from the Maritime Continent, tropical Indian Ocean, tropical Pacific Ocean, and Tasman Sea and from the subtropical Indian and Southern Oceans close to the Australian continent. Terrestrial contributions from Australia were at their peak in summer and were highest in the northern and eastern parts of the continent. During summer, some terrestrial moisture (1.1%) was also sourced from Indonesia, East Timor, Papua New Guinea, Solomon Islands, Vanuatu, and New Caledonia. The stronger moisture contribution to the north is due to the summer-dominant rainfall climate of northern Australia during the monsoon season. In autumn, moisture contribution from the north declined sharply (Fig. 2b), and the most important source region became the tropical Pacific Ocean and Tasman Sea. In winter, the terrestrial contribution was negligible except for parts of eastern and southwestern Australia (Fig. 2d). Marine source regions contracted southward in line with the northward progression of the subtropical ridge, where frontal systems extend farther into southern Australia, and the northward progression of the monsoon trough, as northern Australia moves into its dry season. In spring, the marine source regions expanded northward once again, and the terrestrial contribution increased across most of the continent, most strongly in the southeast (Fig. 2c) with the Tasman Sea the dominant source. In all seasons the proportion of moisture sourced from outside the model domain tended to be less than 7% of the total contributed to Australian precipitation (Figs. 2e,f; Table S4 in the online supplemental material).

Figure 3 highlights the summer source regions for selected basins in the northwest, southeast and southwest of Australia. Source regions for all basins and seasons are shown in Figs. S11a and S11b in the online supplemental material. Summer precipitation in the northwest as defined by the Tanami–Timor Sea Coast basin (Fig. 3a) was dominated by moisture from the tropical Indian Ocean, Maritime Continent, and the subtropical Indian and Southern Oceans close to Australia. Some moisture was also sourced from the tropical Pacific Ocean, extending east of New Caledonia in summer. In addition to marine moisture, the Tanami–Timor Sea Coast

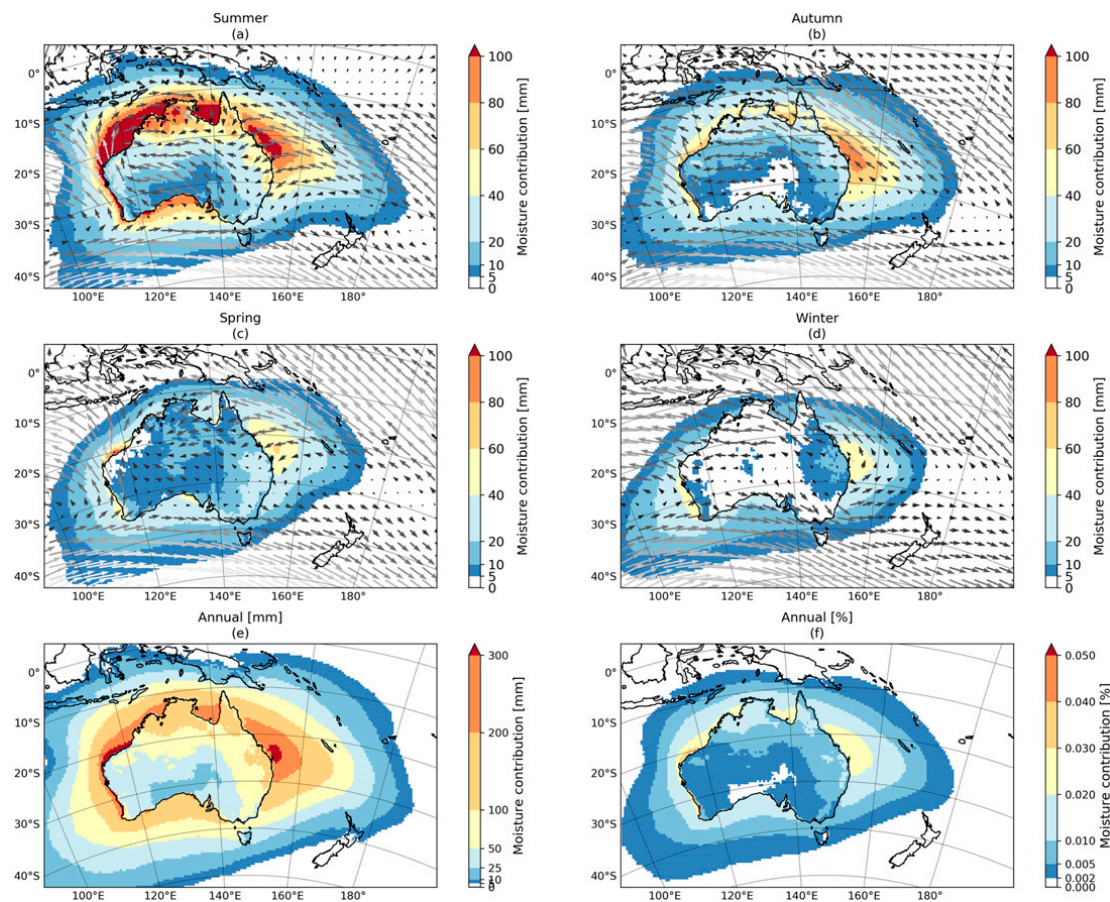


FIG. 2. Mean moisture contribution to Australian precipitation in (a)–(d) each season (mm), with mean climatological low-level wind vectors, (e) annually (mm), and (f) as a percent of annual Australian precipitation (%). Note the nonlinear color scale.

also received significant terrestrial contributions from the basin itself (see section 3b). Total moisture contribution reduced strongly in autumn; was minimal in the dry season and increased again in spring (Fig. S11a). Moisture sourced from outside the model domain was low, reaching a maximum of 3.3% in summer through the western model boundary (Table S4).

Summer precipitation in the southeast as defined by the Murray–Darling Basin (MDB) was primarily sourced from the Tasman Sea, Southern Ocean, and the land within the basin. Secondary contributions were made from the other land and ocean regions, with up to 7.7% of moisture sourced from beyond the southern model boundary (Fig. 3b; Table S4). Unlike the Tanami–Timor Sea Coast, the overall source region for the MDB experienced relatively minor seasonal shifts in spatial contribution (Fig. S11b).

The small moisture contribution to the South West Coast (Fig. 3c) reflects the relatively low seasonal (and annual) precipitation of this comparatively smaller basin. Moisture contribution was constrained to the subtropical Indian and Southern Oceans. Up to 8% of total moisture

was sourced from beyond the southern model boundary in summer, reaching 12.7% through the western boundary in winter (Table S4).

b. Terrestrial and marine contributions

The marine moisture contribution dominated year-round for all basins (Fig. 4). The continent typically received a minimum of 77% of moisture from marine sources in summer and a maximum of 89% in winter (Fig. 4). Terrestrial contributions were greatest in the northern basins compared to the south in summer and autumn and tended to be similar in winter and spring. For all basins, terrestrial contributions peaked in spring and summer.

In summer, north-northwestern basins (North Western Plateau, Tanami–Timor Sea Coast, Carpentaria Coast, and North East Coast) typically received 23% of moisture from terrestrial sources, whereas southeastern basins (MDB; South East Coast, New South Wales; South East Coast, Victoria; Tasmania) received 17% (Fig. 4). The same north-northwestern basins received 12% of moisture from the terrestrial sources during winter (northern dry season),

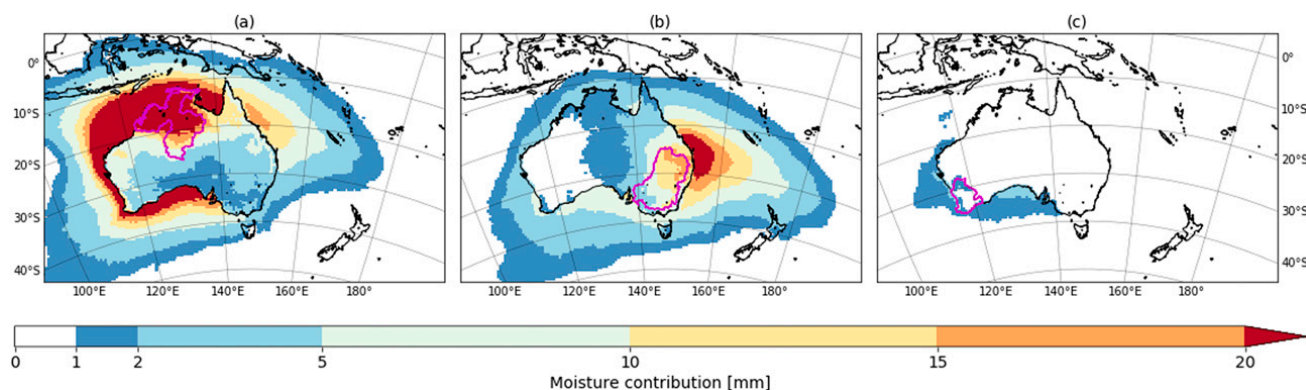


FIG. 3. Mean summer moisture contribution (mm) to precipitation in (a) Tanami–Timor Sea Coast, (b) Murray–Darling Basin, and (c) South West Coast.

compared to the 11% received by southeastern basins. In spring, the southeastern basins received slightly more moisture from the terrestrial sources (18%) relative to north-northwestern basins (17%; Fig. 4).

c. Interannual variability

Interannual variability in terrestrial moisture contribution to Australian precipitation was high for all basins.

Figure 5 shows the mean annual contributions from marine and terrestrial sources, with associated coefficients of variation (CV). The CV is the standard deviation of moisture contributed to the basin normalized by its mean to allow for a direct relative comparison between basins. In a relative sense, interannual moisture contribution from local and nonlocal terrestrial sources (CV 18%) varied more than marine contribution (CV 3%).

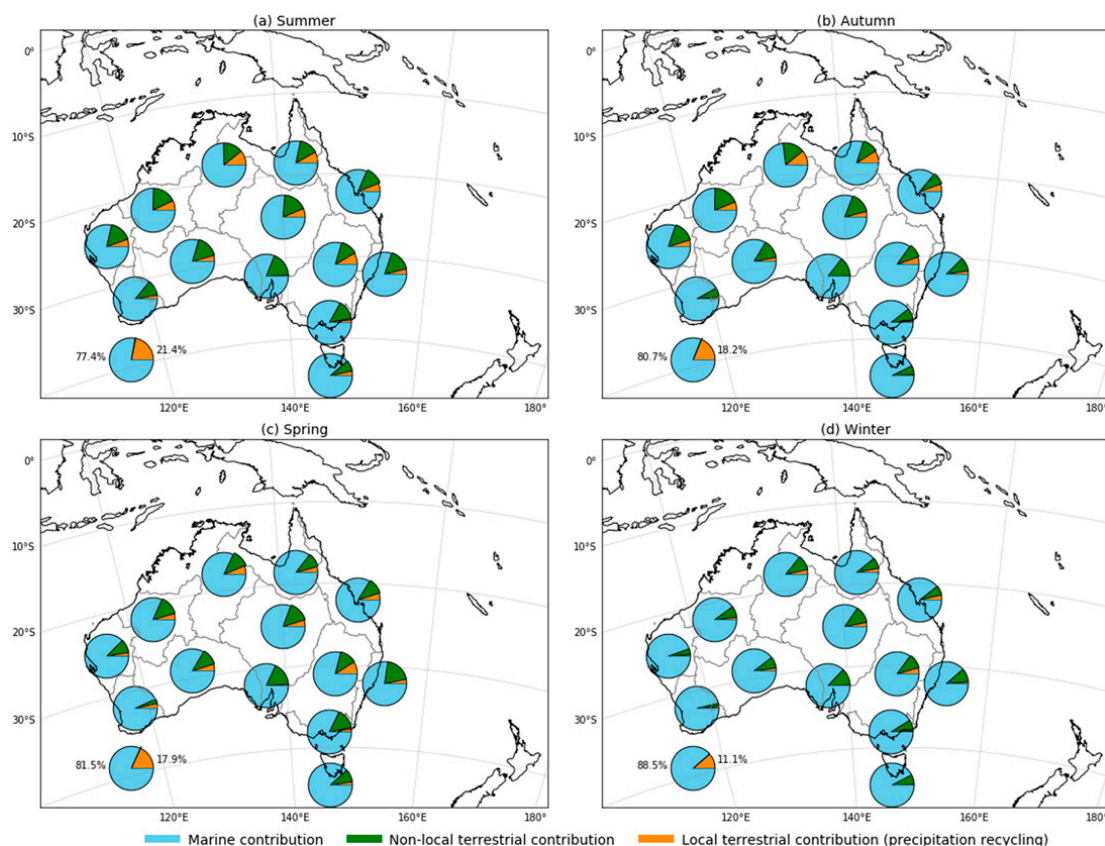


FIG. 4. Mean seasonal contributions to precipitation by basin. Contributions to Australia-wide precipitation are provided in the bottom-left corner of each panel (remaining proportions represent moisture contributed from other countries).

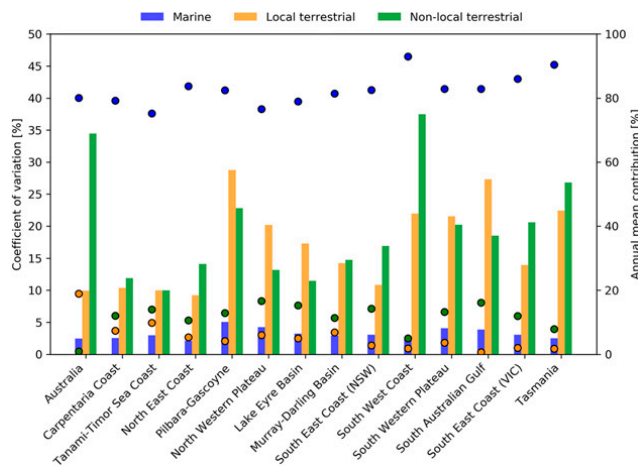


FIG. 5. Interannual variability in marine and terrestrial contribution to precipitation, presented as the coefficient of variation (bars; left axis) with annual mean contribution (dots; right axis).

The annual marine contribution to North East Coast rainfall was the least variable (CV 2.1%; Fig. 5), whereas Pilbara–Gascoyne, located in the westernmost part of Australia (Fig. 1), experienced the largest interannual variability (CV 5%; Fig. 5). The North East Coast and Pilbara–Gascoyne also experienced the lowest (CV 9.2%; Fig. 5) and highest (CV 28.8%; Fig. 5) interannual variability in local terrestrial contribution (i.e., precipitation recycling, see section 3d). The annual nonlocal terrestrial contribution to the Tanami–Timor Sea Coast was the least variable (CV 10%; Fig. 5), and the South West Coast was most variable (CV 37.5%; Fig. 5).

Figure 6 decomposes the interannual variability in the marine contribution by ocean region, with regions defined in Fig. 1. It shows the contribution each ocean region makes to the total interannual variability in moisture contributed to Australia and its subbasins. That is, for each basin, we divide the variance in contribution from each ocean region (mm) by the variance in the total marine contribution (mm). As expected, Fig. 6 shows greater variability in the southern basins compared to the tropical north. In all seasons the Southern Ocean contributed the most to variability of the southern basins (e.g., >50% for Tasmania in all seasons), as well as the Tasman Sea to most basins and especially those on the east coast (e.g., >50% for South East Coast, New South Wales, in all seasons). The tropical Indian Ocean contributed to variability in the northern basins during the wet season, but, like the Maritime Continent, was very stable in the dry season. The subtropical Indian Ocean contributed to variability of the southwestern basins in all seasons and western basins in winter. The South Pacific Ocean, tropical Pacific Ocean, and Maritime Continent contributed the least to interannual variability across Australia. Like

Fig. 5, Fig. 6 shows North East Coast experienced the smallest variability in its source regions.

d. Precipitation recycling

Figure 7 shows the annual cycle of precipitation recycling (ρ) for Australia and each basin. On average 19% of moisture was recycled to contribute to further precipitation across Australia (Fig. 7a). The northern tropical basins (Carpentaria Coast and Tanami–Timor Sea Coast) recycled the largest amount of local moisture, recycling a maximum of 8.8%–11.4% of monthly precipitation (ρ ; Fig. 7). Apart from these, the MDB recycled more precipitation than any of the other basins in the east, south, northwest and northeast of Australia, recycling a maximum of 9.2%, and 6.9% on average across the year (ρ ; Fig. 7h). The least amount of precipitation was recycled in the South Australian Gulf (0.7%), Tasmania (1.7%), and South West Coast (1.8%; Fig. 7). Recycling in the northern basins peaked in March at the end of the wet season, as did the northwestern basins (Pilbara–Gascoyne and North Western Plateau). Recycling in the Lake Eyre Basin and the southern basins peaked between October and January. All southern basins recycled the least amount of precipitation in June. While the northern and northwestern basins experienced a minimum in June/July, the minimum recycling in the Carpentaria Coast was delayed until September, that is, at the very end of the dry season.

The scaled precipitation recycling estimates ρ_s follow the same spatial pattern as the actual estimates, with highest recycling in the northern and southeast basins and lowest in the southwest (Fig. 7). Scaled recycling estimates are discussed and compared to previous studies in section 4c.

e. Trends

Figure 8 shows temporal linear trends (1979–2013) in seasonal moisture contributions to precipitation in each basin, sourced from individual ocean regions (Fig. 1), the Australian landmass outside the basin and the land area within each basin. Trends are expressed as the change in seasonal moisture relative to the mean total seasonal moisture received by each basin (1979–2013). Trends in moisture contribution were frequently positive in spring and summer and negative in autumn and winter (Fig. 8). A positive trend in moisture contribution to northwestern basins is clear, especially in spring (Fig. 8d). Positive contributions occurred over all ocean areas, as well as the local and nonlocal terrestrial sources of moisture.

Trends in moisture contribution may be due to a change in source region evaporation, anomalous

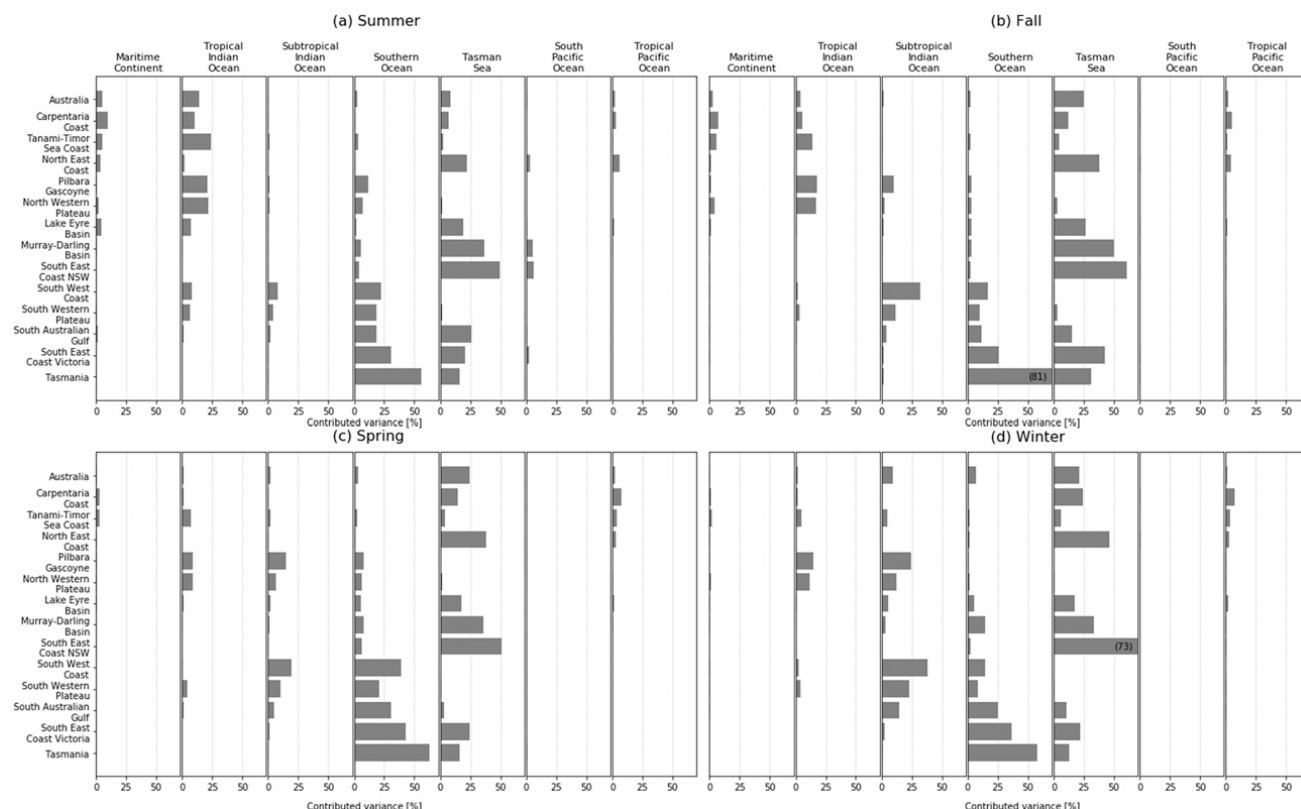


FIG. 6. Contribution to variance in moisture supplied to Australia and its subbasins by each ocean region. Values are provided in parentheses where the bar exceeds the axis limit.

atmospheric circulation (i.e., the moisture was generated but transported elsewhere), a lack of local precipitation-generating mechanisms, land surface control on the atmosphere through coupling processes, or a combination of factors. Considering trends in evaporation of the source regions, we can, to first order, diagnose the processes driving the trends in moisture contribution. Positive spring trends in moisture contributed to the northwest coincides with positive trends in evaporation in the Maritime Continent, subtropical Indian Ocean, and tropical Pacific Ocean (Table S5 in the online supplemental material).

The South Pacific Ocean and the Tasman Sea showed significant positive trends in summer, with the highest trends in the MDB (Fig. 8a). In summer, the net upward trend in seasonal moisture contributed to the MDB amounted to $+0.94\% \text{ yr}^{-1}$ (Fig. 8a). In other words, 0.94% more moisture was available for summer precipitation in the MDB each year, compared to the summer average. Moisture declined by $-1.33\% \text{ yr}^{-1}$ in autumn (Fig. 8b) and $-0.88\% \text{ yr}^{-1}$ in winter (Fig. 8c), and increased in spring by $+0.35\% \text{ yr}^{-1}$ (Fig. 8d), resulting in a net $-0.12\% \text{ yr}^{-1}$ decline in moisture received by the MDB over the 35-yr period. The positive trend in moisture contribution in summer along with the decrease in winter does not coincide with significant

evaporation trends in the key source regions of the Tasman Sea and Southern Ocean (Table S5).

4. Discussion

a. Source regions

Our results show source regions vary markedly across the country. Along with notable terrestrial contributions in the north and southeast, moisture for precipitation in each basin was primarily derived from proximate marine sources. We note our marine evaporative source regions coincide with regions of high marine evaporation (Yu 2007), especially in the Pacific Ocean.

Dirmeyer et al. (2009) estimated similar source regions for the Lake Eyre Basin (available at <http://cola.gmu.edu/wcr/>). Our estimate of the annual terrestrial contributions within Lake Eyre Basin and northeastern Australia was $< 30 \text{ mm yr}^{-1}$ (Fig. S11a) as compared with Dirmeyer et al.'s (2009) estimate of $< 50 \text{ mm yr}^{-1}$. Dirmeyer et al. (2009) also estimated a stronger annual terrestrial contribution from within the MDB (up to $\sim 100 \text{ mm yr}^{-1}$ as compared with our estimate of up to $\sim 50 \text{ mm yr}^{-1}$; Fig. S11b), and a stronger contribution from the Southern Ocean ($\sim 100 \text{ mm yr}^{-1}$ as compared with $\sim 50 \text{ mm yr}^{-1}$ in our study; Fig. S11b). We note Stohl and James (2005) indicated the Tasman Sea to be the most important

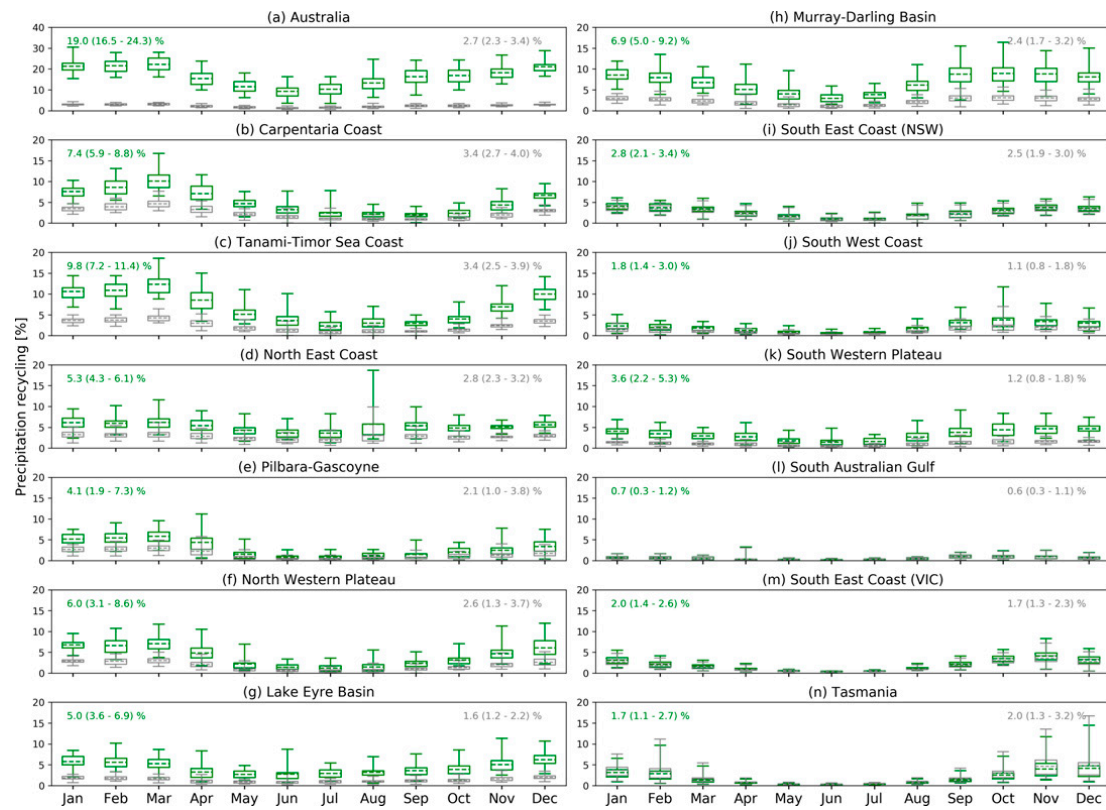


FIG. 7. Mean monthly precipitation recycling (ρ ; green) and scaled precipitation recycling (ρ_s ; gray). Annual mean and range are given in the top-left corner of each panel, and scaled estimates are given in the top-right corner. Note the different vertical scale for Australia in (a).

source of moisture to the MDB, contributing up to $\sim 100 \text{ mm yr}^{-1}$ of moisture to the basin, which is very similar to our results. However, [Stohl and James \(2005\)](#) estimated a greater contribution from the land surface in eastern Australia (up to $\sim 100 \text{ mm yr}^{-1}$) as compared with our estimate of $\sim 50 \text{ mm yr}^{-1}$ (Fig. S11b).

For the whole continent, the dominant annual source regions supplying moisture to precipitation across Australia match estimates by [Dirmeyer et al. \(2009\)](#). In both studies the main sources are proximate oceanic regions as well as the north and east of Australia. However, we estimate a greater contribution from the ocean and a smaller contribution from the land. This is demonstrated in the eastward and southward extension of the Pacific and Southern Oceans source regions relative to [Dirmeyer et al. \(2009\)](#). We estimate contributions up to 200 mm yr^{-1} as far east as $\sim 170^\circ\text{E}$ and as far south as $\sim 40^\circ\text{S}$ (Fig. 2e), as compared with $\sim 155^\circ\text{E}$ and $\sim 35^\circ\text{S}$ by [Dirmeyer et al. \(2009\)](#). While both studies estimate that the greatest terrestrial contributions come from northern and eastern Australia, we estimate contributions up to $\sim 200 \text{ mm yr}^{-1}$ (Fig. 2e) as compared with $\sim 200\text{--}300 \text{ mm yr}^{-1}$ by [Dirmeyer et al. \(2009\)](#).

The importance of moisture from each ocean region varied for precipitation falling in different parts of Australia. Similar to our results, [van der Ent and](#)

[Savenije \(2013\)](#) estimated evaporation from the western tropical Pacific Ocean contributed to annual precipitation over most of the country except the southwestern and southeastern regions during 1990–2009. A similar result was also found by [Gimeno et al. \(2012\)](#), who found evaporation from the Coral Sea (covering part of the regions defined as the tropical Pacific Ocean and Tasman Sea in the present study) supplied moisture for precipitation over much of the continent in summer and northern and eastern Australia in winter, similar to the present study. Differences in source region estimates were expected due to different forcing, moisture tracking algorithms and time periods covered. We used a 0.5° 3D Lagrangian back-tracking algorithm driven by an ERA-Interim-constrained regional simulation over 1979–2013. [Dirmeyer et al. \(2009\)](#) back-tracked moisture at 1.9° resolution using CMAP and NCEP data over 1979–2003. [Stohl and James \(2005\)](#) back-tracked moisture using the 3D Lagrangian flexible particle dispersion model (FLEXPART) at 1° using data from ECMWF over 1999–2003. [Gimeno et al. \(2012\)](#) also used FLEXPART, but with data from ERA-40 over 1980–2000, and forward-tracked moisture from predefined ocean regions. Finally, [van der Ent and Savenije \(2013\)](#) used a 1.5° vertically

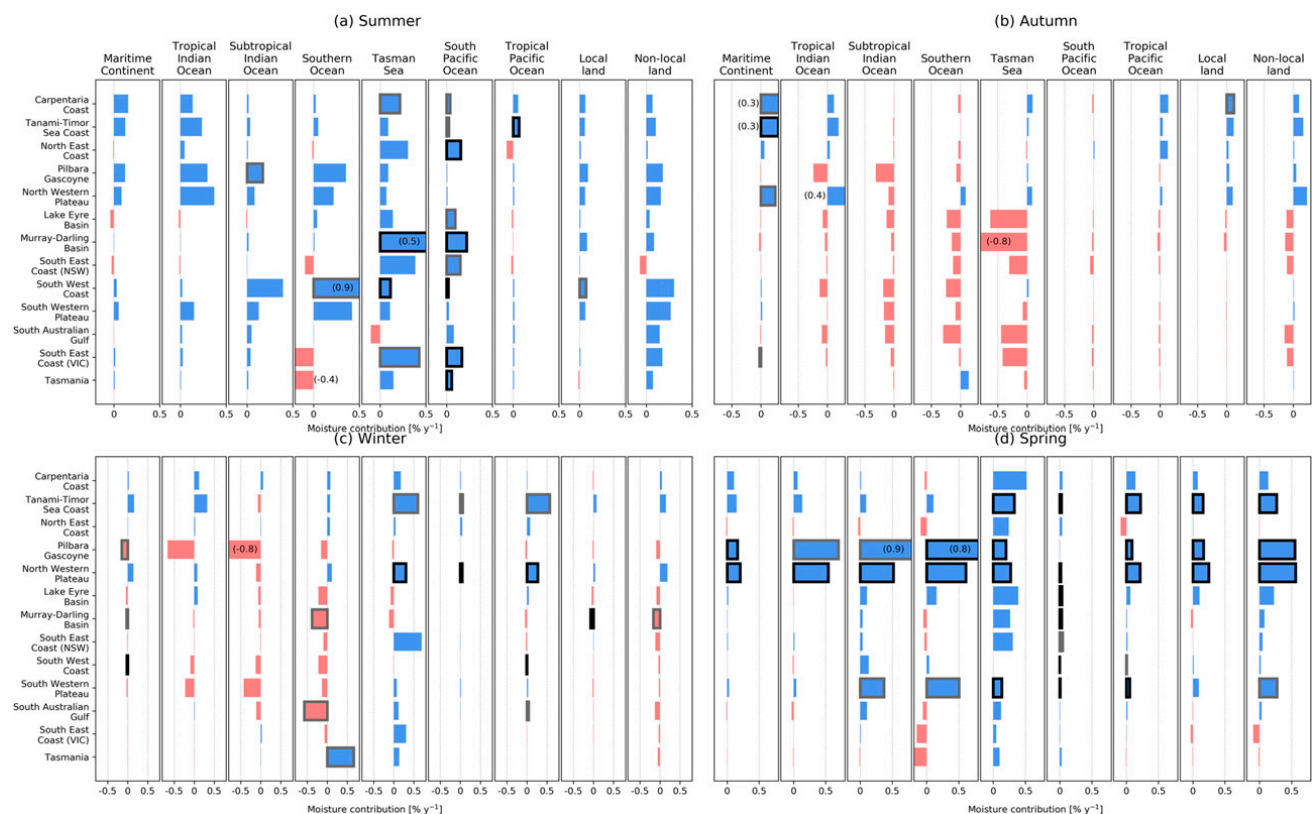


FIG. 8. Trends in seasonal moisture contribution ($\% \text{ yr}^{-1}$). Values represent the change in moisture contributed by each source relative to the mean (1979–2013) total moisture received by each basin each season. Trends that are statistically significant at the 95% level are edged in thick black lines, and those that are significant at the 90% level are edged in thick gray lines. Positive trends are shown in blue; negative trends are shown in red. Note the different axis limits among seasons; values are provided in parentheses where the bar exceeds the axis limit.

averaged 2D Eulerian procedure using ERA-Interim over 1990–2009, and forward-tracked moisture from predefined ocean regions. These methodologies reflect major differences in approach, assumptions, and data that account for differences in the results. We note the higher spatial resolution of forcing used in our study allows for finer representation of precipitation, particularly in areas of high relief such as the mountainous region in southeastern Australia. Furthermore, in some cases the atmospheric and evaporation data used in previous studies was independent of the precipitation estimate, while our approach uses a self-consistent water cycle.

SOURCES OF MOISTURE FOR SOUTHEAST AUSTRALIAN PRECIPITATION

An interesting feature in the identified source regions relates to northwest cloud bands (NWCBS), which commonly extend from the tropics in the northwest to the extratropics in the southeast and have been linked to precipitation in southeast Australia (Bureau of Meteorology 2013). Our back-tracking approach finds no evidence that precipitation in southeast Australia relies on moisture from the northwest. For the MDB and South East

Coast (New South Wales and Victoria) basins, we found moisture is primarily sourced from the Tasman Sea.

The apparent disagreement with the possible role of NWCBS can be reconciled. Reid et al. (2019) shows that days with NWCBS are associated with a northwest–southeast-oriented trough pattern, flanked by high pressure systems to the southwest and north-northeast. The anticyclone to the northeast advects warm, moist tropical air southward where it is lifted over the cooler and drier air in the region of the trough. The location of the southeast's key source region from our results, the Tasman Sea, supports this model. McIntosh et al. (2012) also supports this interpretation. They back-tracked a precipitation event in the Mallee region of southern Australia that appeared associated with a northwest to southeast band of clouds. They found moisture was sourced from the ocean to the northeast of Australia, not the northwest. As the air parcel traveled southward from the northeast it was forced to rise over colder air and subsequently condensed and contributed to precipitation. For the same region Brown et al. (2009) demonstrated that the moisture source, apparently to the west based on a snapshot of winds, was to the northeast when proper consideration was given to the time-

dependent winds and parcel height. Overall, the NWCBS therefore set up the large-scale synoptic conditions that allow oceanic moisture from the Tasman Sea to be advected anticyclonically into the trough, to be subsequently lifted and precipitated in Australia's southeast. Thus, while the NWCBS are an expression of the moisture-advecting process, it is unlikely they are a major source of moisture for precipitation in the southeast.

b. Terrestrial and marine contributions

Our results show advected marine evaporation is relatively more important than terrestrial evapotranspiration as a source of moisture for precipitation across Australia. More than three-quarters of moisture supplying Australia's precipitation is derived from ocean sources throughout the year and can reach over 90% in some basins. While moisture for precipitation in different basins is sourced from different ocean regions, the Tasman Sea is the most important contributor of moisture for all but the western and northwestern basins, where the Indian and Southern Oceans are the most important sources.

While all regions of Australia are dominated by marine contribution, some regions are more reliant on terrestrial contributions than others. The north-northwest basins rely on terrestrial moisture in summer and autumn for around one-quarter of their seasonal precipitation. Southeastern basins rely on terrestrial moisture for around 18% of their spring and summer precipitation and, like the rest of southern Australia, experience higher levels of interannual variability in terrestrial contribution compared to the north. Continentwide terrestrial contributions were around 6 times more variable than marine sources. Since the north-northwest and southeast regions receive more moisture from terrestrial evapotranspiration than others, these areas are most vulnerable to land-cover changes. Potential changes in land cover that lower evapotranspiration will lower the supply of moisture for precipitation (Pitman et al. 2004), especially in regions that rely on it including the North Western Plateau, Tanami–Timor Sea Coast, Carpentaria Coast, North East Coast, MDB, and Lake Eyre. In contrast, the South West Coast is particularly vulnerable to changes in SSTs and atmospheric circulation processes that bring moisture from its relatively small marine source region, which supplies more than 97% of moisture for precipitation in winter.

c. Precipitation recycling

From the source regions, we computed a long-term time series of precipitation recycling for each basin and for the continent. On average, 19% of precipitation was recycled to contribute to further annual precipitation over Australia. Recycling was greatest in spring and summer

and lowest in winter. The seasonal cycle of recycling was evident in all basins, with slight differences in the timing of minima and maxima depending on location.

Land–atmosphere coupling, as measured by precipitation recycling, was strongest in northern and eastern Australia. In summer and autumn, coupling processes amplified available moisture to contribute to further precipitation most strongly in the Carpentaria Coast (average annual maximum of 8.8%) and Tanami–Timor Sea Coast (average annual maximum of 11.4%), semi-arid North Western Plateau (average annual maximum of 8.6%), and Pilbara–Gascoyne (average annual maximum of 7.3%). Terrestrial processes amplified precipitation most strongly in spring and summer in the temperate MDB (average annual maximum of 9.2%). Recycling appeared least important in southwestern regions, approaching 0% in winter. The southwestern basins of South West Coast, South Western Plateau, and South Australian Gulf were dominated by remote processes that advect marine moisture onshore each month.

Our estimates of precipitation recycling show a similar spatial pattern to previous recycling estimates. The spatial pattern of recycling—highest in the north-northwest and southeast, and lowest in the southwest—is similar to van der Ent and Savenije (2011), van der Ent et al. (2010), and Dirmeyer et al. (2009). However, we estimate slightly lower recycling ratios. At a scale of 10^5 km^2 , we estimate recycling to range from an annual average of approximately 1% in the southwest to 3.4% in the north-northwest (Fig. 7), as compared with previous estimates of approximately <2%–8% (Dirmeyer and Brubaker 2007), <3%–8% (Dirmeyer et al. 2009), and <1%–5% (van der Ent and Savenije 2011). Our range of estimates varied little ($\pm 0.1\%$) when we matched the time period to that of Dirmeyer and Brubaker (2007) and Dirmeyer et al. (2009), 1979–2003, or to van der Ent and Savenije (2011), 1999–2008. Moreover, the range of recycling estimated by previous studies fits within the interannual variability estimated here (Fig. 5). Differences in estimates were expected because of different forcing, resolution, and back-trajectory algorithms, as discussed in section 4a.

The relatively low recycling ratios estimated in the present study echo the results of Hope and Watterson (2018), who found limited precipitation persistence across Australia following very wet months. While the analysis did not directly estimate recycling, it indicates that any recycling was limited and declined quickly after the precipitation events.

d. Trends

The positive summer and negative winter trends in moisture contributed to the MDB align with observed

precipitation trends (Bureau of Meteorology 2020). No significant trends were found in the associated marine source region evaporation in this study. This suggests regional moisture contribution changes are not a direct result of changes to marine source region evaporation. Instead these changes may be due to shifts in atmospheric circulation patterns, local land–atmosphere coupling or precipitation-generating mechanisms, or a combination of factors. Indeed, a range of processes have been identified as partially explaining the observed seasonal precipitation changes in southeastern Australia. These include changes in the frequency of El Niño and La Niña events (Cai and Cowan 2008; Freund et al. 2019), the Indian Ocean dipole (Ummenhofer et al. 2009), an increasing influence of the northern dry season (Cai and Cowan 2013), and the upward trend in the southern annular mode (Nicholls 2010).

Long-term changes to regional moisture contribution can also point to potential drivers of MDB precipitation trends. Precipitation simulated by WRF showed a positive trend of $+1.3 \text{ mm yr}^{-1}$ ($p < 0.05$) in summer, and -0.9 mm yr^{-1} ($p \leq 0.15$) in winter, similar to estimates by the Bureau of Meteorology (2010) using gauged precipitation observations for the same period ($+1.5$ and -0.6 mm yr^{-1} in summer and winter, respectively). Of the positive summer trend, 52% ($+0.7 \text{ mm yr}^{-1}$; $p < 0.05$) was associated with rising contributions in summer moisture from the Tasman Sea, and 22% ($+0.3 \text{ mm yr}^{-1}$; $p \leq 0.1$) from the South Pacific Ocean. Of the negative winter trend, 36% (-0.3 mm yr^{-1} ; $p \leq 0.1$) was associated with declining contributions in moisture from the Southern Ocean, 16% (-0.15 mm yr^{-1} ; $p < 0.1$) from the nonlocal land and 7% (-0.06 mm yr^{-1} ; $p < 0.05$) from the local land surface. These results suggest that MDB precipitation is being affected by an increase in the easterly flow of moisture from the Tasman Sea in summer and by a reduction in both terrestrial moisture and the westerly flow of moisture from the Southern Ocean in winter.

We found an upward trend in marine contributions to the northwest of Australia, especially in spring. We also found a significant upward trend in terrestrial contribution, indicating a strengthening of land–atmosphere coupling in this region in spring. Precipitation in northwest Australia has exhibited an increasing trend of more than $30 \text{ mm decade}^{-1}$ since the 1950s (Holper 2011). The attribution of these changes remains uncertain, but our results showed that positive trends in the marine contribution align with positive trends in evaporation in the associated marine source regions. This suggests that intensified evaporation, particularly in the Maritime Continent, subtropical Indian Ocean, and tropical Pacific Ocean, may have led to increased moisture advection over northwest Australia, which may, in turn, have

contributed to the increasing precipitation seen in this region since the 1950s.

Observed precipitation declines in the southwest since the 1960s are not supported by significant declining trends in moisture contribution in this study. Hope et al. (2010) reported a 17% decline in May–July precipitation in southwest Australia between 1969 and 2007, with sharper declines in the 1990s. Declining precipitation in the region has been attributed to a reduction in the number of low pressure systems and increase in persistence of high pressure systems (Hope et al. 2006). While our results indicate negative trends in moisture contributed to the region in winter, these are either small or statistically insignificant.

5. Conclusions

Using a Lagrangian back-trajectory approach, we quantified the evaporative source regions and level of precipitation recycling for Australia and multiple hydrological basins. Presenting the seasonal climatology of the newly established multidecadal time series of source region and recycling, we identify the key marine and terrestrial regions that supply moisture for precipitation across Australia.

We showed, for the first time, that source regions varied markedly across the different hydrological basins within Australia. In the north, key sources included the tropical Indian and Pacific Oceans, the Maritime Continent, and evapotranspiration from the northern Australian land surface. In the southwest, terrestrial contributions were minimal, and moisture was supplied from a small source region within the Southern and subtropical Indian Oceans. The key source regions for the southeast were the Tasman Sea and Southern Ocean, with secondary contributions from terrestrial sources. While the Tasman Sea and the Southern Ocean were the most important source regions for precipitation in the south and east of Australia, they were also the ocean regions to exhibit the greatest interannual variability. Interannual variability of ocean sources was much less than terrestrial sources, whose year-to-year variability was 6 times greater than marine sources on average.

We have shown that advected marine evaporation dominated the moisture contributed to precipitation across Australia in all seasons, compared to terrestrial evapotranspiration. While marine advection was relatively more important, some regions were more reliant on terrestrial contributions than others. Precipitation in the north-northwest and southeast relied on terrestrial moisture for up to one-quarter of its seasonal precipitation. Precipitation in the north-northwest and southeast is therefore most vulnerable to land-cover

changes that may potentially alter the amount of evapotranspiration, and thus the terrestrial moisture available for local precipitation. In contrast, precipitation in the southwest was dominated by remote processes as it received the majority of its moisture from a relatively small ocean region, making it vulnerable to atmospheric circulation changes that advect the moisture necessary for precipitation in this region.

The level of recycling of terrestrial moisture and the strength of land-atmosphere coupling varied across Australia. On average 19% of moisture was recycled across Australia to contribute to further precipitation each year. Recycling was strongest in northern and eastern Australia in spring and summer (~9%), and weakest in the southwest in winter. Winter land-atmosphere coupling strength declined in the MDB over the last 35 years, as demonstrated by the downward trend in precipitation recycling in this region. In contrast coupling strength in the northwestern basins increased, particularly in spring.

Moisture contributed by different ocean regions showed distinct changes over the study period. Summer moisture from the South Pacific Ocean and the Tasman Sea showed positive trends for most basins. The MDB in particular showed positive trends in marine and terrestrial contributions in spring and summer and negative trends in autumn and winter, in line with observed precipitation trends. Furthermore, we found a positive trend in both terrestrial and marine contributions to the northwest of Australia, especially in spring, which is also in line with observed trends in precipitation.

The relative importance of local and remote processes and strength of coupling processes presented here represent the average or climatological condition. A next step is to analyze the relative roles of marine advection versus local recycling during the various stages of drought development. This is particularly relevant in the MDB, a region that has suffered extreme droughts in recent years and where land-atmosphere coupling strength appears relatively strong. Insight into land-atmosphere coupling behavior during drought onset, duration, and termination will help guide our understanding of climate processes and aid the model developments needed to improve the prediction of this region's precipitation and its extremes. However, there are other regions of Australia where the variability or trend in precipitation is impacting natural and human systems. The dataset that forms the basis of this study provides a foundation for future analysis of precipitation in each part of Australia and can be used to explore, for example, the origin of drought-breaking events, the origin of the most intense events, or the role of large-scale drivers in source region variability.

Acknowledgments. This work was made possible by an Australian National University Australian Government Research Training Scholarship for author Holgate and support from the ARC Centre of Excellence for Climate System Science (CE110001028). Holgate and author van Dijk were supported through the ARC Discovery Projects funding scheme (project DP40103679). Authors Evans and Pitman were supported through the ARC Centre of Excellence for Climate Extremes (CE170100023). The authors thank the NCI and its staff for computational support and Jessica Keune and two anonymous reviewers for their constructive feedback. CORDEX-Australasia climate simulations are publicly available online (<https://climatechange.environment.nsw.gov.au/Climate-projections-for-NSW/About-NARCLim/>).

REFERENCES

- Brown, J. N., P. C. McIntosh, M. J. Pook, and J. S. Risbey, 2009: An investigation of the links between ENSO flavors and rainfall processes in southeastern Australia. *Mon. Wea. Rev.*, **137**, 3786–3795, <https://doi.org/10.1175/2009MWR3066.1>.
- Brubaker, K. L., D. Entekhabi, and P. S. Eagleson, 1993: Estimation of continental precipitation recycling. *J. Climate*, **6**, 1077–1089, [https://doi.org/10.1175/1520-0442\(1993\)006<1077:EOCPR.2.0.CO;2](https://doi.org/10.1175/1520-0442(1993)006<1077:EOCPR.2.0.CO;2).
- Bureau of Meteorology, 2010: Australian climate averages—Rainfall (climatology 1961–1990). Bureau of Meteorology, accessed 17 October 2019, http://www.bom.gov.au/jsp/ncc/climate_averages/rainfall/index.jsp.
- , 2012: Australian Hydrological Geospatial Fabric (Geofabric). Bureau of Meteorology, accessed 18 October 2019, <http://www.bom.gov.au/water/about/riverBasinAuxNav.shtml>.
- , 2013: About Australian climate. Bureau of Meteorology, accessed 28 November 2019, <http://www.bom.gov.au/climate/about/?bookmark=nwcloudband>.
- , 2020: Climate change and variability: Tracker: Australian timeseries graphs. Bureau of Meteorology, accessed 11 May 2020, http://www.bom.gov.au/climate/change/index.shtml#tabs=Tracker&tracker=timeseries&tQ=graph%3Ddrain%26area%3Dmdb%26season%3D0608%26ave_yr%3D1.
- Cai, W., and T. Cowan, 2008: Dynamics of late autumn rainfall reduction over southeastern Australia. *Geophys. Res. Lett.*, **35**, L09708, <https://doi.org/10.1029/2008GL033727>.
- , and —, 2013: Southeast Australia autumn rainfall reduction: A climate-change-induced poleward shift of ocean-atmosphere circulation. *J. Climate*, **26**, 189–205, <https://doi.org/10.1175/JCLI-D-12-00035.1>.
- Cortés-Hernández, V. E., F. Zheng, J. Evans, M. Lambert, A. Sharma, and S. Westra, 2016: Evaluating regional climate models for simulating sub-daily rainfall extremes. *Climate Dyn.*, **47**, 1613–1628, <https://doi.org/10.1007/s00382-015-2923-4>.
- Dirmeyer, P. A., and K. L. Brubaker, 1999: Contrasting evaporative moisture sources during the drought of 1988 and the flood of 1993. *J. Geophys. Res.*, **104**, 19 383–19 397, <https://doi.org/10.1029/1999JD900222>.
- , and —, 2007: Characterization of the global hydrologic cycle from a back-trajectory analysis of atmospheric water vapor. *J. Hydrometeorol.*, **8**, 20–37, <https://doi.org/10.1175/JHM557.1>.

- , —, and T. DelSole, 2009: Import and export of atmospheric water vapor between nations. *J. Hydrol.*, **365**, 11–22, <https://doi.org/10.1016/j.jhydrol.2008.11.016>.
- , J. Wei, M. G. Bosilovich, and D. M. Mocko, 2014: Comparing evaporative sources of terrestrial precipitation and their extremes in MERRA using relative entropy. *J. Hydrometeorol.*, **15**, 102–116, <https://doi.org/10.1175/JHM-D-13-053.1>.
- Di Virgilio, G., and Coauthors, 2019: Evaluating reanalysis-driven CORDEX regional climate models over Australia: Model performance and errors. *Climate Dyn.*, **53**, 2985–3005, <https://doi.org/10.1007/s00382-019-04672-w>.
- Eltahir, E. A. B., and R. L. Bras, 1996: Precipitation recycling. *Rev. Geophys.*, **34**, 367–378, <https://doi.org/10.1029/96RG01927>.
- Evans, J. P., A. J. Pitman, and F. T. Cruz, 2011: Coupled atmospheric and land surface dynamics over southeast Australia: A review, analysis and identification of future research priorities. *Int. J. Climatol.*, **31**, 1758–1772, <https://doi.org/10.1002/joc.2206>.
- , F. Ji, G. Abramowitz, and M. Ekström, 2013: Optimally choosing small ensemble members to produce robust climate simulations. *Environ. Res. Lett.*, **8**, 044050, <https://doi.org/10.1088/1748-9326/8/4/044050>.
- , D. Argüeso, R. Olson, and A. Di Luca, 2017: Bias-corrected regional climate projections of extreme rainfall in south-east Australia. *Theor. Appl. Climatol.*, **130**, 1085–1098, <https://doi.org/10.1007/s00704-016-1949-9>.
- Fita, L., J. P. Evans, D. Argüeso, A. King, and Y. Liu, 2017: Evaluation of the regional climate response in Australia to large-scale climate modes in the historical NARCLIM simulations. *Climate Dyn.*, **49**, 2815–2829, <https://doi.org/10.1007/s00382-016-3484-x>.
- Freund, M. B., B. J. Henley, D. J. Karoly, H. V. McGregor, N. J. Abram, and D. Dommenget, 2019: Higher frequency of central Pacific El Niño events in recent decades relative to past centuries. *Nat. Geosci.*, **12**, 450–455, <https://doi.org/10.1038/s41561-019-0353-3>.
- Gimeno, L., and Coauthors, 2012: Oceanic and terrestrial sources of continental precipitation. *Rev. Geophys.*, **50**, RG4003, <https://doi.org/10.1029/2012RG000389>.
- Goessling, H. F., and C. H. Reick, 2013: On the “well-mixed” assumption and numerical 2-D tracing of atmospheric moisture. *Atmos. Chem. Phys.*, **13**, 5567–5585, <https://doi.org/10.5194/acp-13-5567-2013>.
- Hobeichi, S., G. Abramowitz, J. Evans, and A. Ukkola, 2018: Derived Optimal Linear Combination Evapotranspiration (DOLCE): A global gridded synthesis ET estimate. *Hydrol. Earth Syst. Sci.*, **22**, 1317–1336, <https://doi.org/10.5194/hess-22-1317-2018>.
- , —, and —, 2020: Derived Optimal Linear Combination Evapotranspiration—DOLCE v2.0. Research Data Australia, accessed 14 May 2020, <https://doi.org/10.25914/5eab8f533aeae>.
- Holper, P. N., 2011: Australian rainfall—Past, present and future. CSIRO and the Bureau of Meteorology Paper, 18 pp., accessed 15 October 2019, <https://www.cawcr.gov.au/projects/Climatechange/wp-content/uploads/2016/11/rainfall-paper.pdf>.
- Hope, P. K., and I. Watterson, 2018: Persistence of cool conditions after heavy rain in Australia. *J. South. Hemisphere Earth Syst. Sci.*, **68**, 41–64, <https://doi.org/10.22499/3.6801.004>.
- , W. Drosowsky, and N. Nicholls, 2006: Shifts in the synoptic systems influencing southwest Western Australia. *Climate Dyn.*, **26**, 751–764, <https://doi.org/10.1007/s00382-006-0115-y>.
- , B. Timbal, and R. Fawcett, 2010: Associations between rainfall variability in the southwest and southeast of Australia and their evolution through time. *Int. J. Climatol.*, **30**, 1360–1371, <https://doi.org/10.1002/joc.1964>.
- Jones, D. A., W. Wang, and R. Fawcett, 2009: High-quality spatial climate data-sets for Australia. *Aust. Meteor. Oceanogr. J.*, **58**, 233–248, <https://doi.org/10.22499/2.5804.003>.
- McIntosh, P. C., J. S. Risbey, J. N. Brown, and M. J. Pook, 2012: Apparent and real sources of rainfall associated with a cutoff low in southeast Australia. *CAWCR Research Letters*, No. 8, The Centre for Australian Weather and Climate Research, Melbourne, Australia, 4–9, https://www.cawcr.gov.au/researchletters/CAWCR_Research_Letters_8.pdf.
- Merrill, J. T., R. Bleck, and D. Boudra, 1986: Techniques of Lagrangian trajectory analysis in isentropic coordinates. *Mon. Wea. Rev.*, **114**, 571–581, [https://doi.org/10.1175/1520-0493\(1986\)114<0571:TOLTAI>2.0.CO;2](https://doi.org/10.1175/1520-0493(1986)114<0571:TOLTAI>2.0.CO;2).
- Miralles, D. G., and Coauthors, 2016: Contribution of water-limited ecoregions to their own supply of rainfall. *Environ. Res. Lett.*, **11**, 124007, <https://doi.org/10.1088/1748-9326/11/12/124007>.
- Nicholls, N., 2010: Local and remote causes of the southern Australian autumn–winter rainfall decline, 1958–2007. *Climate Dyn.*, **34**, 835–845, <https://doi.org/10.1007/s00382-009-0527-6>.
- Olson, R., J. Evans, A. Di Luca, and D. Argüeso, 2016: The NARCLIM project: Model agreement and significance of climate projections. *Climate Res.*, **69**, 209–227, <https://doi.org/10.3354/cr01403>.
- Pitman, A. J., G. T. Narisma, R. A. Pielke, and N. J. Holbrook, 2004: Impact of land cover change on the climate of southwest Western Australia. *J. Geophys. Res.*, **109**, D18109, <https://doi.org/10.1029/2003JD004347>.
- Reid, K. J., I. Simmonds, C. L. Vincent, and A. D. King, 2019: The Australian northwest cloudband: Climatology, mechanisms, and association with precipitation. *J. Climate*, **32**, 6665–6684, <https://doi.org/10.1175/JCLI-D-19-0031.1>.
- Sharmila, S., and H. H. Hendon, 2020: Mechanisms of multiyear variations of Northern Australia wet-season rainfall. *Sci. Rep.*, **10**, 5086, <https://doi.org/10.1038/s41598-020-61482-5>.
- Stohl, A., and P. James, 2005: A Lagrangian analysis of the atmospheric branch of the global water cycle. Part II: Moisture transports between Earth’s ocean basins and river catchments. *J. Hydrometeorol.*, **6**, 961–984, <https://doi.org/10.1175/JHM470.1>.
- Ummenhofer, C. C., M. H. England, P. C. McIntosh, G. A. Meyers, M. J. Pook, J. S. Risbey, A. S. Gupta, and A. S. Taschetto, 2009: What causes southeast Australia’s worst droughts? *Geophys. Res. Lett.*, **36**, L04706, <https://doi.org/10.1029/2008GL036801>.
- van der Ent, R. J., and H. H. G. Savenije, 2011: Length and time scales of atmospheric moisture recycling. *Atmos. Chem. Phys.*, **11**, 1853–1863, <https://doi.org/10.5194/acp-11-1853-2011>.
- , and —, 2013: Oceanic sources of continental precipitation and the correlation with sea surface temperature. *Water Resour. Res.*, **49**, 3993–4004, <https://doi.org/10.1002/wrcr.20296>.
- , —, B. Schaeffli, and S. C. Steele-Dunne, 2010: Origin and fate of atmospheric moisture over continents. *Water Resour. Res.*, **46**, W09525, <https://doi.org/10.1029/2010WR009127>.
- Yu, L., 2007: Global variations in oceanic evaporation (1958–2005): The role of the changing wind speed. *J. Climate*, **20**, 5376–5390, <https://doi.org/10.1175/2007JCLI1714.1>.
- Zhang, J., W.-C. Wang, and J. Wei, 2008: Assessing land-atmosphere coupling using soil moisture from the global land data assimilation system and observational precipitation. *J. Geophys. Res.*, **113**, D17119, <https://doi.org/10.1029/2008JD009807>.

4.2.1 Supplementary material

Supplementary text: Back-trajectory model assumptions

While testing of the assumptions of a vertically well-mixed atmosphere and height at which precipitation forms is beyond the scope of this study, past attempts to address the uncertainty can be drawn upon to estimate the validity of the assumptions over Australia.

Goessling and Reick (2013) tested the vertical well-mixed assumption by investigating the two main causes of vertical moisture inhomogeneities: vertical wind shear, and the difference in moisture content in the lower and upper parts of the atmosphere. Based on this work, vertical wind shear is not expected to heavily influence moisture source estimates for two reasons. First, unlike 2D back-trajectory models, our 3D model resolves winds vertically. Second, Goessling and Reick (2013) estimate that most parts of Australia typically do not experience strong wind shear, except for the southwest in January and north in July, when in both cases precipitation is low (precipitation in the southwest is winter-dominant, and summer monsoon-dominant in the north). Goessling and Reick (2013) also show that the vertical profile of moisture is typically uniform over Australia during January, indicating that the well-mixed assumption is likely to hold. The authors showed moisture was overrepresented in the lower half of the atmosphere above Australia in July, and above the surrounding oceans in January and July, suggesting the well-mixed assumption may not hold as well in winter over land and over the ocean. Furthermore, in practice the well-mixed assumption means surface evaporation may be added to air parcels at any point along their trajectory (to the extent that moisture has evaporated from the surface at that location, while the parcel is overhead) regardless of the parcel's height. This is a strong assumption when parcels are located high in the atmosphere, when connection between the air parcel and surface fluxes may be minimal. Other back-trajectory models (e.g. FLEXPART, HYSPLIT) add moisture to parcels based on changes in specific humidity, allowing the model to output the net loss or gain of moisture along the trajectory. However these models experience different disadvantages compared to the present approach, most notably the inability to separate precipitation and evaporation.

Van Der Ent and Savenije (2013) tested the effect of releasing parcels from a constant low-level height, compared to a random height, on the spatial distribution of evaporative origin and the recycling ratio for a region in west Africa. While little change to the pattern of evaporative origin was found, considerably more moisture originated within the region. This result was linked to the strong wind shear present in their study area; parcels released at a

low level followed the westerly winds present at low levels, while parcels released higher up followed a more easterly trajectory. As already mentioned, strong wind shear is not expected to heavily influence source regions estimated for Australian precipitation (Goessling and Reick 2013). The impact of the precipitation-formation height assumption is further moderated by the large number of parcels released at each time step. At each 10-minute back-trajectory time step, up to 100 parcels may be released, dependent on the amount of precipitation. As more parcels are released, the importance of the height at which any one parcel is released becomes smaller and the estimate of the evaporative origin converges.

Based on these considerations, it is expected that relaxation of the well-mixed and precipitation-formation height assumptions may have limited effect on the climatological source regions and recycling ratios presented in this study.

Supplementary figures

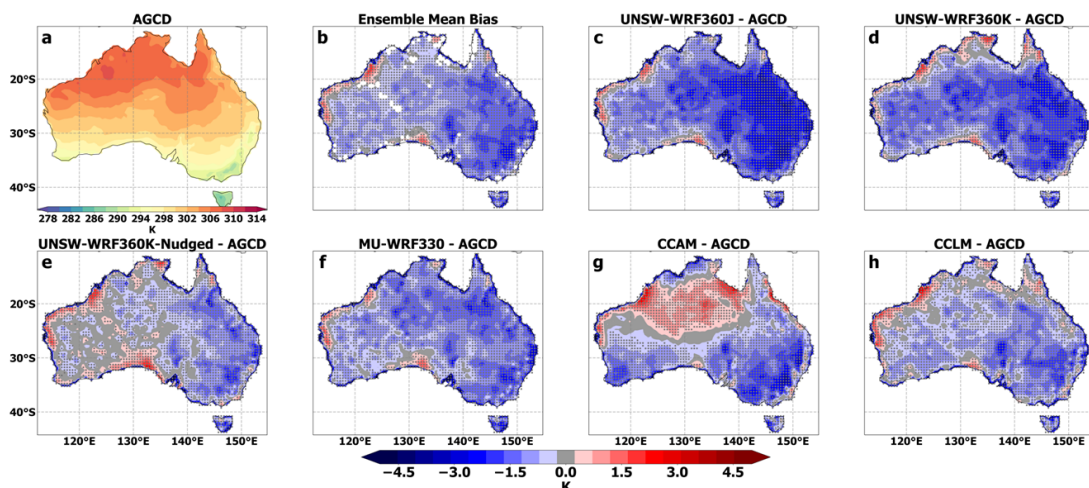


Figure 4.S1: Annual mean near-surface atmospheric maximum temperature bias with respect to Australian Gridded Climate Data (AGCD) observations for the RCMs. Stippled areas indicate locations where an RCM shows statistically significant bias ($p < 0.05$). b Significance stippling for the ensemble mean bias follows Tebaldi et al. (2011). Statistically insignificant areas are shown in colour, denoting that less than half of the models are significantly biased. In significant agreeing areas (stippled), at least half of RCMs are significantly biased, and at least 66% of the significant RCMs agree on the direction of the bias. Significant disagreeing areas are shown in white, which are where at least half of the models are significantly biased and less than 66% significant models agree on the bias direction.

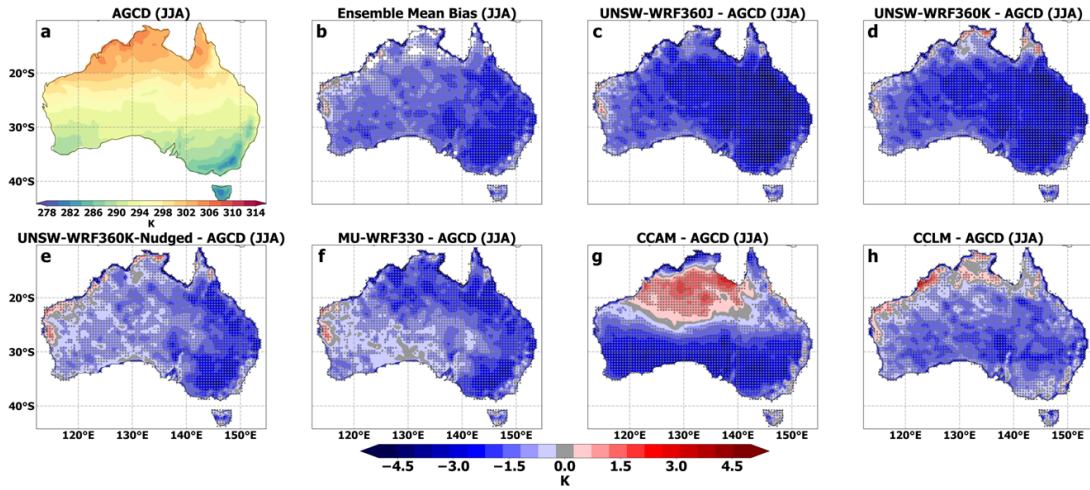


Figure 4.S2: Winter (JJA) maximum temperature bias with respect to AGCD observations with stippling as per Figure 4.S1.

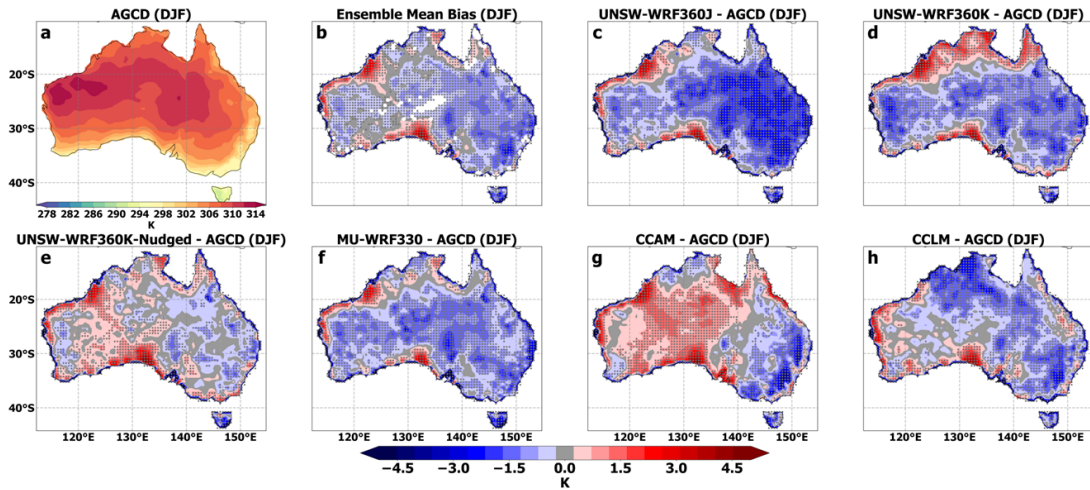


Figure 4.S3: Summer (DJF) maximum temperature bias with respect to AGCD observations with stippling as per Figure 4.S1.

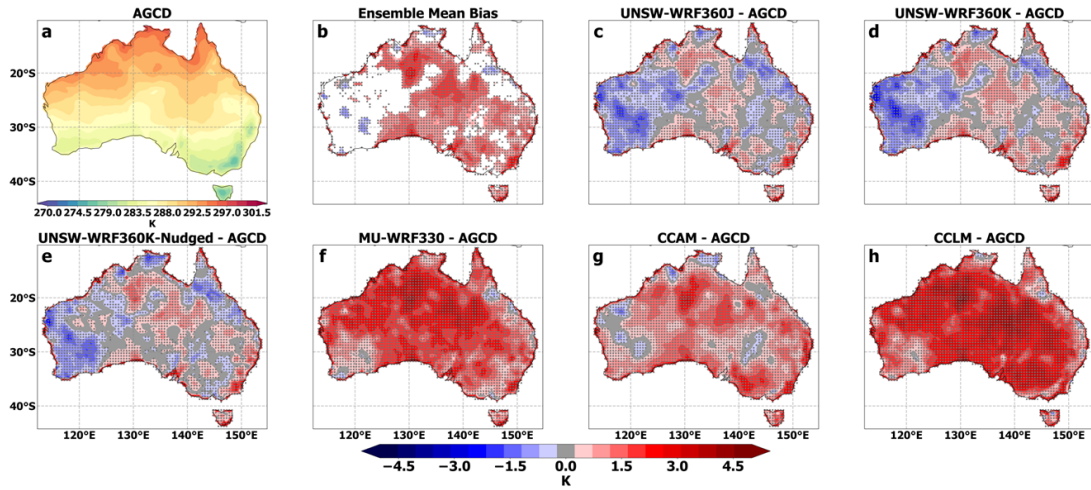


Figure 4.S4: Annual mean minimum temperature bias (K) with respect to AGCD observations for the RCMs with stippling as per Figure 4.S1.

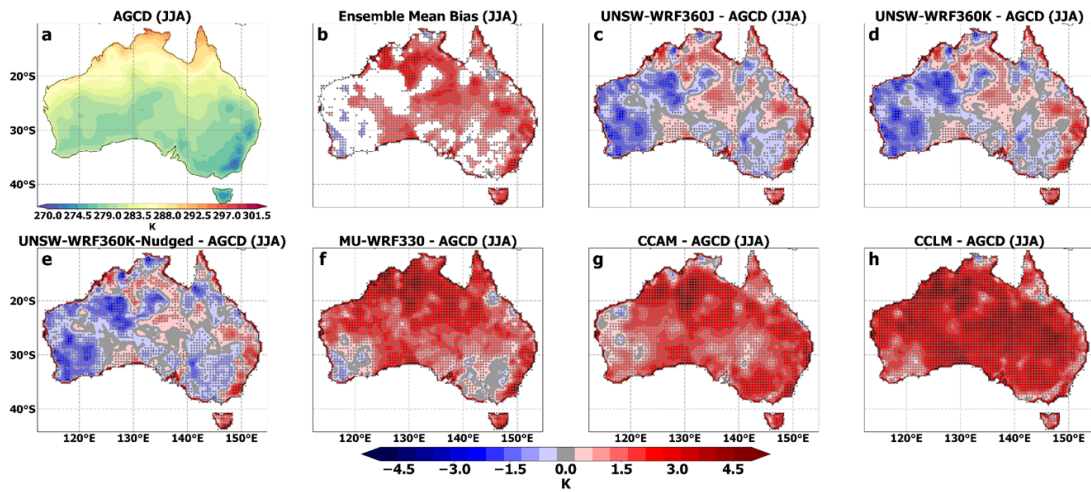


Figure 4.S5: Winter (JJA) minimum temperature bias with respect to AGCD observations with stippling as per Figure 4.S1.

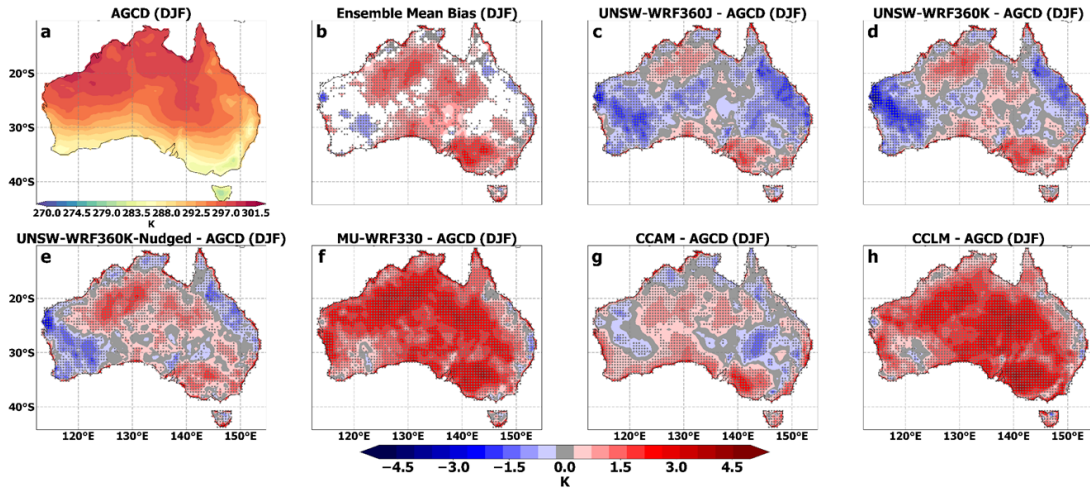


Figure 4.S6: Summer (DJF) minimum temperature bias with respect to AGCD observations with stippling as per Figure 4.S1.

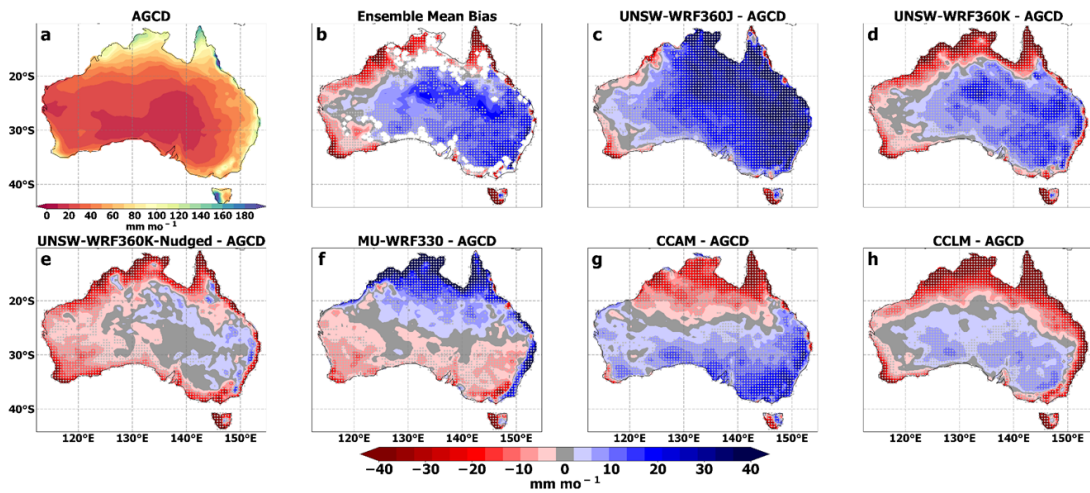


Figure 4.S7: Annual mean precipitation bias of the RCMs with stippling as per Figure 4.S1.

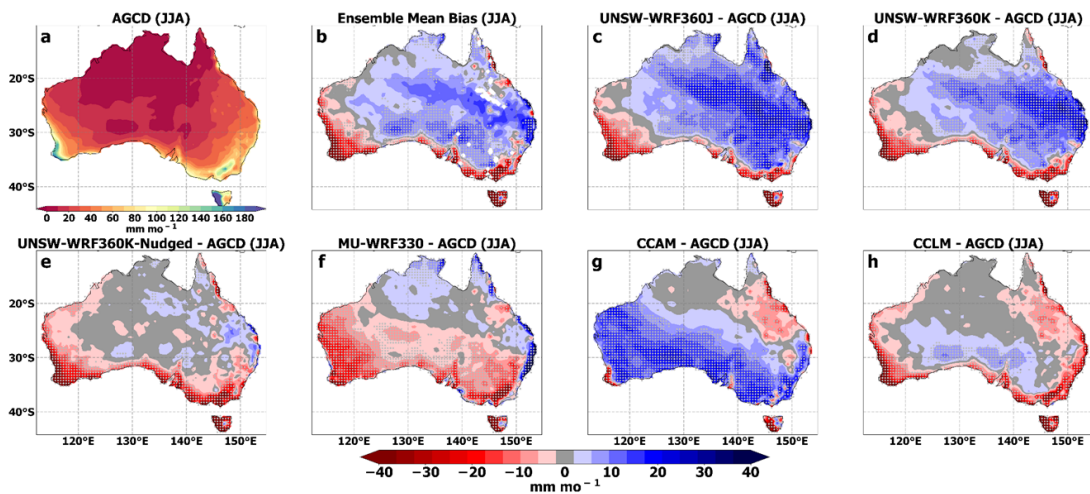


Figure 4.S8: Winter (JJA) precipitation bias with respect to AGCD observations with stippling as per Figure 4.S1.

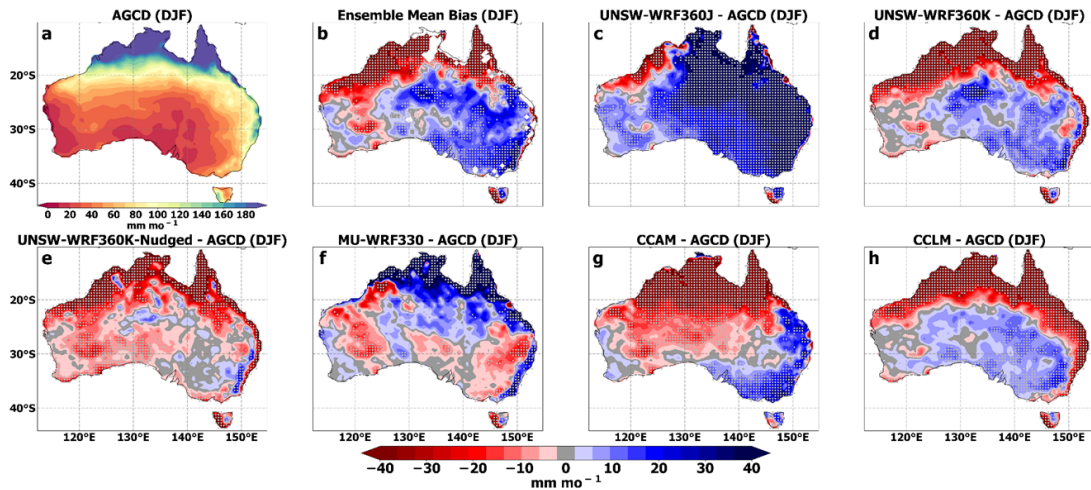


Figure 4.S9: Summer (DJF) precipitation bias with respect to AGCD observations with stippling as per Figure 4.S1.

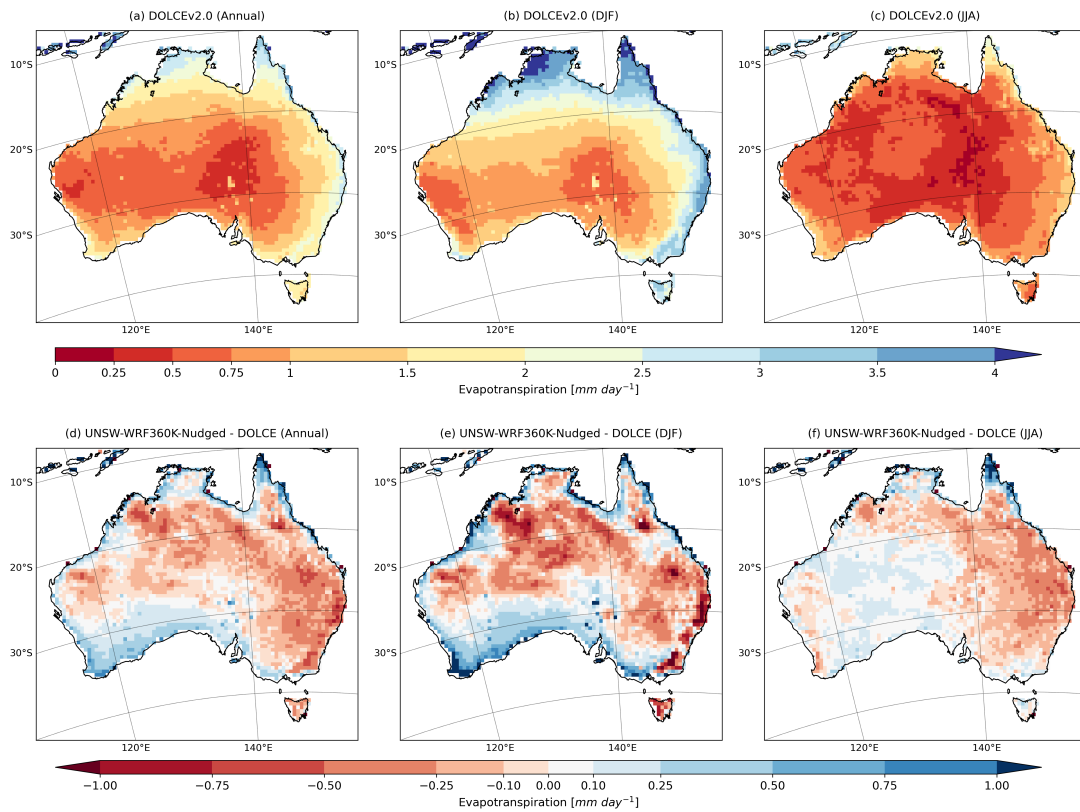


Figure 4.S10: Annual, summer (DJF) and winter (JJA) evapotranspiration bias with respect to DOLCEv2.

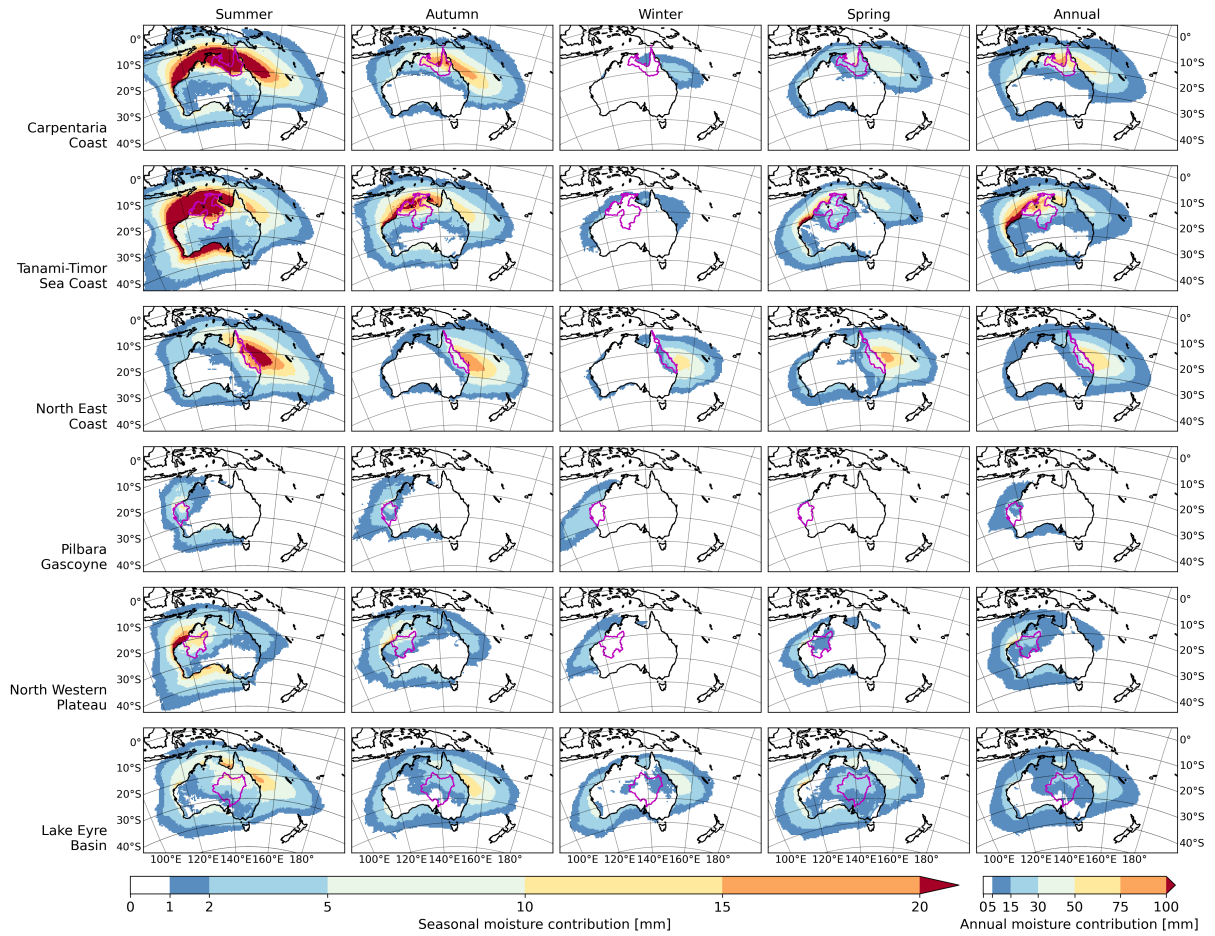


Figure 4.S11: Mean moisture contribution [mm] for precipitation in each basin, both seasonally (first four columns) and annually (rightmost column).

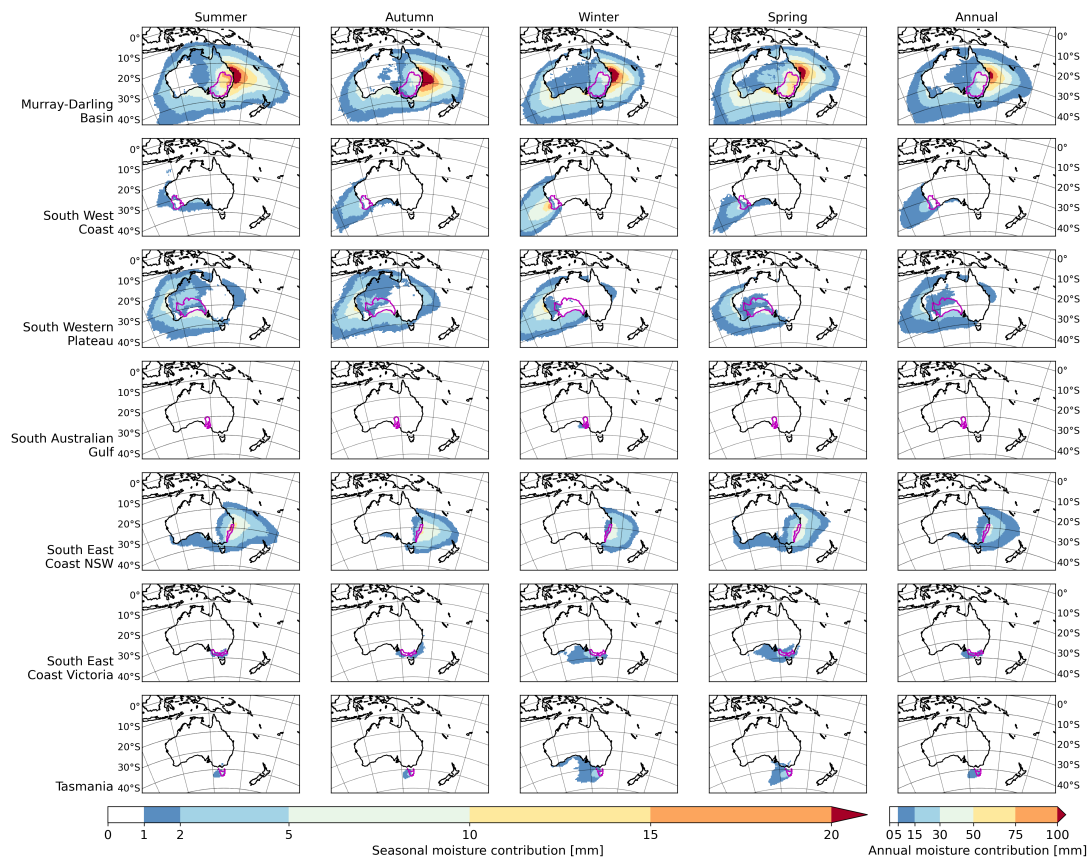


Figure 4.S12: Same as Figure 4.S11 for remaining basins.

Supplementary tables

| Variable | Period | WRF-J | WRF-K | WRF-K-Nudged | MU-WRF | CCAM | CCLM | Ensemble mean |
|---------------------------------|--------|-------|-------|--------------|--------|------|------|---------------|
| Temp. max [K] | Annual | 0.96 | 0.96 | 0.96 | 0.96 | 0.97 | 0.96 | 0.96 |
| | DJF | 0.92 | 0.92 | 0.93 | 0.94 | 0.94 | 0.93 | 0.93 |
| | MAM | 0.96 | 0.96 | 0.96 | 0.97 | 0.96 | 0.97 | 0.96 |
| | JJA | 0.97 | 0.97 | 0.98 | 0.98 | 0.97 | 0.98 | 0.98 |
| | SON | 0.95 | 0.96 | 0.95 | 0.96 | 0.97 | 0.96 | 0.96 |
| Temp. min [K] | Annual | 0.95 | 0.94 | 0.95 | 0.97 | 0.97 | 0.96 | 0.96 |
| | DJF | 0.96 | 0.95 | 0.96 | 0.97 | 0.97 | 0.97 | 0.97 |
| | MAM | 0.94 | 0.94 | 0.94 | 0.96 | 0.95 | 0.95 | 0.95 |
| | JJA | 0.93 | 0.92 | 0.92 | 0.95 | 0.95 | 0.95 | 0.94 |
| | SON | 0.96 | 0.95 | 0.95 | 0.97 | 0.97 | 0.97 | 0.96 |
| Prec. [mm month ⁻¹] | Annual | 0.85 | 0.74 | 0.88 | 0.89 | 0.85 | 0.82 | 0.84 |
| | DJF | 0.92 | 0.84 | 0.93 | 0.94 | 0.90 | 0.90 | 0.91 |
| | MAM | 0.83 | 0.77 | 0.87 | 0.87 | 0.84 | 0.73 | 0.82 |
| | JJA | 0.85 | 0.84 | 0.90 | 0.88 | 0.91 | 0.92 | 0.88 |
| | SON | 0.80 | 0.81 | 0.85 | 0.84 | 0.89 | 0.83 | 0.84 |

Table 4.S1: Mean Pearson correlation between Australian Gridded Climate Data as reference data and six RCMs, for annual and seasonal mean minimum and maximum temperature and precipitation for the period January 1981 to January 2010.

| Variable | Period | WRF-J | WRF-K | WRF-K-Nudged | MU-WRF | CCAM | CCLM | Ensemble mean |
|---------------------------------|--------|-------|--------|--------------|--------|--------|--------|---------------|
| Temp. max [K] | Annual | -1.66 | -1.40 | -0.64 | -1.16 | -0.55 | -0.81 | -1.04 |
| | DJF | -1.27 | -0.78 | -0.24 | -0.97 | 0.09 | -0.80 | -0.66 |
| | MAM | -1.78 | -1.49 | -0.65 | -1.67 | -0.70 | -0.96 | -1.21 |
| | JJA | -2.29 | -2.03 | -1.22 | -1.40 | -1.17 | -1.17 | -1.55 |
| | SON | -1.31 | -1.31 | -0.44 | -0.60 | -0.42 | -0.32 | -0.73 |
| Temp. min [K] | Annual | 0.12 | 0.21 | 0.24 | 1.88 | 1.06 | 2.30 | 0.97 |
| | DJF | -0.13 | 0.13 | 0.38 | 1.81 | 0.37 | 1.72 | 0.71 |
| | MAM | 0.32 | 0.54 | 0.48 | 1.61 | 0.91 | 2.51 | 1.06 |
| | JJA | 0.28 | 0.26 | 0.11 | 1.88 | 1.91 | 2.83 | 1.21 |
| | SON | 0.00 | -0.07 | -0.01 | 2.21 | 1.04 | 2.16 | 0.89 |
| Prec. [mm month ⁻¹] | Annual | 17.04 | -0.92 | -7.59 | 5.12 | 0.02 | -8.26 | 0.90 |
| | DJF | 24.78 | -17.63 | -16.61 | 12.62 | -16.72 | -18.76 | -5.38 |
| | MAM | 18.58 | 4.88 | -6.81 | 8.80 | 0.37 | -7.34 | 3.08 |
| | JJA | 6.20 | 2.71 | -4.85 | -4.15 | 6.09 | -4.24 | 0.29 |
| | SON | 18.61 | 6.37 | -2.09 | 3.20 | 10.35 | -2.72 | 5.62 |

Table 4.S2: Mean biases of six RCMs for annual and seasonal mean minimum and maximum temperature and precipitation for the period January 1981 to January 2010 with Australian Gridded Climate Data as reference data.

| Variable | Period | WRF-J | WRF-K | WRF-K-Nudged | MU-WRF | CCAM | CCLM | Ensemble mean |
|---------------------------------|--------|-------|-------|--------------|--------|------|------|---------------|
| Prec. [mm month ⁻¹] | Annual | 67.8 | 32.5 | 1.0 | 20.9 | 21.5 | 1.5 | 24.2 |
| | DJF | 73.4 | 18.2 | 2.0 | 27.4 | 14.0 | 9.5 | 24.1 |
| | MAM | 75.4 | 55.9 | 4.0 | 28.3 | 29.9 | 19.4 | 35.5 |
| | JJA | 42.7 | 26.1 | 0.8 | 4.4 | 39.6 | 0.2 | 19.0 |
| | SON | 70.0 | 38.9 | 4.4 | 19.6 | 52.8 | 6.8 | 32.1 |

Table 4.S3: Proportion of cells [%] with bias greater than 10 mm month⁻¹.

| Region | Season | North | South | West | East |
|------------------------|--------|-------|-------|-------|-------|
| Australia | DJF | 0.29 | 4.15 | 2.41 | 0.07 |
| | MAM | 0.27 | 3.35 | 2.54 | 0.04 |
| | JJA | 0.01 | 3.09 | 3.64 | 0.02 |
| | SON | 0.01 | 4.51 | 2.56 | <0.01 |
| Carpentaria Coast | DJF | 0.59 | 1.95 | 1.97 | 0.07 |
| | MAM | 0.61 | 1.14 | 1.44 | 0.10 |
| | JJA | 0.10 | 1.48 | 1.03 | 0.24 |
| | SON | 0.04 | 2.06 | 1.78 | 0.02 |
| Tanami-Timor Sea Coast | DJF | 0.35 | 2.80 | 3.29 | 0.03 |
| | MAM | 0.48 | 1.69 | 2.56 | 0.03 |
| | JJA | 0.06 | 1.59 | 1.74 | 0.04 |
| | SON | 0.02 | 2.73 | 2.89 | <0.01 |
| North East Coast | DJF | 0.26 | 2.88 | 0.97 | 0.16 |
| | MAM | 0.34 | 1.95 | 0.95 | 0.10 |
| | JJA | 0.03 | 1.87 | 1.00 | 0.06 |
| | SON | 0.02 | 3.02 | 1.26 | 0.02 |
| Pilbara-Gascoyne | DJF | 0.05 | 5.24 | 3.94 | <0.01 |
| | MAM | 0.06 | 2.56 | 7.63 | <0.01 |
| | JJA | <0.01 | 0.73 | 13.02 | <0.01 |
| | SON | 0.01 | 3.16 | 8.24 | <0.01 |
| North Western Plateau | DJF | 0.12 | 4.74 | 3.71 | 0.01 |
| | MAM | 0.25 | 2.68 | 3.92 | 0.02 |
| | JJA | 0.02 | 1.27 | 4.67 | 0.01 |
| | SON | <0.01 | 3.66 | 4.51 | <0.01 |
| Lake Eyre Basin | DJF | 0.24 | 4.93 | 1.91 | 0.10 |
| | MAM | 0.18 | 4.09 | 1.75 | 0.04 |
| | JJA | 0.02 | 2.86 | 1.51 | 0.03 |
| | SON | 0.01 | 4.44 | 2.46 | <0.01 |
| Murray-Darling Basin | DJF | 0.02 | 7.71 | 1.15 | 0.13 |
| | MAM | 0.04 | 5.57 | 1.17 | 0.02 |
| | JJA | <0.01 | 3.52 | 1.27 | <0.01 |
| | SON | <0.01 | 5.40 | 1.74 | <0.01 |
| South East Coast (NSW) | DJF | <0.01 | 7.00 | 0.86 | 0.10 |
| | MAM | 0.04 | 4.64 | 0.65 | <0.01 |
| | JJA | <0.01 | 2.29 | 0.68 | <0.01 |
| | SON | <0.01 | 4.94 | 1.12 | <0.01 |
| South West Coast | DJF | 0.01 | 7.52 | 4.19 | <0.01 |
| | MAM | 0.01 | 5.82 | 10.75 | <0.01 |
| | JJA | <0.01 | 3.97 | 12.62 | <0.01 |
| | SON | <0.01 | 8.33 | 11.99 | <0.01 |
| South Western Plateau | DJF | 0.05 | 8.01 | 4.02 | 0.02 |
| | MAM | 0.05 | 4.95 | 5.14 | 0.01 |
| | JJA | <0.01 | 2.57 | 6.57 | <0.01 |
| | SON | <0.01 | 5.33 | 4.95 | <0.01 |
| South Australian Gulf | DJF | 0.04 | 10.13 | 2.45 | 0.07 |
| | MAM | 0.04 | 6.88 | 2.78 | 0.02 |
| | JJA | <0.01 | 4.13 | 2.34 | <0.01 |
| | SON | <0.01 | 6.72 | 3.22 | <0.01 |
| South East Coast (VIC) | DJF | <0.01 | 12.69 | 1.22 | 0.08 |
| | MAM | 0.02 | 9.70 | 1.36 | <0.01 |
| | JJA | <0.01 | 6.57 | 1.67 | <0.01 |
| | SON | <0.01 | 8.49 | 2.10 | <0.01 |
| Tasmania | DJF | <0.01 | 22.54 | 1.53 | 0.02 |
| | MAM | <0.01 | 18.87 | 1.86 | <0.01 |
| | JJA | <0.01 | 12.28 | 2.27 | <0.01 |
| | SON | <0.01 | 16.48 | 2.59 | <0.01 |

Table 4.S4: Proportion of total moisture sourced from outside the model domain [%].

| Ocean | Summer | Autumn | Winter | Spring |
|--------------------------|---------|---------|---------|---------|
| Maritime Continent | +0.19** | +0.24** | +0.15** | +0.15* |
| Tropical Indian Ocean | +0.02 | +0.25** | -0.06 | 0 |
| Subtropical Indian Ocean | +0.21 | +0.28** | +0.24** | +0.36** |
| Southern Ocean | -0.22 | - | +0.09 | +0.14** |
| Tasman Sea | +0.04 | +0.13* | +0.07 | +0.19** |
| South Pacific Ocean | -0.06 | -0.24** | +0.03 | -0.04 |
| Tropical Pacific Ocean | +0.13 | -0.01 | +0.07 | +0.10** |

Table 4.S5: Trends in seasonal evaporation over ocean regions [% y^{-1}], (* $p < 0.1$, ** $p < 0.05$).

4.3 Chapter summary

This chapter quantified the strength of land-atmosphere interactions using the precipitation recycling ratio. The results show land-atmosphere interactions have the strongest influence on precipitation in north and southeast Australia, where precipitation recycling is highest ($\sim 9\%$ of monthly precipitation is recycled), and least influence in the southwest ($< 2\%$). Land-atmosphere interactions affect precipitation most strongly in spring and summer, and least in winter.

The analysis identified the sources of moisture contributing to precipitation in each part of Australia for the first time. Moisture sources varied considerably for precipitation falling in different areas. Advected marine moisture was the dominant source of moisture for Australian precipitation, supplying over three-quarters of moisture in all regions and seasons. Specifically, moisture from the Tasman and Coral Seas was most important for precipitation in eastern Australia; moisture from the tropical Indian and Pacific Oceans most important for precipitation in northern Australia, and moisture from the Southern Ocean most important for precipitation in southern regions. Advected ocean moisture varied little from year to year compared to terrestrial sources of moisture.

While advected marine moisture was the dominant supplier of moisture for precipitation across Australia, precipitation in the north and southeast of the continent relied on terrestrial moisture for up to 25% of seasonal precipitation. These regions are therefore most vulnerable to changes in land cover that may change the amount of evapotranspiration available for precipitation. In contrast, the southwest of Australia typically receives less than 3% of moisture from terrestrial sources. Instead, the region relies on marine moisture for up to 97% of winter precipitation, making the region vulnerable to changes to remote ocean and atmosphere processes that bring moisture to the region.

The strength of land-atmosphere interactions presented in this chapter reflects climatological average conditions. The research presented in the next chapter analyses the strength of land-atmosphere interactions, and their relative role compared to remote processes, in controlling Australian precipitation during drought.

Chapter 5

The role of land-atmosphere interactions during drought

5.1 Overview

Droughts are a recurrent feature of the Australian climate and cause severe impacts to ecosystems, water supply, agriculture, people and the economy (Kiem et al. 2016; Van Dijk et al. 2013). Although droughts form part of Australia's naturally variable climate, with evidence of drought dating back hundreds of years (Cook et al. 2016; Gallant and Gergis 2011), the spatiotemporal variation between different droughts has made mechanistic understanding particularly challenging (Van Dijk et al. 2013; Verdon-Kidd et al. 2017). Understanding drought will remain a key concern for Australia (Kiem et al. 2016), as Australia is projected to experience more frequent and intense drought in future (Ukkola et al. 2020).

One region of Australia particularly impacted by drought is southeast Australia. Climate projections indicate the region will in future suffer longer droughts that are more intense (Kirono et al. 2020; Ukkola et al. 2020). The significance of drought to this region and the potential for drought to worsen in future means deeper understanding of underlying physical processes is needed to aid prediction and adaption. This chapter aims to contribute to such understanding. The research presented combines estimates of precipitation recycling and moisture sources with atmospheric circulation to address research question 4: **What role do land-atmosphere interactions play during drought in Australia?**

The research presented in this chapter has been peer-reviewed and published in *Geophysical Research Letters*, and is provided in its published form. Author contributions are outlined in the Statement of Contribution below.

Statement of Contribution

This thesis is submitted as a Thesis by Compilation in accordance with https://policies.anu.edu.au/ppl/document/ANUP_003405

I declare that the research presented in this Thesis represents original work that I carried out during my candidature at the Australian National University, except for contributions to multi-author papers incorporated in the Thesis where my contributions are specified in this Statement of Contribution.

Title: Local and Remote Drivers of Southeast Australian Drought

Authors: Holgate, C. M., A. I. J. M. Van Dijk, J. P. Evans and A. J. Pitman

Publication outlet: Geophysical Research Letters

Current status of paper: Published

Citation: Holgate, C. M., Dijk, A. I. J. M. V., Evans, J. P., & Pitman, A. J. (2020). Local and Remote Drivers of Southeast Australian Drought. Geophysical Research Letters, 47(18), e2020GL090238. <https://doi.org/10.1029/2020GL090238>

Contribution to paper: C. Holgate led the study. C. Holgate designed the study with significant input co-authors. C. Holgate conducted the analysis, prepared the figures and drafted the manuscript. All co-authors contributed to the refinement of the draft manuscript. C. Holgate prepared the submission to the journal and led the revisions of the manuscript following peer-review.

Senior author or collaborating authors endorsement: _____

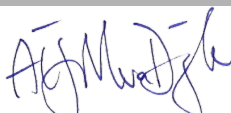
Chiara Holgate
Candidate – Print Name


Signature

26 November 2020
Date

Endorsed

Albert Van Dijk
Primary Supervisor – Print Name


Signature

9/11/2020
Date

Philip Gibbons
Delegated Authority – Print Name


Signature

6/11/20
Date

Geophysical Research Letters

RESEARCH LETTER

10.1029/2020GL090238

Key Points:

- Southeast Australian droughts are driven by circulation anomalies that reduce moisture inflow and a lack of precipitation-generating mechanisms
- Moisture for drought termination is typically sourced from the Tasman and Coral Seas
- Land surface moisture sources amplify drought by up to 6%, minor compared to ocean influence

Supporting Information:

- Supporting Information S1

Correspondence to:

C. M. Holgate,
chiara.holgate@anu.edu.au

Citation:

Holgate, C. M., Van Dijk, A. I. J. M., Evans, J. P., & Pitman, A. J. (2020). Local and remote drivers of southeast Australian drought. *Geophysical Research Letters*, 47, e2020GL090238. <https://doi.org/10.1029/2020GL090238>

Received 10 AUG 2020

Accepted 3 SEP 2020

Accepted article online 9 SEP 2020

Local and Remote Drivers of Southeast Australian Drought

C. M. Holgate^{1,2} , A. I. J. M. Van Dijk¹ , J. P. Evans^{3,4} , and A. J. Pitman^{3,4} 

¹Fenner School of Environment and Society, Australian National University, Canberra, ACT, Australia, ²ARC Centre of Excellence for Climate System Science, UNSW, Sydney, New South Wales, Australia, ³ARC Centre of Excellence for Climate Extremes, UNSW, Sydney, New South Wales, Australia, ⁴Climate Change Research Centre, UNSW, Sydney, New South Wales, Australia

Abstract Droughts are associated with large-scale modes of variability, synoptic-scale systems, and terrestrial processes. Quantifying their relative roles in influencing drought guides process understanding, helps identify weaknesses in climate models, and focuses model improvements. Using a Lagrangian back-trajectory approach we provide the first quantification of the change in moisture supply during major droughts in southeast Australia, including the causes of the changes. Drought onset and intensification were driven by reduced moisture supply from the ocean, as moisture was circulated away from the region, combined with an absence of precipitation-generating mechanisms over land. During termination, strengthened moist easterly flows from the Tasman and Coral Seas promoted anomalously high rainfall. Our approach reveals terrestrial moisture sources played a secondary role, amplifying rainfall anomalies by less than 6%. Simulating droughts therefore requires deeper understanding of the relationship between moisture advection and synoptic-scale circulation and how large-scale climate variability and terrestrial processes modify these relationships.

Plain Language Summary The relative roles of atmospheric circulation, weather systems, and land surface processes in recurring droughts in southeast Australia are unclear. We tracked the path of moisture as it moved through the air to find where the rain in southeast Australia comes from and what was different in the atmosphere and land surface during the development, deepening and breaking of three major droughts. We found that the leading cause for drought was that moisture originating from the oceans did not reach the Murray-Darling Basin as often and produced less rain when it did. The drying landscape exacerbated the low rainfall conditions but had a smaller effect than the ocean. The droughts were broken by strong systems from the east carrying moisture from the ocean into the region. To better model and predict drought we therefore need to understand the relationship between ocean moisture and the weather systems that transport it to the land and how the relationship is affected by the land surface and variability within the climate.

1. Introduction

The Millennium Drought (2001–2009) was the longest drought in the instrumental record (Van Dijk et al., 2013) whereas the subsequent, most recent drought (2017–2020) has been the most severe. The impact of drought is exacerbated by global warming such that 2019 was the warmest and driest year on record (Bureau of Meteorology, 2020a). The recent hot and dry conditions contributed to an unprecedented bush-fire season (Boer et al., 2020) and a serious health emergency (Yu et al., 2020). Low inflows led to record low volumes in water storages (Murray-Darling Basin Authority, 2020). One region in southeast Australia particularly susceptible to drought is the Murray-Darling Basin (MDB), where the long-term trend to warmer and drier conditions has affected the profitability of agriculture significantly (Hughes et al., 2019).

Drought in the MDB is associated with large-scale modes of variability. Rainfall variability and periods of above- and below-average rainfall have been linked with the El Niño-La Niña cycle (e.g., Chiew et al., 1998), the Indian Ocean Dipole (e.g., Ashok et al., 2003), the Southern Annular Mode (e.g., Hendon et al., 2007), the Interdecadal Pacific Oscillation (e.g., Power et al., 1999), and combinations of each (e.g., Ummenhofer et al., 2010). These modes of variability act to modify the probability of rainfall over southeast Australia by perturbing the large-scale circulation of the atmosphere and the frequency and location of rain-bearing

synoptic-scale systems. However, the direct, physical processes that drive the onset, intensification, and termination of southeast Australian droughts are not well understood. Anomalously low rainfall can be due to changes in moisture supply from typical evaporative source regions, either via a reduction in evaporation or due to anomalous atmospheric circulation patterns redirecting the moisture elsewhere. Using a Lagrangian back-trajectory approach, we establish the cause of altered atmospheric moisture supply for rainfall during meteorological drought onset, intensification, and termination in southeast Australia. While large-scale modes of variability and interactions with synoptic-scale systems play a role, some contribution from terrestrial processes is also likely. Our approach combines information on moisture sources, circulation change, and land-atmosphere feedbacks across individual stages of drought, building on previous studies of moisture transport variability (e.g., Bosilovich & Chern, 2006; Dirmeyer & Brubaker, 1999; Drumond et al., 2017; Gimeno et al., 2010; Herrera-Estrada et al., 2019; Miralles et al., 2016; Roy et al., 2019; Stojanovic et al., 2017; Van Der Ent et al., 2010; Wei et al., 2016). Our approach can be applied anywhere in the world to establish the cause of modified atmospheric moisture supply, establish whether land processes amplify or dampen rainfall anomalies, and in doing so establish the relative roles of local and remote processes influencing the different stages of drought.

While some progress has been made to understand the role of terrestrial processes during drought (Herrera-Estrada et al., 2019; Roundy et al., 2013; Roy et al., 2019; Zeng et al., 2019; Zhou et al., 2019), for many regions of the world, including southeast Australia, it is uncertain whether local land-atmosphere feedbacks act to amplify or suppress atmospheric moisture during drought. Here, we quantify the amplification of rainfall anomalies by the land surface as droughts intensify and terminate and the relative roles of local and remote processes influencing each drought stage. Proper representation of land-atmosphere feedbacks is essential for realistic drought simulation (Schubert et al., 2016). Our analysis is therefore central to resolving why climate models struggle to simulate droughts well (Ukkola et al., 2018) and helps provide a means to establish whether climate models simulate droughts for the right reasons.

2. Materials and Methods

2.1. Back-Trajectory Model

We estimated the evaporative origin of the moisture for rainfall falling in the northern and southern regions of the MDB with a three-dimensional (3D) Lagrangian back-trajectory model. The model was based on Dirmeyer and Brubaker (1999), but in addition to water vapor we also tracked other forms of atmospheric water (liquid and solid). Moisture supplying rainfall events of $>2 \text{ mm d}^{-1}$ between 1979 and 2013 were tracked. For each day rainfall occurred within a grid cell, moist air parcels were launched from a precipitable water-weighted height in the atmosphere at a rate proportional to the rainfall rate and advected through the atmosphere using 3-D wind fields. As parcels moved across the grid at each 10-minute back-trajectory time step, a proportion of the parcel's moisture was assumed to come from evaporation from the Earth's surface below the parcel at that point in its trajectory. Parcels were tracked until (i) all the precipitable water at the original rain cell was accounted for, (ii) the parcel reached the edge of the model domain (Figure 1a), or (iii) the maximum back-trajectory time (30 days) was reached. The algorithm provided daily maps of evaporated water that contributed to rainfall over the MDB every day during the 35-year time frame. Anomalies of moisture supply to the MDB during droughts were then calculated as deviations from the 35-year climatology.

The back-trajectory model was forced with 3D, six-hourly, 0.5° atmospheric fields of wind, temperature, precipitable water and pressure, and 2-D fields of rainfall and surface fluxes. Atmospheric fields were simulated using the ERA-Interim-driven WRFv3.6.1 simulation. The simulation was spectrally nudged with winds and geopotential height above approximately 500 hPa using ERA-Interim to ensure synoptic-scale systems remained close to the reanalysis. The WRF simulation performed well against observations of temperature and rainfall and was deemed suitable for the purposes of this study. For further detail of the evaluation and back-trajectory model, the reader is directed to Holgate et al. (2020).

2.2. Definition of Drought Stages

The Bureau of Meteorology (2020b) defines drought as rainfall in the lowest decile (i.e., below the tenth percentile) of historical totals, and we adopt their definition in our analysis. Within each lowest decile year,

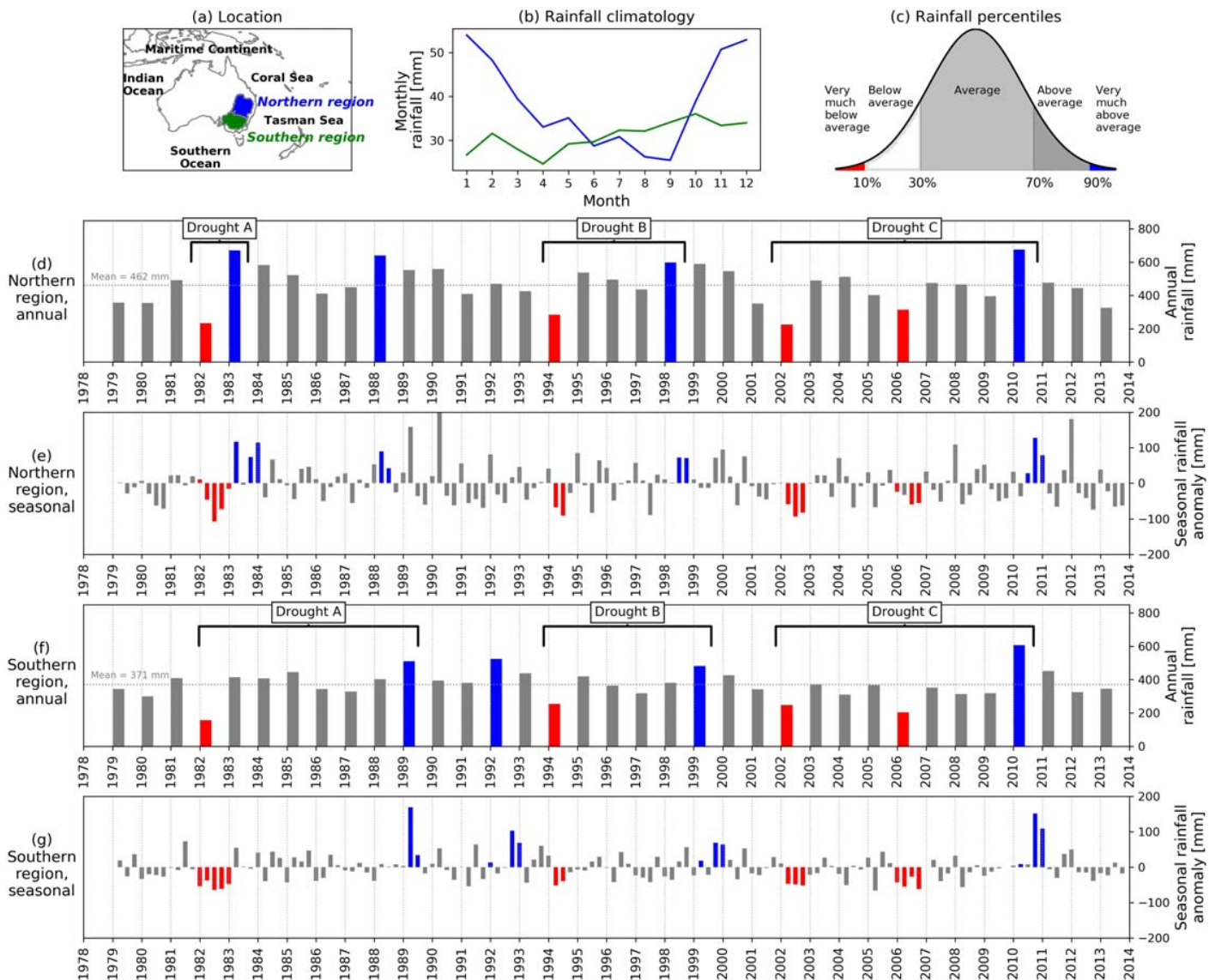


Figure 1. Timeseries of droughts. (a) Location of regions and oceans set within the model domain; (b) rainfall climatology; (c) definition of rainfall percentiles; (d) annual rainfall with mean; and (e) seasonal rainfall anomalies in the northern region; (f) and (g) as (d) and (e) but for the southern region. Years with annual rainfall in the lowest decile and their corresponding seasons with below-average rainfall are marked in red; years in the top decile and their corresponding above-average seasons are marked in blue.

drought seasons are those where the seasonal rainfall was below average (Figure 1c). Drought onset is taken as the first season of drought, with the remaining seasons considered as the drought intensification stage. Drought terminating years are those in the highest decile (i.e., above the 90th percentile). Within terminating years, drought termination seasons are those where the seasonal rainfall was above average (Figure 1c). Based on these definitions, three drought periods occurred starting in 1982 (Drought A), 1994 (Drought B), and 2002 (Drought C). The droughts terminated in different years between the regions, except for Drought C, which terminated in 2010 (Figure 1).

We also estimated drought stages using the Standardized Precipitation Index (SPI, McKee et al., 1993; see supporting information). Results were very similar using the SPI, and therefore, we focus on the percentile-based drought definition. The definitions of drought used rainfall estimated from the WRFv3.6.1 simulation for 1979–2013, to remain consistent with the back-trajectory analysis.

2.3. Estimating Amplification

The degree to which local land-atmosphere feedbacks affected each drought stage was assessed via the rainfall recycling ratio (P_R). The 3-D time series of evaporative origin, obtained with the back-trajectory analysis, was used to calculate the proportion of rainfall in a region A (P_A), whose moisture was derived from evapotranspiration within the same region (M_L): $P_R = M_L/P_A[\%]$. To identify whether land surface processes amplified or dampened rainfall anomalies during drought, we examined the change in the local terrestrial moisture contribution compared to the rainfall anomaly. The anomalies were calculated from the region's seasonal rainfall climatology. For rainfall in a region on any given day, we retained full spatial information on the origin of the precipitated moisture through the back-trajectory results. We calculated an amplification factor (A_L), expressed as follows:

$$A_L = \frac{\Delta M_L}{\Delta P}$$

where ΔM_L (mm) is the anomaly in the contribution of moisture from the local land surface to rainfall and ΔP (mm) is the total anomaly in rainfall. Similarly, we estimated amplification factors for the moisture contributions from the nonlocal land surface (A_{NL}) and the ocean (A_O).

3. Results

3.1. Source Region Change During Drought

Drought onset in the northern (Figures 2a–2d) and southern (Figures 3a–3d) regions was dominated by reduced marine moisture from the Tasman and Coral Seas to the east of Australia (Figure 1a), with low-level winds directing moist marine air away from each region more often than normal (Figure S1). Drought onset was typically associated with reduced terrestrial moisture from the land surface. For the northern region this was within and directly north of the basin. For the southern region, terrestrial anomalies consistently originated from within the northern region.

Drought intensification was also dominated by reduced marine moisture from the Tasman and Coral Seas but covered a larger geographical extent than the onset stage, extending to the subtropical Indian and Southern Oceans (Figures 2e–2h and 3e–3h). For the northern region, terrestrial anomalies remained similar in spatial extent and intensity to those for the onset stage. For the southern region, the spatial extent of terrestrial anomalies increased as droughts intensified from initially the northern region only, to eventually include both regions.

Drought termination in both regions was consistently associated with above-average moisture contribution from the Coral and Tasman Seas, in line with strengthened easterly flow (Figures 2i–2l and 3i–3l) compared to the seasonal expectation (Figure S1). Drought-breaking marine moisture anomalies were similar in spatial extent between events (especially for the northern region), extending from approximately 20 to 30°S and east of the continent to approximately 160°E. Drought-breaking marine moisture contributions were from a larger area for the southern region, encompassing the Tasman Sea and Southern Ocean, but with marine moisture anomalies from the Tasman Sea contributing most strongly to termination. Positive anomalies in moisture supply from terrestrial sources were consistent between termination events and mirrored the negative terrestrial anomalies identified during the intensification stage for both regions.

3.2. Moisture Supply and Rainfall Favorability

To determine whether the anomalously low moisture contribution during drought was due to a reduction in evaporation in the main marine source regions or due to redirection of the moisture elsewhere, we evaluated several hydrometeorological metrics for each drought and compared them to their values for subsequent termination stages (Figure 4). The difference in rainfall during drought years and their respective termination years in the northern region is evident in cumulative rainfall (Figures 4a–4c). For the northern region, the low rainfall during drought years was not due to a reduction in evaporation in the marine source regions (marine evaporation differed little between drought and termination years; Figures 4d–4f). A similar amount of total precipitable water (TPW) was available during the drought year A (1982) and its termination (1983; Figure 4g). In drought year B (1994), the TPW fell below 1998 values in the second half of the year (Figure 4h). For both droughts A and B the 500 hPa maximum vertical wind speed suggests large-scale

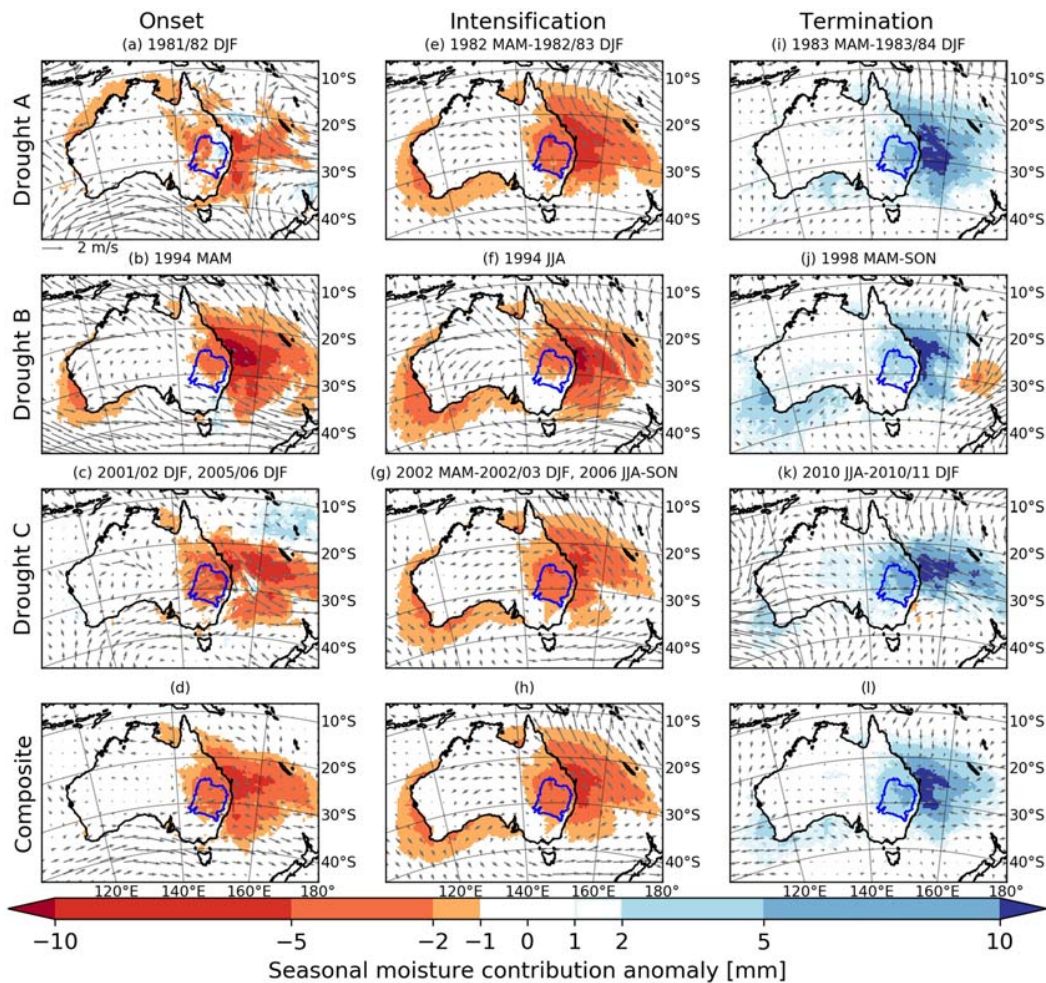


Figure 2. Moisture source anomalies during drought (a–d) onset, (e–h) intensification, and (i–l) termination in the northern region overlain by low-level wind speed anomalies. Droughts A, B, and C are represented in the top three rows, with the bottom row showing their mean.

uplift was greater in the termination year, particularly from April to November (Figures 4j and 4k). This suggests that even if the amount of atmospheric moisture was similar in the drought and termination years of Drought A (and in the first half of Drought B), there was a lack of mechanisms to generate precipitation. In Drought C (the Millennium Drought), both TPW (Figure 4i) and vertical uplift (Figure 4l) were lower than the termination year (2010).

Low rainfall in the southern region could also not be attributed to a reduction in evaporation in the marine source regions (Figures 4d–4f). However, in contrast to the northern region, no consistent difference in precipitation favorability was suggested by vertical wind speed for Droughts A–C (Figures 4j–4l). Instead, during the three droughts, there was an apparent lack of TPW compared to the termination years (Figures 4g–4i).

3.3. Amplification of Drought Stages

In all stages of drought, the local land surface amplified the rainfall anomaly to a similar degree in the northern ($A_L = 5.1\text{--}6\%$) and southern ($3.1\text{--}4.5\%$; Table 1c) regions of the MDB. In the northern region, the local land played a larger role than normal during anomalous rainfall periods: It amplified the negative rainfall anomaly during drought onset and intensification and amplified the positive rainfall anomaly during drought termination (Table 1c). In the southern region local land amplification was limited during each drought stage compared to climatology.

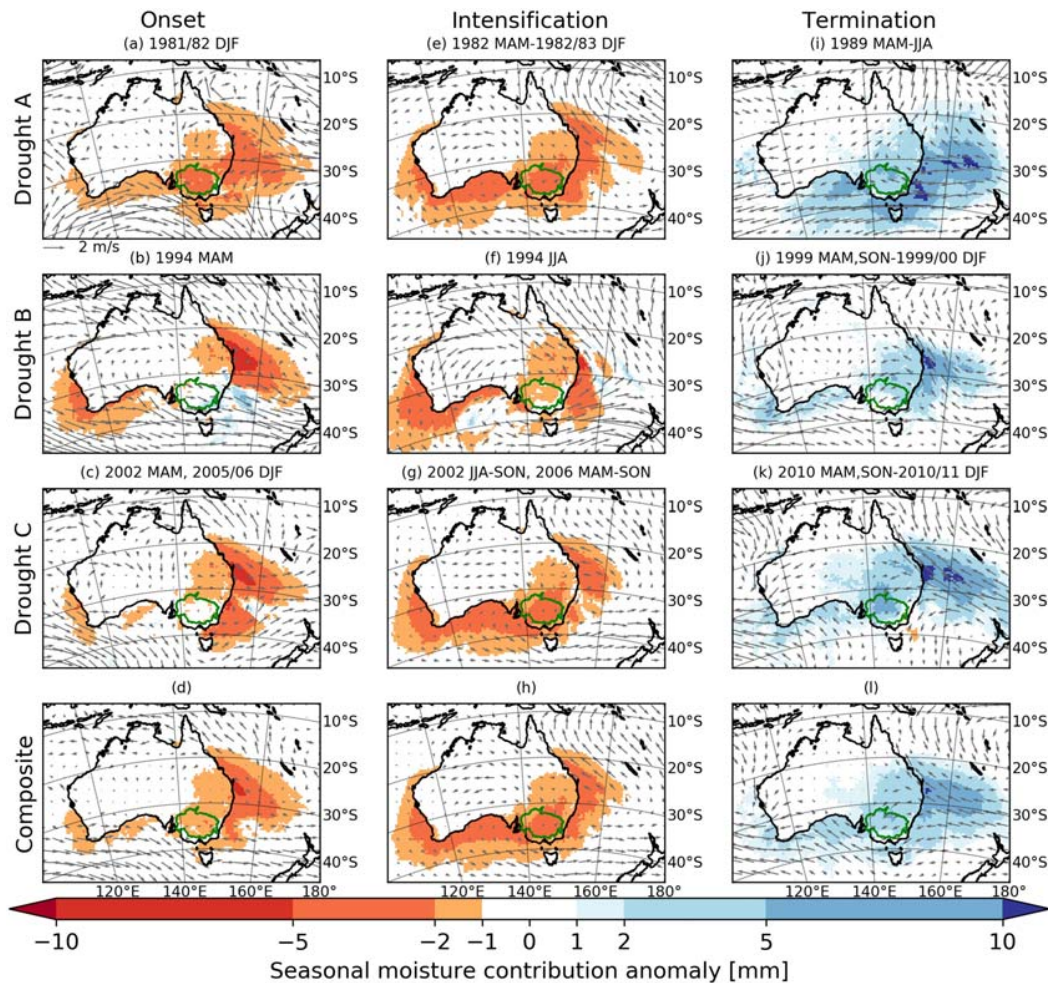


Figure 3. As for Figure 2 but for the southern region.

Rainfall anomalies during drought and termination were also amplified by the ocean and the nonlocal land surface. Rainfall in both basins was most influenced by the ocean ($A_O > 73.9\%$; Table 1c). Land-atmosphere feedbacks, as estimated by rainfall recycling, played a comparatively stronger role in amplifying rainfall anomalies in the northern region (6.4%, 4.8%, and 5.3% during onset, intensification, and termination, respectively) than the southern region (4%, 2.8%, and 3.9% during onset, intensification, and termination, respectively). Comparatively stronger land-atmosphere feedbacks were expected in the northern region compared to the south (Table 1; Figures S1i and S1j).

4. Discussion

Rainfall over the MDB is associated with different synoptic types (e.g., Pook et al., 2006) influenced by large-scale drivers including the El Niño-Southern Oscillation, Indian Ocean Dipole, Southern Annular Mode, and atmospheric blocking (Risbey et al., 2009; Verdon-Kidd & Kiem, 2009). These large-scale modes influence the weather systems during drought and likely also affect the typical sources of moisture. Here, a Lagrangian back-trajectory approach was used to identify changes to moisture supply during major droughts in the MDB. Our results demonstrate the importance of moisture advection during drought and therefore emphasize the need to characterize the relationship between moisture sources and synoptic-scale processes and how the relationship is modified by broader-scale circulation changes. More broadly, our results highlight the importance of understanding the relationship between moisture advection and atmospheric

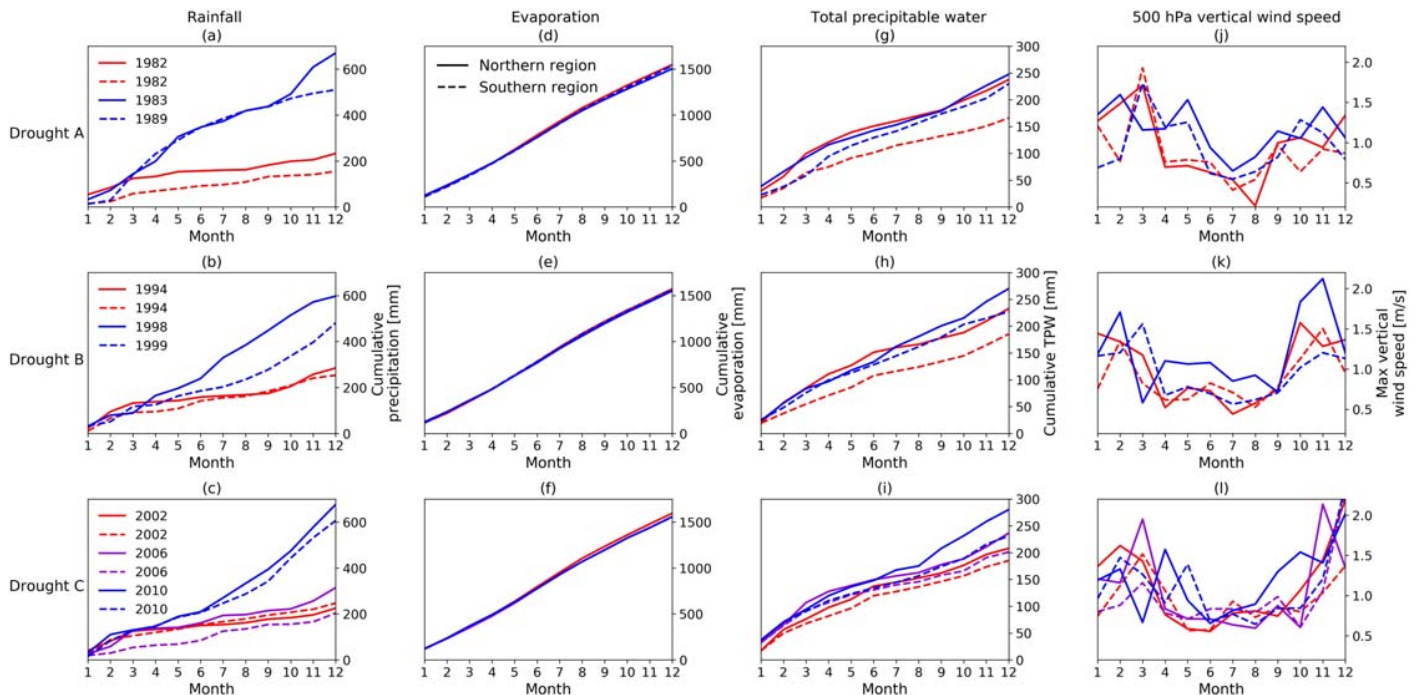


Figure 4. Plots of cumulative monthly (a–c) rainfall, (d–f) marine evaporation, (g–i) total precipitable water, and (j–l) 500 hPa maximum vertical wind speed for Droughts A–C in the northern (solid lines) and southern regions (dashed lines). Drought years are indicated by red/purple lines, termination years by blue lines.

circulation in regions where, like southeast Australia, rainfall is subject to large-scale modes of variability, including parts of the United States, South America, Asia, and Africa.

Our results show that anomalous atmospheric circulation modified the strength of moisture advection from key moisture sources during each drought stage. Climatologically, moist easterlies contribute to year-round rainfall in the MDB and are supplemented by moist westerlies in winter and spring (Figure S1). During drought, anticyclonic conditions over the MDB directed the typical easterly flow of moisture toward the northwest and the typical westerly flow toward the southeast, depriving the basin of moisture (Figures 2 and 3). In contrast, during drought termination moist easterly advection strengthened, bringing enhanced marine moisture for rainfall. Our results are therefore consistent with Rakich et al. (2008) and Pepler et al. (2016) who demonstrated a clear relationship between strong easterlies and higher summer rainfall across southeast Australia and weakened easterlies with lower rainfall. In winter, stronger westerlies were associated with wetter conditions in the southern part of southeastern Australia (Pepler et al., 2016). There is, therefore, a need to investigate the impact of synoptic systems on the relationship between zonal winds, moisture advection, and rainfall during southeast Australian droughts.

In addition to a reduction in advected marine moisture, the land surface also contributed to drought intensification. Drought in the northern region was exacerbated by a reduction in precipitation-generating mechanisms. This may be due to a reduction in local convective activity, suggested by the reduction in rainfall recycling and amplification of dry conditions by the local land surface during drought intensification. In the southern region, the local land surface exacerbated dry conditions but to a smaller degree than normal. In contrast, the typically large role played by ocean moisture in amplifying anomalous rainfall was further enhanced during drought. The suppression of the local land's usual role in generating rainfall and the enhanced role of the ocean both indicate that the ocean and remote processes became an even stronger driver of rainfall anomalies in the southern region during drought.

The nonlocal land surface amplified southern region rainfall anomalies during drought more than local processes. The nonlocal land surface, including the northern part of the MDB, amplified southern

Table 1
 Amplification Factors A Expressed as a Percentage for (a) Seasonal Climatology, (b) Seasons Comprising Drought Stages, and (c) During Drought Stages

| | (a) Climatology (%) | | | | (b) Climatological expectation (%) | | | | (c) A (%) | | | |
|---|---------------------|--------|--------|--------|------------------------------------|-----------------|-------------|-------|-----------------|-------------|-------|-------------|
| | Summer | Autumn | Winter | Spring | Onset | Intensification | Termination | Onset | Intensification | Termination | Onset | Termination |
| Northern region | | | | | | | | | | | | |
| Local land (A_L) | 4.4 | 0.5 | 3.3 | 8.6 | 3.4 | 4.4 | 4.6 | 6.0 | 5.7 | 5.1 | 6.0 | 5.1 |
| Nonlocal land (A_{NL}), total | 25.4 | 12.0 | 8.8 | 13.3 | 22.0 | 13.6 | 14.1 | 16.9 | 17.3 | 12.7 | 16.9 | 12.7 |
| Southern region | | | | | | | | | | | | |
| Ocean (A_O) | 72.1 | 87.4 | 87.5 | 78.4 | 75.9 | 82.2 | 81.7 | 76.5 | 76.4 | 82.2 | 76.5 | 82.2 |
| Local land (A_L) | 4.9 | 3.0 | 2.0 | 13.5 | 4.0 | 5.9 | 6.0 | 3.1 | 4.5 | 4.1 | 3.1 | 4.1 |
| Nonlocal land (A_{NL}), total | 35.3 | 22.7 | 11.4 | 39.8 | 29.0 | 24.6 | 28.7 | 17.3 | 18.3 | 21.7 | 17.3 | 21.7 |
| Nonlocal land (A_{NL}), northern region component | 6.8 | 2.5 | 2.9 | 6.4 | 4.7 | 4.3 | 4.6 | 3.9 | 3.9 | 4.8 | 3.9 | 4.8 |
| Ocean (A_O) | 58.9 | 73.1 | 86.4 | 47.2 | 66.0 | 69.2 | 64.8 | 79.0 | 76.8 | 73.9 | 79.0 | 73.9 |

Note. Values in (c) are bold where they exceed the climatological expectation in (b) and italicized where they are below the climatological expectation. Total amplification (i.e., $A_L + A_{NL} + A_O$) does not add to exactly 100% due to model discrepancy ($<2\%$) between the amount of simulated rainfall and amount of moisture back-tracked.

region rainfall anomalies, especially during drought termination. This means the southern region is partly reliant on moisture advected from the northern region for droughts to terminate and is more vulnerable to land use changes that alter evapotranspiration and thus the supply of moisture for rainfall (Pitman et al., 2004). While past studies have found that land cover changes have increased the severity of droughts in southeast Australia (McAlpine et al., 2009), our analysis indicates that land use and land cover changes in the northern region would have an impact on the supply of atmospheric moisture for rainfall in the southern region. Our results, therefore, highlight a potential mechanism to partly explain declines in rainfall over the southern MDB that requires further investigation.

There are some limitations to our approach. We used a single modeling system—WRFv3.6.1 driven with ERA-Interim reanalyses—together with a Lagrangian back-trajectory algorithm. While WRFv3.6.1 has been shown to work well over southeast Australia when using ERA-Interim (Di Virgilio et al., 2019), and uncertainties in the back-trajectory model are likely to have only a small impact on results (Holgate et al., 2020), we cannot discount that our results are partly dependent on this choice of modeling system.

Simulating droughts in southeast Australia has been an ongoing challenge (Ukkola et al., 2018). Modes of variability, global warming, ozone depletion, sea ice dynamics, land use, and land cover change have all been proposed as partial explanations for drought. Our back-trajectory approach demonstrates that to simulate droughts for the right physical reasons, models need to source moisture from the right marine and terrestrial regions and in the right proportions. Our analysis also suggests that the initiation of droughts, their intensification, and termination have distinct signatures. A climate model used to simulate droughts should match these signatures, which are established by interactions between the modes of variability, in a warming climate, and moderated or ameliorated by land surface feedbacks. This places a considerable demand on climate models, but where models fail to capture these signatures, at least acknowledging these current shortcomings guides where future improvements need to take place.

5. Conclusion

We have shown that major southeast Australian droughts were intensified and terminated chiefly by anomalies of marine moisture from the Tasman and Coral Seas associated with shifts in atmospheric circulation. During drought, anomalous atmospheric circulation patterns redirected moisture away from southeast Australia. This reversed during drought termination, promoting strong advection of moisture from the ocean into the region. This highlights the need to prioritize understanding of the relationship between synoptic-scale circulation and moisture advection, and how this relationship is modified by large-scale climate variability, in drought-prone regions of the world.

While a reduction in advected marine moisture was the dominant cause of drought throughout the MDB, the northern region also experienced a reduction in conditions favorable for the precipitation of available atmospheric moisture. This highlights the need to identify the mechanisms responsible for the suppression of rainfall generation during drought and specifically whether these mechanisms reflect local convective or larger-scale rainfall generating mechanisms.

We showed the land surface acted to amplify rainfall anomalies during all stages of drought. Local terrestrial moisture played a secondary role to ocean moisture contributions which dominated the development and termination of drought in southeast Australia. However, we found evidence that reduced moisture sources in the

northern region might partly explain reductions in rainfall in the southern region, a result that deserves further exploration.

The physical mechanisms leading to drought and its termination shown by our results provide a template for evaluating climate models used for simulating droughts. A research priority is to examine whether any of the current generation of climate models simulate droughts over southeast Australia with signatures and a relative role of marine and terrestrial moisture sources that are in line with the mechanisms we identified. More broadly, our approach provides a framework for investigating causal mechanisms of drought that can be applied to other regions of the world.

Data Availability Statement

CORDEX-Australasia climate simulations used in this study are publicly available (<https://climatedata.environment.nsw.gov.au/>).

Acknowledgments

This work was possible thanks to an Australian National University AGRT Scholarship (C.M.H.) and support from the ARC Centre of Excellence for Climate System Science (CE110001028). C.M.H. and A.I.J.M.v. D. were supported through the ARC Discovery Projects funding scheme (project DP40103679). J.P.E. and A.J.P. were supported via the ARC Centre of Excellence for Climate Extremes (CE170100023). The authors thank the staff at NCI, A. Ukkola, G. di Virgilio, D. Miralles, and R. Van Der Ent.

References

- Ashok, K., Guan, Z., & Yamagata, T. (2003). Influence of the Indian Ocean Dipole on the Australian winter rainfall. *Geophysical Research Letters*, 30(15), 1821. <https://doi.org/10.1029/2003GL017926>
- Boer, M. M., de Dios, V. R., & Bradstock, R. A. (2020). Unprecedented burn area of Australian mega forest fires. *Nature Climate Change*, 10(3), 171–172. <https://doi.org/10.1038/s41558-020-0716-1>
- Bosilovich, M. G., & Chern, J.-D. (2006). Simulation of water sources and precipitation recycling for the MacKenzie, Mississippi, and Amazon River Basins. *Journal of Hydrometeorology*, 7(3), 312–329. <https://doi.org/10.1175/JHM501.1>
- Bureau of Meteorology. (2020a). Annual Australian Climate Statement 2019. Retrieved April 6, 2020, from <http://www.bom.gov.au/climate/current/annual/aus/#tabs=Events>
- Bureau of Meteorology. (2020b). What is drought? Retrieved March 12, 2020, from <http://www.bom.gov.au/climate/drought/knowledge-centre/understanding.shtml>
- Chiew, F. H. S., Piechota, T. C., Dracup, J. A., & McMahon, T. A. (1998). El Nino/Southern Oscillation and Australian rainfall, streamflow and drought: Links and potential for forecasting. *Journal of Hydrology*, 204(1–4), 138–149. [https://doi.org/10.1016/S0022-1694\(97\)00121-2](https://doi.org/10.1016/S0022-1694(97)00121-2)
- Di Virgilio, G., Evans, J. P., Di Luca, A., Olson, R., Argüeso, D., Kala, J., et al. (2019). Evaluating reanalysis-driven CORDEX regional climate models over Australia: Model performance and errors. *Climate Dynamics*, 53(5–6), 2985–3005. <https://doi.org/10.1007/s00382-019-04672-w>
- Dirmeyer, P. A., & Brubaker, K. L. (1999). Contrasting evaporative moisture sources during the drought of 1988 and the flood of 1993. *Journal of Geophysical Research*, 104(D16), 19,383–19,397. <https://doi.org/10.1029/1999JD900222>
- Drumond, A., Gimeno, L., Nieto, R., Trigo, R. M., & Vicente-Serrano, S. M. (2017). Drought episodes in the climatological sinks of the Mediterranean moisture source: The role of moisture transport. *Global and Planetary Change*, 151, 4–14. <https://doi.org/10.1016/j.gloplacha.2016.12.004>
- Gimeno, L., Drumond, A., Nieto, R., Trigo, R. M., & Stohl, A. (2010). On the origin of continental precipitation. *Geophysical Research Letters*, 37, L13804. <https://doi.org/10.1029/2010GL043712>
- Hendon, H. H., Thompson, D. W. J., & Wheeler, M. C. (2007). Australian rainfall and surface temperature variations associated with the Southern Hemisphere annular mode. *Journal of Climate*, 20(11), 2452–2467. <https://doi.org/10.1175/JCLI4134.1>
- Herrera-Estrada, J. E., Martinez, J. A., Dominguez, F., Findell, K. L., Wood, E. F., & Sheffield, J. (2019). Reduced moisture transport linked to drought propagation across North America. *Geophysical Research Letters*, 46, 5243–5253. <https://doi.org/10.1029/2019GL082475>
- Holgate, C. M., Evans, J. P., Van Dijk, A. I. J. M., & Pitman, A. J. (2020). Australian precipitation recycling and evaporative source regions. *Journal of Climate*, 1–40. <https://doi.org/10.1175/JCLI-D-19-0926.1>
- Hughes, N., Galeano, D., & Hatfield-Dodds, S. (2019). The effects of drought and climate variability on Australian farms. In *Australian bureau of agricultural and resource economics and sciences* (Vol. 6, p. 11). Canberra: Australian Bureau of Agricultural and Resource Economics and Sciences. <https://doi.org/10.25814/5de84714f6e08>
- Mcalpine, C. A., Syktus, J., Ryan, J. G., Deo, R. C., McKeon, G. M., McGowan, H. A., & Phinn, S. R. (2009). A continent under stress: Interactions, feedbacks and risks associated with impact of modified land cover on Australia's climate. *Global Change Biology*, 15(9), 2206–2223. <https://doi.org/10.1111/j.1365-2486.2009.01939.x>
- McKee, T. B., Doesken, N. J., & Kleist, J. (1993). The relationship of drought frequency and duration to time scales. In *Proceedings of the 8th Conference of Applied Climatology*, 17–22 January. Anaheim, CA: American Meteorological Society. Retrieved from <https://pdfs.semanticscholar.org/c3f7/136d6cb726b295eb34565a8270177c57f40f.pdf>
- Miralles, D. G., Nieto, R., McDowell, N. G., Dorigo, W. A., Verhoest, N. E., Liu, Y. Y., et al. (2016). Contribution of water-limited ecoregions to their own supply of rainfall. *Environmental Research Letters*, 11(12), 124007. <https://doi.org/10.1088/1748-9326/11/12/124007>
- Murray-Darling Basin Authority. (2020). Water in storages. Retrieved March 12, 2020, from <https://www.mdba.gov.au/managing-water/water-storage>
- Pepler, A. S., Alexander, L. V., Evans, J. P., & Sherwood, S. C. (2016). Zonal winds and southeast Australian rainfall in global and regional climate models. *Climate Dynamics*, 46(1–2), 123–133. <https://doi.org/10.1007/s00382-015-2573-6>
- Pitman, A. J., Narisma, G. T., Pielke, R. A., & Holbrook, N. J. (2004). Impact of land cover change on the climate of southwest Western Australia. *Journal of Geophysical Research*, 109, D18109. <https://doi.org/10.1029/2003JD004347>
- Pook, M. J., McIntosh, P. C., & Meyers, G. A. (2006). The synoptic decomposition of cool-season rainfall in the Southeastern Australian cropping region. *Journal of Applied Meteorology and Climatology*, 45(8), 1156–1170. <https://doi.org/10.1175/JAM2394.1>
- Power, S., Casey, T., Folland, C., Colman, A., & Mehta, V. (1999). Inter-decadal modulation of the impact of ENSO on Australia. *Climate Dynamics*, 15(5), 319–324. <https://doi.org/10.1007/s003820050284>

- Rakich, C. S., Holbrook, N. J., & Timbal, B. (2008). A pressure gradient metric capturing planetary-scale influences on eastern Australian rainfall. *Geophysical Research Letters*, 35, L08713. <https://doi.org/10.1029/2007GL032970>
- Risbey, J. S., Pook, M. J., McIntosh, P. C., Wheeler, M. C., & Hendon, H. H. (2009). On the remote drivers of rainfall variability in Australia. *Monthly Weather Review*, 137(10), 3233–3253. <https://doi.org/10.1175/2009MWR2861.1>
- Roundy, J. K., Ferguson, C. R., & Wood, E. F. (2013). Temporal variability of land–atmosphere coupling and its implications for drought over the Southeast United States. *Journal of Hydrometeorology*, 14(2), 622–635. <https://doi.org/10.1175/JHM-D-12-090.1>
- Roy, T., Martinez, J. A., Herrera-Estrada, J. E., Zhang, Y., Dominguez, F., Berg, A., et al. (2019). Role of moisture transport and recycling in characterizing droughts: Perspectives from two recent U.S. droughts and the CFSv2 system. *Journal of Hydrometeorology*, 20(1), 139–154. <https://doi.org/10.1175/JHM-D-18-0159.1>
- Schubert, S. D., Stewart, R. E., Wang, H., Barlow, M., Berbery, E. H., Cai, W., et al. (2016). Global meteorological drought: A synthesis of current understanding with a focus on SST drivers of precipitation deficits. *Journal of Climate*, 29(11), 3989–4019. <https://doi.org/10.1175/JCLI-D-15-0452.1>
- Stojanovic, M., Drumond, A., Nieto, R., & Gimeno, L. (2017). Moisture transport anomalies over the Danube River basin during two drought events: A Lagrangian analysis. *Atmosphere*, 8(12), 193. <https://doi.org/10.3390/atmos8100193>
- Ukkola, A. M., Pitman, A. J., De Kauwe, M. G., Abramowitz, G., Herger, N., Evans, J. P., & Decker, M. (2018). Evaluating CMIP5 model agreement for multiple drought metrics. *Journal of Hydrometeorology*, 19(6), 969–988. <https://doi.org/10.1175/JHM-D-17-0099.1>
- Ummenhofer, C. C., Sen Gupta, A., Briggs, P. R., England, M. H., McIntosh, P. C., Meyers, G. A., et al. (2010). Indian and Pacific Ocean influences on southeast Australian drought and soil moisture. *Journal of Climate*, 24(5), 1313–1336. <https://doi.org/10.1175/2010JCLI3475.1>
- Van Der Ent, R. J., Savenije, H. H. G., Schaefli, B., & Steele-Dunne, S. C. (2010). Origin and fate of atmospheric moisture over continents. *Water Resources Research*, 46, W09525. <https://doi.org/10.1029/2010WR009127>
- Van Dijk, A. I. J. M., Beck, H. E., Crosbie, R. S., de Jeu, R. A. M., Liu, Y. Y., Podger, G. M., et al. (2013). The millennium drought in Southeast Australia (2001–2009): Natural and human causes and implications for water resources, ecosystems, economy, and society. *Water Resources Research*, 49, 1040–1057. <https://doi.org/10.1002/wrcr.20123>
- Verdon-Kidd, D. C., & Kiem, A. S. (2009). On the relationship between large-scale climate modes and regional synoptic patterns that drive Victorian rainfall. *Hydrology and Earth System Sciences*, 13(4), 467–479. <https://doi.org/10.5194/hess-13-467-2009>
- Wei, J., Jin, Q., Yang, Z.-L., & Dirmeyer, P. A. (2016). Role of Ocean Evaporation in California Droughts and Floods. *Geophysical Research Letters*, 43, 6554–6562. <https://doi.org/10.1002/2016GL069386>
- Yu, P., Xu, R., Abramson, M. J., Li, S., & Guo, Y. (2020). Bushfires in Australia: A serious health emergency under climate change. *The Lancet Planetary Health*, 4(1), e7–e8. [https://doi.org/10.1016/S2542-5196\(19\)30267-0](https://doi.org/10.1016/S2542-5196(19)30267-0)
- Zeng, D., Yuan, X., & Roundy, J. K. (2019). Effect of Teleconnected land–atmosphere coupling on Northeast China persistent drought in spring–summer of 2017. *Journal of Climate*, 32(21), 7403–7420. <https://doi.org/10.1175/JCLI-D-19-0175.1>
- Zhou, S., Williams, A. P., Berg, A. M., Cook, B. I., Zhang, Y., Hagemann, S., et al. (2019). Land–atmosphere feedbacks exacerbate concurrent soil drought and atmospheric aridity. *Proceedings of the National Academy of Sciences*, 116(38), 18,848–18,853. <https://doi.org/10.1073/pnas.1904955116>

5.2.1 Supplementary material

Climatological sources of moisture for each season

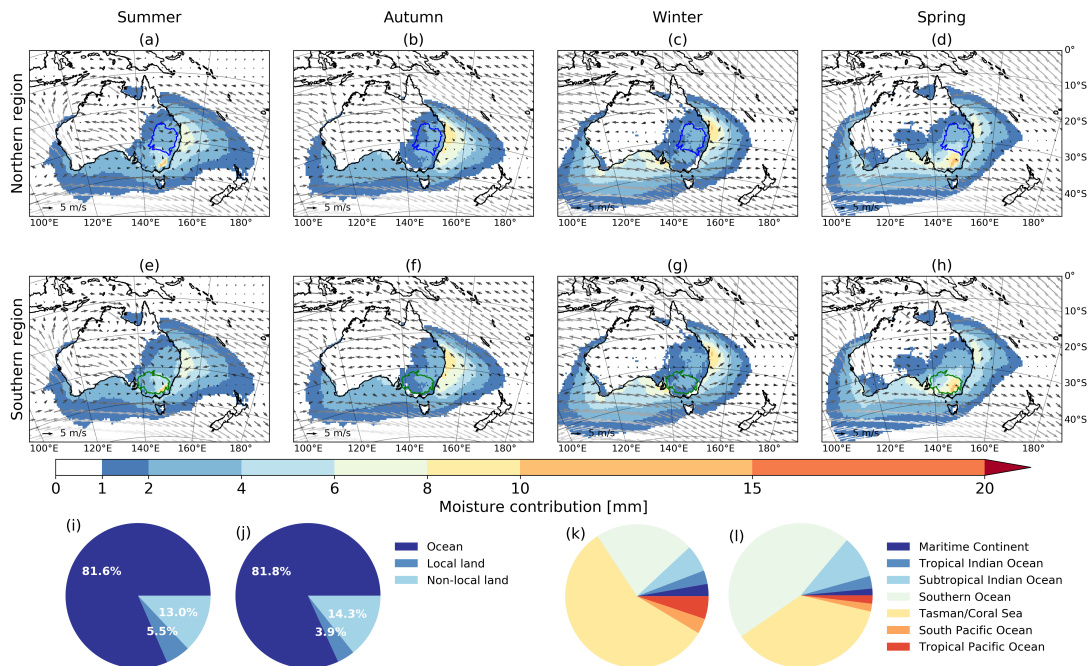


Figure 5.S1: Seasonal climatology of moisture contribution to rainfall in the (a)–(d) northern and (e)–(h) southern region, overlain by climatological low-level wind vectors; proportion of moisture contributed by each source annually to the (i) northern and (j) southern regions, and the proportion of moisture contributed by each ocean region annually to the (k) northern and (l) southern regions.

Drought defined with SPI-12

For comparison we provide drought stages estimated with the Standardized Precipitation Index (SPI), an indicator of how many standard deviations the rainfall lies from the long-term mean over a specified time period (McKee et al. 1993). We first calculated a monthly time series of SPI-12 (Adams 2017). Given the index represents a temporal integration of conditions over the previous 12 months, we define drought as the 12-month window prior to and including months with values of -1.5 or less (“severe” drought McKee et al. 1993). As with the percentile-based method, the first three months are classed as drought onset, with the remainder as drought intensification. Twelve-month windows prior to and including months with values of $+1.5$ are classed as drought termination.

A similar result to that shown in Figure 5.1 was obtained with SPI-12 (Figures 5.S2 and 5.S3 and Tables 5.S1 and 5.S2). Periods identified as drought onset, amplification and termination from the SPI-based method overlapped with those identified from the percentile-based method

but tended to be longer, starting earlier and finishing later. The SPI-based method also identified more droughts than the percentile-based method (three in the northern and one in the southern region), although most were based on only one monthly SPI value below the target threshold.

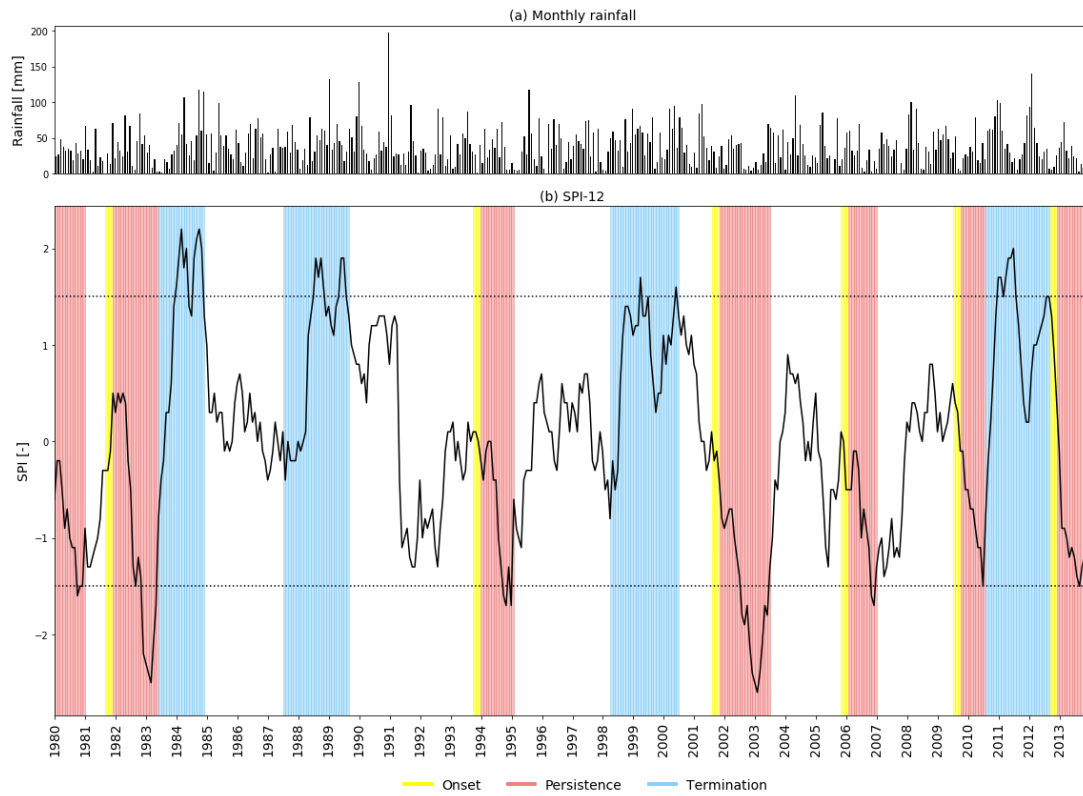


Figure 5.S2: (a) Monthly rainfall in the northern region and (b) SPI-12. Shaded drought intensification periods refer to the 12-months prior to the SPI-12 falling below the -1.5 threshold; the first three months of which are classed as drought onset. Shaded drought termination periods refer to the 12-months prior to the SPI-12 rising above the +1.5 threshold.

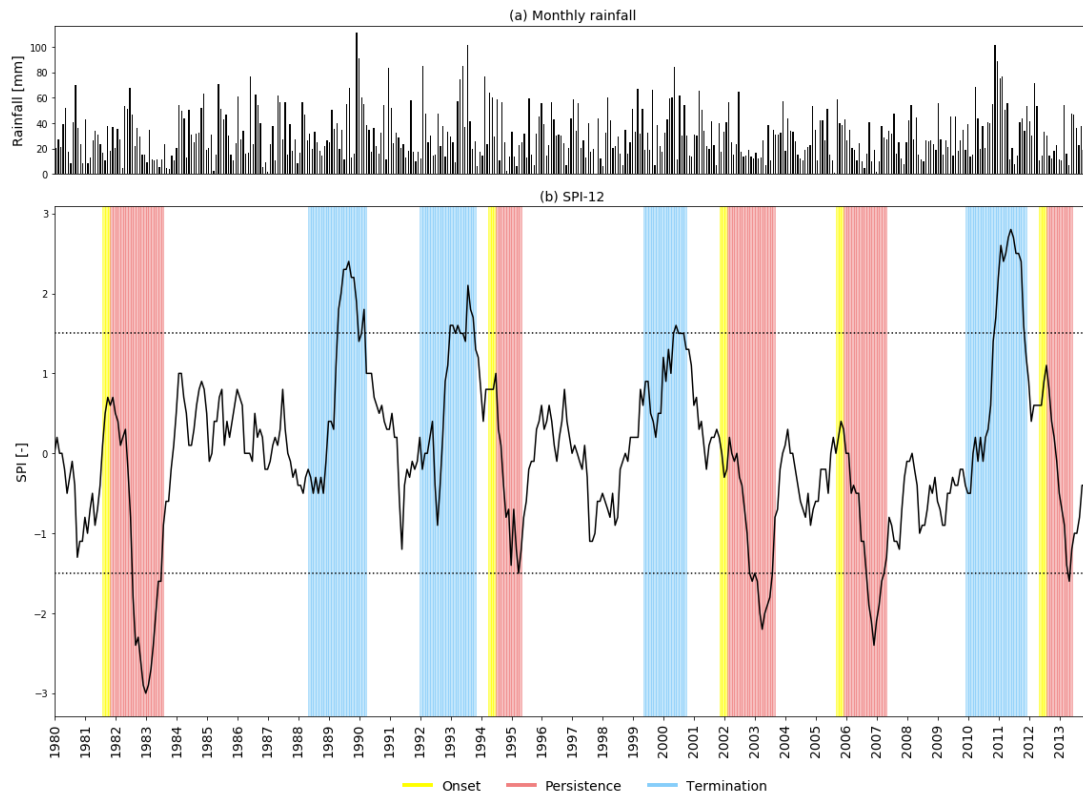


Figure 5.S3: Same as Figure 5.S2, but for the southern region.

Very similar source region anomalies were obtained when drought stages were based on SPI-12 (Figure 5.S4) compared to the percentile-based analysis (Figures 5.2 and 5.3), with negligible difference in the spatial pattern of intensification and termination anomalies. SPI-based anomalies were slightly different during onset; moisture contribution to the northern region was less anomalous over the Tasman Sea and was instead concentrated over Coral Sea (Figure 5.S4a). In the southern region local terrestrial moisture contribution was less anomalous during onset, as were anomalies in the Subtropical Indian and Southern Oceans (Figure 5.S4d). While the monthly time scale of the SPI necessitates the use of monthly anomalies in Figure 5.S4, the magnitude is approximately one-third of the seasonal anomalies in Figures 5.2 and 5.3 to allow direct comparison.

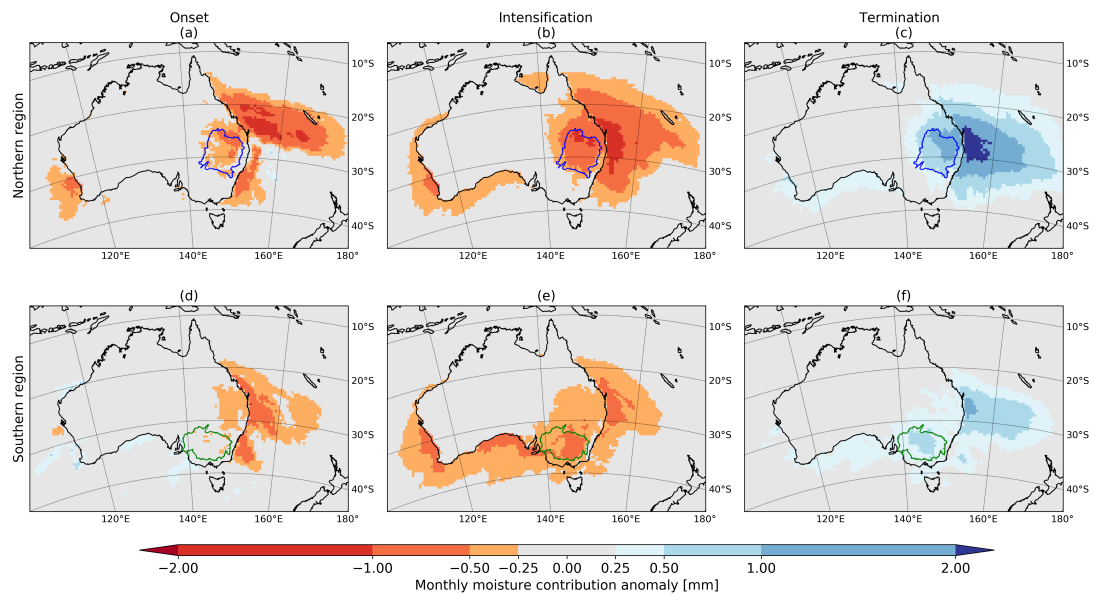


Figure 5.S4: SPI-based composite of monthly moisture source anomalies during drought onset, intensification and termination in the (a)–(c) northern and (d)–(f) southern regions.

| Percentile | | | SPI |
|------------|-----------------|-----------------------------------|--|
| Drought A | Onset | 12/1981–2/1982 | 9/1979–11/1979, 8/1981–10/1981 |
| | Intensification | 3/1982–2/1983 | 12/1979–11/1980, 11/1981–4/1983 |
| | Termination | 3/1983–2/1984 | 5/1983–10/1984, 6/1987–7/1989 |
| Drought B | Onset | 3/1994–5/1994 | 9/1993–11/1993 |
| | Intensification | 6/1994–8/1994 | 12/1993–12/1994 |
| | Termination | 3/1998–11/1998 | 3/1998–5/2000 |
| Drought C | Onset | 12/2001–2/2002, 12/2005–2/2006 | 7/2001–9/2001, 10/2005–12/2005, 6/2009–8/2009, 8/2012–10/2012 |
| | Intensification | 3/2002–2/2003, 6/2006–11/2006 | 10/2001–5/2003, 1/2006–11/2006, 9/2009–6/2010, 11/2012–8/2013 |
| | Termination | 6/2010–2/2011 | 7/2010–7/2012 |

Table 5.S1: Northern region drought stages identified from percentile-based method and corresponding SPI-based stages, given as 'month/year'. SPI-identified periods additional to those from the percentile-based method are listed in grey.

| | | Percentile | SPI |
|-----------|-----------------|-----------------------------------|--|
| Drought A | Onset | 12/1981–2/1982 | 7/1981–9/1981 |
| | Intensification | 3/1982–2/1983 | 10/1981–6/1983 |
| | Termination | 3/1989–8/1989 | 4/1988–2/1990, 12/1991–9/1993 |
| Drought B | Onset | 3/1994–5/1994 | 3/1994–5/1994 |
| | Intensification | 6/1994–8/1994 | 6/1994–3/1995 |
| | Termination | 3/1999–5/1999, 9/1999–2/2000 | 4/1999–8/2000 |
| Drought C | Onset | 3/2002–5/2002, 12/2005–2/2006 | 10/2001–12/2001, 8/2005–10/2005, 4/2012–6/2012 |
| | Intensification | 6/2002–11/2002, 3/2006–11/2006 | 1/2002–7/2003, 11/2005–3/2007, 7/2012–4/2013 |
| | Termination | 3/2010–5/2010, 9/2010–2/2011 | 11/2009–10/2011 |

Table 5.S2: Same as Table 5.S1, but for the southern region.

5.3 Chapter summary

This chapter sought to further understanding of the physical processes driving southeast Australian drought by examining the long term time series of precipitation recycling and moisture sources developed in Chapter 4.

The results show droughts in southeast Australia were driven by anomalous atmospheric circulation that transported important marine moisture away from the region during onset and intensification — a process that reversed during drought termination. This result shows that to more comprehensively understand drought in southeast Australia, and improve its prediction, deeper understanding is needed of the relationship between atmospheric circulation, moisture advection and precipitation, and how this relationship is modified by terrestrial processes and large scale climate variability.

In addition to reduced moisture supply, low precipitation during drought was driven by local land and atmospheric conditions unfavourable to the precipitation of available atmospheric moisture. This result demonstrates that a better understanding is needed of the mechanisms suppressing precipitation generation during drought.

Remote marine moisture played the primary role in drought onset and intensification, with local terrestrial processes playing a secondary role, amplifying the already dry conditions by less than 6%. The results also indicate that the amplification and termination of droughts in the southern region were partly dependent on the land wetness conditions in the northern region. This finding may help explain observed declining precipitation trends in the southern region, and requires further investigation.

Overall, the analysis demonstrates that to improve the simulation and prediction of droughts in southeast Australia, models need to source moisture for precipitation from the correct marine and terrestrial regions in the correct ratio, and amplify precipitation anomalies via land-atmosphere feedback processes. The improved understanding of Australian precipitation and drought provided by this research will contribute to more accurate assessment of how droughts will change in the future, reducing uncertainty associated with future projections.

Chapter 6

Conclusion

The aim of this thesis was to determine the influence of land-atmosphere interactions on Australian precipitation. Process knowledge of land-atmosphere interactions is needed to improve Australia's hydroclimatic prediction capability, including the ability to predict extremes such as drought. Process knowledge of the effect of land-atmosphere interactions on present-day precipitation is needed to grasp what role interactions may play in a future Australian climate, where they are expected to play an increasingly important role.

Despite the potential to improve hydroclimatic prediction, detailed process understanding of land-atmosphere interactions in the Australian region has been limited. Like many parts of the world, uncertainty in the understanding of land-atmosphere interactions stems from a lack of long term observations of the relevant processes, including the relationship between soil moisture and precipitation, and the difficulty of establishing causation in such a complex and interconnected system of feedbacks. In the Australian context, it is uncertain where regional precipitation is strongly impacted by land-atmosphere interactions, and how that impact may vary in time and space. Also uncertain is the relative importance of land-atmosphere interactions compared to larger scale processes, and how interaction between the land and the atmosphere amplifies or suppresses precipitation extremes. In addition to uncertainty in present-day impacts of land-atmosphere interactions on precipitation, it is unknown how interactions may have changed in the past. These uncertainties inevitably lead to uncertainty in how precipitation may be impacted by land-atmosphere interactions in the future.

Confronting these uncertainties, this thesis contributes to the understanding of the impact of land-atmosphere interactions on Australian precipitation by answering the following four research questions:

6.1. Research summary

1. How does the performance of different soil moisture data sets vary across Australia?
2. Where do land-atmosphere interactions affect precipitation across Australia, and how do the interactions vary in time and with spatial scale?
3. How strongly do land-atmosphere interactions affect precipitation across Australia?
4. What role do land-atmosphere interactions play during drought?

The following sections summarise and conclude upon the research presented in this thesis, highlighting the contribution to the field through addressing identified knowledge gaps, and propose future research avenues.

6.1 Research summary

Through its role in controlling the partitioning of available radiative energy, soil moisture plays a key role in linking the land and the atmosphere (Seneviratne et al. 2010). For this reason, soil moisture underpins many of the methods used around the world to analyse land-atmosphere interactions, including the methods used in this thesis. Due to the variety of techniques used to estimate soil moisture, including direct ground measurement and indirect measurement via satellites or models, and the variety of applications employing soil moisture data, numerous soil moisture data sets are available. Which data sets are most suitable for application across Australia, and appropriate for analysing land-atmosphere interactions, is uncertain. This issue motivated the first research question, presented in Chapter 2. The research question was addressed by statistically comparing multiple estimates from satellite and model platforms against observations taken from three ground-based monitoring networks, across a range of Australian landscape and climate types. The comparison showed varying capability across the data sets to reflect ground-based observations, owing to the characteristics of the individual estimation techniques. Among the data sets analysed, soil moisture estimated from SMOS satellite observations and the WaterDyn model stood out for their ability to capture observed soil moisture temporal dynamics. The first scientific contribution of this thesis is, therefore, an evaluation of soil moisture data sets that provides for more informed assessment of the suitability of individual soil moisture data sets to the study of land-atmosphere interactions and other applications.

The second research question identified land-atmosphere interactions by examining the statistical relationship between soil moisture and subsequent precipitation. The research presented in Chapter 3 identified north and southeast Australia as regions where land-atmosphere interactions most strongly affect precipitation. The relationship was seasonal, with a positive correlation between soil moisture and subsequent precipitation found in north Australia in the wet and transition seasons, and a negative correlation in southeast Australia in winter. Inferring local land-atmosphere interactions with a statistical approach like correlation inherently assumes a 1D framing of the physical process. For the first time the consequence of upholding this assumption was demonstrated by specifying spatial and temporal scales to constrain the relationship to local-only physical processes. Thus, the second scientific contribution of this thesis is twofold: first, that north and southeast Australia are regions where land-atmosphere interactions most strongly affect precipitation, and second, that when using correlation to infer land-atmosphere interactions, it must be applied in a way that is consistent with the physical mechanisms it represents.

With regions of land-atmosphere interaction identified, the third research question quantified the strength of the interaction. Using Lagrangian back-trajectory analysis, the research presented in Chapter 4 quantified land-atmosphere interaction with the precipitation recycling ratio, and determined the evaporative source of precipitation falling in each part of Australia for the first time. Strongest land-atmosphere interactions were indicated with higher recycling ratios in the north-northwest and southeast of the continent in spring and summer. Land-atmosphere interactions were weakest in winter, and weakest in the southwest of Australia where precipitation is largely controlled by remote processes. Long term trends in recycling and evaporative source regions were evident in northwest and southeast Australia, which provided new insight into the processes driving the respective upward and downward trends in precipitation observed in these regions. Establishing the sources of moisture supplying precipitation also provided insight to the relative importance of local terrestrial processes to regional precipitation compared to remote processes. Overall, this research contributes knowledge to the processes driving Australian precipitation, its variability and impact from land-atmosphere interactions.

The fourth and final research question of this thesis explored the role of land-atmosphere interactions and their impact on precipitation during drought. The research presented in Chapter 5 combined estimates of precipitation recycling, moisture sources and atmospheric

circulation, with a focus on southeast Australia. The analysis provided the first quantification of the change in moisture supply for precipitation during major droughts in southeast Australia and explicated the causes of the change. The onset and intensification of drought was driven by a reduced supply of moisture from the Tasman and Coral Seas due to anomalies in atmospheric circulation, combined with a lack of precipitation-generating mechanisms. Droughts terminated when atmospheric circulation strengthened the easterly flow of moist marine air into the region to promote anomalously high precipitation. Terrestrial moisture sources played a secondary role in amplifying precipitation anomalies in each drought stage. Beyond Australia, this research provides a framework for evaluating the relationship between atmospheric circulation, moist advection and precipitation in other regions of the world. Lastly, this research directly contributes to the understanding of the physical processes driving drought onset, intensification and termination in southeast Australia.

In conclusion, land-atmosphere interactions have a measurable effect on Australian precipitation, being strongest in north and southeast Australia in spring and summer and weakest in southwest Australia during winter. The sign of the feedback between the land and the atmosphere changes with time and space, but is typically positive in north and southeast Australia in spring and summer and negative in the southeast in winter. During drought, local land-atmosphere feedbacks play a secondary role in amplifying precipitation anomalies compared to remote processes.

6.2 Future work

The research presented in this thesis has highlighted avenues for future research. Three areas of study are recommended as a priority, including: (i) research to understand how moist advection is modified by large scale climate modes to affect Australian precipitation and drought; (ii) detailed examination of the sign of the land-atmosphere feedback in southeast Australia in winter and during drought, and (iii) research to establish the ability of Australia's climate prediction system to simulate precipitation moisture sources and land-atmosphere interactions in line with the mechanisms identified in this thesis. Each priority area is discussed below.

Moisture advection and drought

It is known that Australian precipitation and drought are associated with large scale modes of climate variability such as the El Niño Southern Oscillation (ENSO; Chiew et al. 1998), Indian Ocean Dipole (IOD; Ashok et al. 2003) and Southern Annular Mode (SAM; Hendon et al. 2007). But individual climate modes have only been able to statistically explain up to 50% of precipitation variability, and less than 20% in most regions (Risbey et al. 2009), demonstrating the inherent complexity of the connection between climate modes and Australian precipitation. This thesis has demonstrated the importance of moist marine advection to precipitation in Australia, especially in southeast Australia during drought. Yet it is unknown how climate modes impact Australian precipitation via large scale modification of the supply of marine moisture for precipitation in Australia. There is a need to understand how the IOD and SAM interact with ENSO and it's central and eastern Pacific types to affect the supply of moisture for precipitation, including the weakening or strengthening of moist advection toward Australia to develop or break droughts. Future research is also needed to understand how these large scale climate modes translate into local precipitation impacts through their interaction with synoptic scale and local scale processes. This process understanding can then be used to evaluate the ability of coupled climate models to simulate and predict drought onset, intensification and termination through the circulation-advection-precipitation relationship; understand why potential deficiencies exist and guide subsequent model development.

Negative versus positive feedback

The negative soil moisture-precipitation relationship found in winter over southeast Australia (Chapter 3) contrasts with studies of comparable scale that tend to show a positive or no relationship (Hirsch et al. 2014b; Koster et al. 2006) and with the positive relationship found with precipitation recycling in Chapter 4. The ability of land-atmosphere feedbacks to present as both positive and negative in the same area at different times has been the subject of several previous studies (e.g. Ek and Holtslag 2004; Froidevaux et al. 2013; Guillod et al. 2015; Taylor et al. 2012). Guillod et al. (2015) demonstrated that, for many land regions of the world, a negative spatial feedback (precipitation preferably occurs over drier soils, as shown by Taylor et al. 2012), coincides with a positive temporal feedback (precipitation preferentially occurs over regions that are wetter than normal and heterogeneous). Considering this joint perspective, the soil moisture-precipitation correlation (Chapter 3) reflects a negative temporal

relationship, i.e. greater precipitation depths in winter are associated with colocated drier soils. The precipitation recycling process (Chapter 4) reflects a positive spatial relationship between the land surface and precipitation, i.e. greater precipitation depths in winter are associated with wetter soils in the larger region as a whole. The correlation and precipitation recycling analyses aggregate land-atmosphere interactions over the course of months and seasons. While these analyses were necessary steps to characterise land-atmosphere relationships in Australia, the results demonstrate that southeast Australia is a region of particular uncertainty that will require more detailed examination in time and space.

To determine whether the temporal feedback between the land and the atmosphere in southeast Australia is dominantly positive or negative, and whether it changes with time, future research may consider using a thermodynamic approach such as the CTP method that can more fully characterise boundary layer fluxes on a local, sub-daily time scale (Findell and Eltahir 2003; described in Chapter 1). The method is particularly suited to analysis of both wet and dry days, unlike mixing diagrams where saturated processes are difficult to include (Santanello et al. 2012). The CTP method can identify regions and times when precipitation is more likely to occur over wetter soils, or drier soils, or whether precipitation is likely to occur regardless of the land surface state (i.e. atmospherically controlled events). The method may also be used to understand the tendency of a region toward a particular coupling state as droughts intensify. The paucity of necessary land and atmospheric observations may be overcome by using remotely sensed retrievals of atmospheric temperature and humidity, along with contemporaneous precipitation and soil moisture estimated from either remote sensing or ground stations (e.g. OzFlux, Beringer et al. 2016; OzNet, Smith et al. 2012; CosmOz, Hawdon et al. 2014). Furthermore, the CLASS4GL (<https://class4gl.eu/>; Wouters et al. 2019) platform that integrates global balloon sounding data may be used to further investigate boundary layer sensitivity to land surface states and validate the results gained from the CTP method. Coupling states identified with observations can then be compared to those simulated with coupled climate models. Specific model biases (e.g. precipitation, surface fluxes) revealed by the comparison will guide model modification and subsequent evaluation of its ability to simulate coupling and precipitation in different seasons and stages of drought.

Improving Australia's forecasting capability

The Australian Bureau of Meteorology recently released a decadal research and development plan that, among other things, aims to improve the simulation of land-atmosphere interactions in Australia's climate prediction system, ACCESS (Australian Community Climate and Earth System Simulator; Bureau of Meteorology 2020d). One aim is to reduce uncertainty in precipitation forecasts across time scales. Currently, ACCESS has limited multi-month precipitation forecast prediction skill that changes geographically and seasonally (Hudson et al. 2017).

Next-generation coupled model systems will need to be evaluated against observations of the land-atmosphere system (e.g. Dirmeyer et al. 2018). Wulfmeyer et al. (2018) outlined a modern observational strategy that provides the necessary data to allow comparison between observed and modelled water and energy fluxes. However, collection of these observations involves a significant input of resources to establish the necessary field campaigns, and as such observations remain limited in many parts of the world, including Australia. The sheer expanse of the Australian continent, its diversity of climate zones and low population density all contribute to the challenge of obtaining the necessary observations, at the necessary spatial and temporal scales needed for process understanding and model evaluation. Remote sensing of colocated land surface and atmospheric properties therefore hold promise for future Australian land-atmosphere research.

Finally, process knowledge contributed by this thesis and gained from the above research areas can directly contribute to ACCESS development and evaluation. The magnitude of land-atmosphere interactions and precipitation moisture sources, the geographical variation and the temporal dynamics presented in this thesis provide a valuable baseline for future model evaluation to identify model weaknesses, that, when improved, will enhance Australia's hydroclimatic forecasting capability.

Bibliography

- Adams, J. (2017). *Climate_indices, an open source Python library providing reference implementations of commonly used climate indices*. Climate indices in Python. https://github.com/monocongo/climate_indices. URL: https://github.com/monocongo/climate_indices.
- Albergel, C., C. Rüdiger, D. Carrer, J.-C. Calvet, N. Fritz, V. Naeimi, Z. Bartalis, and S. Hasenauer (2009). "An evaluation of ASCAT surface soil moisture products with in-situ observations in Southwestern France". *Hydrology and Earth System Sciences* 13.2. Publisher: Copernicus GmbH, pp. 115–124. DOI: <https://doi.org/10.5194/hess-13-115-2009>.
- Albergel, C., P. de Rosnay, C. Gruhier, J. Muñoz-Sabater, S. Hasenauer, L. Isaksen, Y. Kerr, and W. Wagner (2012). "Evaluation of remotely sensed and modelled soil moisture products using global ground-based in situ observations". *Remote Sensing of Environment* 118, pp. 215–226. DOI: [10.1016/j.rse.2011.11.017](https://doi.org/10.1016/j.rse.2011.11.017).
- Alfieri, L., P. Claps, P. D'Odorico, F. Laio, and T. M. Over (2008). "An Analysis of the Soil Moisture Feedback on Convective and Stratiform Precipitation". *Journal of Hydrometeorology* 9.2, pp. 280–291. DOI: [10.1175/2007JHM863.1](https://doi.org/10.1175/2007JHM863.1).
- Ashok, K., Z. Guan, and T. Yamagata (2003). "Influence of the Indian Ocean Dipole on the Australian winter rainfall". *Geophysical Research Letters* 30.15. DOI: [10.1029/2003GL017926](https://doi.org/10.1029/2003GL017926).
- Australian Bureau of Statistics (2020). "Measuring natural disasters in the Australian economy". *Australian Bureau of Agricultural and Resource Economics and Sciences, Canberra*. Chief Economist Series. <https://www.abs.gov.au/websitedbs/D3310114.nsf>.
- Baldocchi, D. (2008). "'Breathing' of the terrestrial biosphere: lessons learned from a global network of carbon dioxide flux measurement systems". *Australian Journal of Botany* 56.1. Publisher: CSIRO PUBLISHING, pp. 1–26. DOI: [10.1071/BT07151](https://doi.org/10.1071/BT07151).

- Beck, H. E., A. I. J. M. van Dijk, V. Levizzani, J. Schellekens, D. G. Miralles, B. Martens, and A. de Roo (2017). "MSWEP: 3-hourly 0.25° global gridded precipitation (1979–2015) by merging gauge, satellite, and reanalysis data". *Hydrol. Earth Syst. Sci.* 21.1, pp. 589–615. DOI: 10.5194/hess-21-589-2017.
- Beringer, J. et al. (2016). "An Introduction to the Australian and New Zealand Flux Tower Network – OzFlux". *Biogeosciences* 13.21, pp. 5895–5916. DOI: 10.5194/bg-13-5895-2016.
- Betts, A. K. (2004). "Understanding Hydrometeorology Using Global Models". *Bulletin of the American Meteorological Society* 85.11, pp. 1673–1688. DOI: 10.1175/BAMS-85-11-1673.
- (2009). "Land-Surface-Atmosphere Coupling in Observations and Models". *Journal of Advances in Modeling Earth Systems* 1.3, p. 4. DOI: 10.3894/JAMES.2009.1.4.
- Betts, A. K., J. H. Ball, A. C. M. Beljaars, M. J. Miller, and P. A. Viterbo (1996). "The Land Surface-Atmosphere Interaction: A Review Based on Observational and Global Modeling Perspectives". *Journal of Geophysical Research: Atmospheres* 101 (D3), pp. 7209–7225. DOI: 10.1029/95JD02135.
- Betts, A. K., R. Desjardins, D. Worth, and B. Beckage (2014). "Climate Coupling between Temperature, Humidity, Precipitation, and Cloud Cover over the Canadian Prairies". *Journal of Geophysical Research: Atmospheres* 119.23, 2014JD022511. DOI: 10.1002/2014JD022511.
- Boer, M. M., V. R. d. Dios, and R. A. Bradstock (2020). "Unprecedented burn area of Australian mega forest fires". *Nature Climate Change* 10.3. Number: 3 Publisher: Nature Publishing Group, pp. 171–172. DOI: 10.1038/s41558-020-0716-1.
- Bosilovich, M. G. (2002). "On the vertical distribution of local and remote sources of water for precipitation". *Meteorology and Atmospheric Physics; Wien* 80.1, pp. 31–41. DOI: <http://dx.doi.org/10.1007/s007030200012>.
- Bosilovich, M. G. and J.-D. Chern (2006). "Simulation of Water Sources and Precipitation Recycling for the MacKenzie, Mississippi, and Amazon River Basins". *Journal of Hydrometeorology* 7.3, pp. 312–329. DOI: 10.1175/JHM501.1.
- Brocca, L., G. Zucco, H. Mittelbach, T. Moramarco, and S. I. Seneviratne (2014). "Absolute versus temporal anomaly and percent of saturation soil moisture spatial variability for six networks worldwide". *Water Resources Research* 50.7, pp. 5560–5576. DOI: <https://doi.org/10.1002/2014WR015684>.

- Brocca, L. et al. (2011). "Soil moisture estimation through ASCAT and AMSR-E sensors: An intercomparison and validation study across Europe". *Remote Sensing of Environment* 115.12, pp. 3390–3408. DOI: 10.1016/j.rse.2011.08.003.
- Brown, J. N., P. C. McIntosh, M. J. Pook, and J. S. Risbey (2009). "An Investigation of the Links between ENSO Flavors and Rainfall Processes in Southeastern Australia". *Monthly Weather Review* 137.11, pp. 3786–3795. DOI: 10.1175/2009MWR3066.1.
- Brubaker, K. L., D. Entekhabi, and P. S. Eagleson (1993). "Estimation of Continental Precipitation Recycling". *Journal of Climate* 6.6. Publisher: American Meteorological Society, pp. 1077–1089. DOI: 10.1175/1520-0442(1993)006<1077:E0CPR>2.0.CO;2.
- Budyko, M. (1974). *Climate and Life*. International geophysics series 18. New York Academic Press.
- Bureau of Meteorology (2010). *Australian Climate Averages - Rainfall (Climatology 1961-1990)*. http://www.bom.gov.au/jsp/ncc/climate_averages/rainfall/index.jsp.
- (2012a). *Australian Climate Averages - Climate classifications*. http://www.bom.gov.au/jsp/ncc/climate_averages/climate-classifications/index.jsp.
- (2012b). *Australian Hydrological Geospatial Fabric (Geofabric)*. <http://www.bom.gov.au/water/about/riverBasinAuxNav.shtml>.
- (2013). *About Australian Climate*. <http://www.bom.gov.au/climate/about/>.
- (2020a). *Annual Australian Climate Statement 2019*. <http://www.bom.gov.au/climate/current/annual/aus/#tabs=Events>.
- (2020b). *Climate change and variability: Tracker: Australian timeseries graphs*. <http://www.bom.gov.au/climate/change/index.shtml>.
- (2020c). *Monthly Drought Statement*. <http://www.bom.gov.au/climate/drought/>.
- (2020d). "Research and Development Plan 2020-2030". http://www.bom.gov.au/inside/Research_and_Development_Plan_2020-2030.pdf.
- (2020e). *What is drought?* <http://www.bom.gov.au/climate/drought/t>.
- Cai, W. and T. Cowan (2008). "Dynamics of late autumn rainfall reduction over southeastern Australia". *Geophysical Research Letters* 35.9. DOI: 10.1029/2008GL033727.
- (2012). "Southeast Australia Autumn Rainfall Reduction: A Climate-Change-Induced Poleward Shift of Ocean–Atmosphere Circulation". *Journal of Climate* 26.1, pp. 189–205. DOI: 10.1175/JCLI-D-12-00035.1.

- Centre for International Economics (2014). "Analysis of the benefits of improved seasonal climate forecasting for agriculture". <http://www.climatekelpie.com.au/>.
- Chiew, F. H. S., T. C. Piechota, J. A. Dracup, and T. A. McMahon (1998). "El Nino/Southern Oscillation and Australian rainfall, streamflow and drought: Links and potential for forecasting". *Journal of Hydrology* 204.1, pp. 138–149. DOI: 10.1016/S0022-1694(97)00121-2.
- Choudhury, B. J. and B. J. Blanchard (1983). "Simulating Soil Water Recession Coefficients for Agricultural Watersheds1". *JAWRA Journal of the American Water Resources Association* 19.2. eprint: <https://onlinelibrary.wiley.com/doi/pdf/10.1111/j.1752-1688.1983.tb05321.x>, pp. 241–247. DOI: <https://doi.org/10.1111/j.1752-1688.1983.tb05321.x>.
- Cioni, G. and C. Hohenegger (2017). "Effect of Soil Moisture on Diurnal Convection and Precipitation in Large-Eddy Simulations". *Journal of Hydrometeorology* 18.7, pp. 1885–1903. DOI: 10.1175/JHM-D-16-0241.1.
- Cook, B. I. et al. (2016). "The paleoclimate context and future trajectory of extreme summer hydroclimate in eastern Australia". *Journal of Geophysical Research: Atmospheres* 121.21. eprint: <https://agupubs.onlinelibrary.wiley.com/doi/pdf/10.1002/2016JD024892>, pp. 12, 820–12, 838. DOI: 10.1002/2016JD024892.
- Cortés-Hernández, V. E., F. Zheng, J. Evans, M. Lambert, A. Sharma, and S. Westra (2016). "Evaluating regional climate models for simulating sub-daily rainfall extremes". *Climate Dynamics* 47.5, pp. 1613–1628. DOI: 10.1007/s00382-015-2923-4.
- Crow, W. T., R. Bindlish, and T. J. Jackson (2005). "The added value of spaceborne passive microwave soil moisture retrievals for forecasting rainfall-runoff partitioning". *Geophysical Research Letters* 32.18. DOI: <https://doi.org/10.1029/2005GL023543>.
- CSIRO (2015). *Cosmoz*. Australian Cosmic-Ray Neutron Soil Moisture Monitoring Network. URL: <https://cosmoz.csiro.au/> (visited on 11/20/2020).
- De Jeu, R. A. M., W. Wagner, T. R. H. Holmes, A. J. Dolman, N. C. van de Giesen, and J. Friesen (2008). "Global Soil Moisture Patterns Observed by Space Borne Microwave Radiometers and Scatterometers". *Surveys in Geophysics* 29.4, pp. 399–420. DOI: 10.1007/s10712-008-9044-0.
- Decker, M., A. Pitman, and J. Evans (2015). "Diagnosing the Seasonal Land–atmosphere Correspondence over Northern Australia: Dependence on Soil Moisture State and Correspondence Strength Definition". *Hydrol. Earth Syst. Sci.* 19.8, pp. 3433–3447. DOI: 10.5194/hess-19-3433-2015.

- Desilets, D., M. Zreda, and T. P. A. Ferré (2010). "Nature's neutron probe: Land surface hydrology at an elusive scale with cosmic rays". *Water Resources Research* 46.11. DOI: <https://doi.org/10.1029/2009WR008726>.
- Dharssi, I., K. J. Bovis, B. Macpherson, and C. P. Jones (2011). "Operational assimilation of ASCAT surface soil wetness at the Met Office". *Hydrology and Earth System Sciences* 15.8. Publisher: Copernicus GmbH, pp. 2729–2746. DOI: <https://doi.org/10.5194/hess-15-2729-2011>.
- Di Virgilio, G., J. P. Evans, A. Di Luca, R. Olson, D. Argüeso, J. Kala, J. Andrys, P. Hoffmann, J. J. Katzfey, and B. Rockel (2019). "Evaluating reanalysis-driven CORDEX regional climate models over Australia: model performance and errors". *Climate Dynamics*. DOI: 10.1007/s00382-019-04672-w.
- Dirmeyer, P. A. (2001). "An Evaluation of the Strength of Land-Atmosphere Coupling". *Journal of Hydrometeorology* 2.4, pp. 329–344. DOI: 10.1175/1525-7541(2001)002<0329:AE0TS0>2.0.CO;2.
- (2006). "The Hydrologic Feedback Pathway for Land–Climate Coupling". *Journal of Hydrometeorology* 7.5, pp. 857–867. DOI: 10.1175/JHM526.1.
- (2011). "The Terrestrial Segment of Soil Moisture–climate Coupling". *Geophysical Research Letters* 38.16, p. L16702. DOI: 10.1029/2011GL048268.
- Dirmeyer, P. A. and K. L. Brubaker (1999). "Contrasting Evaporative Moisture Sources during the Drought of 1988 and the Flood of 1993". *Journal of Geophysical Research: Atmospheres* 104 (D16), pp. 19383–19397. DOI: 10.1029/1999JD900222.
- (2007). "Characterization of the Global Hydrologic Cycle from a Back-Trajectory Analysis of Atmospheric Water Vapor". *Journal of Hydrometeorology* 8.1, pp. 20–37. DOI: 10.1175/JHM557.1.
- Dirmeyer, P. A., K. L. Brubaker, and T. DelSole (2009a). "Import and export of atmospheric water vapor between nations". *Journal of Hydrology* 365.1, pp. 11–22. DOI: 10.1016/j.jhydro1.2008.11.016.
- Dirmeyer, P. A., P. Gentine, M. B. Ek, and G. Balsamo (2019). "Chapter 8 - Land Surface Processes Relevant to Sub-seasonal to Seasonal (S2S) Prediction". *Sub-Seasonal to Seasonal Prediction*. Ed. by A. W. Robertson and F. Vitart. Elsevier, pp. 165–181. DOI: 10.1016/B978-0-12-811714-9.00008-5.

- Dirmeyer, P. A., C. A. Schlosser, and K. L. Brubaker (2009b). "Precipitation, Recycling, and Land Memory: An Integrated Analysis". *Journal of Hydrometeorology* 10.1, pp. 278–288. DOI: 10.1175/2008JHM1016.1.
- Dirmeyer, P. A., Z. Wang, M. J. Mbulu, and H. E. Norton (2014). "Intensified Land Surface Control on Boundary Layer Growth in a Changing Climate". *Geophysical Research Letters* 41.4, 2013GL058826. DOI: 10.1002/2013GL058826.
- Dirmeyer, P. A., J. Wei, M. G. Bosilovich, and D. M. Mocko (2013). "Comparing Evaporative Sources of Terrestrial Precipitation and Their Extremes in MERRA Using Relative Entropy". *Journal of Hydrometeorology* 15.1, pp. 102–116. DOI: 10.1175/JHM-D-13-053.1.
- Dirmeyer, P. A. et al. (2012). "Evidence for Enhanced Land–Atmosphere Feedback in a Warming Climate". *Journal of Hydrometeorology* 13.3, pp. 981–995. DOI: 10.1175/JHM-D-11-0104.1.
- Dirmeyer, P. A. et al. (2018). "Verification of Land–Atmosphere Coupling in Forecast Models, Reanalyses, and Land Surface Models Using Flux Site Observations". *Journal of Hydrometeorology* 19.2. Publisher: American Meteorological Society, pp. 375–392. DOI: 10.1175/JHM-D-17-0152.1.
- Dixon, N. S., D. J. Parker, C. M. Taylor, L. Garcia-Carreras, P. P. Harris, J. H. Marsham, J. Polcher, and A. Woolley (2013). "The effect of background wind on mesoscale circulations above variable soil moisture in the Sahel". *Quarterly Journal of the Royal Meteorological Society* 139.673, pp. 1009–1024. DOI: 10.1002/qj.2012.
- Dominguez, F., P. Kumar, X.-Z. Liang, and M. Ting (2006). "Impact of Atmospheric Moisture Storage on Precipitation Recycling". *Journal of Climate* 19.8, pp. 1513–1530. DOI: 10.1175/JCLI3691.1.
- Doran, J. C., W. J. Shaw, and J. M. Hubbe (1995). "Boundary Layer Characteristics over Areas of Inhomogeneous Surface Fluxes". *Journal of Applied Meteorology* 34.2, pp. 559–571. DOI: 10.1175/1520-0450-34.2.559.
- Dorigo, W. A. et al. (2015). "Evaluation of the ESA CCI soil moisture product using ground-based observations". *Remote Sensing of Environment* 162, pp. 380–395. DOI: 10.1016/j.rse.2014.07.023.
- Draper, C. S. (2011). "Near-surface Soil Moisture Assimilation in NWP". PhD thesis. University of Melbourne.

- Draper, C. S., J. P. Walker, P. J. Steinle, R. A. M. de Jeu, and T. R. H. Holmes (2009). "An evaluation of AMSR-E derived soil moisture over Australia". *Remote Sensing of Environment* 113.4, pp. 703–710. DOI: 10.1016/j.rse.2008.11.011.
- Drumond, A., L. Gimeno, R. Nieto, R. M. Trigo, and S. M. Vicente-Serrano (2017). "Drought episodes in the climatological sinks of the Mediterranean moisture source: The role of moisture transport". *Global and Planetary Change. Climate Variability and Change in the Mediterranean Region* 151, pp. 4–14. DOI: 10.1016/j.gloplacha.2016.12.004.
- Duerinck, H. M., R. J. van der Ent, N. C. van de Giesen, G. Schoups, V. Babovic, and P. J.-F. Yeh (2016). "Observed Soil Moisture–Precipitation Feedback in Illinois: A Systematic Analysis over Different Scales". *Journal of Hydrometeorology* 17.6, pp. 1645–1660. DOI: 10.1175/JHM-D-15-0032.1.
- Ek, M. B. and A. a. M. Holtslag (2004). "Influence of Soil Moisture on Boundary Layer Cloud Development". *Journal of Hydrometeorology* 5.1, pp. 86–99. DOI: 10.1175/1525-7541(2004)005<0086:IOSMOB>2.0.CO;2.
- Ek, M. and L. Mahrt (1994). "Daytime Evolution of Relative Humidity at the Boundary Layer Top". *Monthly Weather Review* 122.12, pp. 2709–2721. DOI: 10.1175/1520-0493(1994)122<2709:DEORHA>2.0.CO;2.
- Eltahir, E. A. B. and R. L. Bras (1996). "Precipitation recycling". *Reviews of Geophysics* 34.3, pp. 367–378. DOI: 10.1029/96RG01927.
- Escorihuela, M. J., A. Chanzy, J. P. Wigneron, and Y. H. Kerr (2010). "Effective soil moisture sampling depth of L-band radiometry: A case study". *Remote Sensing of Environment* 114.5, pp. 995–1001. DOI: 10.1016/j.rse.2009.12.011.
- Evans, J. P., D. Argueso, R. Olson, and A. Di Luca (2017). "Bias-corrected regional climate projections of extreme rainfall in south-east Australia". *Theoretical and Applied Climatology* 130.3, pp. 1085–1098. DOI: 10.1007/s00704-016-1949-9.
- Evans, J. P., F. Ji, G. Abramowitz, and M. Ekström (2013). "Optimally choosing small ensemble members to produce robust climate simulations". *Environmental Research Letters* 8.4, p. 044050. DOI: 10.1088/1748-9326/8/4/044050.
- Evans, J. P., A. J. Pitman, and F. T. Cruz (2011). "Coupled Atmospheric and Land Surface Dynamics over Southeast Australia: A Review, Analysis and Identification of Future Research Priorities". *International Journal of Climatology* 31.12, pp. 1758–1772. DOI: 10.1002/joc.2206.

- Ferguson, C. R. and E. F. Wood (2011). "Observed Land–Atmosphere Coupling from Satellite Remote Sensing and Reanalysis". *Journal of Hydrometeorology* 12.6, pp. 1221–1254. DOI: 10.1175/2011JHM1380.1.
- Ferguson, C. R., E. F. Wood, and R. K. Vinukollu (2012). "A Global Intercomparison of Modeled and Observed Land-Atmosphere Coupling". *Journal of Hydrometeorology* 13.3, pp. 749–784. DOI: 10.1175/JHM-D-11-0119.1.
- Findell, K. L. and E. A. B. Eltahir (1997). "An Analysis of the Soil Moisture-Rainfall Feedback, Based on Direct Observations from Illinois". *Water Resources Research* 33.4, pp. 725–735. DOI: 10.1029/96WR03756.
- (2003). "Atmospheric controls on soil moisture-boundary layer interactions: Three-dimensional wind effects". *Journal of Geophysical Research: Atmospheres* 108 (D8), p. 8385. DOI: 10.1029/2001JD001515.
- Findell, K. L., P. Gentine, B. R. Lintner, and B. P. Guillod (2015). "Data Length Requirements for Observational Estimates of Land–Atmosphere Coupling Strength". *Journal of Hydrometeorology* 16.4, pp. 1615–1635. DOI: 10.1175/JHM-D-14-0131.1.
- Findell, K. L., P. Gentine, B. R. Lintner, and C. Kerr (2011). "Probability of afternoon precipitation in eastern United States and Mexico enhanced by high evaporation". *Nature Geoscience* 4.7, pp. 434–439. DOI: 10.1038/ngeo1174.
- Finkele, K., G. A. Mills, G. Beard, and D. Jones (2006). *National daily gridded soil moisture deficit and drought factors for use in prediction of Forest Fire Danger Index in Australia*. <http://www.bom.gov.au/bmrc/pubs/researchreports/RR119.pdf>.
- Fita, L., J. P. Evans, D. Argüeso, A. King, and Y. Liu (2017). "Evaluation of the regional climate response in Australia to large-scale climate modes in the historical NARClIM simulations". *Climate Dynamics* 49.7, pp. 2815–2829. DOI: 10.1007/s00382-016-3484-x.
- Franz, T. E., M. Zreda, T. P. A. Ferre, R. Rosolem, C. Zweck, S. Stillman, X. Zeng, and W. J. Shuttleworth (2012). "Measurement depth of the cosmic ray soil moisture probe affected by hydrogen from various sources". *Water Resources Research* 48.8. eprint: <https://agupubs.onlinelibrary.wiley.com/doi/pdf/10.1029/2012WR011871>. DOI: <https://doi.org/10.1029/2012WR011871>.
- Freund, M. B., B. J. Henley, D. J. Karoly, H. V. McGregor, N. J. Abram, and D. Dommenget (2019). "Higher frequency of Central Pacific El Niño events in recent decades relative to

- past centuries". *Nature Geoscience* 12.6. Number: 6 Publisher: Nature Publishing Group, pp. 450–455. DOI: 10.1038/s41561-019-0353-3.
- Froidevaux, P., L. Schlemmer, J. Schmidli, W. Langhans, and C. Schär (2013). "Influence of the Background Wind on the Local Soil Moisture–Precipitation Feedback". *Journal of the Atmospheric Sciences* 71.2, pp. 782–799. DOI: 10.1175/JAS-D-13-0180.1.
- Frost, A., A. Ramchurn, M. Hafeez, F. Zhao, V. Haverd, J. Beringer, and P. R. Briggs (2015). "Evaluation of AWRA-L: the Australian Water Resource Assessment model". DOI: 10.36334/modsim.2015.12.frost.
- Frost, A., A. Ramchurn, and A. Smith (2018). *Technical Description of the Australian Water Resources Assessment Landscape model version 6*. Commonwealth of Australia.
- Gallant, A. J. E. and J. Gergis (2011). "An experimental streamflow reconstruction for the River Murray, Australia, 1783–1988". *Water Resources Research* 47.12. DOI: 10.1029/2010WR009832.
- Gimeno, L. (2013). "Grand challenges in atmospheric science". *Frontiers in Earth Science* 1. Publisher: Frontiers. DOI: 10.3389/feart.2013.00001.
- Gimeno, L., A. Drumond, R. Nieto, R. M. Trigo, and A. Stohl (2010). "On the origin of continental precipitation". *Geophysical Research Letters* 37.13, p. L13804. DOI: 10.1029/2010GL043712.
- Gimeno, L., A. Stohl, R. M. Trigo, F. Dominguez, K. Yoshimura, L. Yu, A. Drumond, A. M. Durán-Quesada, and R. Nieto (2012). "Oceanic and terrestrial sources of continental precipitation". *Reviews of Geophysics* 50.4. DOI: 10.1029/2012RG000389.
- Goessling, H. F. and C. H. Reick (2013). "On the "well-mixed" assumption and numerical 2-D tracing of atmospheric moisture". *Atmospheric Chemistry and Physics* 13.11, pp. 5567–5585. DOI: 10.5194/acp-13-5567-2013.
- Guillod, B. P., B. Orlowsky, D. G. Miralles, A. J. Teuling, and S. I. Seneviratne (2015). "Reconciling Spatial and Temporal Soil Moisture Effects on Afternoon Rainfall". *Nature Communications* 6, p. 6443. DOI: 10.1038/ncomms7443.
- Guo, Z. et al. (2006). "GLACE: The Global Land-Atmosphere Coupling Experiment. Part II: Analysis". *Journal of Hydrometeorology* 7.4, pp. 611–625. DOI: 10.1175/JHM511.1.
- Haverd, V., M. R. Raupach, P. R. Briggs, J. G. Canadell, P. Isaac, C. Pickett-Heaps, S. H. Roxburgh, E. van Gorsel, R. A. Viscarra Rossel, and Z. Wang (2013). "Multiple observation types reduce uncertainty in Australia's terrestrial carbon and water cycles". *Biogeosciences*

- 10.3. Publisher: Copernicus GmbH, pp. 2011–2040. DOI: <https://doi.org/10.5194/bg-10-2011-2013>.
- Haverd, V. and M. Cuntz (2010). “Soil–Litter–Iso: A one-dimensional model for coupled transport of heat, water and stable isotopes in soil with a litter layer and root extraction”. *Journal of Hydrology* 388.3, pp. 438–455. DOI: 10.1016/j.jhydrol.2010.05.029.
- Hawdon, A., D. McJannet, and J. Wallace (2014). “Calibration and correction procedures for cosmic-ray neutron soil moisture probes located across Australia”. *Water Resources Research* 50.6. eprint: <https://agupubs.onlinelibrary.wiley.com/doi/pdf/10.1002/2013WR015138>, pp. 5029–5043. DOI: <https://doi.org/10.1002/2013WR015138>.
- Hendon, H. H., D. W. J. Thompson, and M. C. Wheeler (2007). “Australian Rainfall and Surface Temperature Variations Associated with the Southern Hemisphere Annular Mode”. *Journal of Climate* 20.11. Publisher: American Meteorological Society, pp. 2452–2467. DOI: 10.1175/JCLI4134.1.
- Herrera-Estrada, J. E., J. A. Martinez, F. Dominguez, K. L. Findell, E. F. Wood, and J. Sheffield (2019). “Reduced Moisture Transport Linked to Drought Propagation Across North America”. *Geophysical Research Letters* 46.10, pp. 5243–5253. DOI: 10.1029/2019GL082475.
- Hirsch, A. L., A. J. Pitman, and J. Kala (2014a). “The Role of Land Cover Change in Modulating the Soil Moisture–Temperature Land–Atmosphere Coupling Strength over Australia”. *Geophysical Research Letters* 41.16, pp. 5883–5890. DOI: 10.1002/2014GL061179.
- Hirsch, A. L., A. J. Pitman, S. I. Seneviratne, J. P. Evans, and V. Haverd (2014b). “Summertime Maximum and Minimum Temperature Coupling Asymmetry over Australia Determined Using WRF”. *Geophysical Research Letters* 41.5, pp. 1546–1552. DOI: 10.1002/2013GL059055.
- Hirsch, A. L., J. Kala, A. J. Pitman, C. Carouge, J. P. Evans, V. Haverd, and D. Mocko (2014c). “Impact of Land Surface Initialization Approach on Subseasonal Forecast Skill: A Regional Analysis in the Southern Hemisphere”. *Journal of Hydrometeorology* 15.1, pp. 300–319. DOI: 10.1175/JHM-D-13-05.1.
- Hirsch, A. L. et al. (2019). “Amplification of Australian Heatwaves via Local Land–Atmosphere Coupling”. *Journal of Geophysical Research: Atmospheres* 124.24, pp. 13625–13647. DOI: 10.1029/2019JD030665.

- Hobeichi, S., G. Abramowitz, and J. P. Evans (2020). "Derived Optimal Linear Combination Evapotranspiration - DOLCE v2.0". *Research Data Australia*. DOI: doi:10.25914/5eab8f533aeae.
- Hobeichi, S., G. Abramowitz, J. Evans, and A. Ukkola (2018). "Derived Optimal Linear Combination Evapotranspiration (DOLCE): a global gridded synthesis ET estimate". *Hydrology and Earth System Sciences* 22.2. Publisher: Copernicus GmbH, pp. 1317–1336. DOI: <https://doi.org/10.5194/hess-22-1317-2018>.
- Hohenegger, C., P. Brockhaus, C. S. Bretherton, and C. Schär (2009). "The Soil Moisture–Precipitation Feedback in Simulations with Explicit and Parameterized Convection". *Journal of Climate* 22.19, pp. 5003–5020. DOI: 10.1175/2009JCLI2604.1.
- Holgate, C. M., A. I. J. M. V. Dijk, J. P. Evans, and A. J. Pitman (2019). "The Importance of the One-Dimensional Assumption in Soil Moisture - Rainfall Depth Correlation at Varying Spatial Scales". *Journal of Geophysical Research: Atmospheres* 124.6, pp. 2964–2975. DOI: 10.1029/2018JD029762.
- (2020a). "Local and Remote Drivers of Southeast Australian Drought". *Geophysical Research Letters* 47.18, e2020GL090238. DOI: 10.1029/2020GL090238.
- Holgate, C. M., J. P. Evans, A. I. J. M. van Dijk, A. J. Pitman, and G. Di Virgilio (2020b). "Australian Precipitation Recycling and Evaporative Source Regions". *Journal of Climate* 33.20, pp. 8721–8735. DOI: 10.1175/JCLI-D-19-0926.1.
- Holgate, C. M. et al. (2016). "Comparison of Remotely Sensed and Modelled Soil Moisture Data Sets across Australia". *Remote Sensing of Environment* 186, pp. 479–500. DOI: 10.1016/j.rse.2016.09.015.
- Holgate, C. M., A. I. J. M. v. Dijk, G. J. Cary, and M. Yebra (2017). "Using alternative soil moisture estimates in the McArthur Forest Fire Danger Index". *International Journal of Wildland Fire*. DOI: 10.1071/WF16217.
- Holmes, A., C. Rüdiger, B. Mueller, M. Hirschi, and N. Tapper (2017). "Variability of soil moisture proxies and hot days across the climate regimes of Australia". *Geophysical Research Letters* 44.14, 2017GL073793. DOI: 10.1002/2017GL073793.
- Holper, P. (2011). *Australian rainfall - past, present and future*. Australian Climate Change Science Program. Australian Climate Change Science Program, p. 18.

- Hope, P. K., W. Drosowsky, and N. Nicholls (2006). "Shifts in the synoptic systems influencing southwest Western Australia". *Climate Dynamics* 26.7, pp. 751–764. DOI: 10.1007/s00382-006-0115-y.
- Hope, P., B. Timbal, and R. Fawcett (2010). "Associations between rainfall variability in the southwest and southeast of Australia and their evolution through time". *International Journal of Climatology* 30.9, pp. 1360–1371. DOI: 10.1002/joc.1964.
- Hope, P. and I. Watterson (2018). "Persistence of cool conditions after heavy rain in Australia". *Journal of Southern Hemisphere Earth System Science* 68.1. DOI: 10.22499/3.6801.004.
- Hudson, D., L. Shi, O. Alves, M. Zhao, H. Hendon, and G. Young (2017). *Performance of ACCESS-S1 for key horticultural regions*. Bureau Research Report. Series: Bureau Research Report. Bureau of Meteorology. DOI: 10.22499/4.0020.
- Hughes, N., D. Galeano, and S. Hatfield-Dodds (2019). "The effects of drought and climate variability on Australian farms". *Australian Bureau of Agricultural and Resource Economics and Sciences, Canberra*. 6, p. 11. DOI: doi.org/10.25814/5de84714f6e08.
- Hughes, N., K. Lawson, and H. Valle (2017). "Farm performance and climate: Climate-adjusted productivity for broadacre cropping farms". *Australian Bureau of Agricultural and Resource Economics and Sciences, Canberra*, p. 71.
- Imaoka, K. et al. (2010). "Global Change Observation Mission (GCOM) for Monitoring Carbon, Water Cycles, and Climate Change". *Proceedings of the IEEE* 98.5. Conference Name: Proceedings of the IEEE, pp. 717–734. DOI: 10.1109/JPROC.2009.2036869.
- Jackson, T. J., M. H. Cosh, R. Bindlish, P. J. Starks, D. D. Bosch, M. Seyfried, D. C. Goodrich, M. S. Moran, and J. Du (2010). "Validation of Advanced Microwave Scanning Radiometer Soil Moisture Products". *IEEE Transactions on Geoscience and Remote Sensing* 48.12. Conference Name: IEEE Transactions on Geoscience and Remote Sensing, pp. 4256–4272. DOI: 10.1109/TGRS.2010.2051035.
- Jackson, T. J. et al. (2012). "Validation of Soil Moisture and Ocean Salinity (SMOS) Soil Moisture Over Watershed Networks in the U.S." *IEEE Transactions on Geoscience and Remote Sensing* 50.5. Conference Name: IEEE Transactions on Geoscience and Remote Sensing, pp. 1530–1543. DOI: 10.1109/TGRS.2011.2168533.
- Johnson, F., C. J. White, A. van Dijk, M. Ekstrom, J. P. Evans, D. Jakob, A. S. Kiem, M. Leonard, A. Rouillard, and S. Westra (2016). "Natural hazards in Australia: floods". *Climatic Change* 139.1, pp. 21–35. DOI: 10.1007/s10584-016-1689-y.

- Jones, D., W. Wang, and R. Fawcett (2009). "High-Quality Spatial Climate Data-Sets for Australia". *Australian Meteorological and Oceanographic Journal* 58, pp. 233–248.
- Jones, P. W. (1999). "First- and Second-Order Conservative Remapping Schemes for Grids in Spherical Coordinates". *Monthly Weather Review* 127.9, pp. 2204–2210. DOI: 10.1175/1520-0493(1999)127<2204:FASOCR>2.0.CO;2.
- Keetch, J. J. and G. M. Byram (1968). *A Drought Index for Forest Fire Control*. Google-Books-ID: zUiUwKYMq_8C. U.S. Department of Agriculture, Forest Service, Southeastern Forest Experiment Station. 36 pp.
- Kerr, Y. H. et al. (2010). "The SMOS Mission: New Tool for Monitoring Key Elements of the Global Water Cycle". *Proceedings of the IEEE* 98.5. Conference Name: Proceedings of the IEEE, pp. 666–687. DOI: 10.1109/JPROC.2010.2043032.
- Kerr, Y. H. et al. (2012). "The SMOS Soil Moisture Retrieval Algorithm". *IEEE Transactions on Geoscience and Remote Sensing* 50.5. Conference Name: IEEE Transactions on Geoscience and Remote Sensing, pp. 1384–1403. DOI: 10.1109/TGRS.2012.2184548.
- Kiem, A. S. et al. (2016). "Natural hazards in Australia: droughts". *Climatic Change* 139.1, pp. 37–54. DOI: 10.1007/s10584-016-1798-7.
- Kim, S., Y. Y. Liu, F. M. Johnson, R. M. Parinussa, and A. Sharma (2015). "A global comparison of alternate AMSR2 soil moisture products: Why do they differ?" *Remote Sensing of Environment* 161, pp. 43–62. DOI: 10.1016/j.rse.2015.02.002.
- King, A. D., D. Hudson, E.-P. Lim, A. G. Marshall, H. H. Hendon, T. P. Lane, and O. Alves (2020). "Sub-seasonal to seasonal prediction of rainfall extremes in Australia". *Quarterly Journal of the Royal Meteorological Society* 146.730, pp. 2228–2249. DOI: 10.1002/qj.3789.
- Kirono, D. G. C., V. Round, C. Heady, F. H. S. Chiew, and S. Osbrough (2020). "Drought projections for Australia: Updated results and analysis of model simulations". *Weather and Climate Extremes* 30, p. 100280. DOI: 10.1016/j.wace.2020.100280.
- Kohler, M. A. and R. K. Linsley (1951). *Predicting the Runoff from Storm Rainfall*. Google-Books-ID: XMtaTBhT5p4C. U.S. Department of Commerce, Weather Bureau. 12 pp.
- Koster, R. D., P. A. Dirmeyer, A. N. Hahmann, R. Ijpelaar, L. Tyahla, P. Cox, and M. J. Suarez (2002). "Comparing the Degree of Land-Atmosphere Interaction in Four Atmospheric General Circulation Models". *Journal of Hydrometeorology* 3.3, pp. 363–375. DOI: 10.1175/1525-7541(2002)003<0363:CTDOLA>2.0.CO;2.

- Koster, R. D., M. J. Suarez, R. W. Higgins, and H. M. Van den Dool (2003). "Observational Evidence that Soil Moisture Variations Affect Precipitation". *Geophysical Research Letters* 30.5, p. 1241. DOI: 10.1029/2002GL016571.
- Koster, R. D. et al. (2004). "Regions of Strong Coupling Between Soil Moisture and Precipitation". *Science* 305.5687, pp. 1138–1140. DOI: 10.1126/science.1100217.
- Koster, R. D. et al. (2006). "GLACE: The Global Land-Atmosphere Coupling Experiment. Part I: Overview". *Journal of Hydrometeorology* 7.4, pp. 590–610. DOI: 10.1175/JHM510.1.
- Kurita, N. and H. Yamada (2008). "The Role of Local Moisture Recycling Evaluated Using Stable Isotope Data from over the Middle of the Tibetan Plateau during the Monsoon Season". *Journal of Hydrometeorology* 9.4. Publisher: American Meteorological Society, pp. 760–775. DOI: 10.1175/2007JHM945.1.
- Lei, F., W. T. Crow, H. Shen, R. M. Parinussa, and T. R. H. Holmes (2015). "The Impact of Local Acquisition Time on the Accuracy of Microwave Surface Soil Moisture Retrievals over the Contiguous United States". *Remote Sensing* 7.10. Number: 10 Publisher: Multidisciplinary Digital Publishing Institute, pp. 13448–13465. DOI: 10.3390/rs71013448.
- Liu, D., Z. Yu, and A. K. Mishra (2016). "Evaluation of soil moisture-precipitation feedback at different time scales over Asia". *International Journal of Climatology*. DOI: 10.1002/joc.4943.
- Liu, Y. Y., W. A. Dorigo, R. M. Parinussa, R. A. M. de Jeu, W. Wagner, M. F. McCabe, J. P. Evans, and A. I. J. M. van Dijk (2012). "Trend-Preserving Blending of Passive and Active Microwave Soil Moisture Retrievals". *Remote Sensing of Environment* 123, pp. 280–297. DOI: 10.1016/j.rse.2012.03.014.
- Liu, Y. Y., R. M. Parinussa, W. A. Dorigo, R. A. M. De Jeu, W. Wagner, A. I. J. M. van Dijk, M. F. McCabe, and J. P. Evans (2011). "Developing an improved soil moisture dataset by blending passive and active microwave satellite-based retrievals". *Hydrol. Earth Syst. Sci.* 15.2, pp. 425–436. DOI: 10.5194/hess-15-425-2011.
- Liu, Y. Y., A. I. J. M. v. Dijk, R. A. M. d. Jeu, and T. R. H. Holmes (2009). "An analysis of spatiotemporal variations of soil and vegetation moisture from a 29-year satellite-derived data set over mainland Australia". *Water Resources Research* 45.7. DOI: <https://doi.org/10.1029/2008WR007187>.
- Liu, Y., R. A. M. d. Jeu, A. I. J. M. v. Dijk, and M. Owe (2007). "TRMM-TMI satellite observed soil moisture and vegetation density (1998–2005) show strong connection with

- El Niño in eastern Australia". *Geophysical Research Letters* 34.15. DOI: <https://doi.org/10.1029/2007GL030311>.
- Liu, Z., M. Notaro, J. Kutzbach, and N. Liu (2006). "Assessing Global Vegetation–Climate Feedbacks from Observations". *Journal of Climate* 19.5, pp. 787–814. DOI: 10.1175/JCLI3658.1.
- Loew, A. (2014). "Terrestrial satellite records for climate studies: how long is long enough? A test case for the Sahel". *Theoretical and Applied Climatology* 115.3, pp. 427–440. DOI: 10.1007/s00704-013-0880-6.
- Lorenz, R., A. J. Pitman, A. L. Hirsch, and J. Srbinovsky (2015). "Intraseasonal versus Interannual Measures of Land-Atmosphere Coupling Strength in a Global Climate Model: GLACE-1 versus GLACE-CMIP5 Experiments in ACCESS1.3b". *Journal of Hydrometeorology* 16.5, pp. 2276–2295. DOI: 10.1175/JHM-D-14-0206.1.
- Maeda, T. and Y. Taniguchi (2013). *Descriptions of GCOM-W1 AMSR2 Level 1R and Level 2 Algorithms*. https://suzaku.eorc.jaxa.jp/GCOM_W/data/doc/NDX-120015A.pdf.
- Mcalpine, C. A., J. Syktus, J. G. Ryan, R. C. Deo, G. M. Mckeen, H. A. McGowan, and S. R. Phinn (2009). "A Continent under Stress: Interactions, Feedbacks and Risks Associated with Impact of Modified Land Cover on Australia's Climate". *Global Change Biology* 15.9, pp. 2206–2223. DOI: 10.1111/j.1365-2486.2009.01939.x.
- McIntosh, P. C., J. S. Risbey, J. N. Brown, and M. J. Pook (2012). "Apparent and real sources of rainfall associated with a cutoff low". *CAWCR Research Letters*.
- McKee, T. B., N. J. Doesken, and J. Kleist (1993). "The relationship of drought frequency and duration to time scales". *Proceedings of the 8th Conference of Applied Climatology, 17-22 January*. Anaheim, CA: American Meteorological Society.
- McVicar, T. R., T. G. Van Niel, L. T. Li, M. L. Roderick, D. P. Rayner, L. Ricciardulli, and R. J. Donohue (2008). "Wind speed climatology and trends for Australia, 1975–2006: Capturing the stilling phenomenon and comparison with near-surface reanalysis output". *Geophysical Research Letters* 35.20. DOI: 10.1029/2008GL035627.
- Meesters, A. G. C. A., R. A. M. D. Jeu, and M. Owe (2005). "Analytical derivation of the vegetation optical depth from the microwave polarization difference index". *IEEE Geoscience and Remote Sensing Letters* 2.2. Conference Name: IEEE Geoscience and Remote Sensing Letters, pp. 121–123. DOI: 10.1109/LGRS.2005.843983.

- Mei, R. and G. Wang (2011). "Impact of Sea Surface Temperature and Soil Moisture on Summer Precipitation in the United States Based on Observational Data". *Journal of Hydrometeorology* 12.5, pp. 1086–1099. DOI: 10.1175/2011JHM1312.1.
- Meng, X. H., J. P. Evans, and M. F. McCabe (2014). "The Impact of Observed Vegetation Changes on Land-Atmosphere Feedbacks During Drought". *Journal of Hydrometeorology* 15.2, pp. 759–776. DOI: 10.1175/JHM-D-13-0130.1.
- Merlin, O., C. Rudiger, A. A. Bitar, P. Richaume, J. P. Walker, and Y. H. Kerr (2012). "Disaggregation of SMOS Soil Moisture in Southeastern Australia". *IEEE Transactions on Geoscience and Remote Sensing* 50.5, pp. 1556–1571. DOI: 10.1109/TGRS.2011.2175000.
- Merrill, J. T., R. Bleck, and D. Boudra (1986). "Techniques of Lagrangian Trajectory Analysis in Isentropic Coordinates". *Monthly Weather Review* 114.3, pp. 571–581. DOI: 10.1175/1520-0493(1986)114<0571:TOLTAI>2.0.CO;2.
- Miralles, D. G., R. Nieto, N. G. McDowell, W. A. Dorigo, N. E. Verhoest, Y. Y. Liu, A. J. Teuling, A. J. Dolman, S. P. Good, and L. Gimeno (2016). "Contribution of water-limited ecoregions to their own supply of rainfall". *Environmental Research Letters* 11.12, p. 124007. DOI: 10.1088/1748-9326/11/12/124007.
- Miralles, D. G., A. J. Teuling, C. C. van Heerwaarden, and J. Vilà-Guerau de Arellano (2014). "Mega-Heatwave Temperatures due to Combined Soil Desiccation and Atmospheric Heat Accumulation". *Nature Geoscience* 7.5, pp. 345–349. DOI: 10.1038/ngeo2141.
- Mladenova, I., V. Lakshmi, T. J. Jackson, J. P. Walker, O. Merlin, and R. A. M. de Jeu (2011). "Validation of AMSR-E soil moisture using L-band airborne radiometer data from National Airborne Field Experiment 2006". *Remote Sensing of Environment* 115.8, pp. 2096–2103. DOI: 10.1016/j.rse.2011.04.011.
- Mount, A. B. (1972). *The derivation and testing of a soil dryness index using run-off data*. In collab. with F. C. of Tasmania. Bulletin no.4. Hobart: Forestry Commission, Tasmania. 30 pp.
- Murray-Darling Basin Authority (2020). *Water in storages*. <https://www.mdba.gov.au/managing-water/water-storage>.
- Naeimi, V., K. Scipal, Z. Bartalis, S. Hasenauer, and W. Wagner (2009). "An Improved Soil Moisture Retrieval Algorithm for ERS and METOP Scatterometer Observations". *IEEE Transactions on Geoscience and Remote Sensing* 47.7. Conference Name: IEEE Transac-

- tions on Geoscience and Remote Sensing, pp. 1999–2013. DOI: 10.1109/TGRS.2008.2011617.
- Nicholls, N. (2010). "Local and remote causes of the southern Australian autumn-winter rainfall decline, 1958–2007". *Climate Dynamics* 34.6, pp. 835–845. DOI: 10.1007/s00382-009-0527-6.
- Nicholls, N., W. Drosowsky, and B. Lavery (1997). "Australian Rainfall Variability and Change". *Weather* 52.3, pp. 66–72. DOI: 10.1002/j.1477-8696.1997.tb06274.x.
- Northcote, K. H. (1960). *Digital Atlas of Australian Soils*. Digital Atlas of Australian Soils. Last Modified: 2019-11-19T23:19:39.914274 type: dataset. URL: <https://data.gov.au/data/dataset/9e7d2f5b-ff51-4f0f-898a-a55be8837828> (visited on 11/20/2020).
- Northcote, K. H., G. D. Hubble, R. F. Isbell, C. H. Thompson, and E. Bettenay (1975). *A description of Australian soils*. CSIRO.
- Notaro, M. (2008). "Statistical Identification of Global Hot Spots in Soil Moisture Feedbacks among IPCC AR4 Models". *Journal of Geophysical Research: Atmospheres* 113 (D9), p. D09101. DOI: 10.1029/2007JD009199.
- (2018). "Enhancement of vegetation-rainfall feedbacks on the Australian summer monsoon by the Madden–Julian Oscillation". *Climate Dynamics* 51.7, pp. 3093–3109. DOI: 10.1007/s00382-018-4067-9.
- Olson, R., J. Evans, A. Di Luca, and D. Argüeso (2016). "The NARCLiM project: model agreement and significance of climate projections". *Climate Research* 69.3, pp. 209–227. DOI: 10.3354/cr01403.
- Orlowsky, B. and S. I. Seneviratne (2010). "Statistical Analyses of Land Atmosphere Feedbacks and Their Possible Pitfalls". *Journal of Climate* 23.14, pp. 3918–3932. DOI: 10.1175/2010JCLI3366.1.
- Owe, M., R. d. Jeu, and J. Walker (2001). "A methodology for surface soil moisture and vegetation optical depth retrieval using the microwave polarization difference index". *IEEE Transactions on Geoscience and Remote Sensing* 39.8. Conference Name: IEEE Transactions on Geoscience and Remote Sensing, pp. 1643–1654. DOI: 10.1109/36.942542.
- Owe, M., R. d. Jeu, and T. Holmes (2008). "Multisensor historical climatology of satellite-derived global land surface moisture". *Journal of Geophysical Research: Earth Surface* 113 (F1). eprint: <https://agupubs.onlinelibrary.wiley.com/doi/pdf/10.1029/2007JF000769>. DOI: <https://doi.org/10.1029/2007JF000769>.

- Panciera, R. et al. (2014). "The Soil Moisture Active Passive Experiments (SMAPEX): Toward Soil Moisture Retrieval From the SMAP Mission". *IEEE Transactions on Geoscience and Remote Sensing* 52.1. Conference Name: IEEE Transactions on Geoscience and Remote Sensing, pp. 490–507. DOI: 10.1109/TGRS.2013.2241774.
- Parinussa, R. M., T. R. H. Holmes, N. Wanders, W. A. Dorigo, and R. A. M. de Jeu (2015). "A Preliminary Study toward Consistent Soil Moisture from AMSR2". *Journal of Hydrometeorology* 16.2. Publisher: American Meteorological Society, pp. 932–947. DOI: 10.1175/JHM-D-13-0200.1.
- Pepler, A. S., L. V. Alexander, J. P. Evans, and S. C. Sherwood (2016). "Zonal winds and southeast Australian rainfall in global and regional climate models". *Climate Dynamics* 46.1, pp. 123–133. DOI: 10.1007/s00382-015-2573-6.
- Petrova, I. Y., C. C. van Heerwaarden, C. Hohenegger, and F. Guichard (2018). "Regional co-variability of spatial and temporal soil moisture–precipitation coupling in North Africa: an observational perspective". *Hydrol. Earth Syst. Sci.* 22.6, pp. 3275–3294. DOI: 10.5194/hess-22-3275-2018.
- Pielke, R. A. (2001). "Influence of the spatial distribution of vegetation and soils on the prediction of cumulus Convective rainfall". *Reviews of Geophysics* 39.2, pp. 151–177. DOI: 10.1029/1999RG000072.
- Pitman, A. J., G. T. Narisma, R. A. Pielke, and N. J. Holbrook (2004). "Impact of land cover change on the climate of southwest Western Australia". *Journal of Geophysical Research: Atmospheres* 109 (D18). DOI: 10.1029/2003JD004347.
- Pook, M. J., P. C. McIntosh, and G. A. Meyers (2006). "The Synoptic Decomposition of Cool-Season Rainfall in the Southeastern Australian Cropping Region". *Journal of Applied Meteorology and Climatology* 45.8, pp. 1156–1170. DOI: 10.1175/JAM2394.1.
- Power, S., T. Casey, C. Folland, A. Colman, and V. Mehta (1999). "Inter-decadal modulation of the impact of ENSO on Australia". *Climate Dynamics* 15.5, pp. 319–324. DOI: 10.1007/s003820050284.
- Pozzi, W. et al. (2013). "Toward Global Drought Early Warning Capability: Expanding International Cooperation for the Development of a Framework for Monitoring and Forecasting". *Bulletin of the American Meteorological Society* 94.6. Publisher: American Meteorological Society, pp. 776–785. DOI: 10.1175/BAMS-D-11-00176.1.

- Rakich, C. S., N. J. Holbrook, and B. Timbal (2008). "A pressure gradient metric capturing planetary-scale influences on eastern Australian rainfall". *Geophysical Research Letters* 35.8. eprint: <https://agupubs.onlinelibrary.wiley.com/doi/pdf/10.1029/2007GL032970>. DOI: 10.1029/2007GL032970.
- Raupach, M. R., P. R. Briggs, V. Haverd, E. King, M. Paget, and C. M. Trudinger (2009). *Australian Water Availability Project (AWAP): CSIRO Marine and Atmospheric Research Component: Final Report for Phase 3*. CAWCR Technical Report No. 013. Aspendale: CSIRO Marine and Atmospheric Research. 72 pp.
- Reichle, R. H., R. D. Koster, J. Dong, and A. A. Berg (2004). "Global Soil Moisture from Satellite Observations, Land Surface Models, and Ground Data: Implications for Data Assimilation". *Journal of Hydrometeorology* 5.3. Publisher: American Meteorological Society, pp. 430–442. DOI: 10.1175/1525-7541(2004)005<0430:GSMFSO>2.0.CO;2.
- Reid, K. J., I. Simmonds, C. L. Vincent, and A. D. King (2019). "The Australian Northwest Cloudband: Climatology, Mechanisms, and Association with Precipitation". *Journal of Climate* 32.20, pp. 6665–6684. DOI: 10.1175/JCLI-D-19-0031.1.
- Renzullo, L. J., A. I. J. M. van Dijk, J. M. Perraud, D. Collins, B. Henderson, H. Jin, A. B. Smith, and D. L. McJannet (2014). "Continental satellite soil moisture data assimilation improves root-zone moisture analysis for water resources assessment". *Journal of Hydrology* 519, pp. 2747–2762. DOI: 10.1016/j.jhydro1.2014.08.008.
- Risbey, J. S., M. J. Pook, P. C. McIntosh, M. C. Wheeler, and H. H. Hendon (2009). "On the Remote Drivers of Rainfall Variability in Australia". *Monthly Weather Review* 137.10, pp. 3233–3253. DOI: 10.1175/2009MWR2861.1.
- Rodell, M. et al. (2004). "The Global Land Data Assimilation System". *Bulletin of the American Meteorological Society* 85.3. Publisher: American Meteorological Society, pp. 381–394. DOI: 10.1175/BAMS-85-3-381.
- Roundy, J. K., C. R. Ferguson, and E. F. Wood (2013). "Temporal Variability of Land–Atmosphere Coupling and Its Implications for Drought over the Southeast United States". *Journal of Hydrometeorology* 14.2. Publisher: American Meteorological Society, pp. 622–635. DOI: 10.1175/JHM-D-12-090.1.
- Roy, T., J. A. Martinez, J. E. Herrera-Estrada, Y. Zhang, F. Dominguez, A. Berg, M. Ek, and E. F. Wood (2019). "Role of Moisture Transport and Recycling in Characterizing

- Droughts: Perspectives from Two Recent U.S. Droughts and the CFSv2 System". *Journal of Hydrometeorology* 20.1, pp. 139–154. DOI: 10.1175/JHM-D-18-0159.1.
- Salvucci, G. D., J. A. Saleem, and R. Kaufmann (2002). "Investigating Soil Moisture Feedbacks on Precipitation with Tests of Granger Causality". *Advances in Water Resources* 25.8, pp. 1305–1312. DOI: 10.1016/S0309-1708(02)00057-X.
- Santanello, J. A., M. A. Friedl, and M. B. Ek (2007). "Convective Planetary Boundary Layer Interactions with the Land Surface at Diurnal Time Scales: Diagnostics and Feedbacks". *Journal of Hydrometeorology* 8.5, pp. 1082–1097. DOI: 10.1175/JHM614.1.
- Santanello, J. A., C. D. Peters-Lidard, A. Kennedy, and S. V. Kumar (2012). "Diagnosing the Nature of Land Atmosphere Coupling: A Case Study of Dry/Wet Extremes in the U.S. Southern Great Plains". *Journal of Hydrometeorology* 14.1, pp. 3–24. DOI: 10.1175/JHM-D-12-023.1.
- Santanello, J. A., C. D. Peters-Lidard, and S. V. Kumar (2011). "Diagnosing the Sensitivity of Local Land Atmosphere Coupling via the Soil Moisture-Boundary Layer Interaction". *Journal of Hydrometeorology* 12.5, pp. 766–786. DOI: 10.1175/JHM-D-10-05014.1.
- Santanello, J. A., C. D. Peters-Lidard, S. V. Kumar, C. Alonge, and W.-K. Tao (2009). "A Modeling and Observational Framework for Diagnosing Local Land Atmosphere Coupling on Diurnal Time Scales". *Journal of Hydrometeorology* 10.3, pp. 577–599. DOI: 10.1175/2009JHM1066.1.
- Santanello, J. A., J. Roundy, and P. A. Dirmeyer (2015). "Quantifying the Land Atmosphere Coupling Behavior in Modern Reanalysis Products over the U.S. Southern Great Plains". *Journal of Climate* 28.14, pp. 5813–5829. DOI: 10.1175/JCLI-D-14-00680.1.
- Santanello, J. A. et al. (2018). "Land–Atmosphere Interactions: The LoCo Perspective". *Bulletin of the American Meteorological Society* 99.6, pp. 1253–1272. DOI: 10.1175/BAMS-D-17-0001.1.
- Schmugge, T. J. (1983). "Remote Sensing of Soil Moisture: Recent Advances". *IEEE Transactions on Geoscience and Remote Sensing* GE-21.3. Conference Name: IEEE Transactions on Geoscience and Remote Sensing, pp. 336–344. DOI: 10.1109/TGRS.1983.350563.
- Schubert, S. D. et al. (2016). "Global Meteorological Drought: A Synthesis of Current Understanding with a Focus on SST Drivers of Precipitation Deficits". *Journal of Climate* 29.11. Publisher: American Meteorological Society, pp. 3989–4019. DOI: 10.1175/JCLI-D-15-0452.1.

- Sekizawa, S., H. Nakamura, and Y. Kosaka (2018). "Interannual Variability of the Australian Summer Monsoon System Internally Sustained Through Wind-Evaporation Feedback". *Geophysical Research Letters* 45.15, pp. 7748–7755. DOI: 10.1029/2018GL078536.
- Seneviratne, S. I., T. Corti, E. L. Davin, M. Hirschi, E. B. Jaeger, I. Lehner, B. Orlowsky, and A. J. Teuling (2010). "Investigating Soil Moisture-climate Interactions in a Changing Climate: A Review". *Earth-Science Reviews* 99.3, pp. 125–161. DOI: 10.1016/j.earscirev.2010.02.004.
- Seneviratne, S. I. et al. (2006). "Soil Moisture Memory in AGCM Simulations: Analysis of Global Land-Atmosphere Coupling Experiment (GLACE) Data". *Journal of Hydrometeorology* 7.5, pp. 1090–1112. DOI: 10.1175/JHM533.1.
- Sharmila, S. and H. H. Hendon (2020). "Mechanisms of multiyear variations of Northern Australia wet-season rainfall". *Scientific Reports* 10.1. Number: 1 Publisher: Nature Publishing Group, pp. 1–11. DOI: 10.1038/s41598-020-61482-5.
- Smith, A. B., J. P. Walker, A. W. Western, R. I. Young, K. M. Ellett, R. C. Pipunic, R. B. Grayson, L. Siriwardena, F. H. S. Chiew, and H. Richter (2012). "The Murrumbidgee soil moisture monitoring network data set". *Water Resources Research* 48.7, W07701. DOI: 10.1029/2012WR011976.
- Stenson, M. et al. (2012). "Operationalising the Australian Water Resources Assessment (AWRA) system". *Science Symposium Proceedings*. Water Information Research and Development Alliance. CSIRO.
- Stohl, A. and P. James (2004). "A Lagrangian Analysis of the Atmospheric Branch of the Global Water Cycle. Part I: Method Description, Validation, and Demonstration for the August 2002 Flooding in Central Europe". *Journal of Hydrometeorology* 5.4, pp. 656–678. DOI: 10.1175/1525-7541(2004)005<0656:ALAOTA>2.0.CO;2.
- Stojanovic, M., A. Drumond, R. Nieto, and L. Gimeno (2017). "Moisture Transport Anomalies over the Danube River Basin during Two Drought Events: A Lagrangian Analysis". *Atmosphere* 8.10. Number: 10 Publisher: Multidisciplinary Digital Publishing Institute, p. 193. DOI: 10.3390/atmos8100193.
- Su, C.-H., D. Ryu, R. I. Young, A. W. Western, and W. Wagner (2013). "Inter-comparison of microwave satellite soil moisture retrievals over the Murrumbidgee Basin, southeast Australia". *Remote Sensing of Environment* 134, pp. 1–11. DOI: 10.1016/j.rse.2013.02.016.

- Taylor, C. M. (2015). "Detecting Soil Moisture Impacts on Convective Initiation in Europe". *Geophysical Research Letters* 42.11, 2015GL064030. DOI: 10.1002/2015GL064030.
- Taylor, C. M., C. E. Birch, D. J. Parker, N. Dixon, F. Guichard, G. Nikulin, and G. M. S. Lister (2013). "Modeling soil moisture-precipitation feedback in the Sahel: Importance of spatial scale versus convective parameterization". *Geophysical Research Letters* 40.23, 2013GL058511. DOI: 10.1002/2013GL058511.
- Taylor, C. M., R. A. M. de Jeu, F. Guichard, P. P. Harris, and W. A. Dorigo (2012). "Afternoon Rain More Likely over Drier Soil". *Nature* 489.7416, pp. 423–426. DOI: 10.1038/nature11377.
- Tebaldi, C., J. M. Arblaster, and R. Knutti (2011). "Mapping model agreement on future climate projections". *Geophysical Research Letters* 38.23. DOI: 10.1029/2011GL049863.
- Timbal, B., S. Power, R. Colman, J. Viviand, and S. Lirola (2002). "Does Soil Moisture Influence Climate Variability and Predictability over Australia?" *Journal of Climate* 15.10, pp. 1230–1238. DOI: 10.1175/1520-0442(2002)015<1230:DSMICV>2.0.CO;2.
- Trenberth, K. E., J. T. Fasullo, and J. Mackaro (2011). "Atmospheric Moisture Transports from Ocean to Land and Global Energy Flows in Reanalyses". *Journal of Climate* 24.18. Publisher: American Meteorological Society, pp. 4907–4924. DOI: 10.1175/2011JCLI4171.1.
- Trenberth, K. E., L. Smith, T. Qian, A. Dai, and J. Fasullo (2007). "Estimates of the Global Water Budget and Its Annual Cycle Using Observational and Model Data". *Journal of Hydrometeorology* 8.4. Publisher: American Meteorological Society, pp. 758–769. DOI: 10.1175/JHM600.1.
- Tuttle, S. and G. Salvucci (2016). "Empirical Evidence of Contrasting Soil Moisture-Precipitation Feedbacks across the United States". *Science* 352.6287, pp. 825–828. DOI: 10.1126/science.aaa7185.
- Ukkola, A. M., A. J. Pitman, M. G. De Kauwe, G. Abramowitz, N. Herger, J. P. Evans, and M. Decker (2018). "Evaluating CMIP5 Model Agreement for Multiple Drought Metrics". *Journal of Hydrometeorology* 19.6. Publisher: American Meteorological Society, pp. 969–988. DOI: 10.1175/JHM-D-17-0099.1.
- Ukkola, A. M., M. G. D. Kauwe, M. L. Roderick, G. Abramowitz, and A. J. Pitman (2020). "Robust Future Changes in Meteorological Drought in CMIP6 Projections Despite Un-

- certainty in Precipitation". *Geophysical Research Letters* 47.11, e2020GL087820. DOI: 10.1029/2020GL087820.
- Ummenhofer, C. C., M. H. England, P. C. McIntosh, G. A. Meyers, M. J. Pook, J. S. Risbey, A. S. Gupta, and A. S. Taschetto (2009). "What causes southeast Australia's worst droughts?" *Geophysical Research Letters* 36.4. DOI: 10.1029/2008GL036801.
- Ummenhofer, C. C., A. Sen Gupta, P. R. Briggs, M. H. England, P. C. McIntosh, G. A. Meyers, M. J. Pook, M. R. Raupach, and J. S. Risbey (2010). "Indian and Pacific Ocean Influences on Southeast Australian Drought and Soil Moisture". *Journal of Climate* 24.5, pp. 1313–1336. DOI: 10.1175/2010JCLI3475.1.
- Van Der Ent, R. J. and H. H. G. Savenije (2011). "Length and time scales of atmospheric moisture recycling". *Atmospheric Chemistry and Physics* 11.5, pp. 1853–1863. DOI: <https://doi.org/10.5194/acp-11-1853-2011>.
- Van Der Ent, R. J. and H. H. G. Savenije (2013). "Oceanic sources of continental precipitation and the correlation with sea surface temperature". *Water Resources Research* 49.7, pp. 3993–4004. DOI: 10.1002/wrcr.20296.
- Van Der Ent, R. J., H. H. G. Savenije, B. Schaefli, and S. C. Steele-Dunne (2010). "Origin and Fate of Atmospheric Moisture over Continents". *Water Resources Research* 46.9, W09525. DOI: 10.1029/2010WR009127.
- Van der Schalie, R., Y. H. Kerr, J. P. Wigneron, N. J. Rodríguez-Fernández, A. Al-Yaari, and R. A. M. de Jeu (2016). "Global SMOS Soil Moisture Retrievals from The Land Parameter Retrieval Model". *International Journal of Applied Earth Observation and Geoinformation*. Advances in the Validation and Application of Remotely Sensed Soil Moisture - Part 1 45, Part B, pp. 125–134. DOI: 10.1016/j.jag.2015.08.005.
- Van der Schalie, R., R. M. Parinussa, L. J. Renzullo, A. I. J. M. van Dijk, C. -.-H. Su, and R. A. M. de Jeu (2015). "SMOS soil moisture retrievals using the land parameter retrieval model: Evaluation over the Murrumbidgee Catchment, southeast Australia". *Remote Sensing of Environment* 163, pp. 70–79. DOI: 10.1016/j.rse.2015.03.006.
- Van Dijk, A. I. J. M., H. E. Beck, R. S. Crosbie, R. A. M. de Jeu, Y. Y. Liu, G. M. Podger, B. Timbal, and N. R. Viney (2013). "The Millennium Drought in Southeast Australia (2001–2009): Natural and Human Causes and Implications for Water Resources, Ecosystems, Economy, and Society". *Water Resources Research* 49.2, pp. 1040–1057. DOI: 10.1002/wrcr.20123.

- Van Dijk, A., M. Yebra, and G. Cary (2015). *A model-data fusion framework for estimating fuel properties, vegetation growth, carbon storage and the water balance at hillslope scale*. <https://www.bnhcrc.com.au/sites/default/files/managed/downloads/>.
- Vaze, J. et al. (2013). "The Australian Water Resource Assessment Modelling System (AWRA)". 20th International Congress on Modelling and Simulation, p. 8.
- Verdon-Kidd, D. C. and A. S. Kiem (2009). "On the relationship between large-scale climate modes and regional synoptic patterns that drive Victorian rainfall". *Hydrology and Earth System Sciences* 13.4. Publisher: Copernicus GmbH, pp. 467–479. DOI: <https://doi.org/10.5194/hess-13-467-2009>.
- Verdon-Kidd, D. C., B. R. Scanlon, T. Ren, and D. N. Fernando (2017). "A comparative study of historical droughts over Texas, USA and Murray-Darling Basin, Australia: Factors influencing initialization and cessation". *Global and Planetary Change* 149, pp. 123–138. DOI: 10.1016/j.gloplacha.2017.01.001.
- Verhoest, N. E. C., H. Lievens, W. Wagner, J. Álvarez-Mozos, M. S. Moran, and F. Mattia (2008). "On the Soil Roughness Parameterization Problem in Soil Moisture Retrieval of Bare Surfaces from Synthetic Aperture Radar". *Sensors* 8.7. Number: 7 Publisher: Molecular Diversity Preservation International, pp. 4213–4248. DOI: 10.3390/s8074213.
- Viney, N. R., J. Vaze, J. Vleeshouwer, A. Yang, A. van Dijk, and A. Frost (2014). "The AWRA modelling system". *Hydrology and Water Resources Symposium 2014*. Publisher: Engineers Australia, p. 1018.
- Viney, N., J. Vaze, R. Crosbie, B. Wang, W. Dawes, and A. Frost (2015). "AWRA-L v5.0: Technical description of model algorithms and inputs". Publisher: CSIRO. DOI: <https://doi.org/10.4225/08/58518bc790ff7>.
- Vinnikov, K. Y., A. Robock, S. Qiu, and J. K. Entin (1999). "Optimal design of surface networks for observation of soil moisture". *Journal of Geophysical Research: Atmospheres* 104 (D16), pp. 19743–19749. DOI: <https://doi.org/10.1029/1999JD900060>.
- Vreugdenhil, M., W. A. Dorigo, W. Wagner, R. A. M. d. Jeu, S. Hahn, and M. J. E. v. Marle (2016). "Analyzing the Vegetation Parameterization in the TU-Wien ASCAT Soil Moisture Retrieval". *IEEE Transactions on Geoscience and Remote Sensing* 54.6. Conference Name: IEEE Transactions on Geoscience and Remote Sensing, pp. 3513–3531. DOI: 10.1109/TGRS.2016.2519842.

- Wagner, W., W. Dorigo, R. de Jeu, D. Fernandez, J. Benveniste, E. Haas, and M. Ertl (2012). "Fusion of active and passive microwave observations to create an essential climate variable data record on soil moisture". *ISPRS Annals of the Photogrammetry, Remote Sensing and Spatial Information Sciences (ISPRS Annals)* 7, pp. 315–321.
- Wagner, W., G. Lemoine, M. Borgeaud, and H. Rott (1999a). "A study of vegetation cover effects on ERS scatterometer data". *IEEE Transactions on Geoscience and Remote Sensing* 37.2. Conference Name: IEEE Transactions on Geoscience and Remote Sensing, pp. 938–948. DOI: 10.1109/36.752212.
- Wagner, W., G. Lemoine, and H. Rott (1999b). "A Method for Estimating Soil Moisture from ERS Scatterometer and Soil Data". *Remote Sensing of Environment* 70.2, pp. 191–207. DOI: 10.1016/S0034-4257(99)00036-X.
- Wagner, W. et al. (2013). "The ASCAT Soil Moisture Product: A Review of its Specifications, Validation Results, and Emerging Applications". *Meteorologische Zeitschrift*. Publisher: Schweizerbart'sche Verlagsbuchhandlung, pp. 5–33. DOI: 10.1127/0941-2948/2013/0399.
- Wanders, N., D. Karssenbergh, A. de Roo, S. M. de Jong, and M. F. P. Bierkens (2014). "The suitability of remotely sensed soil moisture for improving operational flood forecasting". *Hydrology and Earth System Sciences* 18.6. Publisher: Copernicus GmbH, pp. 2343–2357. DOI: <https://doi.org/10.5194/hess-18-2343-2014>.
- Wang, J. R. and T. J. Schmugge (1980). "An Empirical Model for the Complex Dielectric Permittivity of Soils as a Function of Water Content". *IEEE Transactions on Geoscience and Remote Sensing* GE-18.4. Conference Name: IEEE Transactions on Geoscience and Remote Sensing, pp. 288–295. DOI: 10.1109/TGRS.1980.350304.
- Wang, Y.-P., B. Z. Houlton, and C. B. Field (2007). "A model of biogeochemical cycles of carbon, nitrogen, and phosphorus including symbiotic nitrogen fixation and phosphatase production". *Global Biogeochemical Cycles* 21.1. DOI: <https://doi.org/10.1029/2006GB002797>.
- Wei, J., R. E. Dickinson, and H. Chen (2008). "A Negative Soil Moisture Precipitation Relationship and Its Causes". *Journal of Hydrometeorology* 9.6, pp. 1364–1376. DOI: 10.1175/2008JHM955.1.

- Wei, J., Q. Jin, Z.-L. Yang, and P. A. Dirmeyer (2016). "Role of Ocean Evaporation in California Droughts and Floods". *Geophysical Research Letters* 43.12, 2016GL069386. DOI: 10.1002/2016GL069386.
- Wigneron, J. et al. (2007). "L-band Microwave Emission of the Biosphere (L-MEB) Model: Description and calibration against experimental data sets over crop fields". *Remote Sensing of Environment* 107.4, pp. 639–655. DOI: 10.1016/j.rse.2006.10.014.
- Wouters, H., I. Y. Petrova, C. C. v. Heerwaarden, J. Vilà-Guerau de Arellano, A. J. Teuling, V. Meulenbergh, J. A. Santanello, and D. G. Miralles (2019). "Atmospheric boundary layer dynamics from balloon soundings worldwide: CLASS4GL v1.0". *Geoscientific Model Development* 12.5, pp. 2139–2153. DOI: <https://doi.org/10.5194/gmd-12-2139-2019>.
- Wulfmeyer, V. et al. (2018). "A New Research Approach for Observing and Characterizing Land–Atmosphere Feedback". *Bulletin of the American Meteorological Society* 99.8, pp. 1639–1667. DOI: 10.1175/BAMS-D-17-0009.1.
- Al-Yaari, A. et al. (2014). "Global-scale comparison of passive (SMOS) and active (ASCAT) satellite based microwave soil moisture retrievals with soil moisture simulations (MERRA-Land)". *Remote Sensing of Environment* 152, pp. 614–626. DOI: 10.1016/j.rse.2014.07.013.
- Yang, L., G. Sun, L. Zhi, and J. Zhao (2018). "Negative soil moisture-precipitation feedback in dry and wet regions". *Scientific Reports* 8.1, p. 4026. DOI: 10.1038/s41598-018-22394-7.
- Yee, J. P. Walker, G. Dumedah, A. Moneris, and C. Rudiger (2013). "Towards land surface model validation from using satellite retrieved soil moisture". *Piantadosi, J., Anderssen, R.S. and Boland J. (eds) MODSIM2013, 20th International Congress on Modelling and Simulation*. 20th International Congress on Modelling and Simulation (MODSIM2013). Modelling, Simulation Society of Australia, and New Zealand (MSSANZ), Inc. DOI: 10.36334/modsim.2013.L14.yee.
- Yu, L. (2007). "Global Variations in Oceanic Evaporation (1958–2005): The Role of the Changing Wind Speed". *Journal of Climate* 20.21. Publisher: American Meteorological Society, pp. 5376–5390. DOI: 10.1175/2007JCLI1714.1.
- Yu, P., R. Xu, M. J. Abramson, S. Li, and Y. Guo (2020). "Bushfires in Australia: a serious health emergency under climate change". *The Lancet Planetary Health* 4.1, e7–e8. DOI: 10.1016/S2542-5196(19)30267-0.

- Zeng, D., X. Yuan, and J. K. Roundy (2019). "Effect of Teleconnected Land–Atmosphere Coupling on Northeast China Persistent Drought in Spring–Summer of 2017". *Journal of Climate* 32.21, pp. 7403–7420. DOI: 10.1175/JCLI-D-19-0175.1.
- Zhang, H. (2004). "Analyzing the Potential Impacts of Soil Moisture on the Observed and Model-Simulated Australian Surface Temperature Variations". *Journal of Climate* 17.21, pp. 4190–4212. DOI: 10.1175/JCLI3141.1.
- Zhang, J., W.-C. Wang, and J. Wei (2008). "Assessing Land-Atmosphere Coupling Using Soil Moisture from the Global Land Data Assimilation System and Observational Precipitation". *Journal of Geophysical Research: Atmospheres* 113 (D17), p. D17119. DOI: 10.1029/2008JD009807.
- Zhao, M., H. Zhang, and I. Dharssi (2019). "On the soil moisture memory and influence on coupled seasonal forecasts over Australia". *Climate Dynamics* 52.11, pp. 7085–7109. DOI: 10.1007/s00382-018-4566-8.
- Zhou, S., A. P. Williams, A. M. Berg, B. I. Cook, Y. Zhang, S. Hagemann, R. Lorenz, S. I. Seneviratne, and P. Gentile (2019). "Land–atmosphere feedbacks exacerbate concurrent soil drought and atmospheric aridity". *Proceedings of the National Academy of Sciences*, p. 201904955. DOI: 10.1073/pnas.1904955116.
- Zou, G. Y. (2007). "Toward Using Confidence Intervals to Compare Correlations". *Psychological Methods* 12.4, pp. 399–413. DOI: 10.1037/1082-989X.12.4.399.
- Zreda, M., D. Desilets, T. P. A. Ferré, and R. L. Scott (2008). "Measuring soil moisture content non-invasively at intermediate spatial scale using cosmic-ray neutrons". *Geophysical Research Letters* 35.21. DOI: <https://doi.org/10.1029/2008GL035655>.